Author:
Breen, Charles Edward Pitt

Title:
Impact damage in thick carbon fibre reinforced plastic laminated composites

University of BRISTOL

IMPACT DAMAGE IN THICK CARBON FIBRE REINFORCED PLASTIC LAMINATED COMPOSITES

CHARLES EDWARD PITT BREEN

A dissertation submitted to the University of Bristol in accordance with the requirements of the degree of Doctor of Philosophy in the Faculty of Engineering, Department of Mechanical Engineering. February 2007

Word Count: 51 330

ABSTRACT

Thick carbon fibre composite laminates are to be used in the structure of large civil aircraft, in particular wing skins which can be up to 30 mm thick. These structures are susceptible to low velocity impacts, for example from accidental tool drops. Whilst it is known that thin laminates (up to approximately 3 mm thick) can sustain critical sub-surface damage from such impacts, little research has been undertaken on the low velocity impact of thick laminates. In addition free edges are commonplace on a wing and little is known about thick laminate impact near a free edge (defined as 20 mm from the edge). The aim of this research is to use experiment and analysis to understand the response and damage to thick laminates impacted centrally and near a free edge.

An instrumented drop weight impact tower was designed and built to perform impact experiments, measuring the impact and rebound velocity, and impact force. Carbon fibre epoxy composite laminates up to 12 mm thick were manufactured using non-crimped fabrics and a standard autoclave cure cycle.

Composite plates of three thicknesses (4, 8 and 12 mm) were impacted with three different energies (100, 200 and 350 J) in two locations (edge and central). Damage was evaluated using ultrasonic C-scan, deply and residual strength measurements. It was observed for all impact energies that delamination was the dominant damage mode in edge impacts, whereas in central impacts it was fibre breakage. This leads to lower residual compressive strength for edge impacted plates, and conversely lower residual tensile strength for centrally impacted plates.

In parallel an explicit finite element study was performed studying the effect of the plate dimensions. In particular it was shown that the maximum stress becomes largely independent of panel diameter for thicker panels. Qualitative agreement with experiment was achieved.

It was concluded that the location of impact has a great influence on the resulting damage in a thick laminate. This means that inspection for impact damage near a free edge is much more important in structures that carry compressive loads than tensile loads.

PAGE
MISSING
IN
ORIGINAL

ACKNOWLEDGEMENTS

I would like to thank Airbus UK and the Needham Cooper Trust for financially supporting the research.

I would like to thank my supervisors Dr Martyn Pavier and Dr Felicity Guild for their support, advice and enthusiasm throughout the research. Also I would like to thank Dr Bruce Drinkwater for his advice and use of his ultrasonic scanning equipment, and Kevin Potter for his advice on many subjects. Also I would like to thank the various members of the Solid Mechanics group for their advice and support.

There are several members of the technical staff who helped me during my research; Brian Exon, Mike Jones and John Skinner I would like to thank especially.

Finally I would like to thank Nadia, Mum and Dad for their unwavering support.

PAGE
MISSING
IN
ORIGINAL

DECLARATION

I declare that the work in this dissertation was carried out in accordance with the regulations of the University of Bristol. The work is original except where indicated by special reference in the text and no part of the dissertation has been submitted for any other degree. Any views expressed in the dissertation are those of the author and in no way represent those of the University of Bristol. The dissertation has not been presented to any other University for examination either in the United Kingdom or overseas.

Signed: .....

Date: 11 JUNE 2007

PAGE
MISSING
IN
ORIGINAL

CONTENTS

PAGE
MISSING
IN
ORIGINAL

FIGURES

TABLES

PAGE
MISSING
IN
ORIGINAL

PUBLICATIONS

Journal Papers

1. Breen, C. E. P., F. J. Guild and M. J. Pavier, "Impact Damage to Thick Carbon Fibre Reinforced Plastic Composite Laminates", To appear in the Journal of Materials Science
2. Bateman, M. G., O. H. Miller, T. J. Palmer, C. E. P. Breen, E. J. Kingston, D. J. Smith and M. J. Pavier, (2005), "Measurement of Residual Stress in Thick Composite Laminates using the Deep-Hole Method", International Journal of Mechanical Sciences, 47, pp 1718-1739
3. Breen, C. E. P., F. J. Guild and M. J. Pavier, (2005), "Impact of Thick CFRP Laminates: The Effect of Impact Velocity", Composites: Part A, 36, pp 205 – 211

Conference Papers

1. Breen CEP, Guild FJ, Pavier MJ, "Thick NCF Composite Laminates: Low Velocity Impact Performance", Proceedings of 15th International Conference on Composite Materials, Durban, South Africa, July, 2005.
2. Breen CEP, Guild FJ, Pavier MJ, "Influence of a near free edge on the impact of thick CFRP panels", Proceedings of 2nd Composites Testing and Model Identification, Bristol, UK, September, 2004.
3. Breen CEP, Guild FJ, Pavier MJ, "Impact of Thick CFRP Laminates: Near Free Edge Impact", Proceedings of 11th European Conference on Composite Materials, Rhodes, Greece, May, 2004.
4. Breen CEP, Guild FJ, Pavier MJ, "Finite Element Simulation of The Impact Response Of Thick Carbon Fibre Reinforced Laminates", Proceedings of 17th ABAQUS UK Users' Group Conference, Derby, UK, November, 2003.
5. Breen CEP, Guild FJ, Pavier MJ, "Impact of Thick Carbon Fibre Composite Laminates: A Parametric Study", Proceedings of 14th International Conference on Composite Materials, San Diego, California, USA, July, 2003
6. Breen CEP, Guild FJ, Pavier MJ, "Impact of Thick CFRP Laminates: The Effect of Impact Velocity", Proceedings of 7th Deformation and Fracture of Composites, Sheffield, UK, April, 2003

CHAPTER 1

INTRODUCTION

1.1 COMPOSITES AND AEROSPACE STRUCTURES

Composites are in wide use on civil and military aircraft structures. This application of composites has been typically led by the military; however their use on large civil aircraft is becoming more widespread, especially with the next generation of aircraft, for example the Airbus A350 and the Boeing 787. Consequently there is a requirement to calculate allowable loading for these materials in order that structures can be designed and analysed.

Aerospace structures need to be lightweight, stiff, strong and in a configuration that facilitates analysis. Due to their specific properties fibre reinforced composites are attractive and feature heavily in current and future designs. The aircraft mentioned above have very ambitious targets for efficiency, weight and range which require that fibre reinforced composites are used, as traditional and advanced metal alloys cannot deliver the same performance.

Composites are not a panacea for aircraft design however and more care must be applied. Manufacture of parts with complex geometry may be possible but there are limitations. Manufacturing tolerances can be difficult to reduce, though careful use of machining can improve this. Out-of-plane, composites are weak and as such need to be protected from out of plane loads, but with exposed composite components such as wing skins this is impossible.

Despite these limitations, the potential benefits outweigh the additional complexity in manufacture, design and analysis. The composites industry the world over is growing so the need for composites research will not dwindle.

1.2 BACKGROUND TO IMPACT

Composite laminates have poor properties (strength and elastic modulus) out-of-plane, and as such should be protected from out-of-plane loads. Where composites are used as an external component like a wing skin, rather than an internal component like a rib or spar, impacts are more probable as they will most likely come from an external foreign object. An impact onto a composite wing skin will create damage and compromise the structure.

An impact is typically divided into two categories. High velocity, or ballistic, impact is usually from a small mass that penetrates the target. This can come from gunfire, or small objects flicked up from the runway during takeoff. In the laboratory high velocity impact is simulated using pressurised gas guns. Low velocity impact is typically a large mass that does not penetrate the target. The source for this type of impact could come from a toolbox or refuelling nozzle dropped from hand height or higher. The sort of response and damage from each type of impact is very different. The high velocity impact will create local, visible damage. A slow velocity impact can create damage that is below the surface and invisible to the naked eye (Barely Visible Impact Damage, BVID). Although high and low velocity impacts of the same energy may produce damage of equal severity, because the low velocity impact damage could go unnoticed the influence of such damage must be well understood and aircraft are designed assuming BVID is present. The damage imparted to a composite component is important to be understood as it will have a limiting effect on that component's ability to perform its function. The damage will reduce its elastic modulus and strength and be more susceptible to fatigue failure. Both types of impact are of interest to designers and are modelled experimentally and in analysis.

The shape and material of the impactor is of importance also. The shape of the impacting object will change the nature of the damage and the response of the target, as will its stiffness. A sharp object will certainly create surface visible damage and perhaps its impact energy will be absorbed by surface matrix crushing. A more blunt nosed impactor

will more likely create sub-surface damage that is not visible to the naked eye. Both are likely to happen in service. The dropped tool box could fall on its corner or on a flat side. Often in research the impactor shape is idealised as a hemisphere, a point, blunt nose or a line contact. Often this choice is made based on what has happened in previous tests, or to allow ease of analysis. It is difficult to analyse the impact from a real situation as there are many random elements. In addition the composition of the impactor is important. An impactor with a low stiffness or strength will not damage the composite as much as a stiff or strong impactor as the energy will be absorbed within the impactor. In research steel impactors are common so that the relative amount of energy absorbed by the impactor is small.

Consideration to how the impact target is held in place is given much thought also. Usually a standard method is employed; these have been developed by Airbus and other organisations to give some consistency to impact experiments (see Short (2001) for a comparison). The usual boundary conditions are clamped or an approximation to free. The type of impact and component has influence on the fixture required. For example, as a low velocity impact generates a response from the whole structure, the impact specimen will need to be large. Each specimen can only really be impacted once making the cost of the tests prohibitive in most cases. More commonly the coupon will be much smaller and through analysis the results related to whole structure response. If the impact is of a high enough velocity compared to the specimen dimensions, the boundary conditions become less important as the effect of impact becomes more localised.

As ultimately the aim of any research is to predict and understand what will happen to a real structure under impact, thought should be given to what that structure is actually like. There could be stiffeners, stringers for example, and the surface could be curved rather than flat. These additional parameters add further dimensions to the possible experiments, and their effects are not trivial and have been studied. The higher apparent stiffness of a component near a stiffener, or with convex curvature will mean the response and damage will be different.

Often an impact will be classified simply by the incident kinetic energy of the impactor. However there are many more parameters that should be included before an impact can be fully characterised. Impactor mass and velocity give more information than just the

energy. The tup shape and material are also important. Also the target mass, stiffness, geometry and constraints all contribute to the response, and should be considered when designing impact experiments.

Impact can be modelled through all the usual techniques: analytical solutions have been found, usually with limited applicability, and numerical solutions are common. For an analytical solution there are often gross assumptions made to enable the solution. In numerical and finite element solutions much care has to be taken in setting up the model in order to ensure accuracy, in particular how contact is defined and the boundary conditions. Impact is commonly assumed to be quasi-static which means simpler tests can be performed (using a static test machine) and simpler analysis carried out. This is a valid assumption where the impact is low velocity and any dynamic transient effects can be ignored. Where this is not the case more complex analysis is carried out using explicit finite element solvers for example.

1.3 AIMS OF THE WORK

There is currently a desire to use composite laminates throughout the structure of large civil aircraft. In particular, use of composites for wing skins is being investigated, where thicknesses up to 24mm are being considered. As shown in Chapter 2, there is little research looking at the impact of thick composite structures and as there is a need for their use, research is required, hence this research programme. Of particular interest is the effect of impacting thick section composite structures near free edges, and how the proximity of such a free edge affects the response of the plate to impact and any resulting damage. A free edge is inevitable on a real structure and it is unknown how the resulting stress state will influence the resulting damage.

The general aims of the project are to manufacture, impact and assess the damage of thick composite laminates impacted near and far from a free edge. Also, in parallel to the experimental work the aim is to gain a qualitative understanding of the impact event. Thus, the overriding aim is to obtain better understanding of thick section composite laminates under impact including the influence of a near free edge, in particular the types of damage prevalent and residual properties. The following paragraphs explain in more detail the aims of each component of the project.

The materials for the project have been supplied by the project sponsor Airbus UK, who have required that a specific lay-up and manufacturing technique be used. The aim was to develop experience in the use of this technique to allow the manufacture of the required number of thick laminates to a high quality, efficiently, with existing equipment.

As there is limited experience in the impact testing of thick laminates no standard test rigs have been developed. It was necessary to design and build an instrumented impact machine to produce impacts with the desired range of impact velocities and energies in a repeatable and efficient way and have instrumentation that allows recording of quality live data for subsequent analysis.

Following impact it is important to evaluate the damage, and existing methods (developing them where necessary for thick composites) were used in order to obtain accurate measurement. The desired measurements are of fibre damage, delamination and residual strength; the use of non-destructive and destructive techniques is expected.

The aim of the parallel analysis work is to develop the use of ABAQUS/Explicit (with ABAQUS/CAE) to analyse dynamically the impact event in order to obtain better understanding of the effects of geometric and impact parameters on the elastic impact response of composite plates, and obtain qualitative agreement and better understanding of results from experiment.

1.4 STRUCTURE OF THE THESIS

Chapter 2 presents the literature review, where the background to impact in composites, manufacturing techniques, non-destructive analysis methods, analysis and experimental investigations of composite impact and thick laminate analysis are discussed.

Chapter 3 presents the materials used in the project and their properties. The laminate manufacturing methods are discussed.

Chapter 4 presents the impact experiments and the design of the impact machine. The test schedule, the range and type of experiments conducted and the manner in which they were conducted are shown. The results from the impact tests are presented and discussed.

Chapter 5 presents the efforts to evaluate the damage in the impacted plates. The techniques employed include non-destructive ultrasonic C-scanning for delamination, resin burn-off and deply for fibre breakage and coupon tension and compression testing for residual strength measurement. The results are presented and discussed.

Chapter 6 shows the efforts to analyse the impact using linear elastic, explicit, finite element analysis. A parametric investigation of the geometric properties of the target component and impact parameters is shown. Also analysis to verify the design of the impact rig is presented.

Chapter 7 gives the thesis discussion, and Chapter 8 the conclusions and recommendations for further work.

The appendices contain detailed listings of experimental results and other miscellaneous items. Appendix A contains the designs of the adapters for fitting the hydraulic grips to the existing Mayes hydraulic static test machine, Appendix B contains the impact tests tabulated results and Appendix C contains the tabulated results from the residual strength tests.

CHAPTER 2

LITERATURE REVIEW

2.1 INTRODUCTION

In this chapter previous research in composites and impact is reviewed and summarised, subdivided into sections by subject: impact, non-destructive testing, destructive testing and analysis. In each some history is given, and the more recent developments.

2.2 HISTORY

The idea of fibrous reinforcement is ancient, with references to straw used in mud bricks thousands of years ago one of the earliest known applications. The first carbon fibres were manufactured in the UK less than 50 years ago, and carbon fibre composite aircraft components were in use by the end of the 1960s (Daniel and Ishai, 1994). Since then the development of fibres and resins has accelerated and now there are many systems available for applications such as: leisure, medical, automotive, space and aircraft industries.

Much of the early research effort was on the characterisation of composite materials, experimental analysis of their mechanical properties and development of analytical techniques. For example, the methods to calculate properties based on generalised Hooke's law for anisotropic elasticity were investigated by Whitney (1967) and numerical methods for calculation of laminate elastic properties developed by Chen and Cheng (1967). Whitney (1969) developed closed form solutions to give the elastic deflections of a composite laminated plate subjected to bending, vibration and buckling.

Impact was also considered at this time. Two-dimensional or planar impact was studied by using a planar projectile thus producing a planar stress pulse in the square specimens of Schuster and Reed (1969). This technique was used to investigate spalling of different composites systems used in thin shell applications. The impact stress pulse induces the spalling: after reflection off the back face it becomes tensile. The more general case of impact by a spherical projectile to the centre of a plate was studied by Moon (1972). A modified version of Mindlin's plate theory showed that both extensional and bending waves are created in the impacted plate, and the magnitudes of these stress waves were calculated. These two types of impact were high velocity, typically from small objects where any damage is likely to be local, although the propagation of the stress wave was important as this can lead to damage far from the impact site where the stress waves reflect off structural features. The problem of stress wave propagation was further investigated by Takeda, Sierakowski and Malvern (1981) in an experimental study using surface and embedded strain gauges. Agreeing with the previous analytical work of Moon (1972) it was shown that tensile and flexural stress waves are created by the impact. The finite difference method was employed in a computer code to study numerically wave propagation in impacted composites (Chen and Lee, 1979). The fibre orientation was found to play a large part in determining the shape of the wave surfaces; this would be expected as the fibre direction determines the stiffness, and the stiffness the wave velocity. They showed that the asymmetric wave patterns resembled those in isotropic solids under asymmetric loads.

Low velocity impact was identified as a critical load case, and the response of laminates to this type of impact as opposed to the more localised response of a high velocity impact was studied (McQuillen, Gause and Llorens, 1976). They determined that in a low velocity impact transverse wave propagation was unimportant and is dominated by structural response. The ratio of the impactor to specimen mass was found to be a determining factor for the specimen's response. Five damage and response mechanisms were identified: structural flexural shear, in-plane wave, spallation, indentation and shear-out (see Figure 2.1). The actual response of a structure will be a mixture of some or all of these mechanisms.

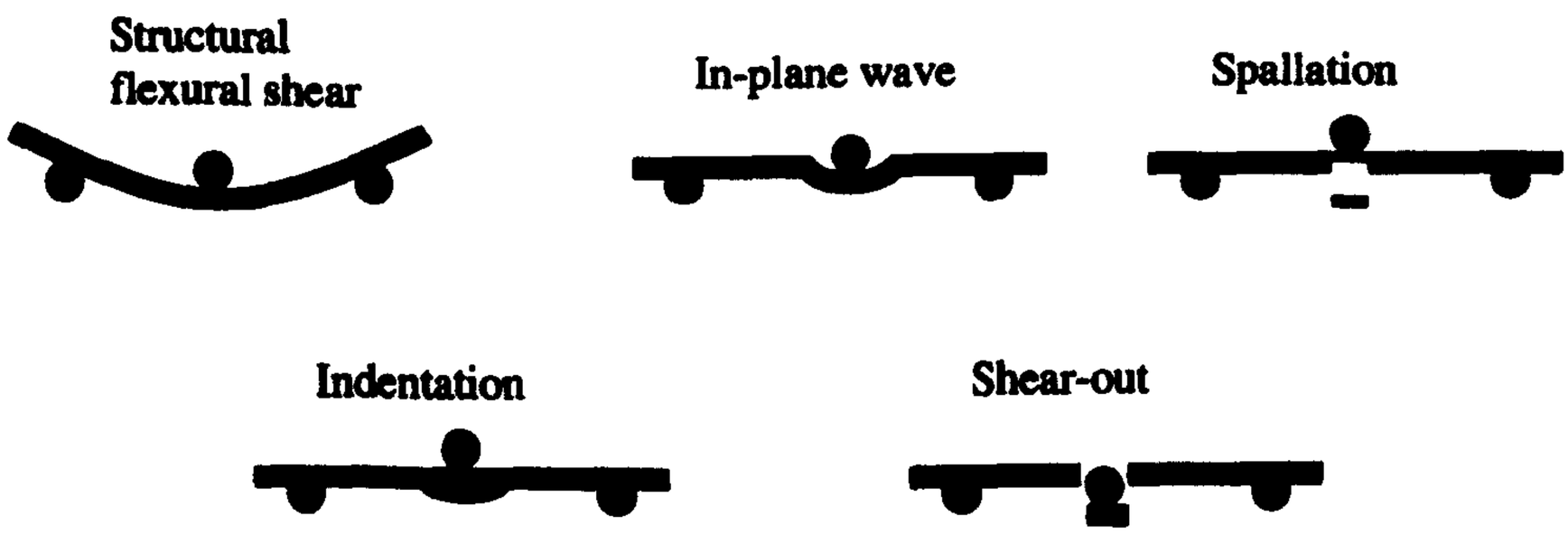

Figure 2.1 - Types of plate response to impact

The earliest paper that was found to use the finite element method to analyse the dynamic response of composites was by Reddy (1982). Unidirectional and cross-ply laminates were loaded with time dependent pressures and the time dependent response was shown to match well with a closed form solution; it was found that the shear deformation and plate thickness were important in determining the amplitude and period of transverse deflection.

The non-destructive testing of composites was first published by Lord and Hay (1972) where their ultrasonics experiments on metal-metal composites showed the initial promise of the technique.

Perhaps the most important paper was that by Waddoups, Jackson and Rogers (1972) which summarised the potential of composite materials in aerospace applications, yet also warning against simply substituting metal for composite and designing so-called black aluminium. In fact this kind of design can mean that the advantage of composites is negated. In their paper, the authors emphasised the importance of designing to the strengths of composites, a point eloquently put by Vasiliev and Razin (2005).

In the last 10 to 15 years the number of papers published in the field of composites research, and on the subject of impact has increased. Many reviews are available such as those by Abrate (1991 and 1994), Richardson and Wisheart (1996) and Pickett (2002).

2.3 MANUFACTURING

There are several composite manufacturing methods in use currently. The simplest method is termed "bucket and brush" whereby the fibres are laid dry into a mould and the resin applied in a liquid form using a brush. This method is ideal for large structures where the quality (in terms of thickness control, fibre alignment etc.) of the resulting composite is not important, e.g. ship building. The most common method is to use rolled sheets of pre-impregnated composite. The laminate shape can be cut out and laid up with relative geometric precision and consistent resin content. The resulting laminate is cured using cycles of heat and pressure. Alternative methods exist such as resin transfer moulding where liquid resin is pumped under pressure or vacuum to infuse a fibre preform.

The use of non-crimped fabrics is a relatively new advancement in the manufacture of laminates. They allow multiple plies stitched together in a blanket to be laid at once thus allowing rapid building up of the laminate thickness. The non-structural stitching maintains the geometric integrity of the blanket so that fibre alignment is maintained. As the blankets are supplied dry, without resin, the manufacture method must include some system for resin infiltration. One method is to use liquid resin with a vacuum pressure differential. This however requires special tooling and equipment. A cheaper and hence more attractive way is to use solid resin film either stacked at the bottom of the laminate or interleaved in a standard autoclave cure; during cure the resin turns liquid and permeates the fibres. This method does require that the transverse permeability of the dry laminates be of an acceptable level so that the fibres are fully wetted and this implies a combination of low viscosity resin, short permeation distance and acceptable permeability. The stitching plays an important role in this part of the manufacturing process too. The stitching density has been shown to be directly related to the transverse permeability of non-crimped fabrics (Drapier et al, 2002); the resin flows along the stitching and then longitudinally between stitches.

The normal requirement of composites is that they are fully cured, with low void content and other defects to allow the maximum potential use of the constituents. The manufacturing method described above, Resin Film Infusion (RFI), is particularly vulnerable to the creation of voids as, besides the volatiles produced by the resin, the air in the blankets must escape fully. This is a subject that has received much attention, with the

development of much specialised cure-monitoring equipment e.g. Chen et al. (1999). This allows the development of optimised cure cycles that ensure complete curing of the resin and ideal dwell times. The internal defects that are inevitable following cure can significantly reduce the interlaminar strength of a laminate depending on their size, type and distribution (Ziao and Tao, 1996). Generally the defects act as crack initiation sites although it was found that their effect on interlaminar shear strength is less than on interlaminar tensile strength.

The final manufacturing parameter that can have serious influence on the quality of laminates is the skill of the technician. It is essential that the correct fibre orientations are achieved with minimal deviation, that lay-up be performed in a clean environment. As with all materials a size effect is present with composites, where larger specimens have a higher probability of containing a large defect. It has been shown that specimens four times larger have an interlaminar tensile strength 1/5 lower than that of the smaller specimen; a similar reduction in strength is possible for a laminate that is poorly manufactured (Wisnom, Jones and Hill, 2001).

2.4 NON-DESTRUCTIVE EVALUATION

Non-destructive evaluation encompasses the range of techniques that are used to characterise materials without causing lasting damage. With impacted composites use of such techniques is important due to the likely presence of critical sub-surface damage that is invisible to the naked eye. Techniques available include x-radiography, ultrasonic evaluation, acoustography, thermography and free vibration methods. Ultrasonic evaluation is of great interest due to the high level of automation available and its relative maturity compared to some other methods. It is in wide use in the marine, aerospace and military industries especially where a high level of component integrity is required.

Ultrasonic methods have been used to detect damage in composites, in particular impact damage for some time. Three scan types are available. A-scan gives the amplitude-time plot for a single point and B-scan a 3D plot of A-scans for a series of points along the specimen. The C-scan has been found to be the most useful method. It takes a given feature of the A-scan (e.g. maximum amplitude within a certain time window), and measured this across the whole specimen to produce a 2d contour plot. This is achieved

using a transducer attached to a 2-axis motion controller which is stepped across the specimen with either the full waveform or particular characteristics of the waveform saved at each position. The emitted ultrasonic pulse is reflected by material interfaces and defects. These reflections can be recorded individually for a detailed examination of the damage. Of particular use is to examine the time domain plot at each position on the scan and shift the data collection gate so that defects at different locations through the thickness can be determined, in particular delaminations at particular ply interfaces thus developing 3D damage maps (Kaczmarek, 1995; Potel et al., 1998; Aymerich and Meili, 2000; Scarponi and Briotti, 2000). This technique has been used to show the development of delaminations in laminates that have been impacted at incrementally higher impact forces (Kaczmarek, 1993). By using force-time impact histories and the C-scan results Kaczmarek was able to determine matrix cracking and delamination threshold impact force levels, that delamination propagation follows matrix crack growth and that initially delaminations are larger nearer the front face, but with larger impact forces the back face delaminations are larger.

Delaminations are relatively straightforward to detect, as they are naturally perpendicular to the emission of the ultrasonic pulse. Matrix cracks involve more complex methods. Kaczmarek (1995) showed a method that allowed the use of the standard normal incidence ultrasonic scanning equipment that also showed matrix cracks. For this method a through-transmission system was used as opposed to the pulse-echo system usually used for delamination detection; the ultrasonic signal emitted by a focussed 20MHz transducer being attenuated by scattering on the crack tip. The results compared favourably with x-radiography. An alternative method is oblique incidence ultrasonics (Bar-Cohen and Crane, 1982 and Gorman, 1991). In this method reflections from the crack are detected by inclining the pulse-echo transducer at an oblique angle to the specimen, so that the cracks are not parallel to the direction of propagation of the ultrasonic wave.

The higher the difference in acoustic impedance, the higher the amplitude of the signal reflected off an interface or defect within the specimen. Hence the back and front face will generate high amplitude reflections in the same way that delaminations do. With a delamination, as the separation between delaminated plies decreases nearer the delamination edge, the amplitude of the reflection decreases and so the delamination

boundary is smeared. The depth of the delamination can be visualised by plotting time of flight results based on a threshold amplitude for a reflection (Aymerich and Meili, 2000).

Choice of transducer is important, especially when scanning thick laminates; although with a lower frequency transducer enhanced penetration is achieved, resolution is sacrificed (Scarponi and Briotti, 2000).

Other NDE methods have limited applicability due to specialised equipment or techniques required. Acoustography requires the use of a special transducer that scans a large area at once, with the through transmitted signal captured to show the extent of the damage. This system has been successfully used in situ to monitor fatigue delamination growth, with a fatigue limit being demonstrated (Chen, Almond and Harris, 2001). Free vibrations techniques exist whereby damaged specimens are excited into vibrational modes, and the frequency and damping of these modes measured and compared against that for undamaged specimens. For small beams this method has shown some success (Kyriazoglou, 2003). However for thicker laminates with thickness up to 10 mm similar techniques have been found to be insensitive to small and medium sized delaminations (Penn el al., 1999).

2.5 IMPACT ANALYSIS

The impact response of composite plates can be categorised into three: where the impact duration is in the order of the transition time of the through thickness waves and is dominated by 3D wave propagation; where the impact is longer the impact is governed by flexural and shear waves; when the impact duration is longer than that needed for these waves to reach the plate boundaries the lowest vibration mode of the impactor-plate system pre-dominates, and the response is quasi-static. The first type can typically be caused by ballistic impact. The latter types can be caused by lightweight object impact, for example hail or runway debris, in the intermediate case and more heavy object impact, for example heavy tool drop, in the last case. The latter types can be considered more critical as they cause barely visible impact damage. However small mass impacts (i.e. the impacts with smaller impact durations) will cause more severe damage as less energy is absorbed through global elastic deflection.

Olsson (2000) researched this method of impact characterisation, and showed that impact damage is more influenced by impact duration (and hence impactor mass) than impact energy. This is a key result as most impacts in the literature are classified by impact energy sometimes with little reference to the other impact parameters. The type of plate response is important in knowing what kind of analysis to perform.

Three 1-dimensional models were proposed by Olsson to simulate the plate response for each impact duration time: the fast impact can be modelled as a mass-spring-mass system, the intermediate case as a mass-spring-damper system, and the slow impact modelled as a spring-mass model (spring stiffnesses for contact, shear, bending and membrane) where the plate's response is global and effectively quasi-static.

Olsson based the criteria for determining which type of model should be used on the ratio of the mass of the impactor and the effected area of the plate. It is effectively the relative inertias of the impactor and plate that determines the plate's response. Thus, with a small duration impact the response is dominated by 3-dimensional wave propagation and is very local. Effects of the through thickness waves will only be significant if their transition time is similar to the impact duration. For intermediate mass impacts, the response is complicated where higher modes of vibration are superimposed on the fundamental vibration. Once the flexural waves hit a boundary the response becomes more dominated by static deformation. The criteria are, for small mass impact:

$$M_{impactor} / M_{plate} \leq 0.29 \text{ (circular plate)}$$
$$M_{impactor} / M_{plate} \leq 0.23 \text{ (square plate)}$$

For large mass impact (quasi-static):

$$M_{impactor} / M_{plate} >> 0.25$$

For intermediate impact:

$$0.2 < M_{impactor} / M_{plate} < 2$$

These criteria give boundaries to different types of impact (high velocity versus low velocity) where previously in literature the boundaries are the subject of some disagreement. The criteria mean that small mass impact analysis does not need to include the boundaries, or can be performed with small sized coupons. Of course the models can only be applied up to damage initiation. The criteria are simplistic however and it might be difficult to determine the correct effective mass of the target when a structure is impacted.

A similar analytical model to Olsson's for large mass impact was used by Helms, Li and Pang (2001) where impact was modelled as a 1-dimensional spring mass damper system, using a lumped stiffness for the plate and a modified Hertzian contact law to determine the contact force (Sun and Yang, 1980) and assuming a quasi-static plate response. Also Caprino, Langella and Lopresto (2002) showed that for thicker laminates (i.e. small mass impacts) the Hertzian contact plays a greater role in affecting the plate behaviour, meaning that the response is more local. Where the plate was thinner (i.e. larger mass impacts) non-linear deformation became more dominant.

Although it is known that impact force is a function of bending, membrane and shear, Caprino, Langella and Lopresto postulated that if the thickness/width ratio was less than 0.2 (i.e. thin laminates) shear can be neglected and if the ratio of maximum deflection to thickness was less than 0.2 (i.e. small deflections) membrane effects can be ignored. As found by Olsson (2000) the solutions showed that the maximum indentation and impactor force (i.e. plate response) are related to the impact duration, and also in common found that once damage was initiated the proposed models diverge significantly from experiment.

A different approach was taken by Christoforou and Yigit (1996); their analytical solution assumed an instantaneous impact based on the impulse-momentum principal. A coefficient of restitution from an elastic plastic contact law was defined and the onset of the plastic deformation phase of the laminate calculated using the critical indentation depth calculated from the ply shear strength.

Chandrashekhara and Schroeder (1995) and Joshi and Sun (1985) both used modified Hertzian contact laws to define the loading of the plate, whereas Sun and Chen (1985) used a contact law derived from experiment - a power law that takes into account cratering (the

permanent deformation, or dent, under the impactor). Sun and Chen's work looking at the effect of plate pre-stress is analogous to Chandrashekhara and Schroeder's where the plate curvature was studied. Plate tension pre-stress and increased convex curvature both increase the target's apparent stiffness and effect the response accordingly: shorter impact durations and greater impact forces. Both papers also show evidence of multiple contacts within an impact event, although Sun and Chen showed that with larger impactor masses continuous contact is possible. Both authors showed that with greater apparent plate stiffness hence higher natural frequencies the second contact happens sooner.

Sun and Chen (1985) showed that with a positive tension pre-stress the contact force increases and the contact time decreases. With a negative compressive pre-stress the deflection decreases.

In Joshi and Sun's (1985) work, the analysis was used to show qualitative agreement with experiment where plane strain 9-node elements with no rotation were used to model beam impact. The results showed that although flexural stress dominates, the peak through thickness shear stress approximately predicts the location of the shear cracks in the top surface.

Tu and Chao (1999) used their elastic finite element model (Chao and Tu, 1999) for a more esoteric aim, to look at the effect of surface friction in oblique impact. Almost all analysis assumes a normal impact with frictionless contact, that any surface parallel velocity component will have negligible effect. Their research showed, however, that with anisotropic friction assumed (where two coefficients of friction are defined, one for each material direction of the top ply), the orientation of the top layer has a great influence over the resulting stress distribution and that larger friction coefficients give rise to smaller contact forces.

Satish Kumar and Mukhopadhyay (2002) developed a finite element that incorporated the effect of an arbitrarily oriented stiffener (hat, blade or I type) without the need for additional beam or plate elements. This resulted in an efficient model that does not require specific mesh refinement and no loss in accuracy when compared with published work or analysis in a commercial code.

Damage can be modelled in many ways. The simplest way is to include an energy sink (dashpot) in line with an elastic plate model that will absorb energy in a way proportionate to what is observed in experiment. As damage is not initiated immediately during impact use of a gap element is necessary to engage the dashpot once a critical impact force is reached (Oguibe and Webb, 1999). This method will only give an idea of the energy that has been absorbed through damage, but will enable the response of a damaged laminate to be studied.

To model the damage initiation and propagation, failure criteria can be embedded into the code. Typically a stress based criteria is used, where laminate strengths are derived using experiments. Often the challenge comes in defining these strengths as the laminate in situ properties will be different to those in a coupon due to the effect of the surrounding plies and boundary conditions. Choi, Wu and Chang (1991) were concerned with the in situ laminate strengths. Their finite element model focussed on predicting the matrix cracks and the delaminations that initiate from them. The Hashin failure criterion (Hashin, 1980) was adopted:

$$(S_{yy}/Y_t)^2 + (S_{yz}/S_i)^2 = e_M^2 \; ; \; e_M \geq 1 = \text{failure}$$

Where S_{yy} and S_{yz} are the ply transverse stress and interlaminar shear stress respectively, and Y_t and S_i the relevant in situ strengths. The actual measured coupon strengths were modified using an empirical formula to determine in situ strengths. When an element met the failure criterion (i.e. $e_M \geq 1$) its properties were reduced so that additional tension stress or transverse shear load could not be sustained, and then the stress field was re-calculated. The authors achieved reasonable agreement with experiment, and also predicted a damage threshold impact energy which was dependent on layer thicknesses and orientation. It is known that composites have an impact damage energy threshold (e.g. Schoeppner and Abrate, 2000), and the fact that this is dependent on the difference between the orientation angle of adjacent plies, known as the ply clock angle, and thickness is unsurprising as the greater the clock angle the weaker the interlaminar interface, and the thicker the ply the weaker it is in-plane. This work was performed in 2-dimensional models to match with experiments on line-loaded coupons. It was followed up in Choi and Chang (1992) where delamination was predicted in a 3-dimensional impact situation. They employed the same matrix cracking criteria and a delamination criterion in a similar form, again based on

modified strengths to approximate in situ values. They showed that delamination induced by a shear crack is initially controlled by Mode I and later by Mode II loading, and is unstable in the direction of the fibres in the lower ply. For bending crack-induced delamination Mode I is dominant and crack extension is stable.

In more recent work, Hou et al. (2000) used a very similar approach, where a set of criteria were embedded in the finite element code and once the failure criteria were met reduced properties were assigned to those elements. The in-built Chang-Chang failure criteria (Chang and Chang, 1987) were used, but modified to give more realistic failure analysis. In this research, despite not using in situ values for ply strengths, good agreement with experiment was achieved.

Fuoss, Straznicky and Poon (1994) used a bending stiffness mismatch method to determine the onset of damage in their analytical solution for two ply laminates. Wu and Springer (1988a) used a similar dimensional analysis method in a finite element model by examining the stiffness difference between plies adjacent to the delamination and mode I stress intensity factor. They assumed that the dominant stress in delamination is through thickness tension in a simplified version of the delamination criteria described above. Fleming (2001) also used a fracture mechanics approach, employing the virtual crack closure technique for delamination prediction. Fleming used spring elements along the interface where it was known the delamination would propagate. This technique of placing special elements along the predicted crack or delamination interface to model the special local properties of the interlaminar region was also used by Geubelle and Baylor (1998) where cohesive elements were used. These elements are essentially non-linear springs that once they have opened beyond a given amount (the crack has opened) the tractions go to zero.

Zou et al. (2002) combined the stress based and fracture mechanics approaches. A stress based criterion, this time modified Tsai-Wu (Fish and Lee, 1989), was used to determine the initiation of delamination, based on interlaminar shear stresses. The delamination growth criteria was mixed mode (modes I, II and III), based on the critical and local strain energy release rates for each mode. In common with Hou et al. (2000), it was postulated that compressive through thickness stresses retard delamination and cause the area directly under the impactor to be free from such damage.

Johnson, Kempe and Simon (2000) used their models to optimise the design of a composite wing access cover without the need for a costly test programme.

2.6 IMPACT EXPERIMENTS

There is a wealth of research on the experimental impact of composite laminates. There have been many ways of impacting employed: drop weight (e.g. Farrow et al., 2000), pendulum (e.g. Sjöblom, Hartness and Cordell, 1988) and gas gun (e.g. Wu and Springer, 1988b). There have been many geometries of impactor used: flat/blunt ended (e.g. Zhou and Davies, 1994), line nosed (e.g. Choi, Downs and Chang, 1991) and most commonly point nosed (e.g. Cantwell and Morton, 1989). Target geometries have been variously beams (e.g. Choi, Wang and Chang, 1992), rectangular (e.g. Raju, Liu and Dang, 1998) and circular (e.g. Zhou, Lloyd and McGuirk, 2001) plates, tubes/rods (e.g. Potter, Schweickhardt and Wisnom, 2000), composite lap joints (e.g. Farrow et al., 2000), sandwich panels (e.g. Kim and Jun, 1992), cylindrical shells (e.g. Lin and Lee, 1990) and curved plates (e.g. Short, 2001).

Despite this variety, it is still possible to capture some common themes:

1. Impact can be classified into three categories (as has been seen in the section on simulation and analysis of impact): low velocity, where the response can be represented as quasi-static; intermediate where the response is more dynamic with wave propagation becoming more important; and high velocity where wave propagation and vibration are dominant and boundary conditions are negligible (Sjöblom, Hartness and Cordell, 1988).
2. Initial damage is in the form of matrix cracking, typically as shear cracks at 45° to the loading direction (Choi, Downs and Chang, 1991). Delamination forms between plies with different fibre orientations and initiates from these matrix cracks, and spreads unstably, typically in a direction following the fibres of the lower ply (Wu and Springer, 1988b). Matrix cracking in the lower plies can be common, especially in slower impacts with more flexible targets, due to bending generated tension stresses. Finally with larger impact energies and forces, fibre breakage occurs (Cantwell and Morton, 1989). Other damage modes that can occur

include surface fibre micro-buckling when the contact forces are large generating significant surface compressive stresses, and fibre shear-out which is associated with final plate failure and penetration (Zhou and Davies, 1994).

3. Composite laminates will not exhibit any damage below a given impact energy: the impact damage threshold. The value of the threshold depends on many things such as the target geometry, boundary conditions, impact configuration and lay-up. Certainly the laminate lay-up can be considered an important design variable when designing impact damage resistant composite structures (Cantwell and Morton, 1989, Choi, Downs and Chang, 1991 and Schoeppner and Abrate, 2000).
4. Any pre-existing damage in the laminate prior to impact, due to manufacturing or other defects will significantly reduce the impact energy threshold. As the threshold is based on the matrix shear strength, and other damage modes such as delamination can occur freely after matrix cracking, the presence of significant residual thermal stresses or cracking due to these stresses will reduce the laminate strength (Choi, Downs and Chang, 1991).

Farrow et al. (2000), in looking at the impact of adhesively bonded composite single lap joints showed similar results to simple composite plate impact. The top adherend showed typical delaminations growing in size towards the back. In the adhesive shear cracks were evident. In the lower laminate there were more delaminations, growing in size towards the back face, starting smaller than the biggest delamination in the top laminate and growing to be larger. 50% joint strength reduction is shown after impact at the barely visible impact damage level, with delaminations fully contained in the width of the specimen. The joint failed in the laminate with a significant contribution from the offset in loading from the single lap joint configuration. The failure was in the 0^{o} ply interface nearest the adhesive in the top laminate.

Green, Morrison and Luo (2000) were interested in the more practical aspect of plates with holes or cut-outs – features that are inevitable in real engineering structures. An impact energy damage threshold was observed, which was shown to drop as holes are added to the plate. Matrix cracks were observed to form directly from the hole, away from the impact site with the delamination area under the impactor decreasing in area. When the holes are close together and the energy is sufficient to spread the delamination to the holes, the damage was seen to spread over a much wider area than would have otherwise.

2.7 THICK LAMINATES

There have not been many papers that study thick laminates for a number of reasons. Thick laminates cost more to produce so experimental programmes can be more difficult to fund. There are technical challenges in manufacturing thick laminates in addition to those normally associated with thinner laminates: larger residual stresses, escape of volatiles etc. Finally thick laminates have not seriously been considered for use in structural applications until recently, hence there has been no industrial driver.

The problem that needs to be solved is when thick laminates have through thickness stresses. The traditional analysis techniques for thin laminates usually assume a plane stress condition and hence are unable to solve for these cases. Where a laminate consists of many repeating sub-laminates the analysis can be simplified when the characteristic length of deformation is larger than the thickness of the sub laminate. The repeating lay-up is likely as lay-ups are commonly designed like this to help prevent warping due to curing stresses. Effective smeared elastic moduli for the repeating sub laminate can be evaluated and thus the whole laminate is modelled as homogenous anisotropic. The effective global stresses can be calculated, from which the lamina stresses can be recovered. This technique cannot be applied where high stress or strain gradients are present, e.g. near crack tips, so a global-local method can be employed to model the local stress field near a feature. In the local model the real properties of the laminate are retained. This method was proposed and used to give good agreement with finite element analysis when analysing delamination cracks and free edge stresses by Sun and Liao (1990).

Another approach is to use finite element analysis, however when considering a thick laminate with many layers it becomes expensive to use a single element for each ply. Hence a finite element that can represent multiple plies was proposed by Chang, Perez and Chang (1990) to analyse a thick curved composite beam under eccentric end load with reasonable correlation with experiment.

Strain gauges and Moiré interferometry can be used to determine the edge stresses in thick section composite specimens cut from thick walled cylinders (Guo, Post and Han, 1992). The Moiré technique revealed the ply shear and normal strains for in-plain and

interlaminar compression. High interlaminar normal strains and very high shear strains were measured at the free edge. Hence the free edge effects are not insignificant in thick laminates and should be considered.

2.8 SUMMARY

Impact of composites have been a subject of serious research for many years and the development of the subject has been discussed.

Despite the amount of research available there is still a large amount of uncertainty with predicting failure and damage growth. Many of the failure criteria are particular to a given material system and geometry and have limited scope outside of the parameters for which they were developed.

Most of the research has centred on thin laminates, usually no more than 3 – 4 mm thick. There is a need to understand the impact response of thicker laminates and the damage resulting from such an impact. There is also a need for research on impacts that occur near free edges, a subject that has not been covered yet.

CHAPTER 3

MATERIALS, MANUFACTURING METHODS AND PROPERTIES

3.1 INTRODUCTION

The materials used throughout this research are introduced in this Chapter. The fibre and matrix type, lay-up and laminate manufacturing method used are presented in detail. The efforts to measure lamina and laminate properties are also presented and discussed here. As with all composite manufacture residual stresses are developed during the cure of the laminates. In the thicker laminates considered here residual stress may become more significant so in the final part of this Chapter, attempts to measure the residual stress in the laminates are described.

3.2 COMPOSITE LAMINAE AND LAMINATES

3.2.1 Composites

A composite is made up of two or more distinct materials. In the case of this research a plastic resin and carbon fibres. It is the properties of the fibres that are being exploited as they have excellent strength and stiffness to weight ratios thanks to the very small amount of material defects in a fibre that is less than 10μm in diameter. The plastic resin allows load transfer between fibres and more complex fibre architectures to be used. The plastic resin can take many forms (epoxy, polyester, bismaleimide etc.) but will usually be engineered to have one or two particular properties enhanced depending on the application.

For example to aid manufacturing it may have very low viscosity at high temperature so that it can fully infiltrate and be able to bond to the fibres. To aid the mechanical properties it needs to be able to transfer load between the fibres through a strong fibre-matrix bond and good elastic shear modulus and strength and be tough to prevent crack growth.

Table 3.1 compares typical specific strength and elastic modulus and strain to failure for a selection of engineering materials relative to a plain carbon steel, including some composites. It shows that, per unit density, unidirectional glass fibre laminates although not as stiff as steel, are considerably stronger and that unidirectional carbon fibre laminates are considerably stronger and stiffer than steel, and other metals. As their strain to failure is an order of magnitude lower than that of metals, a composite structure will be more geometrically stable, though this does infer that failure is mostly brittle, and hence sudden and catastrophic.

Table 3.1 - Typical properties of a selection of engineering materials (Callister, 1997)

Material	Relative specific elastic modulus	Relative specific tensile strength	Relative strain to failure
Plain carbon steel	1.00	1.00	1.00
Titanium	0.92	1.18	2.50
Aluminium	0.97	0.96	1.10
UD Glass fibre reinforced epoxy ($V_f = 0.6$)	0.81	2.21	0.23
UD Carbon fibre reinforced epoxy ($V_f = 0.6$)	3.44	3.53	0.09

The fibres can be either short or continuous. Continuous aligned fibres offer superior structural reinforcement, whereas short randomly oriented fibre laminates are usually inexpensive and are often good enough for non-structural components, for example dinghy hulls.

A composite lamina is a single layer of fibres and resin where all the fibres are continuous and aligned in the same direction (unidirectional). It will be characterised by excellent properties in the longitudinal direction as the fibres support the load, see Figure 3.1. In the transverse directions, however, these properties are much reduced as the fibres do not provide any mechanical reinforcement and the matrix supports a high proportion of the load. In fact the transverse strength is worse than that of the matrix by itself as the stress

has to redistribute around the relatively stiff fibres creating many areas of stress concentration.

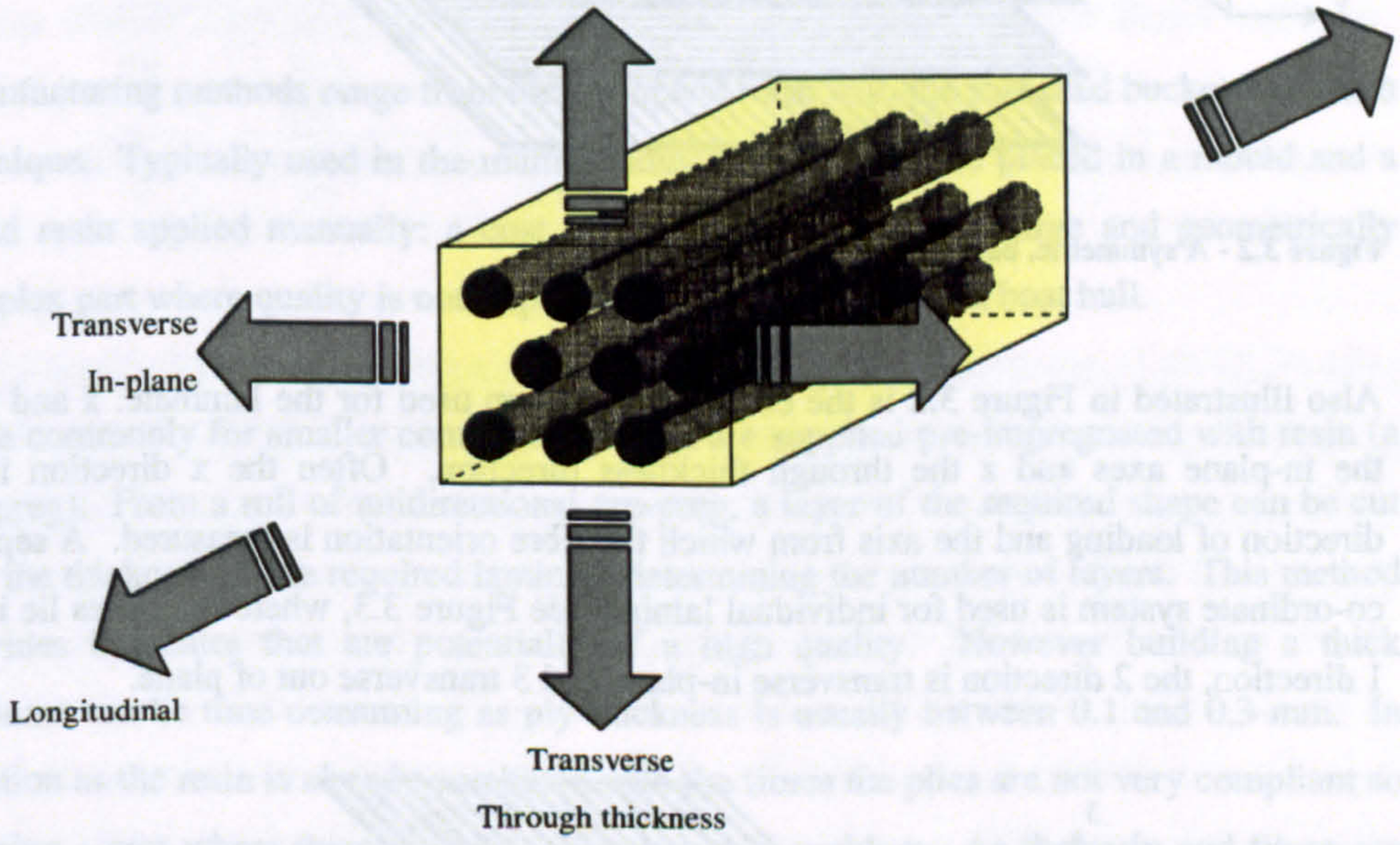

Figure 3.1- A small section of a unidirectional laminate

To provide a viable structural material a laminate is used; this is where several lamina are layered, orienting the fibres in different directions. A cross-ply laminate, one with fibres oriented at 0^{o} and 90^{o}, is illustrated in Figure 3.2. This laminate is also symmetric providing the plies are also the same thickness, as there is a plane of symmetry in the lay-up and geometry about its centre plane. As there are equal numbers of plies at 0^{o} and 90^{o} the laminate could also be termed balanced (also if there are equal numbers of $+\theta$ and $-\theta$ plies).

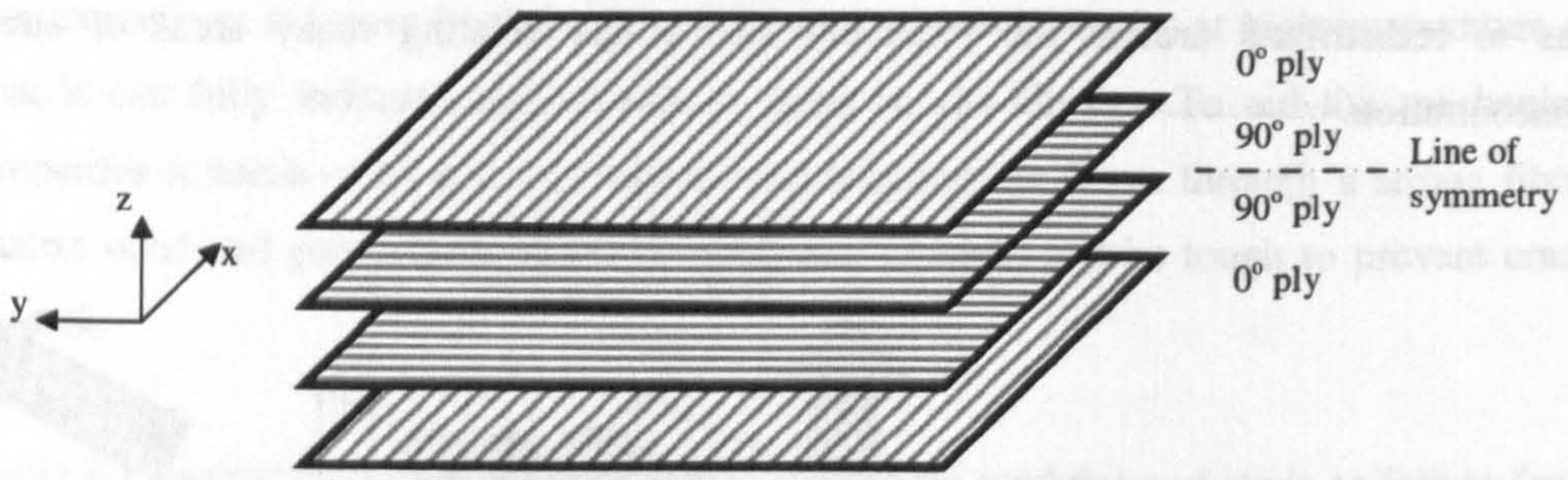

Figure 3.2 - A symmetric, balanced, cross-ply laminate

Also illustrated in Figure 3.2 is the co-ordinate system used for the laminate: x and y are the in-plane axes and z the through thickness direction. Often the x direction is the direction of loading and the axis from which the fibre orientation is measured. A separate co-ordinate system is used for individual lamina, see Figure 3.3, where the fibres lie in the 1 direction, the 2 direction is transverse in-plane and 3 transverse out of plane.

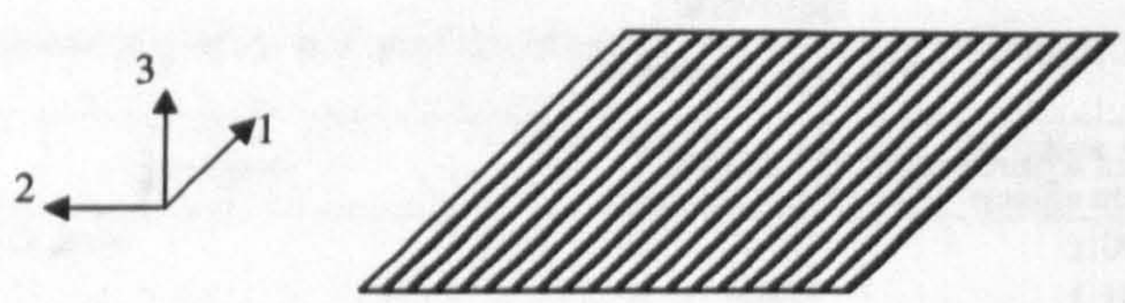

Figure 3.3 - Lamina co-ordinate system

A commonly employed lay-up is one that gives in-plane isotropic properties to the laminate. There are many lay-ups that can achieve this, but a common one will have equal numbers of plies oriented at 0°, +45°, -45° and 90° in a symmetrical lay-up termed $[0, +45, -45, 90]_s$.

3.2.2 Manufacturing Methods

There are many ways to manufacture a composite and the correct choice is important in ensuring the finished product has suitable characteristics. The main considerations are deciding the best way to combine the fibres with the resin and the geometry of the part to be manufactured, particularly its thickness and presence of any geometric complexities all at acceptable cost.

Fibres and resin both come in many forms. Resin can be liquid, or a tacky solid gel (usually in a thin sheet). The fibres can be pre-impregnated with resin, or dry. Fibres in different directions can be woven (crimped) or stitched (non-crimped) together.

Manufacturing methods range from their simplest form with the so-called bucket and brush technique. Typically used in the marine industry, dry fibres are placed in a mould and a liquid resin applied manually: a cost effective way to create a large and geometrically complex part where quality is not of paramount importance, e.g. a boat hull.

More commonly for smaller components fibres are supplied pre-impregnated with resin (a pre-preg). From a roll of unidirectional pre-preg, a layer of the required shape can be cut out; the thickness of the required laminate determining the number of layers. This method provides laminates that are potentially of a high quality. However building a thick laminate can be time consuming as ply thickness is usually between 0.1 and 0.3 mm. In addition as the resin is already combined with the fibres the plies are not very compliant so forming a part where there is double curvature is a problem. As the resin and fibres are already mixed, the fibre volume fraction cannot be changed unless additional resin only film is added.

Storage can be an issue with pre-pregs. At room temperature, epoxy, and all thermosetting resins have a shelf life of only a few days, as the resin will start to cure. If stored at -18°C (normal domestic freezer temperature) then their shelf life is extended to several years. Thus, the time allowed to prepare the laminates has a finite limit.

Alternative methods are being researched. A popular method is Vacuum Assisted Resin Transfer Moulding or VARTM. This method has the benefit of allowing the use of dry fibre blankets and hence better shape conformability and the possibility of making thick laminates. A liquid resin is pumped through this dry fibre pre-form under a vacuum bag. The technique does require specialised equipment.

A further method is Resin Film Infusion or RFI. Dry fibre blankets are interleaved with sheets of resin film and then cured in a similar way to pre-pregs. Used in conjunction with non-crimped fabrics (NCFs) this method has many advantages. A single sheet of NCF can

be relatively thick with several layers stitched together (with a non-structural polyester thread) thus reducing the total number of layers needed to make a thick laminate. A further benefit of NCFs over woven fabrics is that there is no degradation of in-plane properties associated with the crimp (although it is still not as good as UD pre-preg), and any fibre angles can be incorporated. Also, compared with pre-pregs, freezer space is conserved as only the resin is stored (although not the case with two part epoxies); the manufacturer has control over fibre volume fraction; and more complex shapes can be formed.

Use of NCFs is not without its drawbacks. Cutting a thick carbon fibre blanket to an accurate shape can be difficult and the sharpness of the cutting tool is important. Also the cutting of dry fibre blankets has health and safety issues with the potential of releasing many tiny fibre fragments into the air hence the correct personal protective equipment should be used (for example coveralls, goggles and air filter face mask). Because the resin is not already mixed with the fibres, it is introduced by interleaving the layers of NCF with layers of resin. With pre-pregs the resin is already infused throughout the fibres and during the cure cycle the resin from each layer only has to mix with that from its neighbours, not necessarily penetrating any fibre layers. With NCFs, however, the resin has to infuse throughout the fibres and bond the fibre layers together. This means long dwell times at high temperatures during the cure and the necessity for the resin to have a low viscosity at cure temperature compared to resins used, for example, in pre-pregs.

3.2.3 Materials Used

Throughout this project four different types of non-crimped fabric were used: two three layer types and two single layer types, all with the same fibre. The fabrics were supplied by Airbus, and the source of the fabrics cannot be divulged due to legal reasons. The orientation of the layers and the proportion of fibres in each layer define which type they are. Table 3.2 shows the definitions of the four NCF types used.

Table 3.2 - NCF type definitions

Type	Layer Orientation	Layer Areal Weight (g/m^2)	Total Areal Weight (g/m^2)	Nominal Thickness (V_f = 0.6) (mm)
2A	+45°	267.5	642	0.6
	90°	107		
	-45°	267.5		
2B	-45°	267.5	642	0.6
	90°	107		
	+45°	267.5		
6	0°	642	642	0.6
7	0°	321	321	0.3

All the types of NCF feature stitching to keep the fibres together, a white polyester thread being used for that reason. Figure 3.4 shows the photographs of type 2A and 7 with the polyester stitch clearly visible. Type 2B is identical to 2A except for the orientation of the top and bottom layers to allow for symmetric laminates and types 6 and 7 are identical except for their weight per unit area (areal weight).

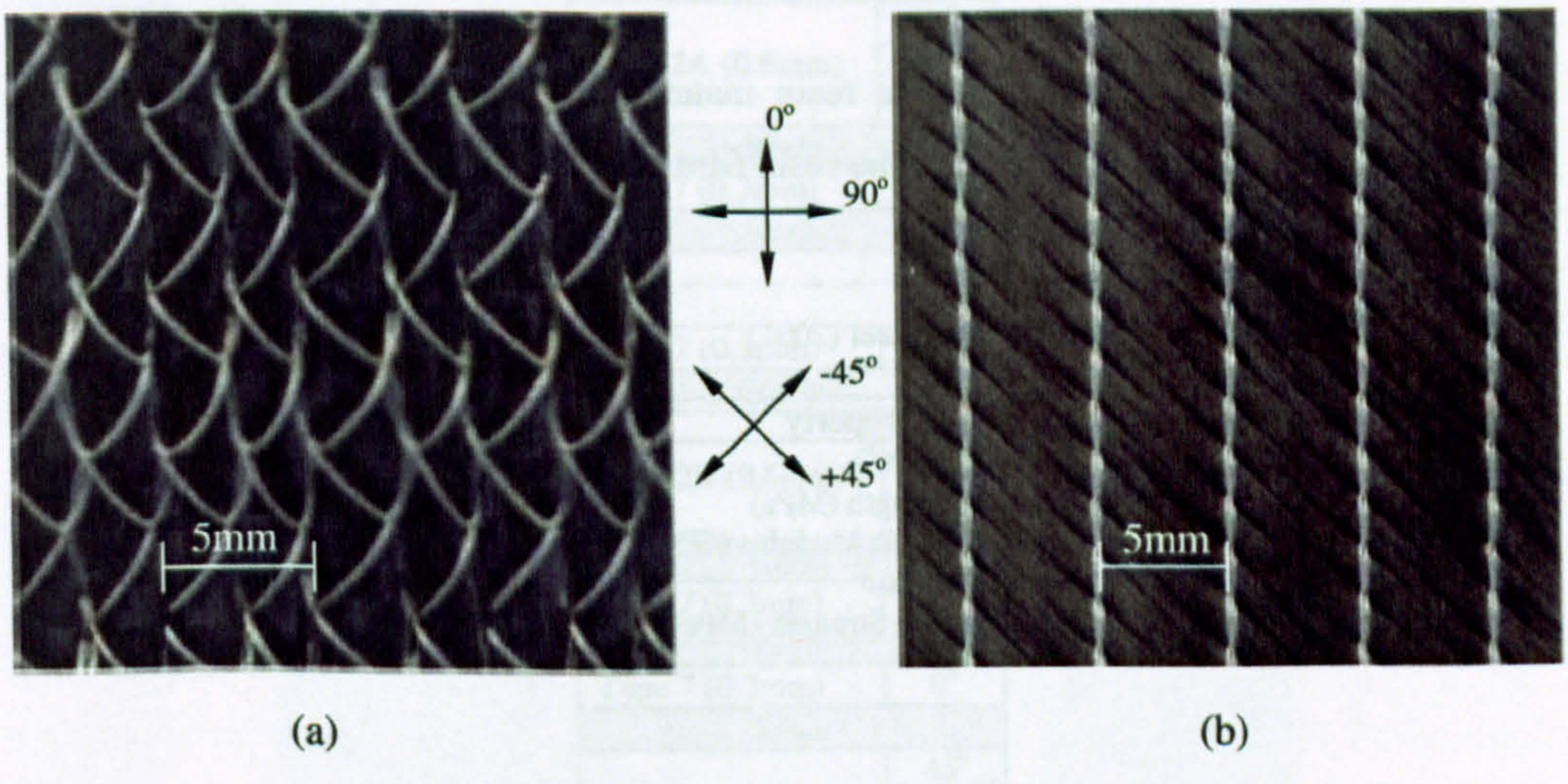

Figure 3.4 - Type (a) 7 and (b) 2A NCF supplied for the project. White polyester stitching clearly visible

The fibres, designated HTS 5131, in the NCFs are defined as high strength fibre with a standard elastic modulus, good for most applications with good processability and

excellent spreadability performance. The fibre properties are given in Table 3.3 with a comparison to a plain carbon steel.

Table 3.3 - HTS 5131 fibre properties, Tenax (unknown)

Property	HTS 5131 Fibre	Plain Carbon Steel
Density (kg/m^3)	1770	7850
Tensile Strength (MPa)	4300	<1700
Tensile Elastic Modulus (GPa)	238	207
Strain to Failure (%)	1.5	20

As can be seen from Table 3.3 the properties of pure carbon fibre compared to plain carbon steel show potential with a density 4.5 times smaller, a strength up to 2.5 times bigger and a comparable stiffness. Unfortunately fibres have to be combined with a plastic resin to form a useful structural material, and that resin usually has very low strength and elastic modulus. As already mentioned, the fibres have a very small strain to failure compared to steel; the steel will exhibit significant plastic deformation before failure whereas the fibres will not. This has its advantages and disadvantages: it means that the fibrous component will be more geometrically stable but will give little warning to impending failure.

Table 3.4 shows the properties of the resin material used in this project, Hexply M36 epoxy film resin. The areal weight of the resin film used for this research was 175 g/m^2.

Table 3.4 - M36 resin material properties, Hexcel (2001)

Property	Value
Density (kg/m^3)	1170
Tensile Strength (MPa)	81
Tensile Elastic Modulus (GPa)	3.5
Poisson's Ratio	0.42
Compressive Strength (MPa)	146

It is the proportion of resin to fibres that will determine how much of the fibres' properties are retained in the final material (at least in the longitudinal direction). Designing for a fibre volume fraction V_f of 60% is common.

3.3 LAMINATE MANUFACTURE

All laminates for this research have been manufactured using the RFI process with NCF blankets. Here the laminate lay-up is discussed and the manufacturing method presented in detail.

3.3.1 Lay-up

Using the NCF blankets defined in Table 3.2 a laminate block with a nominal cured thickness of 4.2mm was defined. As the block was symmetric it could be repeated two or three times to produce laminates with approximate thicknesses of 4, 8 and 12mm. Figure 3.5 shows the lay-up block used, showing that resin is inserted between every fibre layer thus giving it the smallest possible distance to travel.

Type 2B (0.6mm)	-45°
	90°
	45°
Resin	
Type 7 (0.3mm)	0°
Resin	
Type 7 (0.3mm)	0°
Resin	
Type 2A (0.6mm)	45°
	90°
	-45°
Resin	
Type 7 (0.3mm)	0°
Resin	

Symmetry

Type 7 (0.3mm)	0°
Resin	
Type 2B (0.6mm)	-45°
	90°
	45°
Resin	
Type 7 (0.3mm)	0°
Resin	
Type 7 (0.3mm)	0°
Resin	
Type 2A (0.6mm)	45°
	90°
	-45°

Figure 3.5 - Lay-up used in specimen manufacture showing ply angle

Thus, this lay-up creates the laminate lay-ups shown in Table 3.5, where there was always a -45 degree layer at each outer surface.

Table 3.5 - Laminate lay-ups used

Nominal Laminate Thickness (mm)	Laminate Lay-up
4.2	$(45/90/-45/0_2/-45/90/45/0)s$
8.4	$((45/90/-45/0_2/-45/90/45/0)s)_2$
12.6	$((45/90/-45/0_2/-45/90/45/0)s)_3$

Initially type 7 UD NCF was used in the laminates as the 0° reinforcement. Part of the way through the project it was substituted for type 6 UD NCF. The reason for this was ease of manufacture, as type 6 is twice as thick as type 7, and material availability. In the lay-up detailed above the type 7 layers are in pairs so simply replacing these with a single layer of type 6 was all that was required. Tests described later in the section show that there is little mechanical difference from changing the UD fabrics.

Other methods of inserting the resin were investigated, such as placing all of the resin together underneath the fibre layers and having the resin at fewer positions in the lay-up, but these methods were found to give poorer quality laminates, e.g. laminates with patches of low resin content. At each fibre layer interface, often more than one sheet of resin was inserted; the total number of sheets determined by the desired volume fraction.

The exact amount of resin (N number of layers) that needs to be inserted to achieve a given fibre volume fraction (V_f) can be easily calculated using equation 3.1, knowing the density of the fibres (ρ_f) and resin (ρ_r), and their total areal weights (m_f and m_r).

$$N = \frac{m_f \rho_r}{m_r \rho_f}\left(\frac{1}{V_f} - 1\right) \tag{3.1}$$

Usually this amount has to be increased slightly to take into account some resin bleed off.

Once cured, the actual volume fraction can be calculated using equation 3.2 once the mass (M) and in-plane dimensions (area A) of the laminate are known.

$$V_f = \frac{Am_f}{Am_f + \frac{\rho_f}{\rho_r}(M - Am_f)} \tag{3.2}$$

This method has been found to be extremely reliable in producing laminates with fibre volume fractions very close to the design value. Typically the variation is no more than 0.5% in 55% V_f. The V_f was never measured, however the same proportion of resin to fibres was used during the manufacture of the laminates so that the V_f was consistent. Void content was never measured, although voids were never found during the extensive ultrasonic C-scanning of the laminates, or the few micrographs taken of laminate sections. The effect of the stiching fibre is unknown. The proportion of stitching fibre to resin is unknown, but thought to be small.

3.3.2 Manufacturing Method

The resin film infusion method involves creating a lay-up where dry fibre blankets of NCF are alternately layered with sheets of resin film. This lay-up is then autoclave cured under vacuum. What follows is a detailed explanation of the manufacturing process.

Using a template to cut around, all the required sheets of fibre need to be cut from the rolls of NCF, see Figure 3.6. It is essential to use an extremely sharp knife, otherwise the fibres are dragged along with the cut, hence the fibres' and the cut's straightness is lost. Pushing down on the template helps to grip the blanket thus ensuring a good cut.

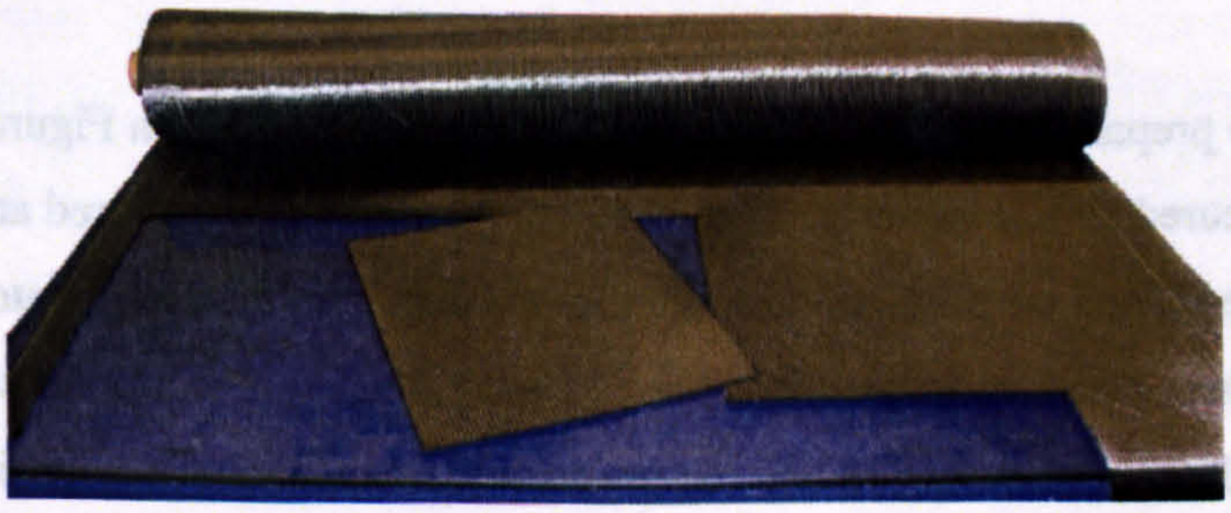

Figure 3.6 - Cutting a fibre layer from a roll of NCF

The same was performed for the resin, though a template was not used; instead the shape required was approximately measured and cut out. The resin was removed from the

freezer at least five hours before cutting to ensure that it had thawed. It was not removed from its plastic bag until thawed to prevent any condensation forming on the resin. Once finished it was replaced into the plastic bag and the freezer, noting the total time that it had been removed from the freezer.

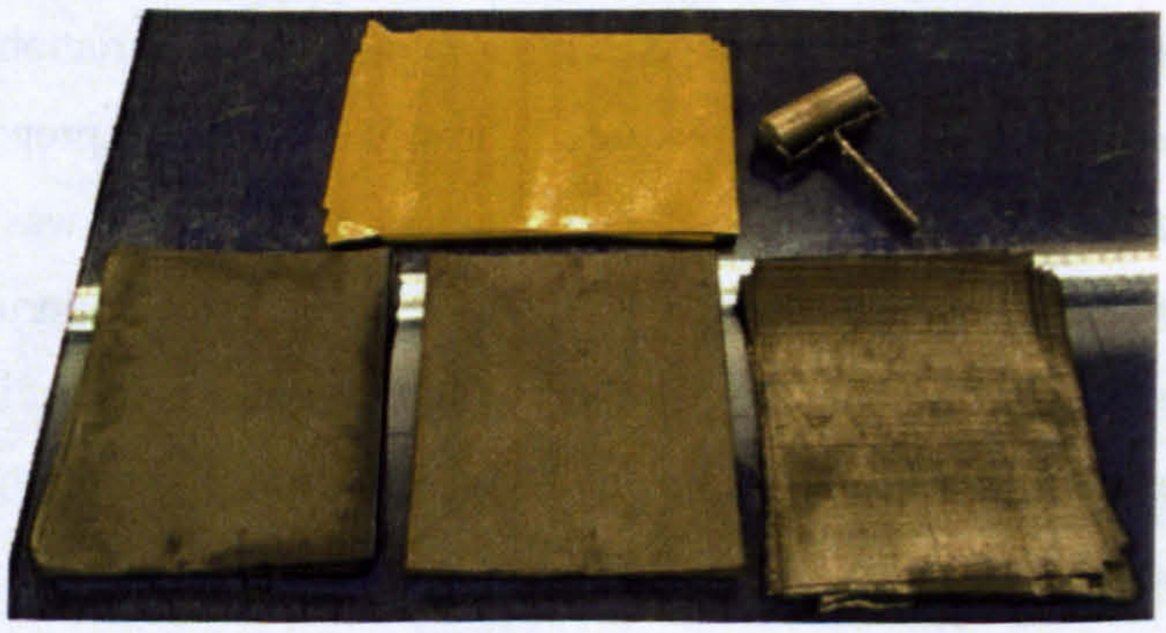

Figure 3.7 - Fibre and resin sheets ready for laying up

Figure 3.7 shows the squares of NCF (three types, 2A, 2B and 7, see Table 3.2) and resin (on its yellow backing paper). In the top right of the figure is a metal roller that was important during lay-up: to ensure that the resin has adhered to the NCF square to enable easy removal of the backing paper pressure was applied.

As previously mentioned the lay-up involves carefully placing the fibre layers in the order prescribed interspersed with at least one sheet of resin. A length of L-section aluminium was clamped to the table to provide a straight edge to position reliably the NCF. Once all the layers had been positioned the next step was to prepare the laminate for the autoclave.

The process to prepare the laminate for the autoclave is illustrated in Figure 3.8 where two laminates are cured simultaneously: more than one laminate can be cured at once. First the laminates were placed on a flat smooth aluminium plate (the tool) separated by a sheet of release film, then a cork resin dam was erected around the full perimeter of the laminates. Next another sheet of release film and the pressure plates are carefully positioned. For the pressure plates 5mm thick aluminium was used as this gave a good balance between imposing a flat smooth surface and thermal conductivity. Then a layer of breather material was placed on top and the breach valve feet positioned. The breach valves pierce the vacuum bag and allow the removal of air via a non-return valve and a vacuum pump.

Finally strips of tacky tape were laid, noting the importance of "shark's fins": additional flaps of tacky tape that are used to ensure the vacuum bag is loose over the laminates when fitted so that on application of the vacuum it can conform to the shape of the laminates and hence provide a uniform pressure. Figure 3.9 shows a sketch of a section view of a laminate prior to being cured.

(a) Place laminates onto lay-up tool on a sheet of release film.

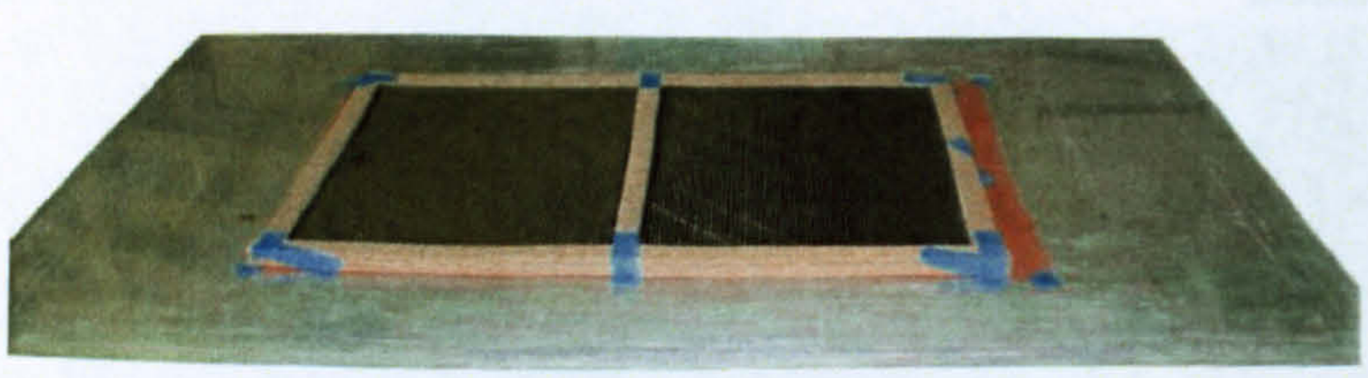

(b) Place cork resin dam around the laminates.

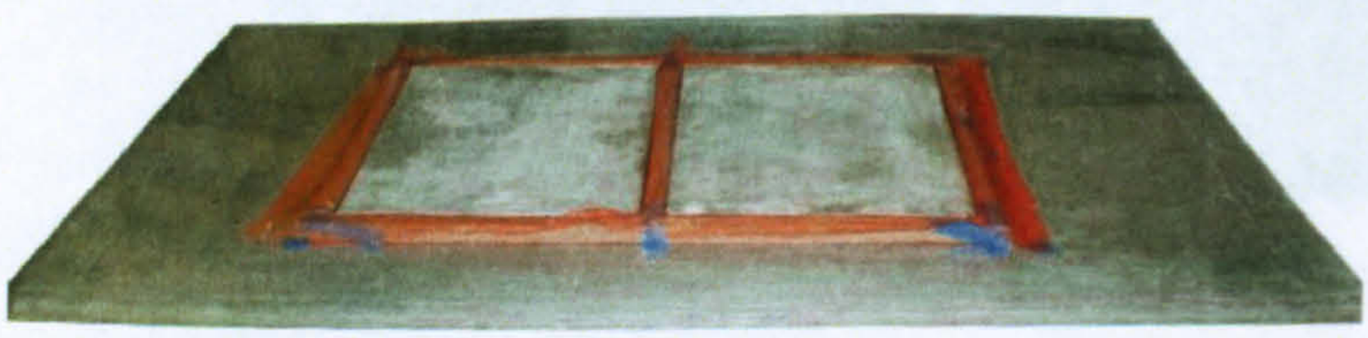

(c) Place on top another sheet of release film and the pressure plates.

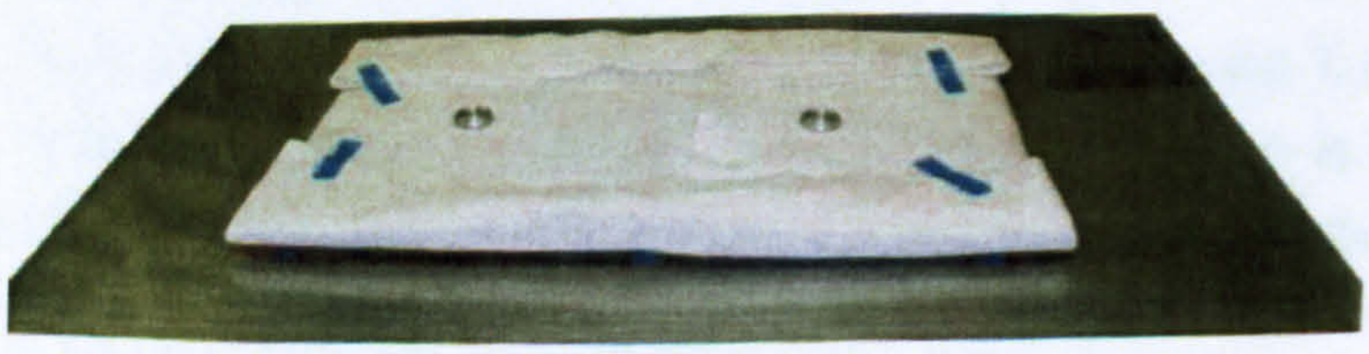

(d) Place breather cloth on top and the feet to the breach valves.

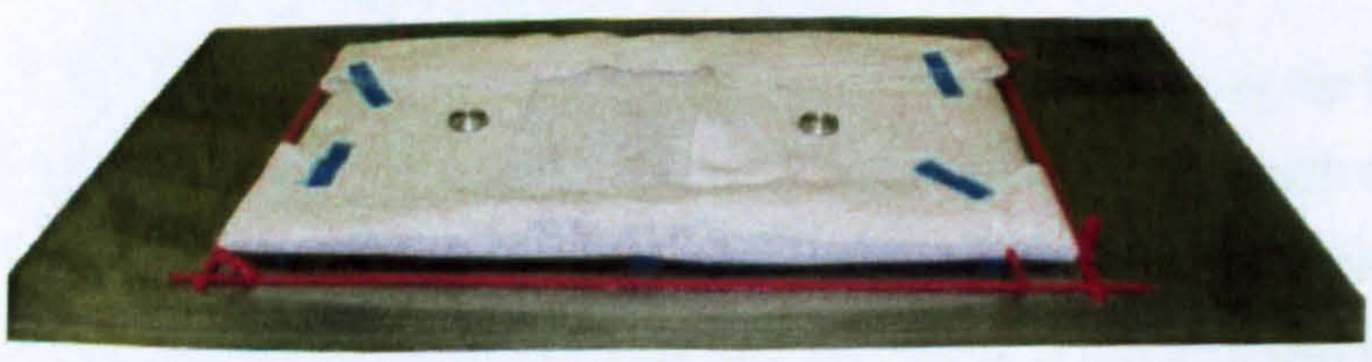

(e) Put a strip of tacky tape around the outside, remembering "shark's fins".

(f) Fit vacuum bag and the breach valves.

Figure 3.8 - Six stages of laying up a pair of laminate

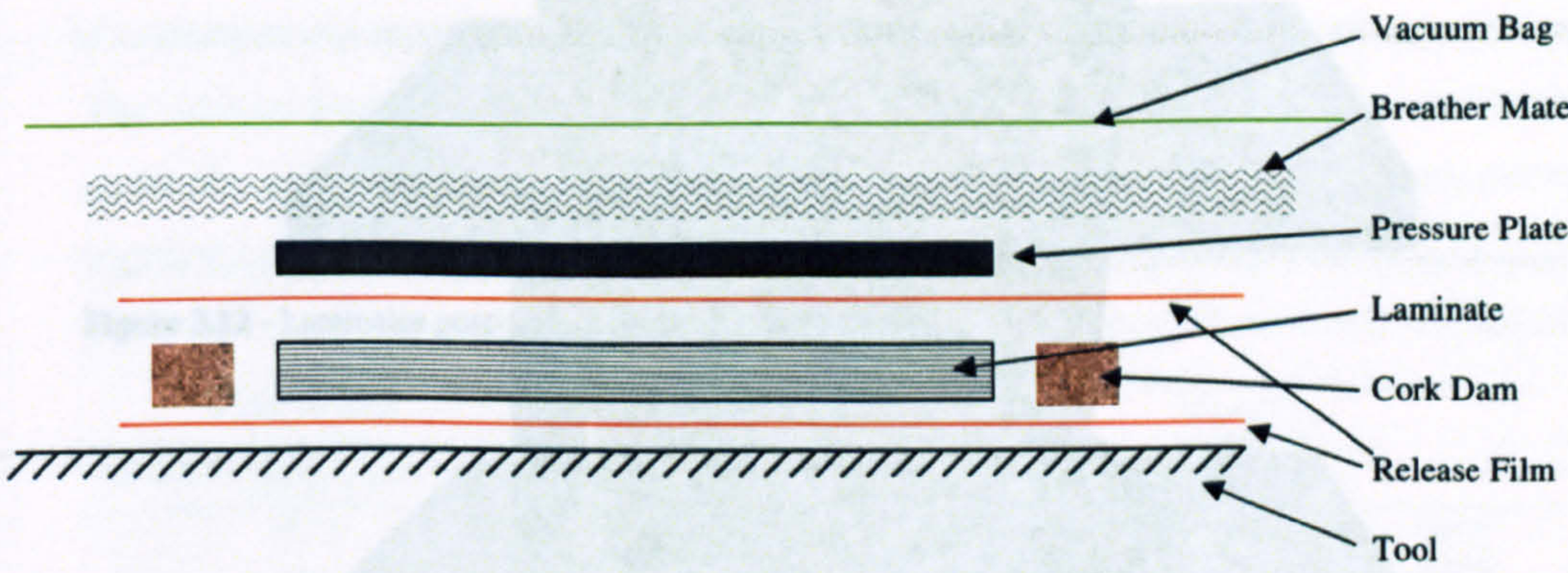

Figure 3.9 - Section view of laminate prior to curing

The next step was to apply the vacuum and check the quality of the seal between the vacuum bag and tacky tape, see Figure 3.10. Thermocouples are attached to the laminates in order to monitor their temperature during the cure. A special trolley was devised to support the laminates in the autoclave. The autoclave was an LBBC (Leeds and Bradford Boiler Company) Ltd Quicklock Thermoclave, with 1 m diameter, 1.5 m working length, maximum temperature of 250°C and maximum pressure of 690 kPa with Eurotherm 903P controllers. The trolley could roll into the centre of the autoclave and supported the tool so that it could be at the widest part. This trolley sat on a second trolley that enabled it to be positioned in front of the autoclave.

The autoclave maintained the vacuum and applied an external pressure and temperature variation following the pattern in Figure 3.11. Characteristic of this cure schedule are the long dwell times that enable the resin to permeate the fibres. Although the curves in the figure are idealised the measured pressure and temperature profiles match these curves closely. Thermal lag was measured and was minimal, dwell times at the correct temperature were maintained.

Figure 3.10 - Laminates with vacuum applied ready to enter autoclave

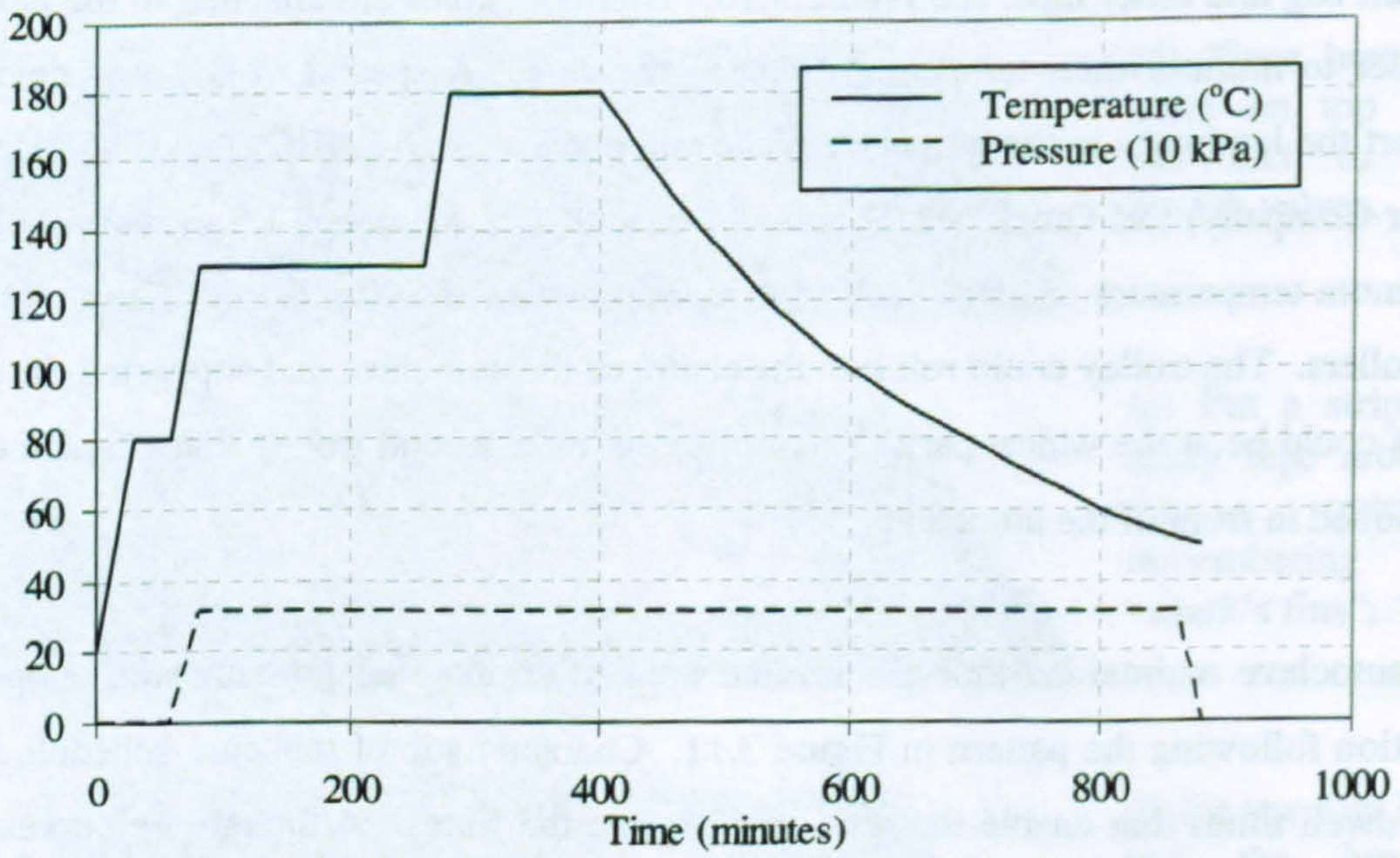

Figure 3.11 - Cure temperature and pressure profile

Once the laminates have cooled to approximately 50°C they are removed from the autoclave, see Figure 3.12, and the various vacuum bag, release films and breather layers can be removed, see Figure 3.13. During the cure the laminates reduce in thickness by up to 5 mm and consequently the release film is torn in some areas to fit around the edges of the pressure plate. These tears allow small amounts of resin to escape and soak into the breather layer, some such patches are visible in Figure 3.12.

Figure 3.12 - Laminates post-cure showing some resin bleed

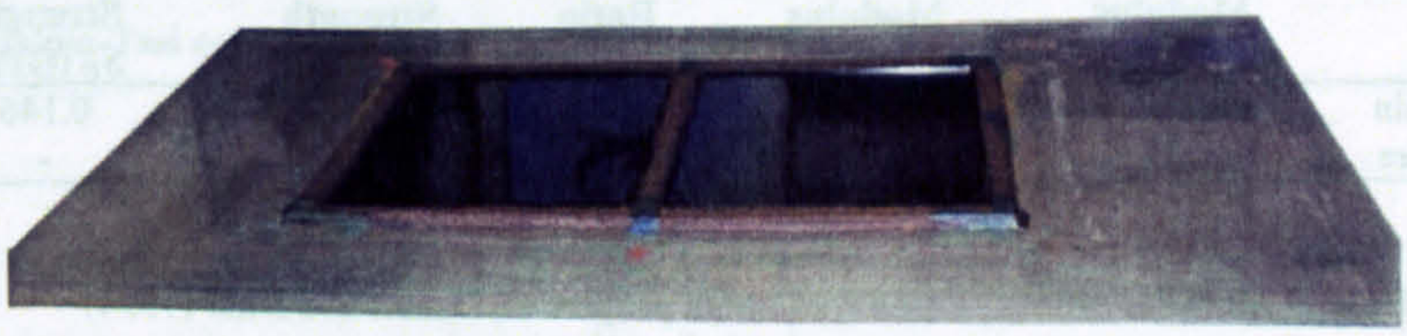

Figure 3.13 - Newly cured laminates

The final process was to trim off the cork resin dam, and cut the desired size of laminate from the cured plates. A commercially available wet cut circular diamond saw was used to perform this task, wasting approximately 25mm of laminate around each plate. The cutting datum was the white stitching still visible after the curing process, and running in the 0^{o} direction.

3.4 LAMINA AND LAMINATE PROPERTIES

It is essential to characterise properly the materials in use in this research. This will enable accurate modelling and benchmarking of tests. The material properties for single UD lamina have been measured, and then used to calculate the properties of the laminates. In addition type 7 and 6 UD NCFs are compared. Firstly however, the lamina properties are calculated using standard formulae to predict the elastic moduli and strengths.

3.4.1 Calculation of Lamina Properties

In this section two methods are used to estimate the lamina properties from the raw fibre and matrix properties: the Rule of Mixtures and the Halpin-Tsai equations.

The fibre and matrix material properties are presented in Table 3.6, taken from their respective manufacturers' data sheets: Hexcel (2001) and Tenax (unknown). The

manufacturer did not provide the properties marked with an asterisk: they were approximated by scaling values found in the literature. Using the appropriate estimates the lamina properties can be predicted, see Table 3.7.

Table 3.6 - Resin and fibre manufacturers' quoted properties (* values not provided and scaled from values found in literature)

	Young's Modulus E (GPa)	Elastic Shear Modulus G (GPa)	Poisson's Ratio ν	Tensile Strength S_T (GPa)	Compressive Strength S_C (GPa)
Resin	3.5	1.23	0.42	0.081	0.146
Fibre	238	27 *	0.15 *	4.3	-

Table 3.7 – Rule of Mixtures estimates used for lamina properties, Daniel and Ishai (1994)

Lamina Property	Estimate	Equation
E_1	Voigt: matrix and fibres have same strain	$E_1=E_fV_f+E_m(1-V_f)$
E_2	Reuss: matrix and fibres have same stress	$E_2 = \frac{E_f E_m}{E_m V_f + E_f(1-V_f)}$
ν_{12}	Voigt	$\nu_{12}=\nu_fV_f+\nu_m(1-V_f)$
G_{12}	Matrix and fibres have same shear stress	$\frac{1}{G_{12}} = \frac{V_f}{G_f} + \frac{1-V_f}{G_m}$

The results for this analysis are presented in Table 3.8. In addition the strength of the lamina can be predicted. Using the Voigt estimate and using the strength and elastic modulus values quoted in Table 3.6, failure strains can be calculated for the matrix and fibres. Assuming the lamina fails when the fibres fail, the lamina stress at the fibre failure strain is its strength. These strength predictions are also given in Table 3.8. The fibre failure strain is 0.018, and 0.023 for the matrix.

Table 3.8 - Lamina properties calculated using the Rule of Mixtures

V_f (%)	E_1 (GPa)	E_2 (GPa)	ν_{12}	G_{12} (GPa)	S_T (GPa)
50	121	6.90	0.285	2.35	2.19
51	123	7.04	0.282	2.40	2.22
52	125	7.18	0.280	2.44	2.26
53	128	7.33	0.277	2.49	2.31
54	130	7.48	0.274	2.54	2.35
55	132	7.64	0.272	2.59	2.39
56	135	7.81	0.269	2.64	2.44
57	137	7.98	0.266	2.70	2.48
58	140	8.17	0.263	2.76	2.53
59	142	8.36	0.261	2.82	2.57
60	144	8.56	0.258	2.88	2.60

The Halpin-Tsai equations are based on more rigorous mathematical modelling and generally give more accurate values of E_2 and G_{12}. In addition to the constituents' properties, the equations rely on an empirical constant dependent on the packing and the particular material system: ξ, or the reinforcement factor. Table 3.9 details the equations.

Table 3.9 - Halpin-Tsai equations, Daniel and Ishai (1994)

Property	Equation	ξ value
E_2	$\frac{(1+\xi\eta V_f)}{(1-\eta V_f)}E_m$	2
G_{12}	$\frac{(1+\xi\eta V_f)}{(1-\eta V_f)}G_m$	1

Accurate values for ξ have not been calculated. The values used, shown in Table 3.9, are typical. η is a function of the elastic modulus ratio (relevant fibre elastic modulus divided by the relevant matrix elastic modulus), R, and is given in equation 3.3. The results are shown in Table 3.10.

$$\eta = \frac{R-1}{R+\xi} \tag{3.3}$$

Table 3.10 - Lamina properties calculated using the Halpin-Tsai equations

V_f (%)	E_2 (GPa)	G_{12} (GPa)
50	13.1	3.30
51	13.5	3.37
52	13.9	3.45
53	14.3	3.54
54	14.7	3.62
55	15.2	3.71
56	15.6	3.80
57	16.1	3.90
58	16.6	4.00
59	17.1	4.10
60	17.7	4.21

These results show that Halpin-Tsai method tends to predict values of E_2 and G_{12} that are greater than those using the Rule of Mixtures. As the multi-directional laminates are

manufactured to have a volume fraction of 55%, we now know what the lamina properties at best can be expected to approach.

3.4.2 *Experimental Measurement of UD Laminate Properties*

Specimens were designed to follow the CRAG specification of Curtis (1985), and the dimensions are shown in Figure 3.14. Although more modern specifications exist, the most experience within the Department was with CRAG. Chamfered aluminium end tabs were bonded to the specimens using a two part structural adhesive. Although fiddly to apply aluminium end tabs individually, this was the cheaper option compared to using glass fibre tabs. Using a simple weight analysis (knowing the weight and in-plane dimensions of the specimens, the areal weight of the NCF, and the fibre and resin density) the volume fraction was estimated. Using three layers of type 7 NCF, specimens with a volume fraction of 50% were manufactured, lower than the 55% volume fraction for the multi-directional laminates.

The results of these tests are shown in Table 3.11. These tests were carried out on a Zwick 100 kN ball screw driven test machine, with some strain gauging to allow accurate measurement of the elastic modulus.

Table 3.11 - Experimentally measured unidirectional laminate properties

Tensile Strength S_T (GPa)	Elastic Modulus E_1 (GPa)	Poisson's Ratio ν_{12}
1.46	100	0.41

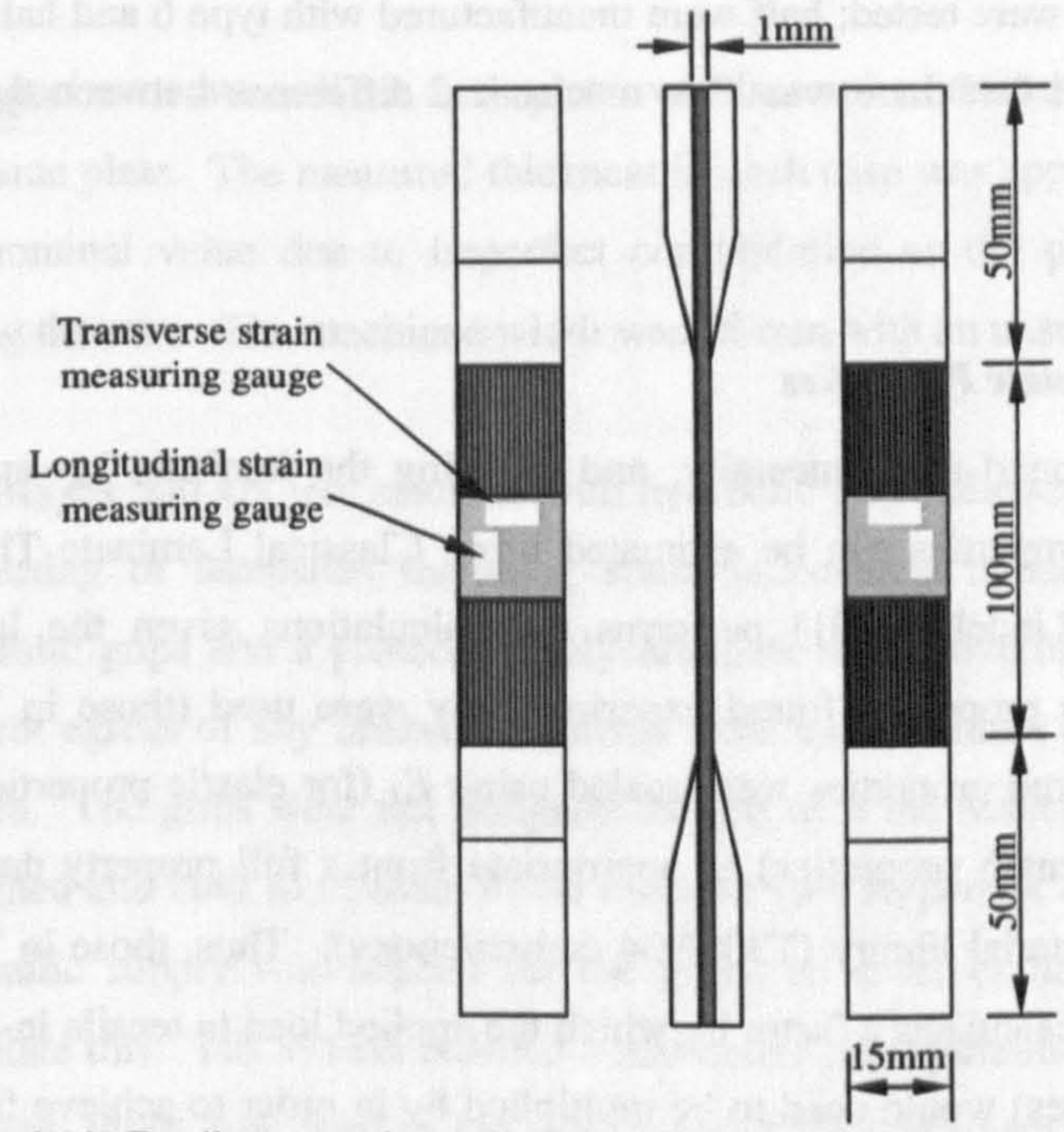

Figure 3.14 - Tensile test specimen dimensions

Comparison of these values to those calculated in section 3.4.1 shows that the manufactured specimens have not achieved the full potential indicated by their constituents. This is to be expected for a number of reasons. Firstly, the fibres are not perfectly straight; this will contribute to the apparently degraded value of elastic modulus. In fact this is a feature of NCFs in that by stitching the fibres together to form the fabric, the penetration of the fibre layer by the polyester thread induces some fibre waviness. Also, although care is taken to achieve fibre layer alignment during manufacture, there will inevitably be some misalignment and this will further contribute to the reduced elastic modulus. The strength is lower than the predicted value and this most likely due to the stitching; it acts to create pockets of resin-rich areas. These areas are likely to start cracking at a load lower than the specimen strength. Once these cracks have grown to a critical size the specimen will fail at a lower, effective, strength.

There was a need to verify the assumption that there is no mechanical difference between using one layer of type 6 NCF instead of two layers of type 7. They are identical, except for their areal weights and thickness, where type 6 is twice that of type 7. A programme of testing was undertaken whereby specimens 0.6 mm and 1.2 mm thick, of the same

geometry as in Figure 3.14, were tested; half were manufactured with type 6 and half with type 7. The results showed that there was little mechanical difference between the two NCFs (Vasudevan, 2004).

3.4.3 Calculation of Laminate Properties

Using the lamina values found experimentally, and knowing the laminate lay-up (see Figure 3.5), the laminate properties can be estimated using Classical Laminate Theory. The software Laminator (Lindell, 2001) performs the calculations given the lamina properties and lay-up. The properties found experimentally were used (those in Table 3.11). The remaining required properties were scaled using E_1 (for elastic properties) or the tensile strength (for strength properties) as appropriate from a full property data set available in Laminator's material library (T300/934 carbon/epoxy). Thus, those in Table 3.12 were used. Laminator calculates a factor by which the applied load (a tensile in-plane load aligned with the 0° fibres) would need to be multiplied by in order to achieve failure in that ply. The failure stresses quoted in Table 3.13 are obtained by calculating that failure load and dividing by the net cross-sectional area; the load is applied in units of force per unit width, so the results only need to be divided by the laminate total thickness. Table 3.13 also shows the laminate apparent elastic moduli.

Table 3.12 - Lamina properties used in the laminate property prediction

E_1 (GPa)	E_2 (GPa)	G_{12} (GPa)	ν_{12}	X_t (GPa)	Y_t (MPa)	S (MPa)
100	6.523	3.075	0.41	1.46	47.4	53.5

Table 3.13 - Predicted laminate properties using Laminator (x = 1 direction etc.)

E_x (GPa)	E_y (GPa)	G_{xy} (GPa)	ν_{xy}	90° Ply Failure Stress (MPa)	0° Ply Failure Stress (MPa)	±45° Ply Failure Stress (MPa)
52.3	24.3	13.8	0.49	470	765	610

3.4.4 Experimental Measurement of Laminate Properties

The strength and approximate elastic modulus of the laminates were measured using specimens cut from undamaged sections of laminate. Three each were tested in tension and compression to obtain baseline measurements from which to compare subsequent impact damaged laminate strength.

The specimens were all cut from plates with a nominal thickness of 8.4 mm, each set from the same plate. The measured thickness in each case was approximately 9 mm, more than the nominal value due to imperfect consolidation as the pressure plate bends slightly during the cure. The machined width was 25 mm with an unsupported length of 150 mm.

The Mayes 500 kN test machine with hydraulic grips, shown in Figure 3.15, was used in all testing of laminates including static indentation impact simulation tests. It has hydraulic grips and a protective polycarbonate sheet covering the grips and specimen to prevent egress of any broken fragments from the specimen during testing and especially failure. The grips were not designed for use with the Mayes so four steel adapters were designed and built to fit them to the machine (see Appendix A). In addition a pressurised hydraulic supply was needed for the grips, so a set of hand-pumps were installed to facilitate this. The system enabled a maximum grip hydraulic pressure of 21 MPa. A flat, serrated, insert was used in the grips to hold the specimens which were not end-tabbed. Alignment of the specimen in every case was ensured by careful placement and measuring of the position of the specimen.

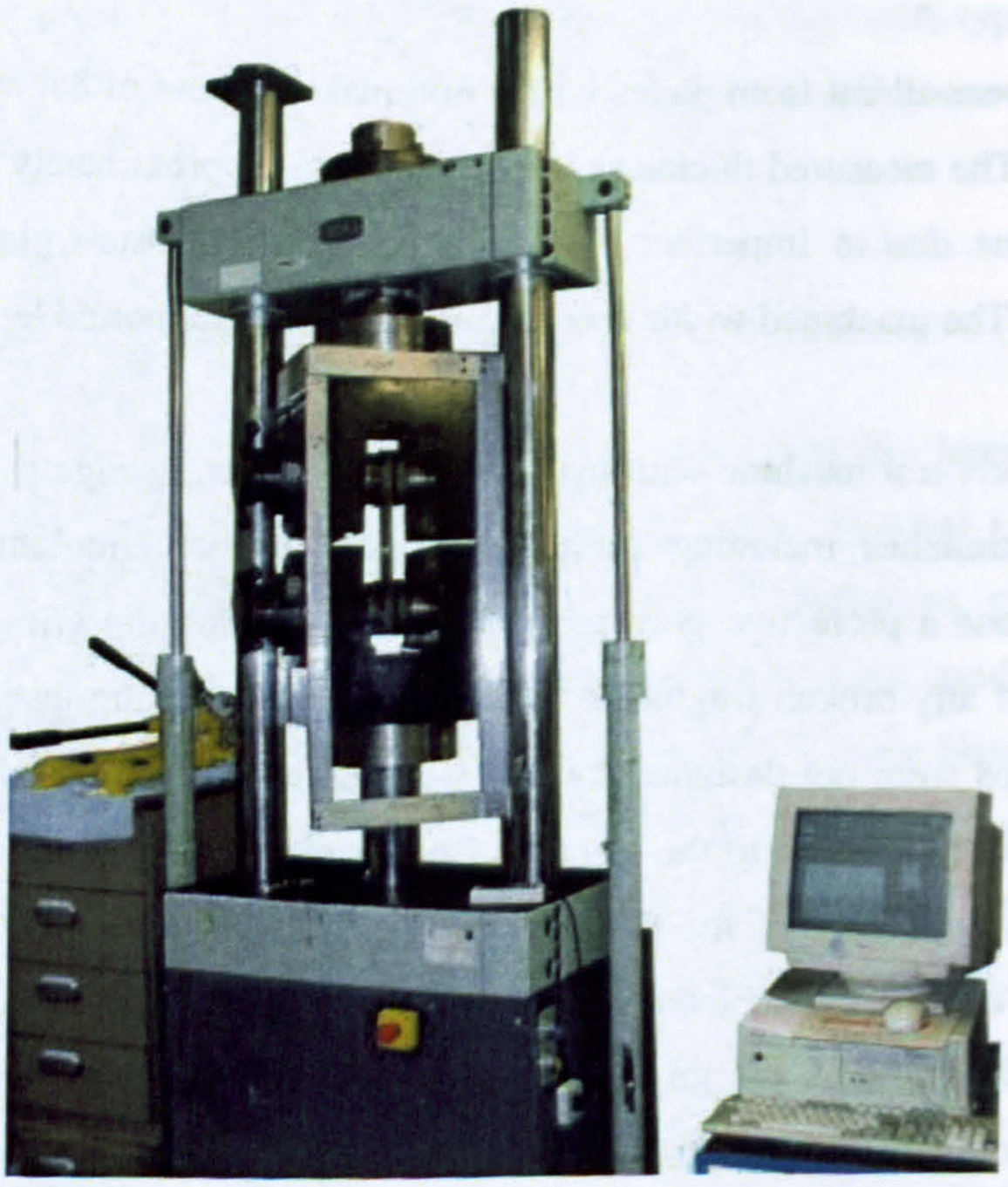

Figure 3.15 - Mayes 500 kN hydraulic testing machine

The machine was used in displacement control mode, with a desktop personal computer recording crosshead displacement and load cell readings for subsequent analysis. Figure 3.16 and Figure 3.17 show the results from the six specimen tests. Table 3.14 summarises the results.

Table 3.14 - Undamaged tension and compression results

Specimen	Width (mm)	Thickness (mm)	Strength (MPa)	Strain to Failure	Elastic Modulus (GPa)
			Tension		
1	25.36	9.13	922	0.029	40.1
2	27.22	9.08	978	0.034	40.5
3	26.48	8.94	977	0.034	38.2
Average	26.35	9.05	959	0.032	39.6
			Compression		
1	25.59	8.99	386	0.014	38.4
2	26.97	8.95	338	0.011	44.3
3	26.61	8.85	343	0.011	41.9
Average	26.39	8.93	356	0.012	41.5

The results show good agreement between each test. The stress-strain (strain calculated using crosshead displacement) curves are not perfectly linear, and this is due to some slippage in the grips from the serrated inserts damaging the top surface of the laminate. However this is not a problem as failure occurred across the gauge length in each case, most likely due to the compressive gripping force preventing damage initiation. Whilst it is not best practice to use crosshead displacements for strain measurement, the purpose of the experiments was to measure strength. The elastic moduli calculated are merely illustrative, as being based on the crosshead displacement they are inaccurate. The initial part of each stress-strain curve is used for this calculation, typically up to a strain level of 0.002.

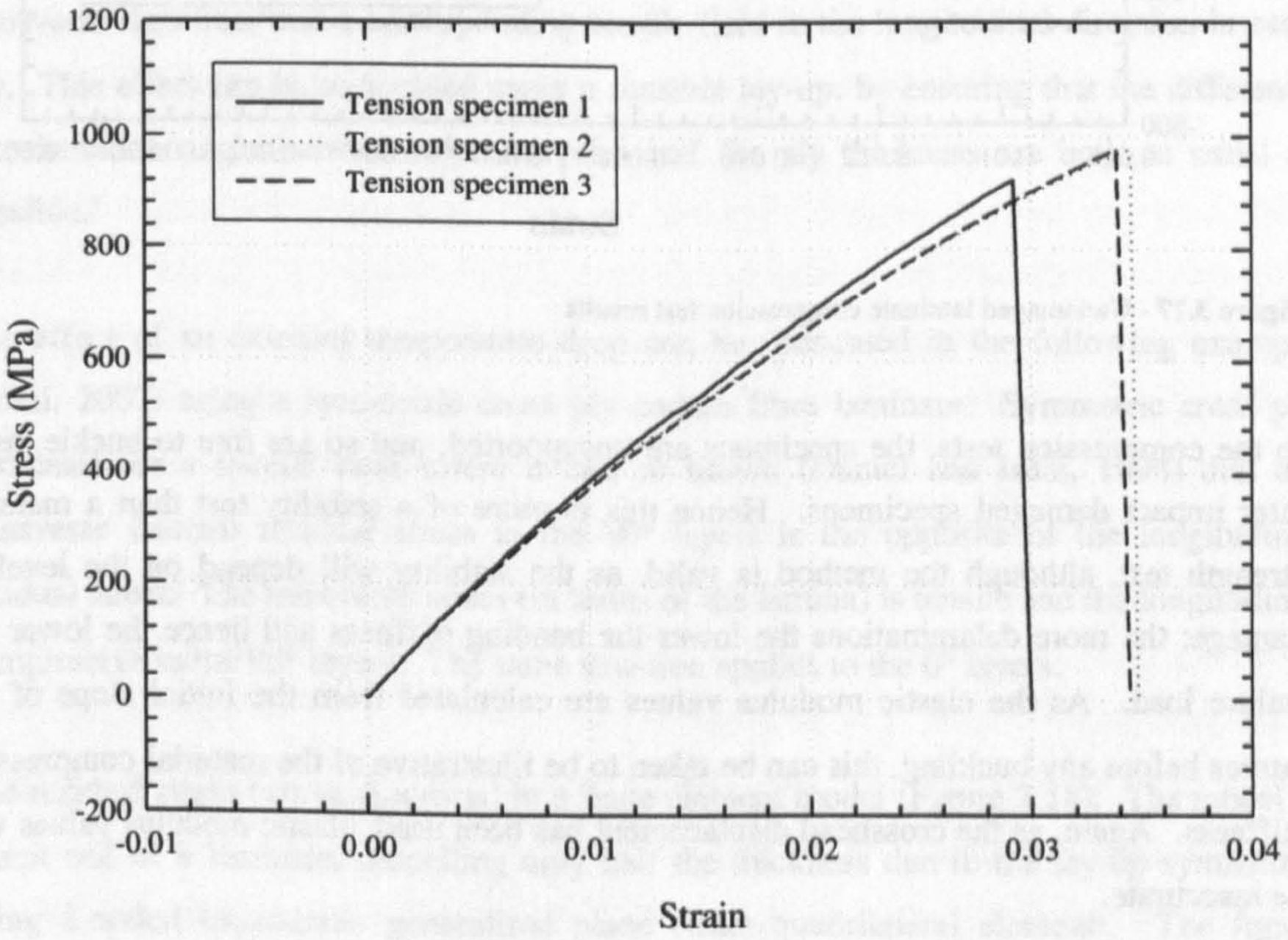

Figure 3.16 - Undamaged laminate tensile test results

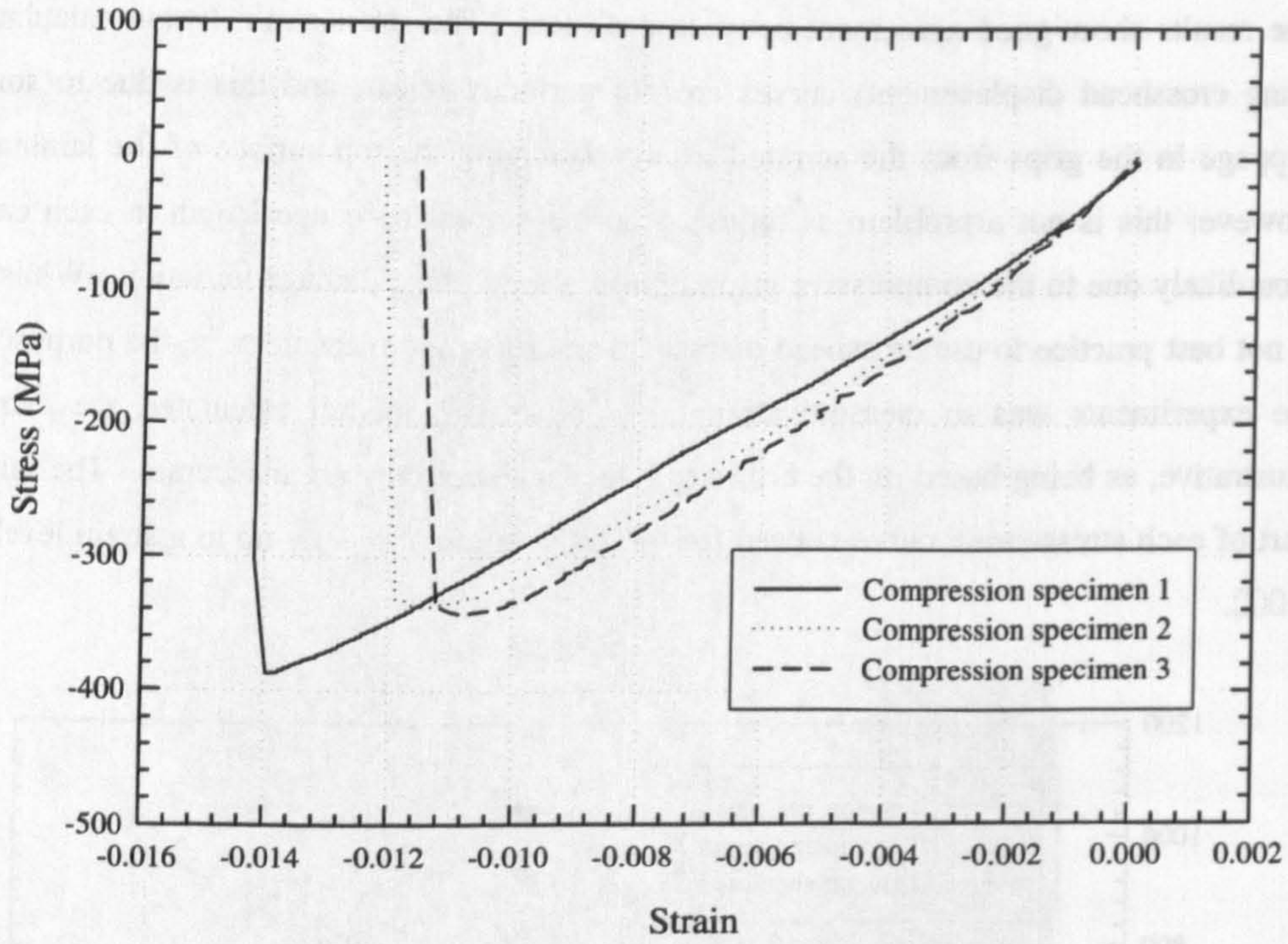

Figure 3.17 - Undamaged laminate compression test results

In the compression tests, the specimens are unsupported, and so are free to buckle, as in later impact damaged specimens. Hence this is more of a stability test than a material strength test, although the method is valid, as the stability will depend on the level of damage: the more delaminations the lower the bending stiffness and hence the lower the failure load. As the elastic modulus values are calculated from the initial slope of the curves before any buckling, this can be taken to be illustrative of the material compressive stiffness. Again, as the crosshead displacement has been used, elastic modulus values will be inaccurate.

The measured laminate strengths (Table 3.14) are somewhat greater than those predicted earlier (Table 3.13). The average tensile strength of the laminates (959 MPa) is 20% larger than that predicted for 0^{o} ply failure (765 MPa). It is the 0^{o} plies that will govern the laminate failure as they take the majority of the end load. The 90^{o} ply predicted failure load of 470 MPa is well below the measured strengths as the matrix is the dominant load carrier in these plies. Matrix cracks may lead ultimately to other more critical failure modes but will not immediately lead to laminate failure. The reason the predictions are off

the real values is a measure of the quality of the laminates and the crudeness of the maximum stress criterion used to derive them. The elastic modulus is below that predicted, and this can be attributed the fact that the crosshead displacement was used for strain measurement.

3.5 RESIDUAL STRESS

Residual stress can be a problem in composite laminates, and one that increases with the thickness of the laminate. They arise during the manufacture of the laminate: during the cure, as the resin cools back to room temperature it will try to contract. As there is a stiffness mismatch between plies, there will be a residual compressive stress field in the transverse direction, and a corresponding tensile field in the longitudinal direction in each ply. This effect can be minimised using a sensible lay-up: by ensuring that the difference in orientation angle between adjacent plies and the ply thickness are both as small as possible.

The effect of an external temperature drop can be illustrated in the following example (Balhi, 2007) using a symmetric cross ply carbon fibre laminate. Symmetric cross ply laminates are a special case where it can be shown (Daniel and Ishai, 1994) that the transverse thermal residual stress in the 90° layers is the opposite of the longitudinal residual stress. The transverse stress (in terms of the lamina) is tensile and the longitudinal compressive in the 90° layers. The same situation applies to the 0° layers.

The residual stress can be simulated in a finite element model (Figure 3.18). The model is a unit cell of a laminate, modelling only half the thickness due to the lay-up symmetry, using 8-noded biquadratic generalised plane strain quadrilateral elements. The figure shows the stress σ_{11} of a (0/90)s laminate due to a thermal loading of ΔT = -150 K. The longitudinal direction of the laminate is along the 1-axis while the 2-axis is through the thickness – against normal convention, but the way the finite element software presents 2d results.

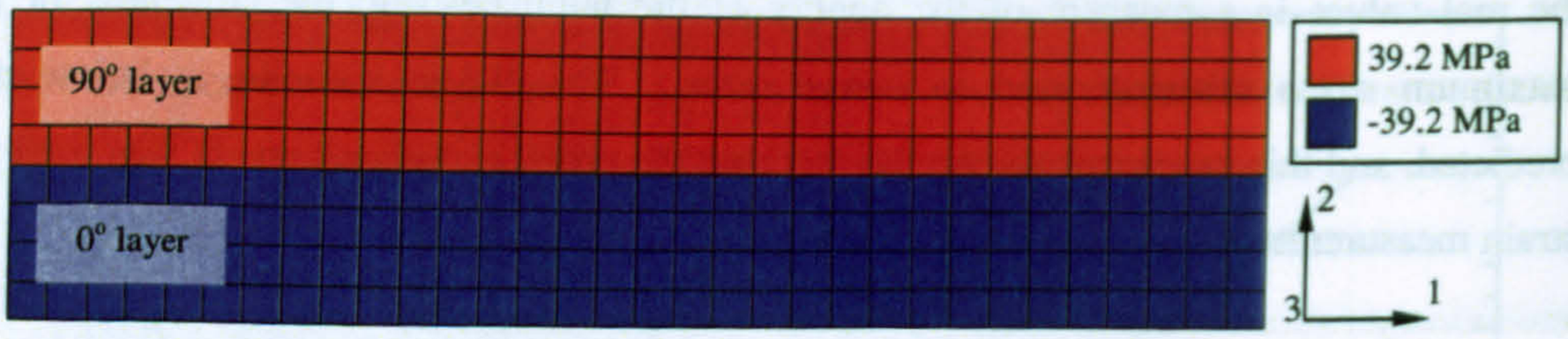

Figure 3.18 - σ_{11} stress in a (0/90)s laminate subject to a temperature drop of 150°C (Balhi, 2007)

Examination of the stress plot in Figure 3.18 and the corresponding plot for σ_{33} indicates a uniform stress distribution in the 90° layers such that σ_{11} = 39.2 MPa and σ_{33} = -39.2 MPa. This agrees exactly with the predictions from Classical Laminate Theory obtained with the software Laminator (Lindell, 2001) when imposing a thermal load of –150 K (noting that the cure cycle for the laminates in this research gives a temperature drop of 160 K).

This example, using a common laminate and a typical cure cycle temperature drop (although different to that in the cure schedule of Figure 3.11), shows that the residual stress can be significant. The residual stresses are undesirable because they will be an additional component to any applied load, and hence the apparent strength will be lower.

There is currently research being undertaken into ways to measure the level of residual stress in a laminate. One such method adapting an existing method used in isotropic materials is called the Deep Hole method. A small diameter reference hole is drilled through the material, and the exact diameter profile measured. Then a column of material containing the reference hole as its axis is trepanned free from the laminate, allowing relaxation of the residual stress. The new hole diameter profile is measured, and compared with the profile before trepanning to provide strain information for subsequent analysis to determine the residual stresses (Bateman et al., 2005).

As this work is on going the residual stress in the laminates used in this research was not measured.

CHAPTER 4

IMPACT TESTING

4.1 INTRODUCTION

4.1.1 Impact and the Impact Machine

One of the first tasks was to design a test procedure and machine that could provide impacts in the manner required. In addition it was important that the various characteristic parameters determining the type of impact could be varied with ease. With this procedure and machine in place the project could continue with confidence.

When designing a new test machine it is important to keep in mind the various standards that may apply, the type of result that is desired, the available resources and the scenario which is being simulated. The tests being undertaken in the laboratory are simulations of what has occurred, in the past, in service. An event that damages a product or component whilst it is being used, and that happens frequently enough to merit further examination, needs to be accurately simulated in the laboratory. Firstly, the event itself needs to be characterised, and then the test designed to mimic those characteristics and hence the event. In the case of this research the event is a tool, toolbox or equivalent dropped onto a composite wing skin from above, for example from a maintenance gantry. This is characterised as a low velocity impact: a blunt object with mass between 1 kg and 10 kg falling under the influence of gravity from between 1 m and 5 m.

4.1.2 Test Schedule

Already there are many parameters to investigate for a thorough experimental exploration: impactor velocity, mass and drop height, and target thickness, in-plane dimensions and type of support. There is a further constraint on the research: available resources in time, materials and finances. Hence a sensible and practical test schedule has to be planned based on these constraints and parameters. The resultant test matrix will form the bulk of the experimental results and will be the basis upon which all understanding and conclusions will be made. Given that there is the inevitable trade off between an extensive study that is not as authenticated as a very focussed study, the ensuing test matrix has to be pragmatic and far reaching without losing credibility.

4.1.3 Chapter Structure

In this chapter the impact test methods and results from three broad areas are presented: central impact, edge impact and variable velocity impact. As is discussed in the following chapter, the impacted plates were non-destructively and destructively examined to quantify the damage. Within each of the three areas there are parameters that are varied to gain an overall impression of their effect: plate thickness, impact energy and impact velocity (or drop height). The thickness and impact energy were varied for central and edge impacts, and only the impact velocity varied when studying variable velocity impact. The first two areas of work are linked; the central impacted plates all have corresponding edge impacted plates, so that comparisons can be drawn. The variable velocity impacted plates constitutes a more stand-alone piece of research. There is some research that shows that with impacts of constant energy, the impact velocity is important (Robinson and Davies, 1992 and Olsson, 2000). Hence a series of tests were planned that looked at this: three different impact velocities, and three correspondingly different impactor masses all at the same impact energy.

Firstly the test schedule is discussed, in particular the range of tests planned, and the parameters investigated. Next, it is the impact machine: the various different types of machine are discussed, finally explaining the choice made. The machine's design is also discussed as this is important for ensuring confidence in its performance. In addition the rig for performing simulated impact with a quasi-static test machine is presented. Following that, the test methods and sample results are presented. The way in which the

plates were impacted, the types of impact that they were subjected to and why, and the type of data that the impact machine created during the impact, and how it is used, are discussed. Finally the results are shown and discussed.

4.2 IMPACT MACHINE

4.2.1 Introduction

In this section the type of impact machine used is defended, citing examples of other configurations. There are three main components to the machine, an impactor that has a known mass, impact energy and means of delivery to the target, a plate fixture and sensors and data acquisition. The design is presented and method of operation is discussed.

The aim is to have a machine that can accurately and repeatedly drop a mass onto a composite laminate thereby creating damage within the plate.

4.2.2 Impact Machine Specifications

The specifications were defined as follows.

i. The impactor must be accurately guided onto a specific point on the plate, whilst ensuring the weight is allowed to fall freely under the influence of gravity.

ii. The plate must be held securely in place by a fixture.

iii. The plate fixture must be able to hold rectangular plates up to 15 mm thick and with in-plane dimensions up to 400 mm.

iv. The plate fixture must be able to allow the plate to be impacted near a free edge.

v. The plate fixture must not rigidly clamp the plate but allow a small amount of rotation at the edge to simulate the impact of a larger panel clamped at its edges.

vi. A drop height or equivalent of at least 4 m is required. The impactor mass needs to be at least 8 kg, giving a maximum impact energy of at least 310 J. Using a mechanism to maintain consistent drop heights, at least two different drop heights should be possible.

vii. The impactor must not be allowed to fall back onto the plate after the first impact.

viii. The plate fixture must be at least a factor of ten stiffer than the plate.

ix. The impactor must be easily modified to change its mass, and thus provide at least three different impact energies from any given drop height.

x. There must be provision for sensors to measure at least the motion of the impactor and its incident velocity.

4.2.3 Choice of Impact Machine Configuration

Impact machines are usually one of three types: ballistic, drop weight and pendulum.

The ballistic type fires an impactor using, for example, compressed gas or a magnetic field. The impactor is guided by a barrel and thus strikes the plate. The ballistic type was not considered as the impactor is released at a much higher velocity in comparison to the other two types and is more often used when studying penetration of the plate, simulating battle damage for example.

Drop weight impact machines can take either a pendulum or a simpler falling weight configuration. Both have advantages, in the case of the pendulum machine the path of the impactor is necessarily controlled, and ensuring low friction is easier with just the need for a rotary bearing. The designer of a falling weight machine has to think carefully about the seemingly conflicting criteria of guiding the impactor accurately to the target and being as free from friction as possible. However, the choice was easily made as the available laboratory space was limited and so a falling weight machine the only viable choice.

A drop weight impact machine is shown schematically in Figure 4.1. A vertically falling mass, or impactor, with a suitable impact tup is guided onto a plate.

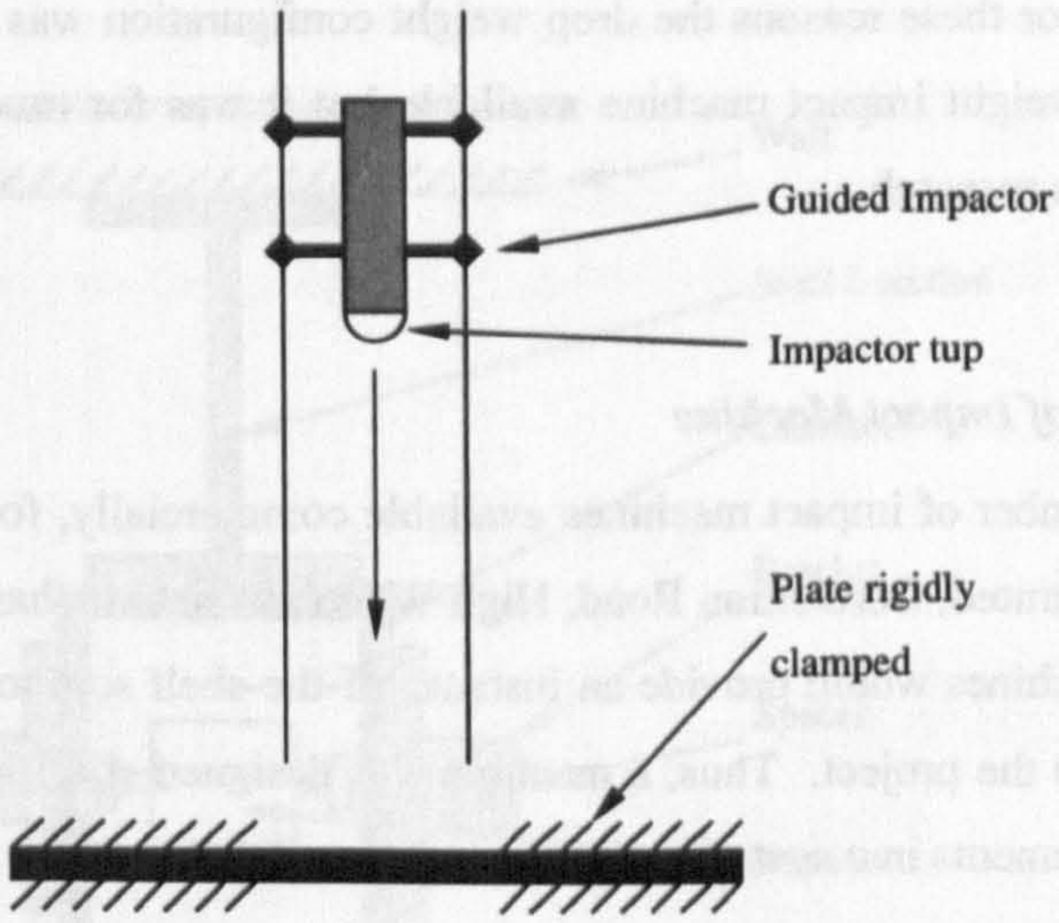

Figure 4.1 - Sketch of a drop weight impact machine

Simply, the machine works by converting gravitational potential energy into kinetic energy at the moment of impact: the incident impact energy. Some commercially available machines use pneumatic pressure or spring loading to provide an initial impulse to the impactor to overcome its lack in available height. If the machine can be built high enough then such complications are not necessary. The impact velocity is governed by the drop height, the impact energy by the mass and velocity, or mass and drop height. For a given impact energy IE and drop height h, the required impactor mass m can be found using equation 4.1, where g is the acceleration due to gravity. For a given drop height the impact velocity v can be calculated using equation 4.2. These equations represent the ideal situation where there are no losses in the system, and are the result of simply equating and rearranging the equations for gravitational potential energy and kinetic energy.

$$m = \frac{E}{gh} \tag{4.1}$$

$$v = \sqrt{2gh} \tag{4.2}$$

A drop weight machine is fairly flexible within its limits; there are potentially unlimited different release heights and impactor masses. In the literature review, all the impact experiments were conducted using either a drop weight machine (for example Potter, Schweickhardt and Wisnom, 2000) or a ballistic impact machine (for example Park and

Jang, 2000). For these reasons the drop weight configuration was chosen. There was an existing drop weight impact machine available but it was for much lower energies than required for this research.

4.2.4 Design of Impact Machine

There are a number of impact machines available commercially, for example the Dynatup from Instron Limited, Coronation Road, High Wycomb, Buckinghamshire, UK. However, whilst their machines would provide an instant, off-the-shelf solution, the cost was beyond that available to the project. Thus, a machine was designed specifically for the project, to meet the requirements in a cost effective way.

The design combines three main components that are all discussed below: the drop tube, impactor and plate fixture. In addition the sensors chosen and the data acquisition system are presented.

4.2.4.1 Drop Tube

Figure 4.10 shows a top down view of the drop tube arrangement. It is essentially a long piece of steel channel section, with long steel flat "rails" bolted to the channel with brackets. This arrangement is then bolted to the wall using two separate lengths of large depth steel I-section. The brackets, bolted at three positions along the tube, ensure a consistent distance between the rails and channel.

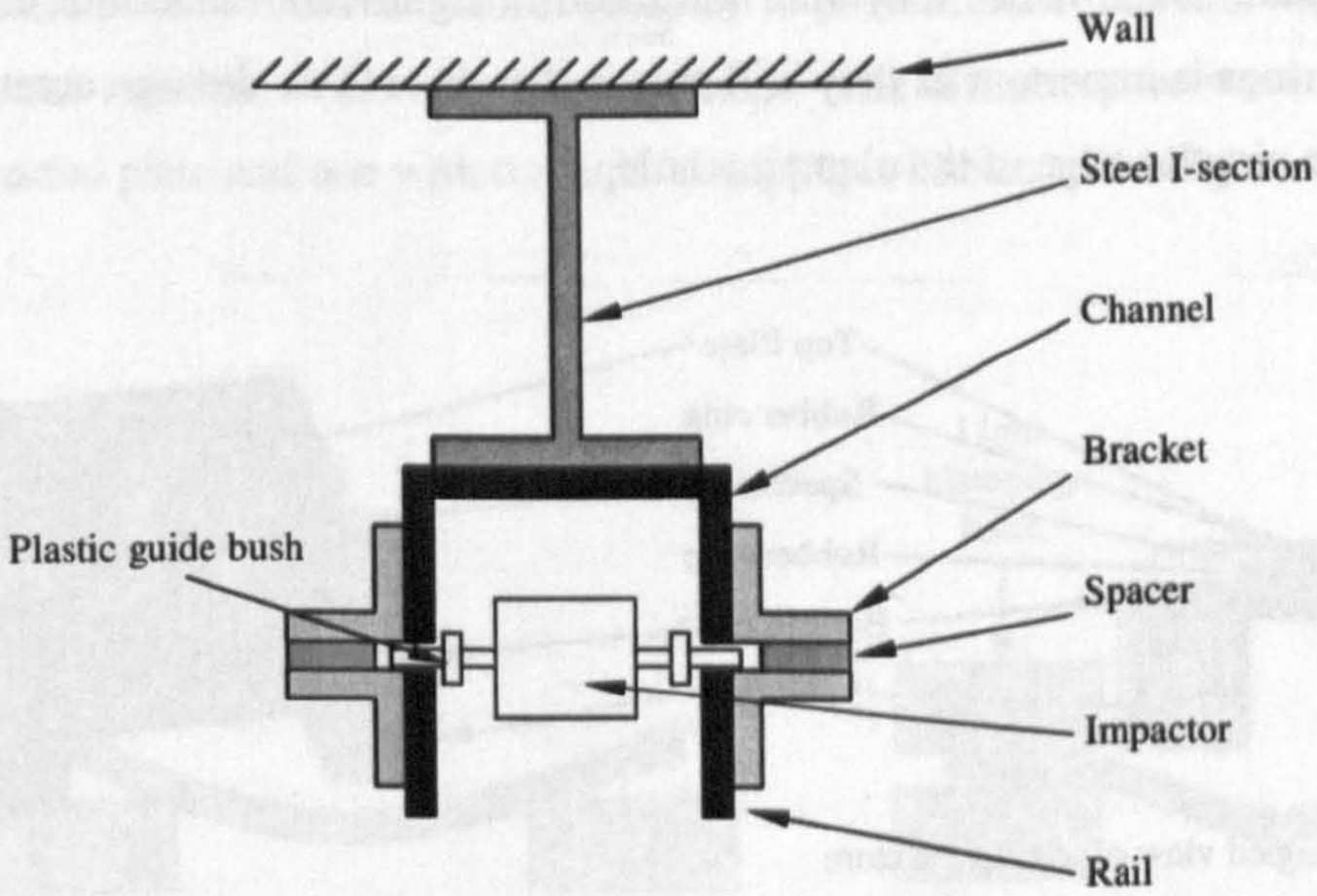

Figure 4.2 - Top-down view of the drop tube arrangement

As can be seen, the impactor has arms with plastic bushes that slide in the slot afforded between the channel and rails, thus guiding the impactor. There is clearance of approximately 1 mm (the slot is 10 mm wide) between the bushes and the edges of the slot, enough to guide the impactor accurately without impeding its descent.

At two positions along its length, there is a catch. Each catch holds the impactor at a given height so the drop height is repeatable. The impactor can be released at the appropriate moment.

4.2.4.2 Plate Fixture

Figure 4.3 shows a side and an angled view of the plate fixture, indicating its key features. The support for the plate has to be as stiff as possible so that it is the plate that dominates the deflection. The 100 x 100 x 100 mm solid steel feet bolt directly onto a concrete floor. The bottom plate is 30mm thick steel, 500mm square, has a 200mm diameter hole cut in the centre and bolts onto the feet. There are rubber rings bonded to the top and bottom plates that allows a softened contact at the clamping edge by allowing a small amount of rotation at the edge of the hole. They are 200 mm inner and 210 outer diameters with a

thickness of 3 mm. The rubber is incompressible and is put into compression by the act of clamping the top plate down, hence they will not absorb a significant amount of energy. Having the rubber rings is important as they will ensure that there is no damage created on the plate around the circular edge of the clamping hole.

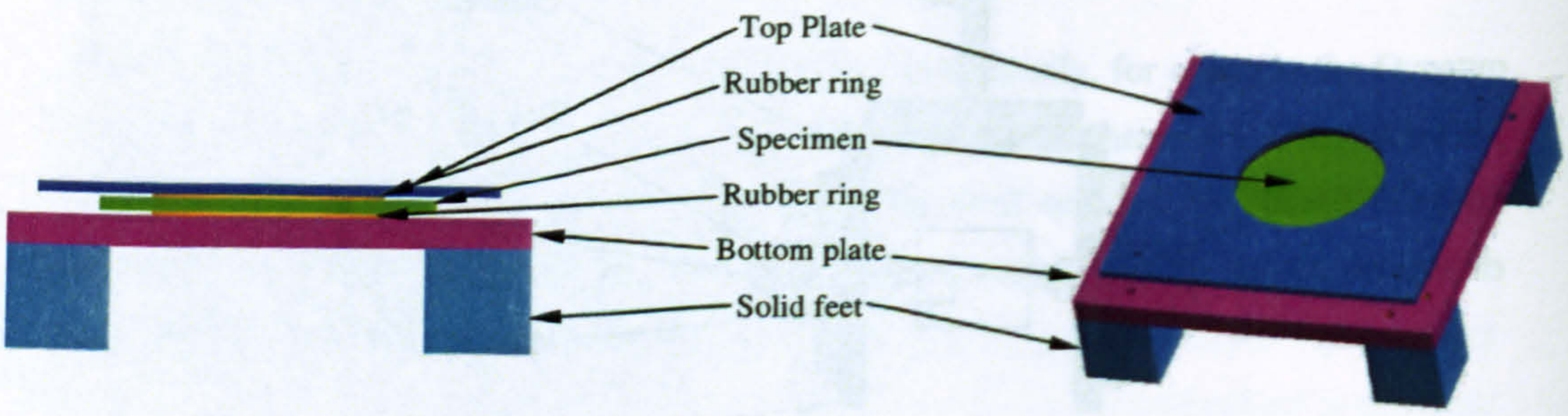

Figure 4.3 - Side and angled view of the plate fixture

The size of the support structure was determined by material availability and constraints on time for manufacture of the plates. Also the dimensions of the support are in the same order as the stringer pitch on the proposed Airbus UK composite wing design where for a 5 to 10 mm thick skin the stringer pitch would be between 150 and 260 mm (Yang, 2005).

The top plate is bolted to the bottom plate at its four corners. The bolts are tightened simultaneously with a torque wrench to the same torque.

No plate fixture for use in low velocity impact experiments has been found in the literature that uses a similar rubber ring arrangement. Typically the plate is either strongly clamped between two metal plates to simulate a built in condition (Aymerich and Meili, 2000), or lightly clamped between two metal plates to simulate a free-free condition whilst preventing rebound of the plate (Yuan, Czigany and Ye, 2000). Some researchers have used circular holes (Green, Morrison and Luo, 2000) whilst others rectangular (Kessler and Bledski, 2000). Impact experiment standards (Boeing, CRAG, NASA, see Short (2001) for a comparison) show much variation between each other in the way the plate is constrained and impacted.

Strongly clamping the plate to simulate a built in condition can cause damage to the plate by the edge of the clamps where there is a high stress concentration due to the geometrical

discontinuity. The simulation of a free-free boundary condition is far from perfect as the top plate in such fixtures, whilst necessary to prevent plate rebound, also tends to constrain the plate rotation at the edge of the clamp. The difference between a genuinely simply supported plate and one with the light clamping is illustrated in Figure 4.4.

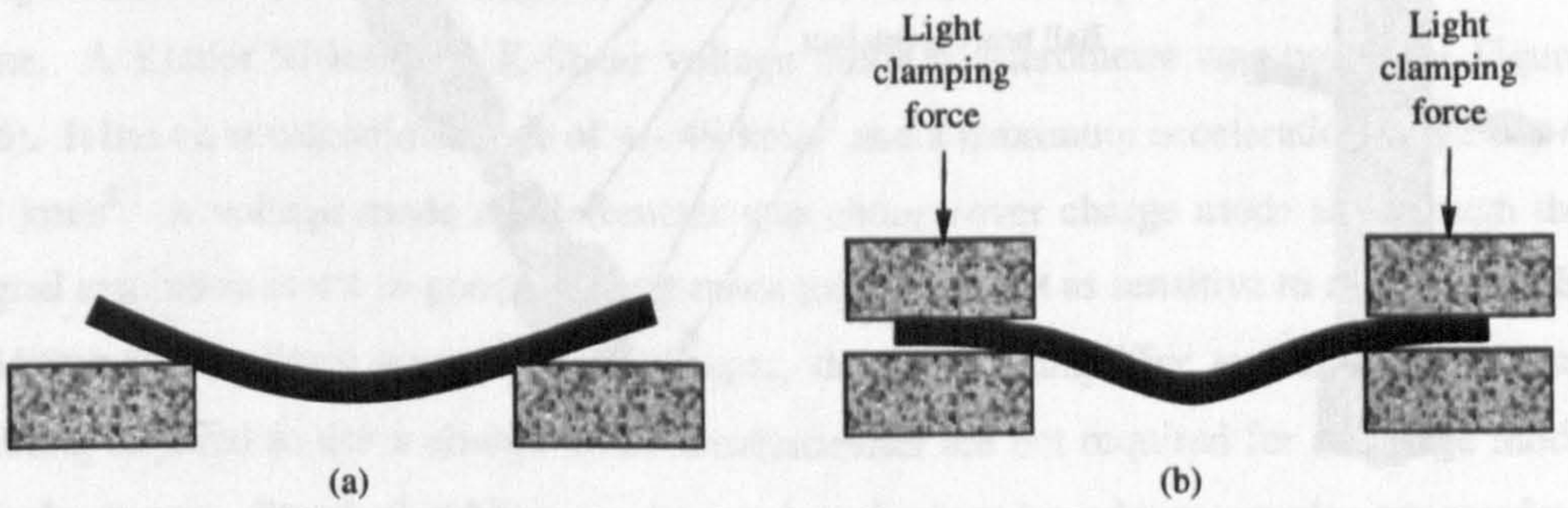

Figure 4.4 – Exaggerated effect of different plate clamping conditions with (a) genuine free-free condition and (b) an experimental simulated free-free

It is important to know exactly how the plate is constrained to model correctly its behaviour and understand the damage caused. The design presented can be used to create strong or light clamping forces, but for all experiments the four clamping bolts were tightened to 8 Nm. Experimentally modelling boundary conditions can be difficult and often it is just a close approximation that is possible. A more practical approach is to understand the limitations of the boundary conditions that are applied, and then knowing how to relate the results to some analysis.

4.2.4.3 The Impactor

The impactor assembly and exploded view are shown in Figure 4.5. The overall length of the impactor is 200mm, and its mass is 2kg, though this can be reduced easily if required by waisting the impactor body. The impactor body, ball bearing holder and ball bearing retainer are all manufactured from aluminium. The ball bearing is made from hardened stainless steel and is 19 mm in diameter. As with the plate fixture, the diameter and geometry of the impact tup in impact experiments varies considerably in the literature.

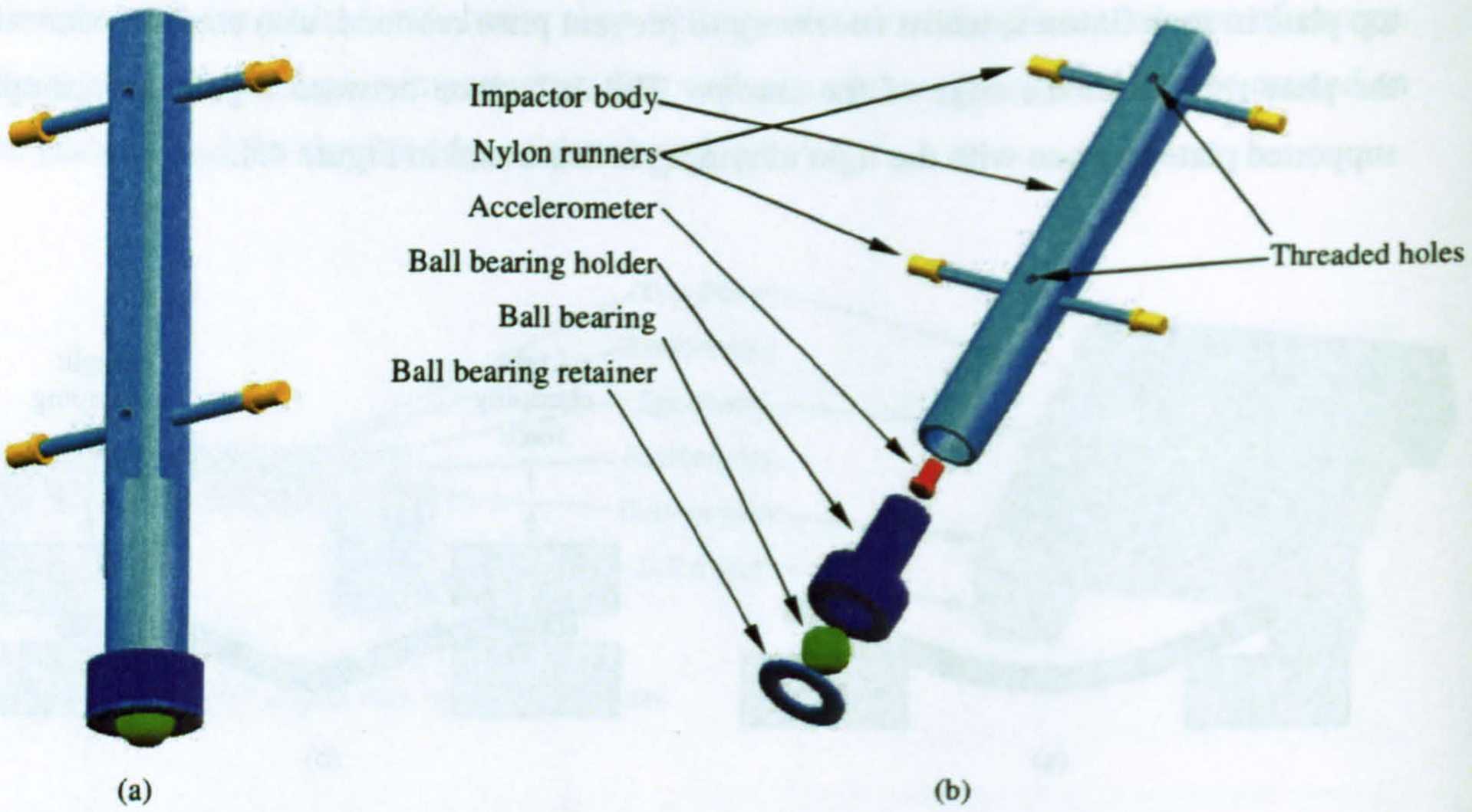

Figure 4.5 - Impactor (a) assembly and (b) exploded view

The ball bearing locates into a hemispherical hole on the ball bearing holder. The ball bearing retainer is attached to the ball bearing holder with four screws. The accelerometer screws to the top of the ball bearing holder. The impactor body then screws onto the ball bearing holder, a recess providing space for the ball bearing holder and accelerometer. There is a narrow hole along the entire length of the impactor body for the accelerometer cable. During an impact experiment the nylon runners slide in the gap between the channel and rails in the drop tube keeping the impactor central. The threaded holes allow extra mass to be secured to the impactor. Two impactors were designed, one with an aluminium body, shown in Figure 4.5, and one with a steel body. They both use the same steel ball bearing assembly so that the accelerometer mounting is common. The main difference between the two designs is that the steel impactor had mass of 4.67 kg whereas the aluminium impactor shown in Figure 4.5 had a mass of 2.47 kg.

The impactor length was chosen to prevent the impactor from jamming in the drop tube due to an axial misalignment whilst also keeping its size manageable. Analysis presented in Chapter 6 shows that the accelerometer should be placed as close as possible to the tup, hence its location inside the impactor body.

4.2.4.4 Sensors and Data Acquisition

An accelerometer on the impactor was used to measure live accelerations during impact. It gives a voltage output that relates to the acceleration it experiences. This signal can then be plotted against time and integrated twice to give impactor displacement, or used in conjunction with the known mass of the impactor to find the impact force as a function of time. A Kistler 8704B5000 K-Shear voltage mode accelerometer was used (see Figure 4.6). It has an acceleration range of +/- 49 km/s^2 and a maximum acceleration range of +/- 98 km/s^2. A voltage mode accelerometer was chosen over charge mode as although the signal resolution is not as good, they are more robust and not as sensitive to cable whip. In addition the ancillary equipment is cheaper, the charge amplifier and high impedance cabling required to use a charge mode accelerometer are not required for a voltage mode accelerometer. Standard cabling can be used, and a low impedance coupler are required instead, in the case of this project a Kistler 5118B2 low impedance coupler is used.

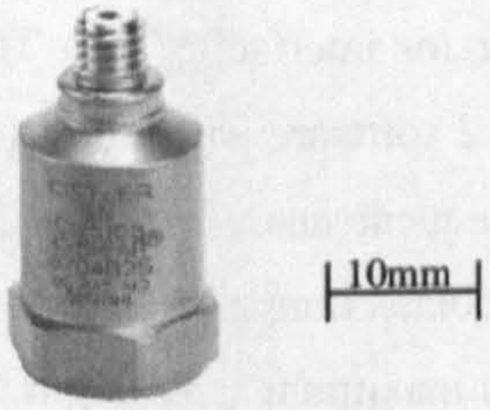

Figure 4.6 - Kistler 8704B5000 K-Shear voltage mode accelerometer

Also, a velocity sensor was permanently installed close to the target, there measuring the impact and rebound velocity. It consists of two pairs of infrared diodes, each pair consisting of one emitter and one receiver. Each pair give a signal of 5 V when the infrared circuit is clear, and 0 V when blocked. A thin 30 mm long aluminium tab affixed near to the tup of the impactor breaks the infrared beam as it passes. The first pair act as a trigger for the data acquisition system to commence recording accelerometer data and data from the second diode pair (see Figure 4.7). The signal from the second pair is used to calculate the velocity of the impactor before and after impact, as the length of the tab is known and the time trace of the signal divulges the time taken for it to pass. These

measurements will be used to calculate the actual incident kinetic energy of the impactor, and the energy absorbed by the plate.

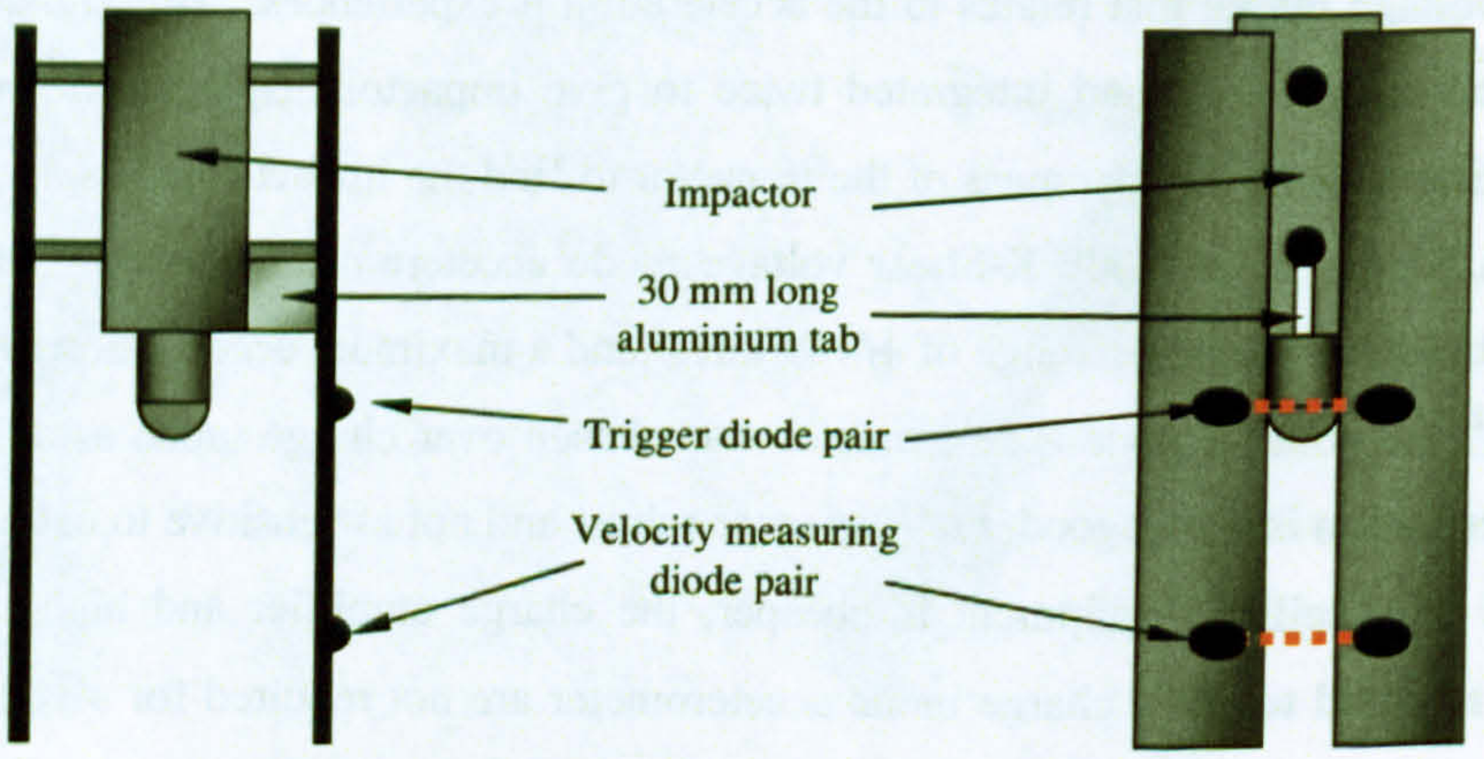

Figure 4.7 - Arrangement of infrared diode pairs. Left: front view; right: side view

For data acquisition the instruNet iNet-100B system was used in conjunction with the iNet-230 PCMCIA card controller for interfacing to a Toshiba Satellite Pro laptop computer. The instruNet World version 2 software was used to control the data acquisition, and save it to the hard disc for subsequent analysis. The iNet-100B is an analogue to digital converter with 16 BNC type connections and several general purpose screw-down terminal connectors. The system has a maximum sampling rate of 166 kHz. The data acquisition is started by the trigger diode pair, at which point the data from the accelerometer and velocity measuring diode pair is recorded for a given length of time. As two channels are being recorded the maximum sampling rate per channel of 83 kHz is used.

Figure 4.8 shows a composite photograph of the impact rig.

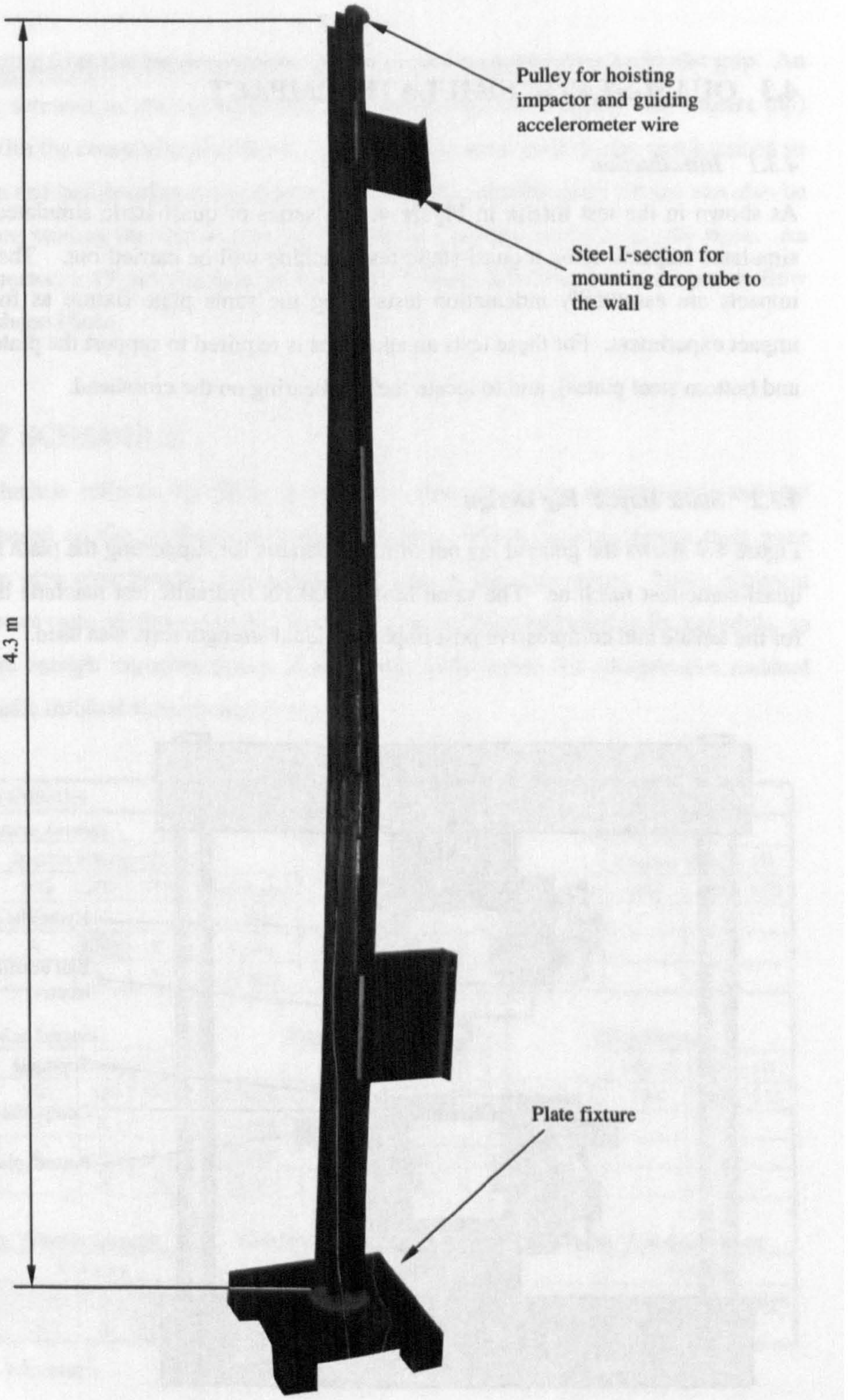

Figure 4.8 - Photograph of the impact rig

4.3 QUASI-STATIC SIMULATED IMPACT

4.3.1 Introduction

As shown in the test matrix in Figure 4.10 a series of quasi-static simulated impacts, or simulated impacts using a quasi-static test machine will be carried out. These simulated impacts are essentially indentation tests using the same plate fixture as for a dynamic impact experiment. For these tests an apparatus is required to support the plate fixture (top and bottom steel plates), and to locate the ball bearing on the crosshead.

4.3.2 Static Impact Rig Design

Figure 4.9 shows the general lay out of the apparatus for supporting the plate fixture in the quasi-static test machine. The same Mayes 500 kN hydraulic test machine that was used for the tensile and compressive post impact residual strength tests was used.

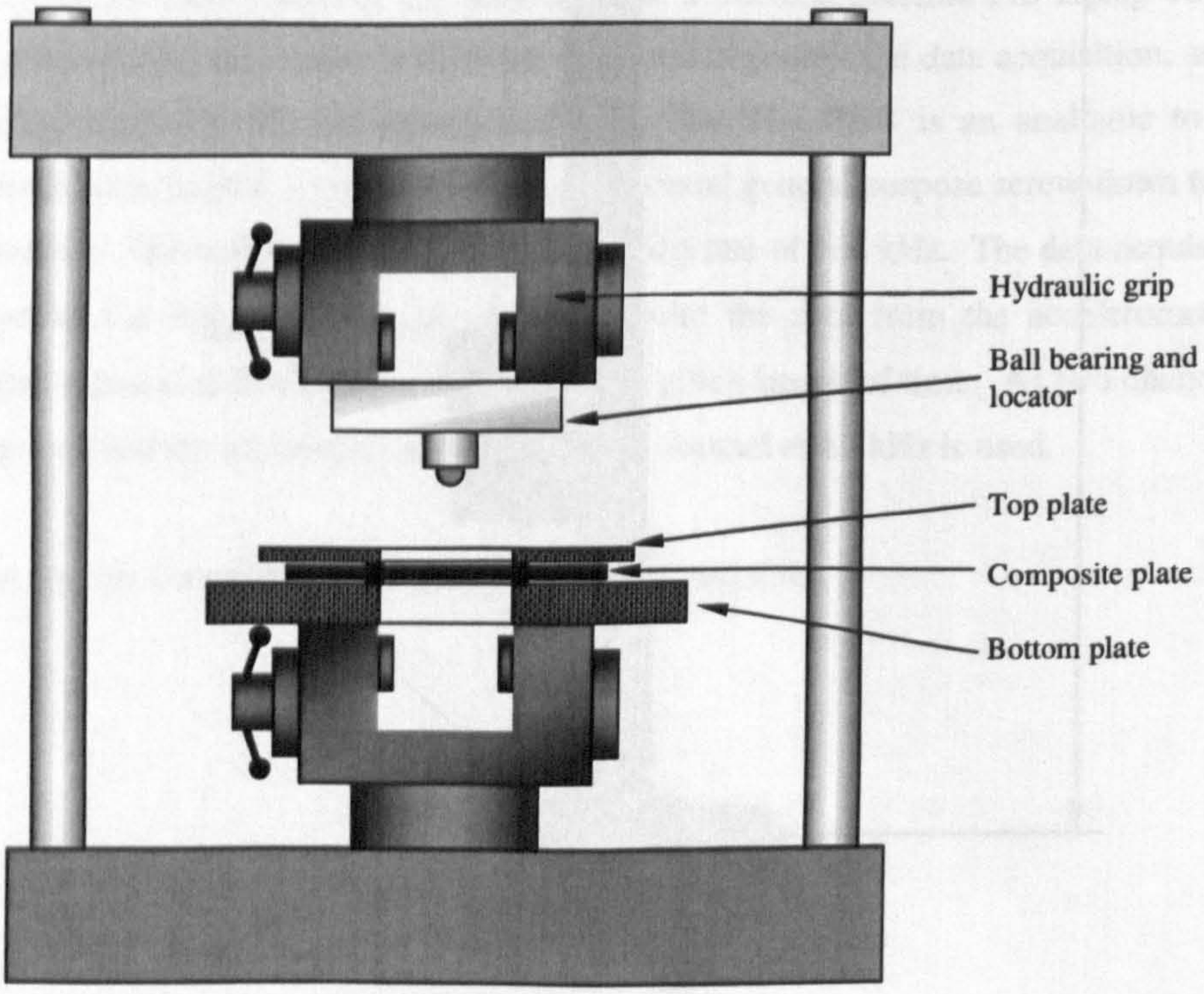

Figure 4.9 - Apparatus for supporting the plate fixture in a quasi-static test machine

The plate fixture from the impact machine is simply rested on the lower hydraulic grip. An arrangement screwed to the top hydraulic grip locates the ball bearing (the impact tup) centrally. With the composite plate loaded, and with its centre marked, the ram is raised so that the plate and ball bearing are just touching. At this point the plate fixture can also be centred before starting the test so that the ball bearing indents centrally on the plate. As with the impactor, a 19 mm diameter ball bearing is used; it is held in place by a shallow spherically shaped hole.

4.4 TEST SCHEDULE

The test schedule reflects the three broad areas that are being investigated, and the limitations based on the available material and time. Where possible repeat tests were performed to give error bounds and variability levels to the data points. Three different destructive tests were performed on the impacted plates; this is reflected in the schedule, so that there are enough impacted plates of each type to be tested for compressive residual strength, tensile residual strength and deply.

TENSION

Central Impact

Thickness	Impact Energy (J) 100	200	375
4 mm	X	X	
8 mm	X	XXX	X
12 mm		X	X

Edge Impact

Thickness	Impact Energy (J) 100	200	375
4 mm	X	X	
8 mm	X	X	X
12 mm		X	X

Variable Velocity Impact

Thickness	Velocity Q-Static	Slow	High
8 mm	XXX	X	XXX

COMPRESSION

Central Impact

Thickness	Impact Energy (J) 100	200	375
4 mm	X	X	
8 mm	X	X	X
12 mm		X	X

Edge Impact

Thickness	Impact Energy (J) 100	200	375
4 mm	X	X	
8 mm	X	XXX	X
12 mm		X	X

Variable Velocity Impact

Thickness	Velocity Q-Static	Slow	High
8 mm	X	X	X

DEPLY

Central Impact

Thickness	Impact Energy (J) 100	200	375
4 mm			
8 mm		X	
12 mm			

Edge Impact

Thickness	Impact Energy (J) 100	200	375
4 mm			
8 mm		X	
12 mm			

Variable Velocity Impact

Thickness	Velocity Q-Static	Slow	High
8 mm	X		

Figure 4.10 - Test matrix

Figure 4.10 shows the test matrix. Each "X" represents a single test, so where the entry is "XXX" this shows where three identical impact tests have been performed. The matrix identifies the destructive damage evaluation method to be used on each impacted plate, be it compressive or tensile residual strength test or deply. The greyed out entries indicate those tests (within each post impact destructive test grouping) that are identical and are not repeated. It can be seen that for the central and edge impact tests, there are three plate thicknesses included: nominally 4 mm, 8 mm and 12 mm, and three impact energies: nominally 100 J, 200 J and 375 J. These impacts are executed at the maximum drop height of the machine (4.3 m); the different energies achieved by changing the impactor mass. 100 J impact tests are not carried out on the 12 mm thick plates, as it would not be possible to fail these plates in subsequent residual strength tests. 375 J impacts are not carried out on the 4 mm thick plates as such impacts would totally destroy the laminate and such tests are not of interest to the project.

The variable velocity tests are only performed on 8 mm thick plates, and at three different impact velocities. The different velocities are achieved using the maximum drop height (4.3 m) of the impact machine (a "high" velocity impact), an intermediate drop height (1.5 m, a "slow" velocity impact) and using a quasi-static test machine to perform a simulated impact (a "Q-static" impact).

Three representative impacts were identified for deply, namely a central and edge impacted 8 mm thick plates at 200 J, and a simulated impact on another 8 mm thick plate.

4.5 IMPACT TEST METHODS AND SAMPLE RESULTS

4.5.1 Introduction

In this section, the test methods used to impact the plates are presented. In particular this means each different type of impact is identified, and the impactor mass and drop height configuration used are described. The method for performing the simulated impact using a quasi-static test machine is presented also. Then the typical results from an impact are presented, showing what information can be garnered from the data.

4.5.2 Impact Types and Impactor Configurations

For drop weight impact tests, there were four different impactor masses, and two different drop heights. The impact energies were chosen to replicate those that the structure might see during manufacture or assembly, for example accidental tool drop from a gantry, or if the component was accidentally knocked against a doorframe for example. These incidents could easily produce impacts with energies in the order of hundreds of joules (Naylor, 2002).

Table 4.1 - Impactor mass, drop height and energy configurations

Impactor body mass (kg)	Additional mass (kg)	Total Impactor mass (kg)	Drop height (m)	Estimated impact velocity (ms^{-1})	Estimated impact energy (J)
2.47	0	2.47	4.3	9.2	104
4.67	0	4.67	4.3	9.2	197
4.67	3.7	8.37	4.3	9.2	353
4.67	7.5	12.17	1.5	5.4	179

Evident are the three impact energies used, all using the full height of the impact rig and three different masses and hence three different impact energies. The fourth impact configuration was designed to provide an impact of comparable energy to the second, but with a slower impact velocity from a lower drop height.

4.5.3 Test Methods

For all the dynamic impacts the same test method was employed. Firstly the size of the plate was chosen so that both a central and an edge impact could be performed on it. This meant a material saving that gave the opportunity to carry out more impacts. Care was always taken to ensure that there was no interaction between damage from the first impact and the second; hence at the highest energy levels separate plates were used for edge and central impacts. The plate dimensions were chosen so that the height was the smallest possible to enable post impact strength tests to be carried out using the hydraulic grips, and the width so that it is possible to fit two impacts.

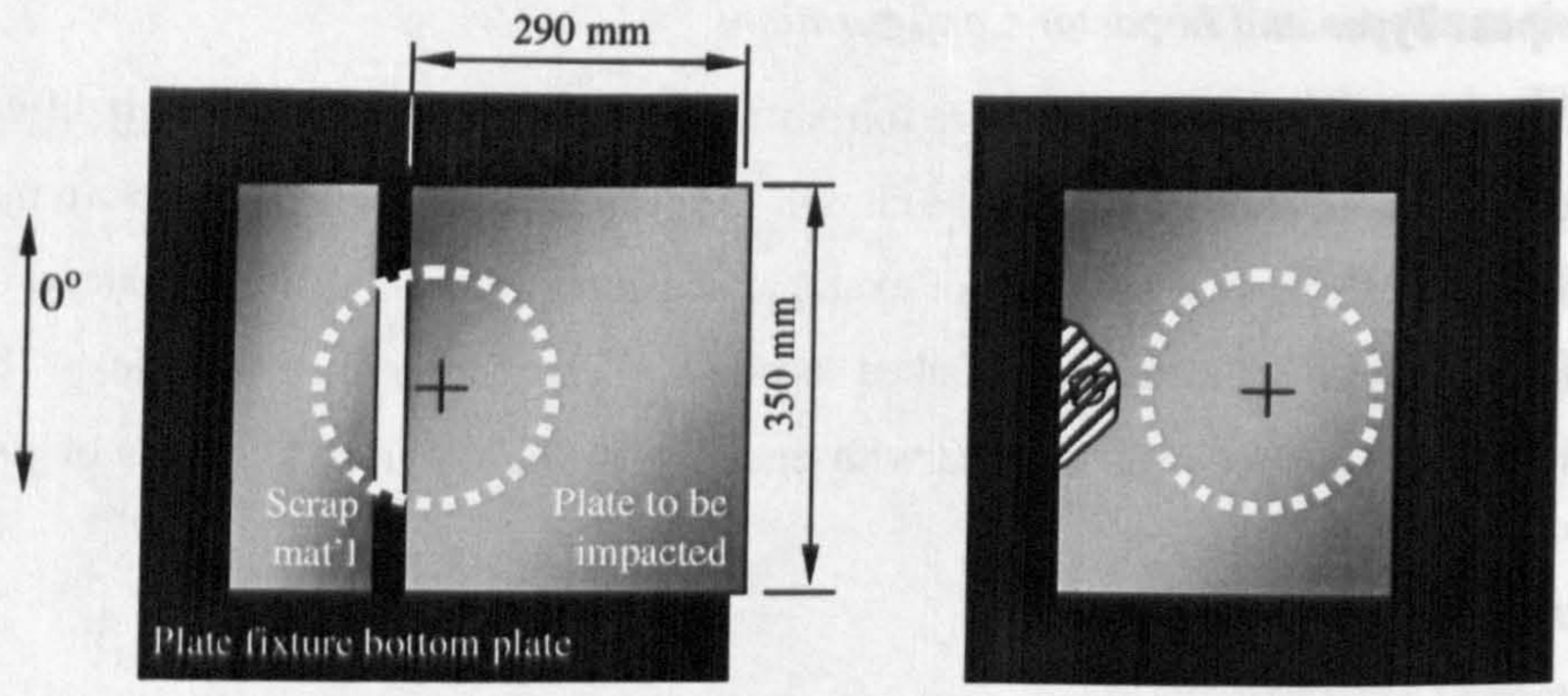

Figure 4.11 – Arrangement for plate to be impacted. Left: edge impact, right: central impact

The edge impact was completed first in each case. Figure 4.11 shows the arrangement used, with the plate fixture bottom plate visible, and the outline of the hole over which the plate is rested. The impact was measured to be 20 mm from the free edge, and a piece of scrap material of the same thickness as the plate used to pack the other side thus ensuring an even clamping force. Following the edge impact, the plate was shifted to the left for the central impact, ensuring that all impact damage is outside of the 100 mm radius central impact zone (Figure 4.11).

For each impact the procedure was as follows. Two operators were necessary to prevent rebound of the impactor.

1. Depending on the impact configuration (see Table 4.1) set-up the catch at the correct drop height and secure additional masses to the impactor as required.
2. Locate the plate on the plate fixture, clamping with the top plate by screwing the bolts down to 8 Nm.
3. Hoist impactor up to desired drop height, and rest on catch. The catch is secured into pre-drilled holes and so the drop height is the same every time.
4. Enable data acquisition system, data acquiring set to commence based on trigger response.
5. Ensure that accelerometer cable is not tangled, and don all relevant safety wear (goggles and ear defenders).

6. Operator 1 releases the impactor by opening the catch. Operator 2 waits by the plate, waits for the impact and then slides across a piece of wood after impact to prevent the impactor from impacting the plate twice.
7. Save the data.

The method for the quasi-static simulated impacts was similar in terms of setting the plates up in the fixture. However a regime needed to be defined where the results from a simulated impact could be compared logically with the equivalent 200 J dynamic impacts, from 1.5 m and 4.3 m. The method was as follows.

1. The plate was located in the fixture as before. The plate then positioned so it was just touching the ball bearing, so the fixture could be positioned in line with the axis of the test machine.
2. Then a short test was performed, where the plate was loaded by the ball bearing under displacement control until the crosshead had displaced by 2 mm. This was deemed to be within the elastic range of the plate, so no damage was incurred. Using the output from this initial test, the plate bending stiffness was calculated, and then the deflection required to create 200 J of stored elastic energy in the plate was calculated assuming linear elastic deflection.
3. Finally the plate was loaded under displacement control, with the maximum crosshead deflection defined from previous step. The crosshead displacement and force data were recorded.

The rationale for this method is similar to that in a dynamic impact. An energy level is chosen for the plate to be subjected to, and some of that energy is absorbed as damage, and the rest is returned, either to rebound the impactor or to provide a reaction force on the crosshead as it returns to the origin. In a dynamic impact an energy level is arbitrarily chosen, without any regard for what the plate might actually experience or absorb, although it is expected that in a perfectly linear elastic impact where inertial and dynamic effects are negligible all the initial energy would in fact be absorbed elastically at maximum deflection. In fact due to inertial effects and the damage propagation, the maximum stored elastic energy in the plate will be different, and less, than the initial impact energy. With a quasi-static simulated impact the initial energy that the plate will be subjected to is the same as if it were a dynamic impact. Again the actual elastic energy

absorbed will be different due to the damage mechanisms (and of course in this case the inertial and dynamic effects will be negligible).

So the premise of the technique is that given that the initial energies chosen for a dynamic and a simulated impact are the same, and are equivalent to that which would be absorbed perfectly elastically by the plate, it is the ensuing differences that are being investigated. These differences will be the amount of energy absorbed by the plate as damage, and the type of damage that predominates.

The other commonly employed method considered was to perform the simulated impacts first and calculate the total absorbed energy in the plate. Then, through a series of trial and error dynamic impact tests find the impact energy level that gives a corresponding level of absorbed energy. This method however does not compare similar impacts, but only the consequential damage. Also there is a need to perform several impact tests in order to find the matching impact energy level. As in this research the interest lay in trying to see the difference between similar impacts be they simulated or dynamic, this method was thought to be inappropriate.

4.5.4 Sample results

In this section sample results from a dynamic impact and a quasi-static simulated impact are presented. In particular the kind of results that can be obtained, and how, are shown.

Three sets of results are compared: two impacts and one simulated impact. The impacts are an edge and a central impact, both onto a nominally 8 mm thick laminate, with a nominal impact energy of 200 J using the 4.67 kg impactor. The simulated impact is a matching result to the central impact, a centrally loaded 8 mm thick plate with an initial energy of 200 J.

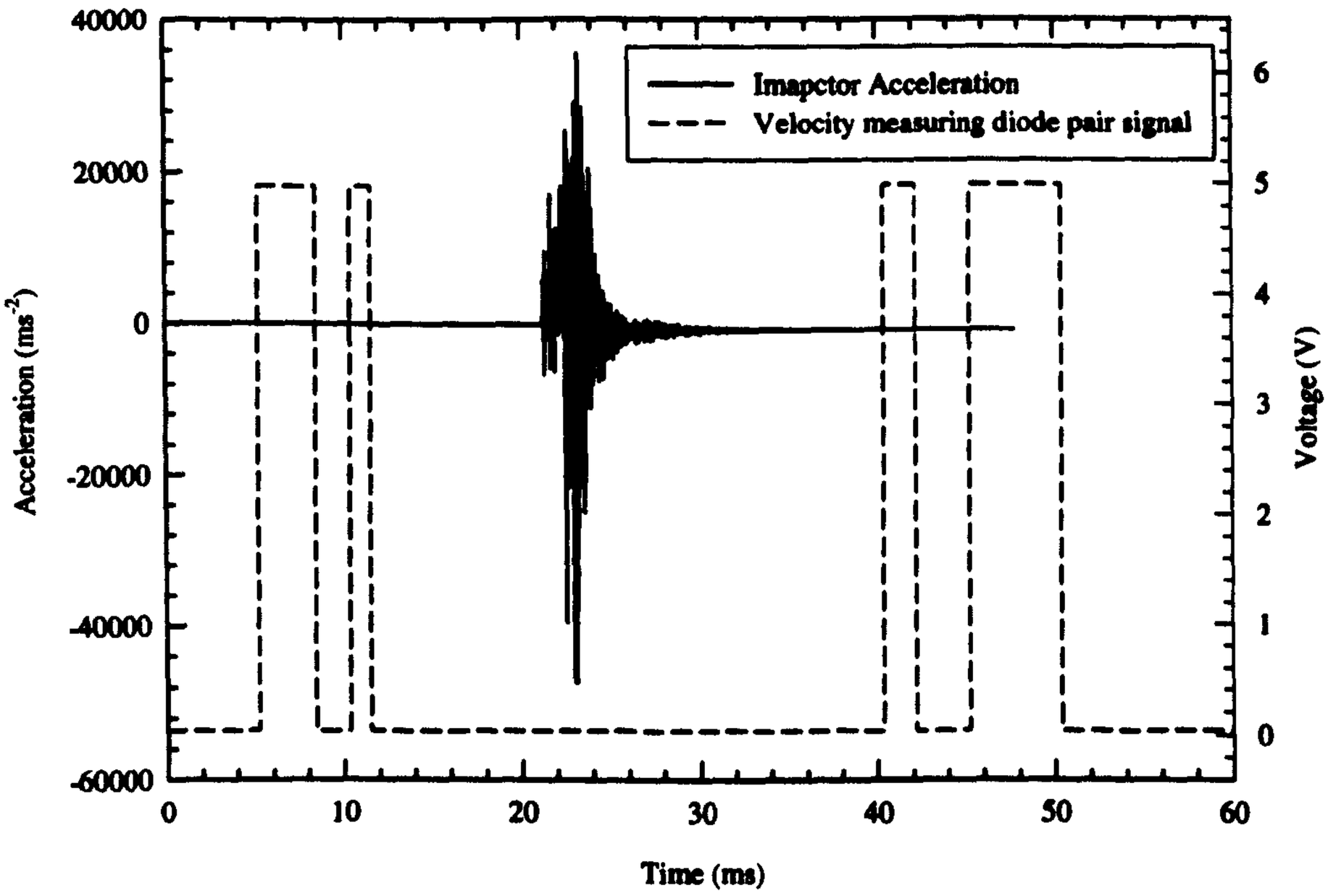

Figure 4.12 - Accelerometer and velocity measuring diode pair signals for 200 J central impact onto an 8 mm thick plate

Figure 4.12 shows the typical results using the central impact results. Firstly the diode signal trace shows four peaks. The first and last are the ones of interest, as the tab fitted to the impactor pass through the beam. The second and third are created by the first of the nylon runners (see Figure 4.5) passing through. As the width of each pulse clearly tells us the length of time it took for the aluminium tab to pass through the infrared beam, and the tab is 30 mm long, so the impact velocity and rebound velocity can be calculated.

The signal from the accelerometer is between the second and third diode signal pulses, of course. The accelerometer outputs a voltage signal proportional to the acceleration at approximately 1000 g per 1 V; the converted data is shown. It shows a considerable amount of noise due to resonance in the impactor, and to clean the signal up so that meaningful information may be gleaned a 15 period moving average was used, see Figure 4.13. In the case of this research it was necessary to find a way to reliably extract comparable data from each impact. Smoothing the data in the way described enabled this, although it can be argued that the noise in the signal is real and should not be averaged out. However it is difficult to state confidently what in the signal is due to signal distortion,

impactor resonance and other such "noise" or from interaction with the composite plate. For this reason the smoothing process was used to give consistent data extraction from the impact results.

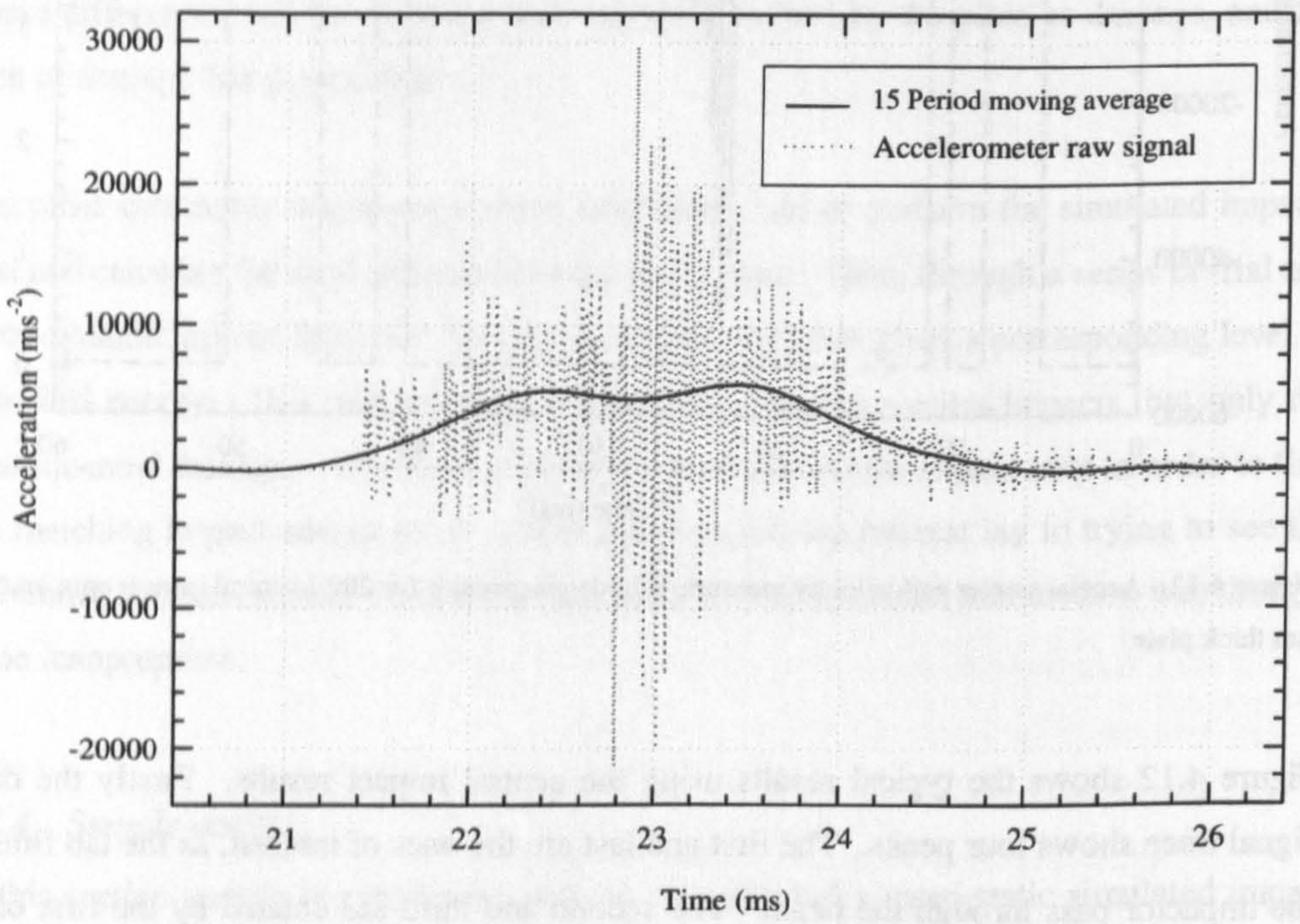

Figure 4.13 - Raw accelerometer signal with a 15 period moving average

The graph in Figure 4.14 compares similar edge and central impacts on an 8 mm thick plate. The information that these plots can offer include the impact event duration, and the maximum impactor force (the product of impactor acceleration and mass). Both plots show a steady increase in acceleration as the plate slows the impactor down with the centrally impacted plate much stiffer. Then in both a drop at approximately 22.5 ms, much more pronounced in the central impact, where the acceleration decreases. Certainly in the case of the central impact, as the drop is so severe, this can be taken to be due to damage in the plate; when damage is initiated and propagated in the plate its stiffness decreases and hence its ability to slow the impactor reduces. The edge impacted plate experiences a lower maximum acceleration (and hence force), but a longer impact event duration.

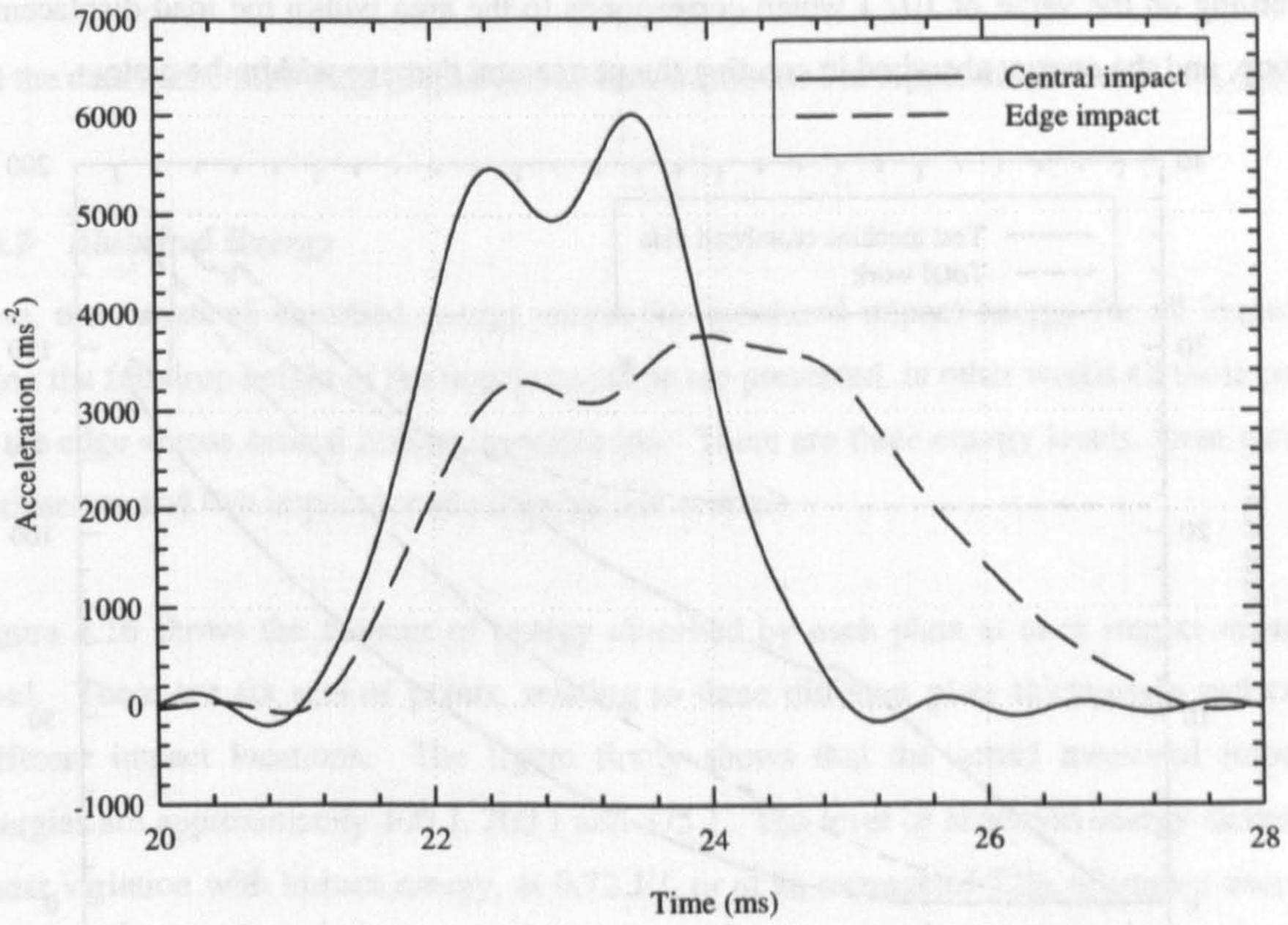

Figure 4.14 - Impactor acceleration trace for similar edge and central impacts

Figure 4.15 shows a typical crosshead force displacement output from a simulated 200 J initial energy central impact on an 8 mm thick plate. The bending stiffness of the plate was found to be 4.3 $kNmm^{-1}$, and so a maximum crosshead displacement of 10 mm was chosen for the test, as this would create 200 J of strain energy in the plate. The initial part of the curve is linear. A small drop in load at approximately 3 mm indicates a small amount of damage. The curve steadily increases up to the maximum load at which point a large load reduction is experienced as more significant damage is created. The damage created is likely to be matrix cracking initially followed by fibre breakage and delamination, in this order as the matrix will fail under much smaller loads compared to the interlaminar region and the fibres. This is, however, conjecture, as no microscopy was carried out. Once the maximum deflection of 10 mm is achieved, the crosshead returns to zero, leaving the plate with a residual permanent deflection (partly indentation and global deflection) of 2.1 mm. Shown also in the figure is the total work (calculated by the cumulative area under the force-displacement curve) done by the plate. The energy absorbed by the plate steadily increases to the maximum at 182 J, and then drops as the cross head returns to zero,

settling on the value of 107 J which corresponds to the area within the load-displacement loop, and the energy absorbed in creating the permanent damage within the plate.

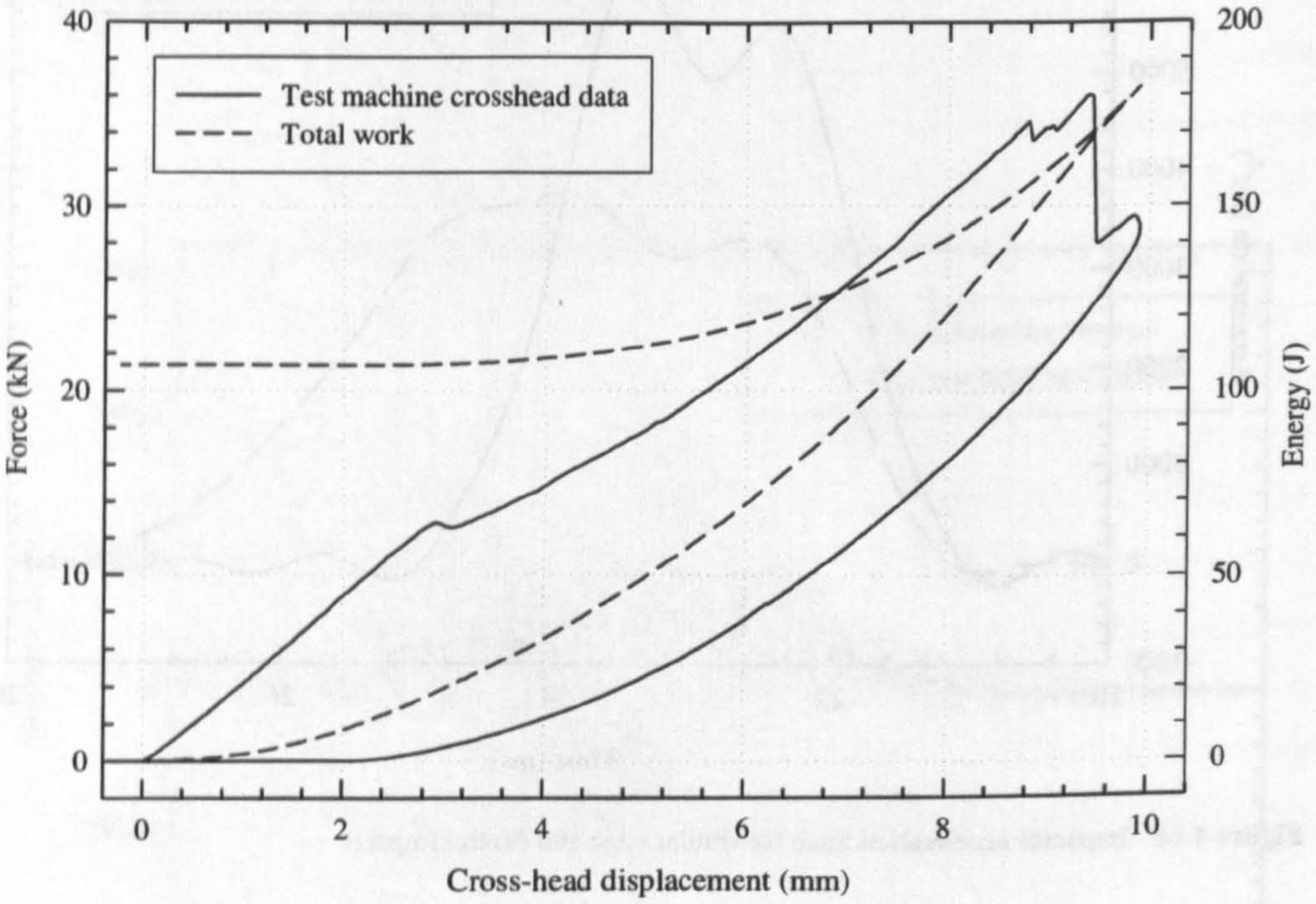

Figure 4.15 - Typical crosshead force-displacement data for a 200 J initial energy simulated impact on an 8 mm thick plate

4.6 RESULTS AND DISCUSSION

4.6.1 Introduction

Now that the test machines, methods and sample data have been shown, the actual results are presented in this section. Using the methods already presented, the impact duration times, maximum impactor forces and absorbed energy are compared for all the impacts as detailed in the test schedule in Figure 4.10.

The comparison between edge and central impacts is made and then the results for the effect of impact velocity are presented, including the applicable results from the simulated impacts. First however, the actual measured impact energy and absorbed energy for each impact are presented.

All the data in the following graphs can be found tabulated in Appendix B.

4.6.2 Absorbed Energy

Here, the measured absorbed energy versus the measured impact energy for all impacts using the full drop height of the impact machine are presented, in other words all those part of the edge versus central impact investigation. There are three energy levels, three panel thicknesses and two impact locations (edge and central).

Figure 4.16 shows the amount of energy absorbed by each plate at each impact energy level. There are six sets of points, relating to three different plate thicknesses and two different impact locations. The figure firstly shows that the actual measured impact energies are approximately 100 J, 200 J and 375 J. The level of absorbed energy shows a linear variation with impact energy, at 0.72 J/J, or at an average of 72% of impact energy absorbed by the plate, so that a larger impact energy entails more energy, or damage, absorbed by the plate. Also, there does not seem to be any clear pattern distinguishing the edge impacts from the central impacts. This is further examined in Figure 4.17 where the percentage of the impact energy is plotted. There is more scatter as might be expected as a ratio of two experimentally measured values is shown, but it shows more accurately that the proportion of the impact energy absorbed by the plate is approximately constant, or slightly increasing with larger impact energies. This increase is due to the nature of the damage that is being accumulated. It required a greater force, and more energy to break fibres compared to delaminations and matrix cracks. So with a higher energy, a different damage mechanism can dominate, and once several fibres have been broken, the plate stiffness drops more significantly than with matrix cracking, so the plate can deflect more, and hence more damage can be generated.

Figure 4.18 and Figure 4.19 show similar plots, on the same axes, for the plates impacted as part of the investigation into the effect of impact velocity. As the energy level in every case was nominally 200 J, there is only one data point cluster on each graph. Two plates were edge impacted in addition to the original test plan in Figure 4.10, one using the intermediate drop height on the impact machine, and one using the simulated impact on the quasi-static test machine.

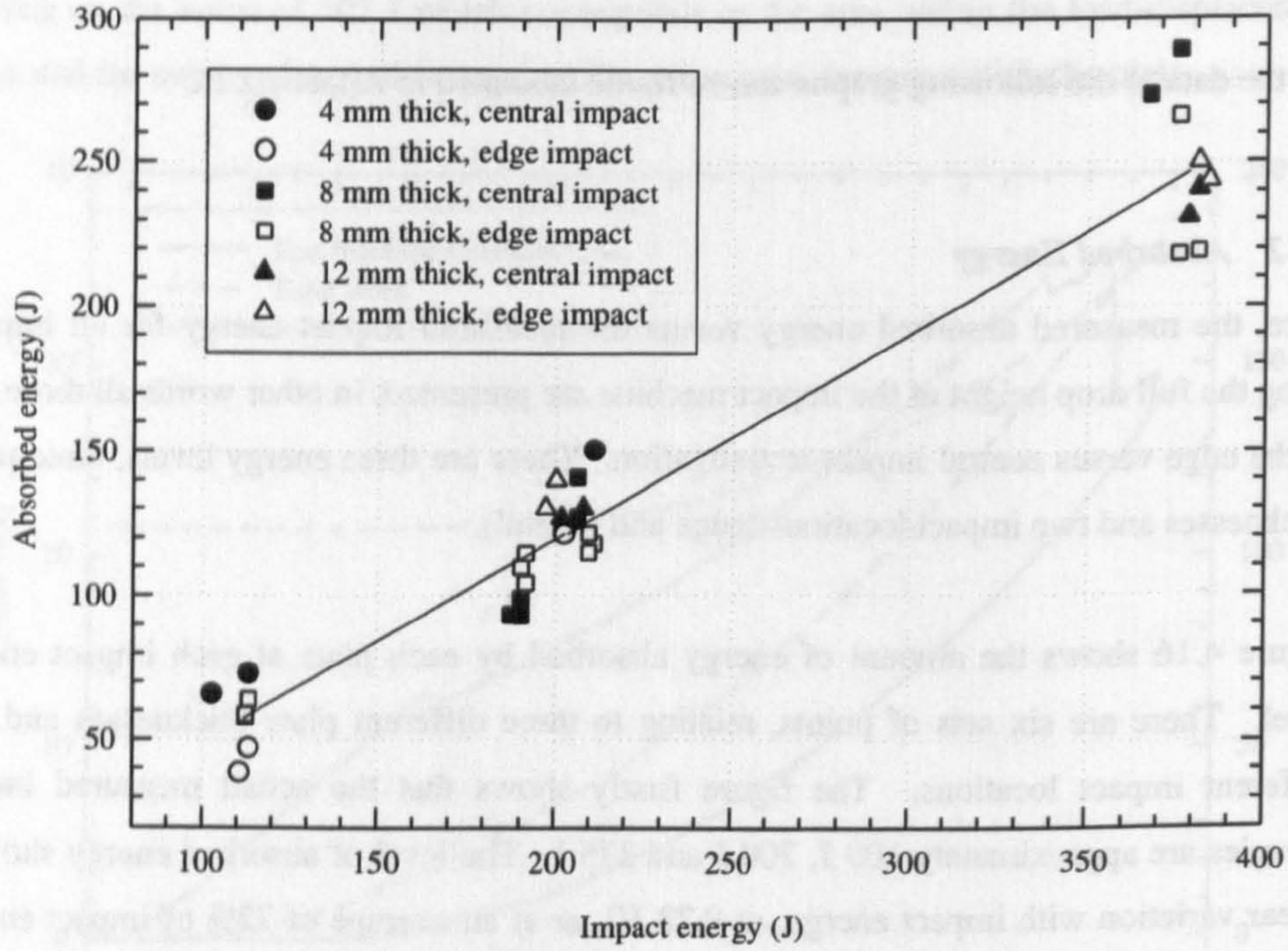

Figure 4.16 – Amount of the impact energy absorbed by the plate for all impacts from 4.3 m

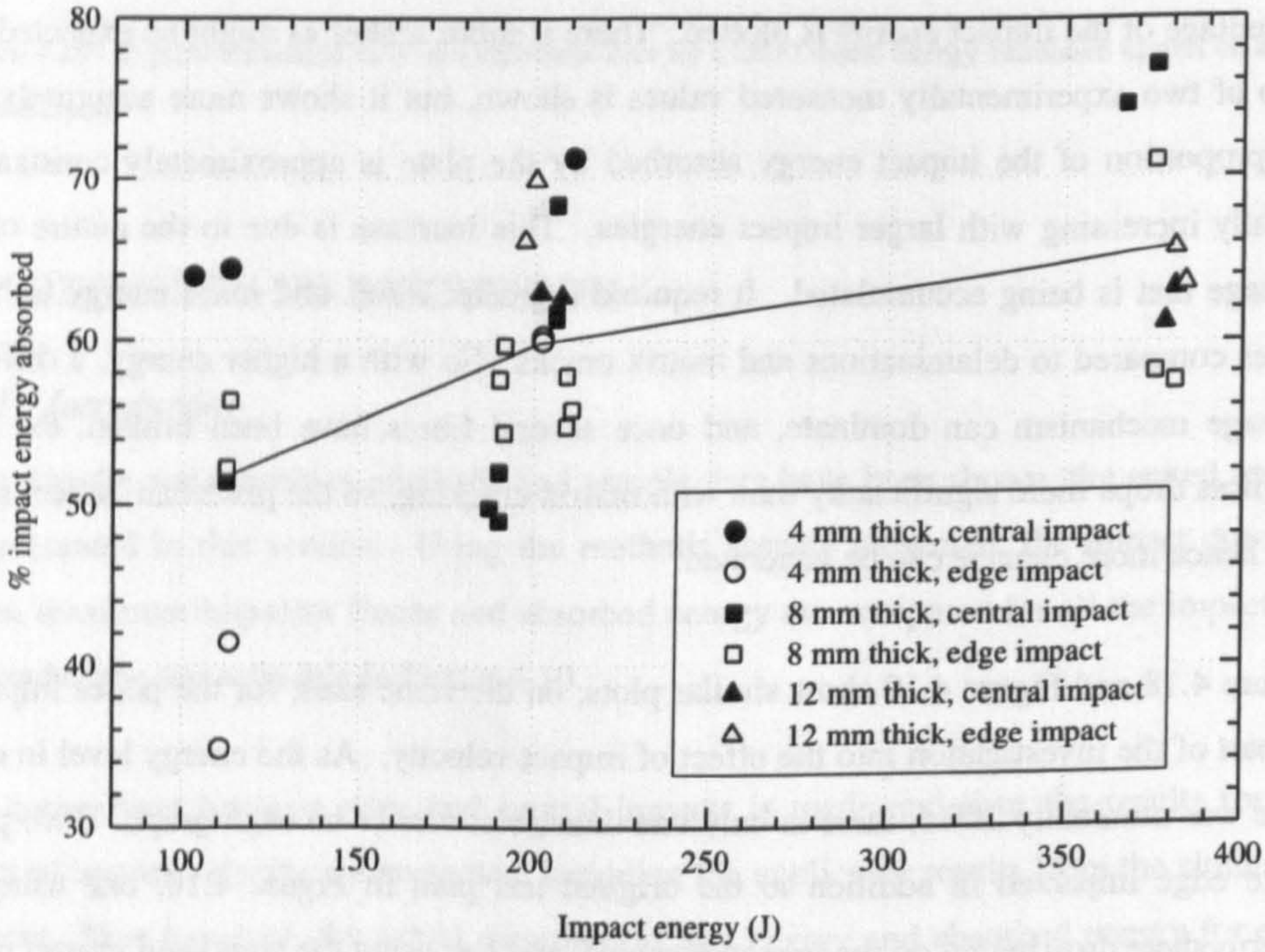

Figure 4.17 - The percentage of the impact energy absorbed by the plate for all impacts from 4.3 m

Again the figures show a good consistency in impact energy around 200 J. For the simulated impacts using a quasi-static test machine, the initial energy was calculated using the maximum deflection in the test and the measured initial bending stiffness.

There is very little difference observed between the edge and central impacts as before, with an overall average absorbed energy of 103 J at 52%, below in both cases compared to the values from Figure 4.16 and Figure 4.17. What can be drawn from this is that lower velocity impacts tend to lead to lower amounts of absorbed energy. Hence the damage is dependant more on inertial stiffening than the momentum of the impactor (see Table 4.2); the higher velocity impacts, though at the same impact energy and smaller momentum, appear stiffer and cannot deflect to absorb the energy and accordingly are damaged.

Table 4.2 - Comparison between impact energy and impactor momentum

Impactor mass (kg)	Impact velocity (ms^{-1})	Nominal impact energy (J)	Impactor momentum ($kgms^{-1}$)
n/a	0	200	0
12.17	5.4	200	65.7
4.67	9.2	200	43.0

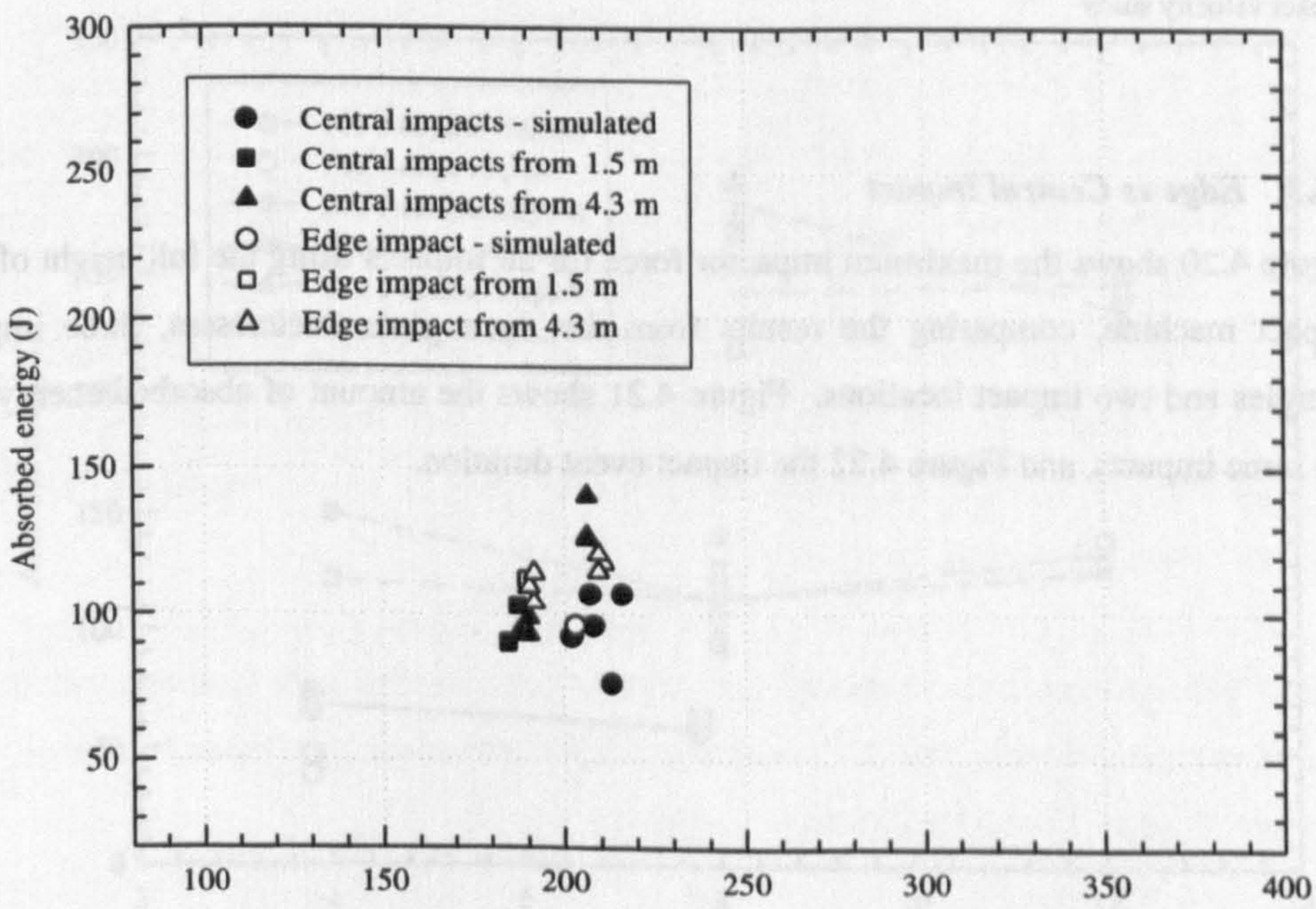

Figure 4.18 - Absorbed energy for all impacts part of the effect of impact velocity study

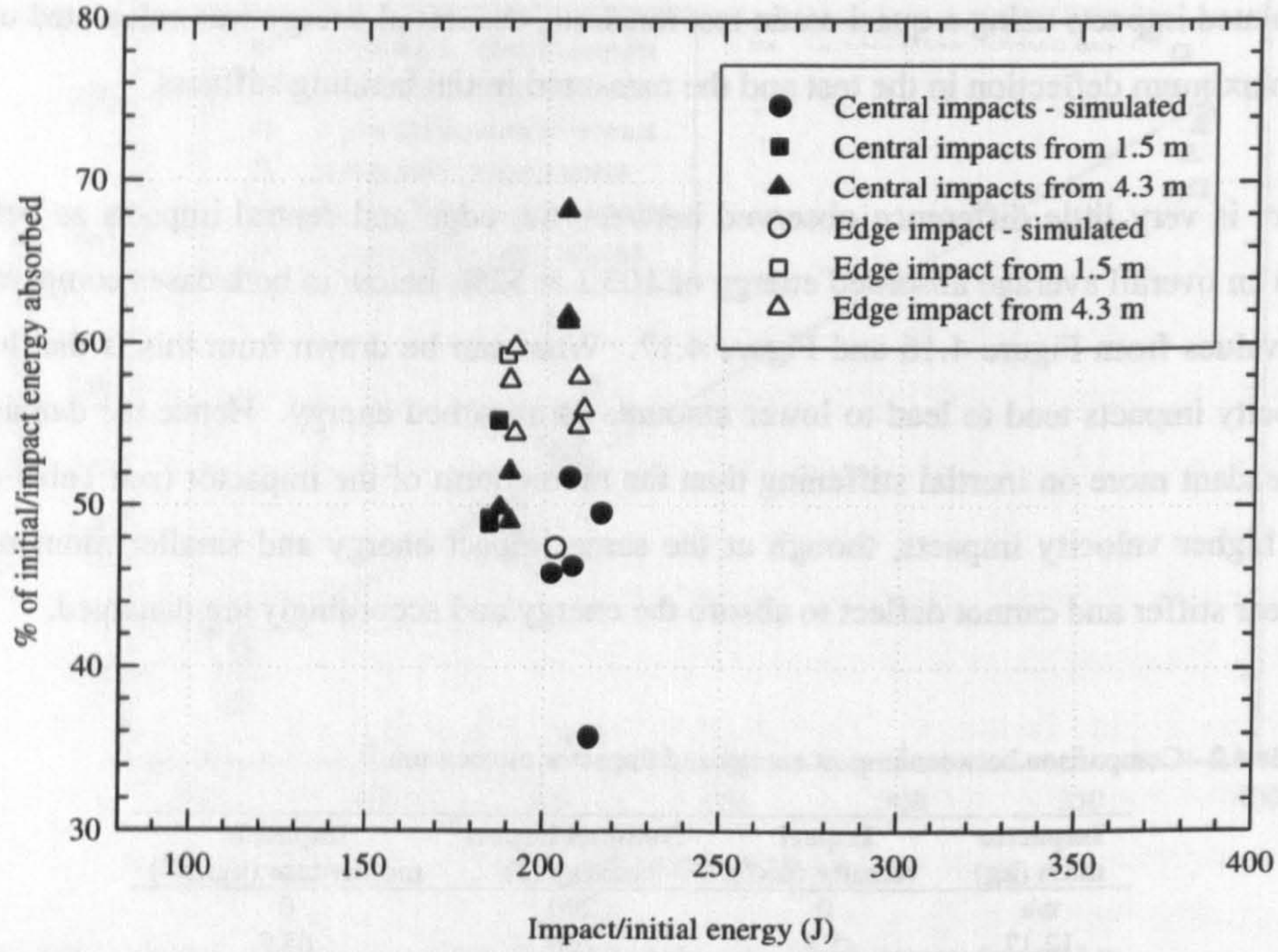

Figure 4.19 - The percentage of the impact energy absorbed by the plate for all impacts part of the effect of impact velocity study

4.6.3 Edge vs Central Impact

Figure 4.20 shows the maximum impactor force for all impacts using the full height of the impact machine, comparing the results from the three plate thicknesses, three impact energies and two impact locations. Figure 4.21 shows the amount of absorbed energy for the same impacts, and Figure 4.22 the impact event duration.

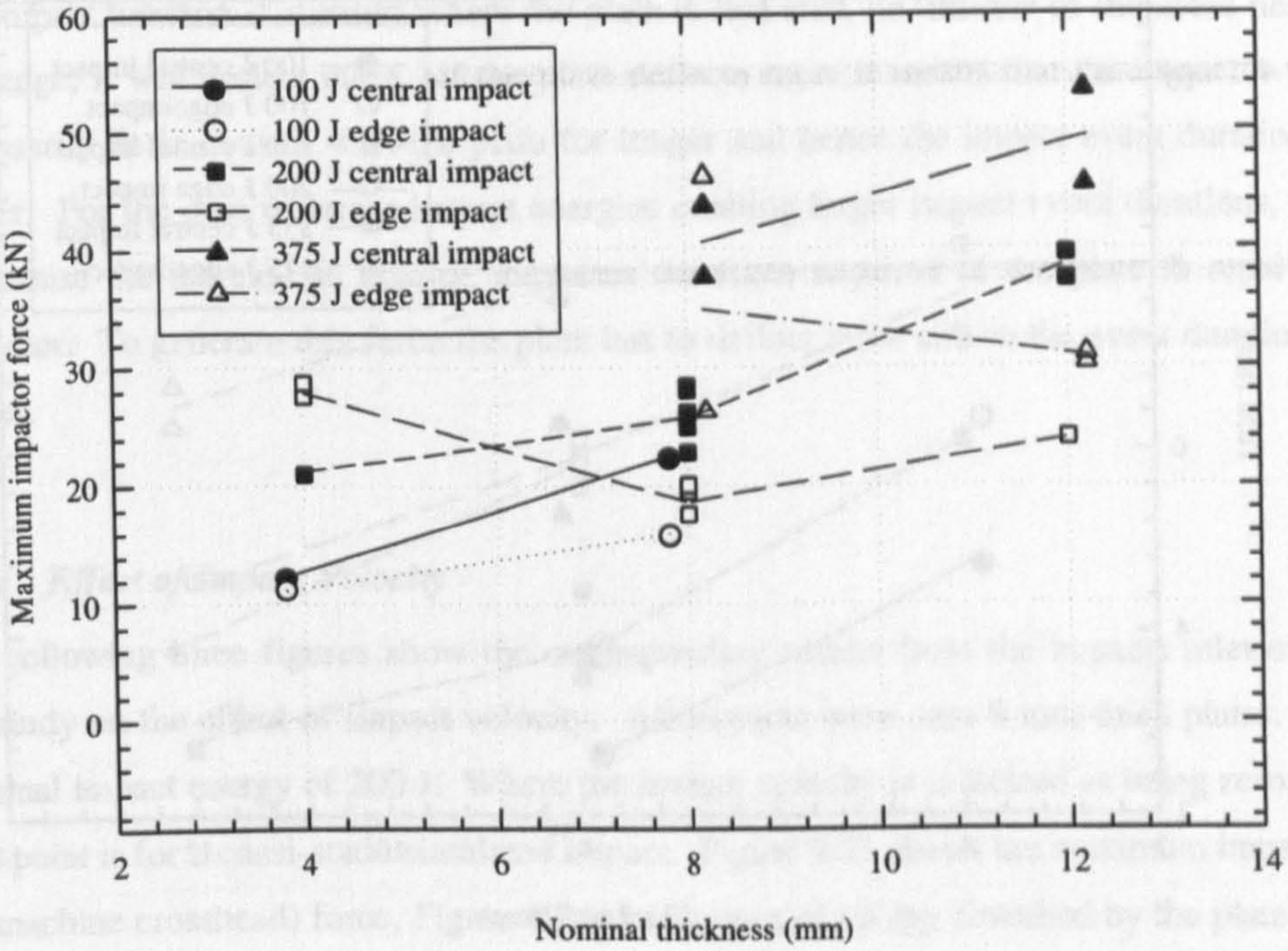

Figure 4.20 - Maximum impactor force for all impacts from 4.3 m

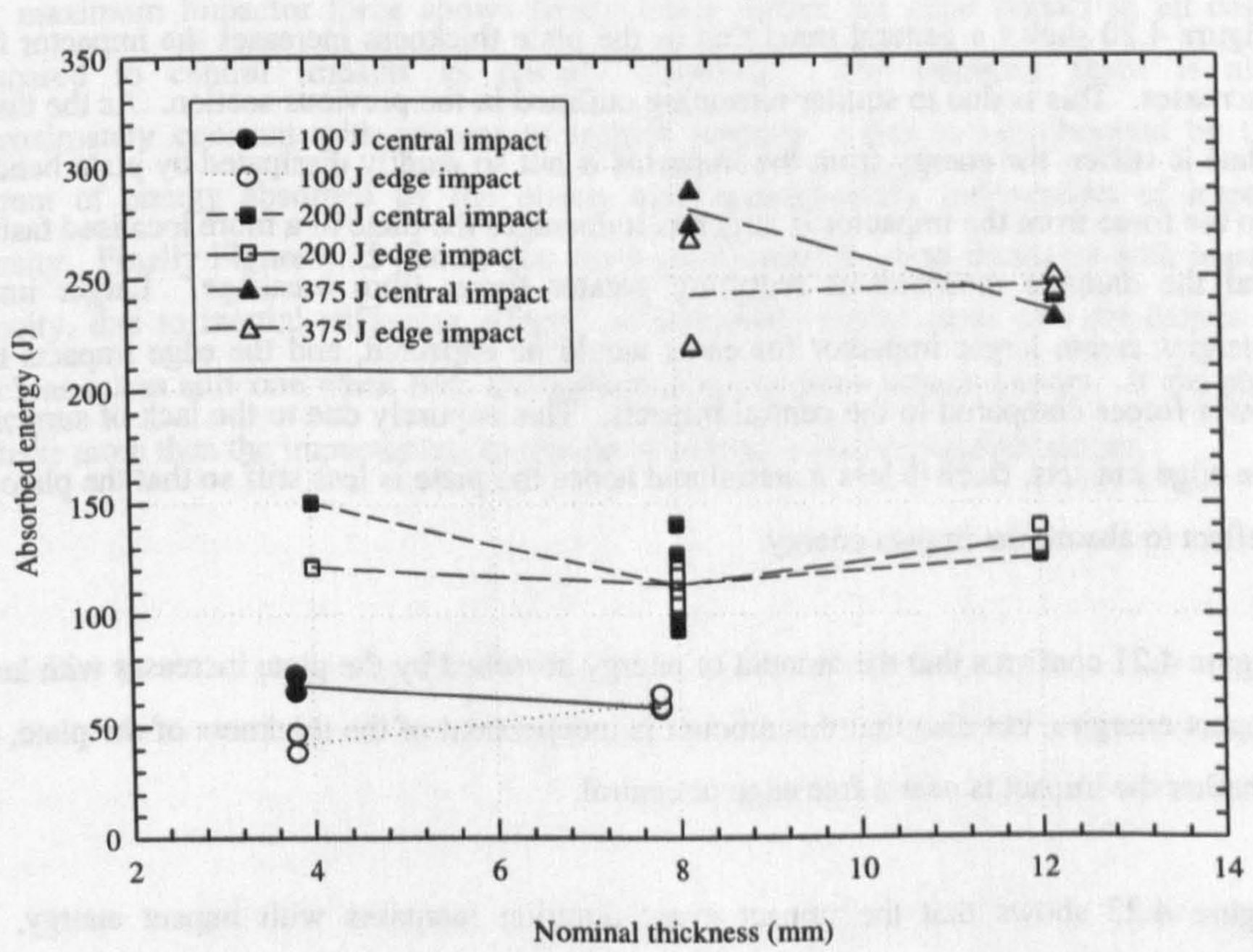

Figure 4.21 - Amount of energy absorbed by the plate in all impacts from 4.3 m

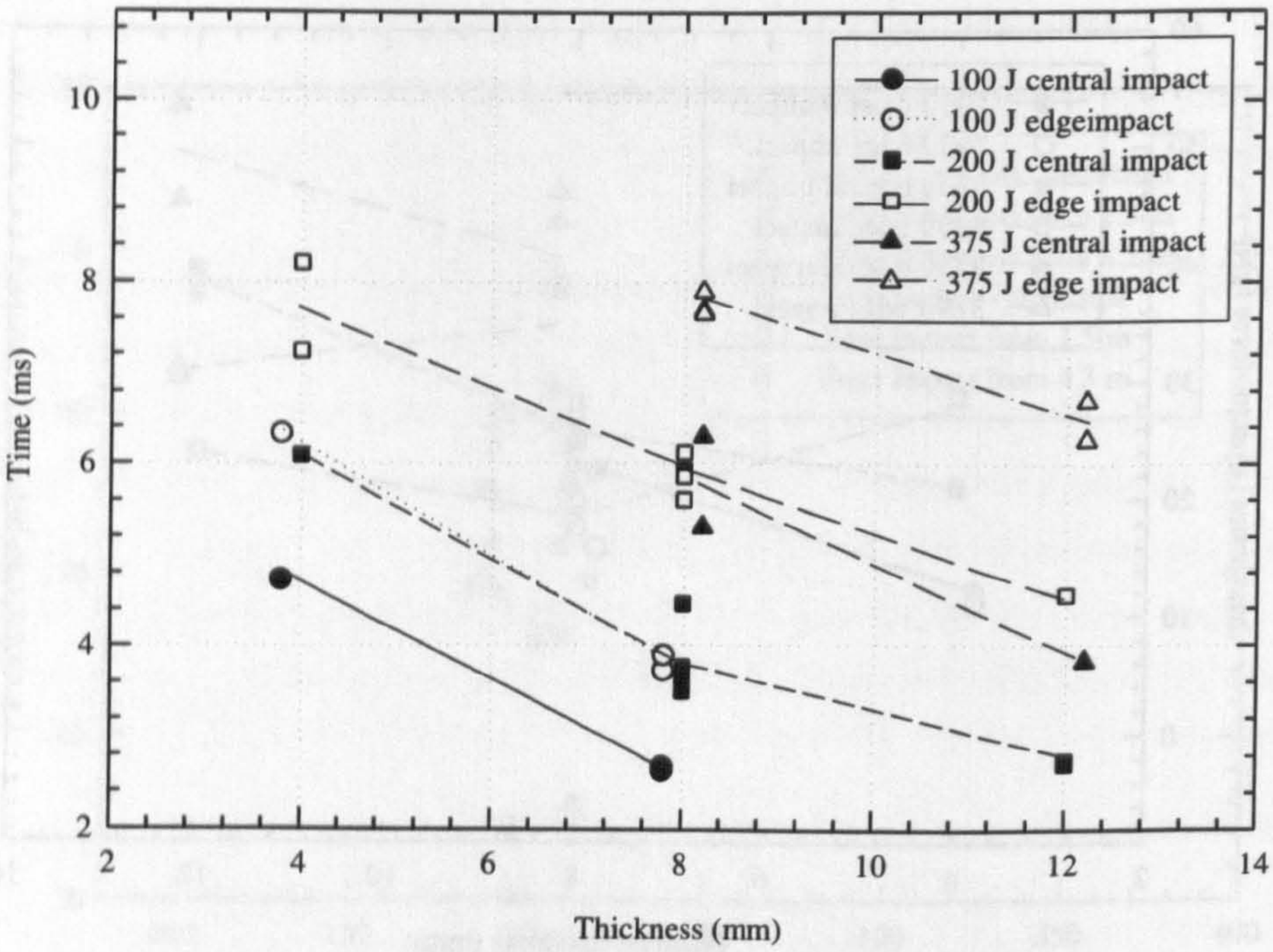

Figure 4.22 – Impact event duration for all impacts from 4.3 m

Figure 4.20 shows a general trend that as the plate thickness increases the impactor force increases. This is due to similar reasoning outlined in the previous section. As the thicker plate is stiffer, the energy from the impactor is not so readily dissipated by plate bending. So the force from the impactor is larger as it damages the plate in a more localised fashion, and the damage mechanisms requiring greater force: fibre breakage. Larger impact energies create larger impactor forces as would be expected, and the edge impacts have lower forces compared to the central impacts. This is purely due to the lack of support in the edge impacts, there is less material and hence the plate is less stiff so that the plate can deflect to absorb the impact energy.

Figure 4.21 confirms that the amount of energy absorbed by the plate increases with larger impact energies, but also that this amount is independent of the thickness of the plate, and whether the impact is near a free edge or central.

Figure 4.22 shows that the impact event duration increases with impact energy, but decreases with thickness and central impacts. The reason for this dependence on thickness

and impact location is similar: where the plate is less stiff, i.e. thinner or impacted near a free edge, it will deflect more. If the plate deflects more it means that the impactor will necessarily be in contact with the plate for longer and hence the impact event duration is longer. For the case of larger impact energies creating larger impact event durations, this is because the increase in energy, increases the force required of the plate to repel the impactor. To generate this force the plate has to deflect more and so the event duration is longer.

4.6.4 Effect of Impact Velocity

The following three figures show the corresponding results from the impacts relevant to the study on the effect of impact velocity. All impacts were onto 8 mm thick plates, at a nominal impact energy of 200 J. Where the impact velocity is indicated as being zero, the data point is for a quasi-static simulated impact. Figure 4.23 shows the maximum impactor (or machine crosshead) force, Figure 4.24 the amount of energy absorbed by the plate and Figure 4.25 the impact event duration for the two dynamic impact types.

The maximum impactor force shows firstly lower values for edge impact in all cases compared to central impacts as already observed. The impactor force is also approximately constant with respect to impact velocity. This is corroborated by the amount of energy absorbed by the plates, also approximately independent of impact velocity. Finally Figure 4.25 shows that the impact event duration decreases with impact velocity, due to inertial stiffening effects: an apparently stiffer plate will not deflect as much as a less stiff one when both are subjected to the same impact energy. If the plate deflects more then the impactor has to remain in contact with the plate for longer.

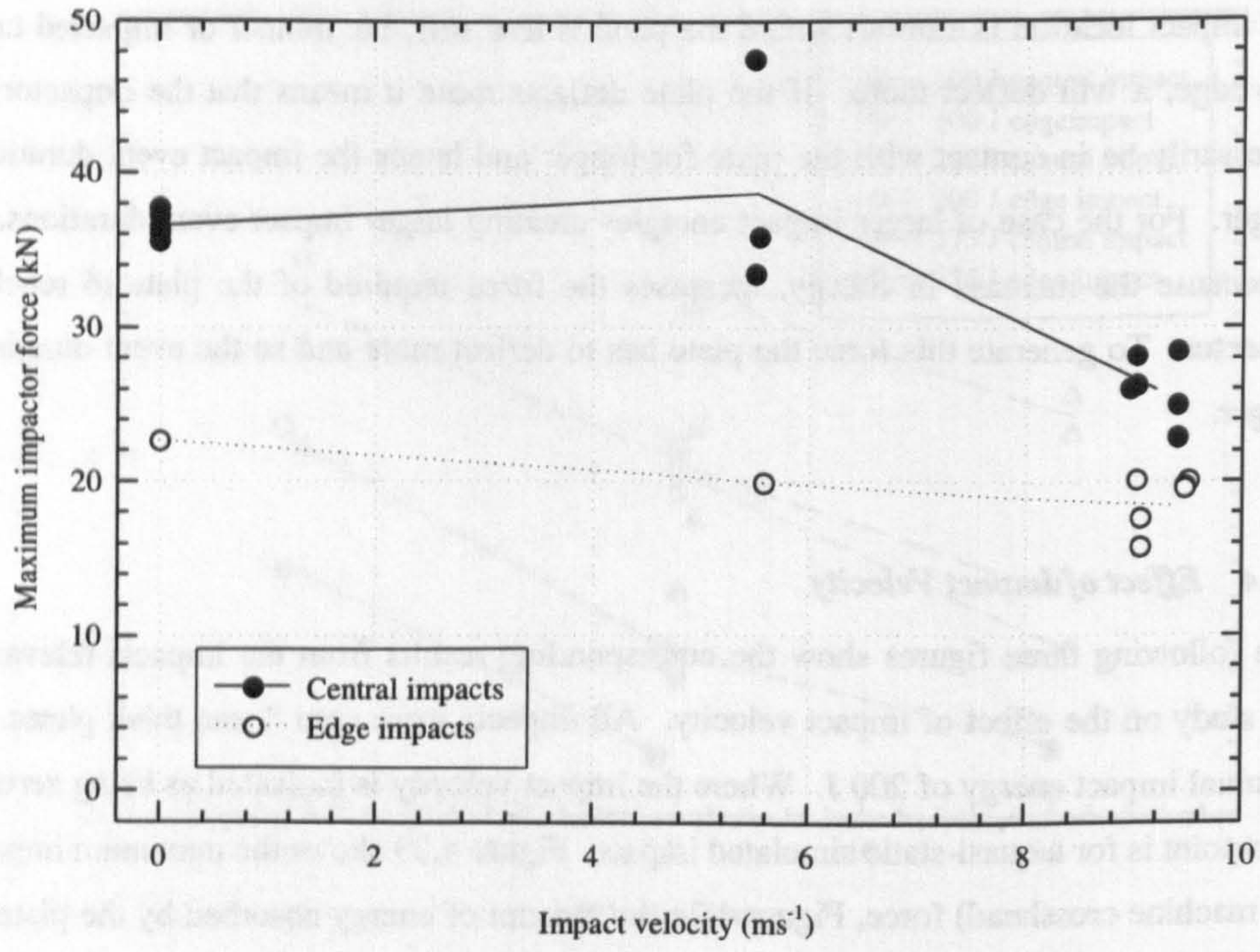

Figure 4.23 - Maximum impactor force for edge and central variable velocity impacts

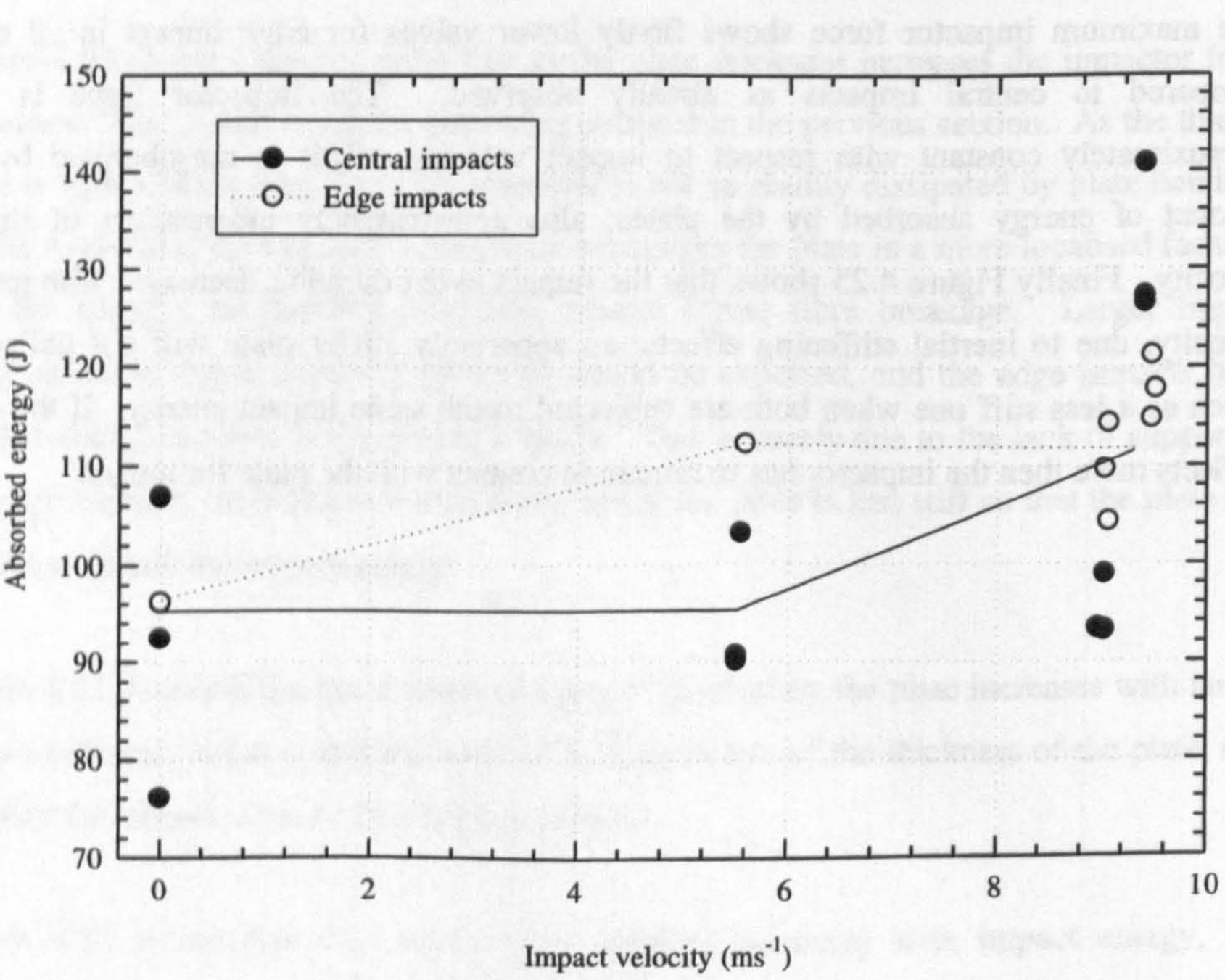

Figure 4.24 - Amount of energy absorbed by the plate for edge and central variable velocity impacts

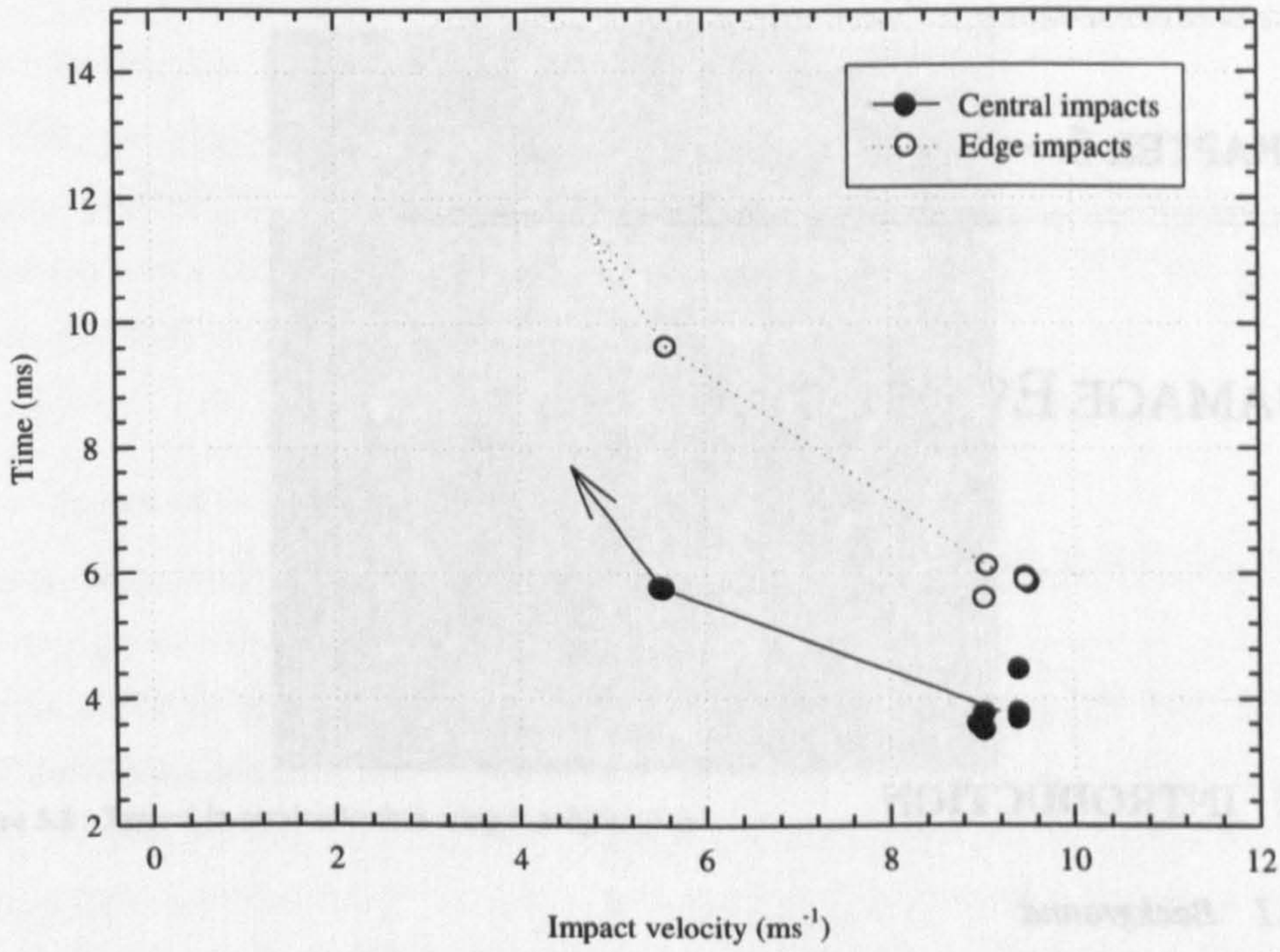

Figure 4.25 - Impact event duration for the slow and fast, edge and central variable velocity impacts

4.7 CONCLUSIONS

In this chapter the design of the impact machine was presented. The test methodology and matrix were also presented.

The data from the instrumented impact machine was successfully analysed to produce impact energy absorption, maximum impact force and impact event duration for each impact. The trends show that the proportion of the impact energy absorbed by the plate is constant with impact energy at 70%, for both central and edge impacts. A consistently larger maximum impact force was recorded for thicker plates for both edge and central impacts whereas the impact event duration consistently decreased. In the impact of constant energy but variable impact velocity, the maximum impactor force is insensitive to the velocity, but the impact event duration decreases with faster impact velocities.

CHAPTER 5

DAMAGE EVALUATION

5.1 INTRODUCTION

5.1.1 Background

In this chapter the efforts to measure and explain the effects of the damage imparted to the composite plates by the impacts administered as per the previous chapter are presented. As already discussed, thick laminates are being designed for use as wing skins on large civil aircraft where the laminate's best property, in-plane elastic modulus and strength, will be exploited. The typical sources of load to a wing are illustrated in Figure 5.1, and include loads due to the aerodynamic lift, the wing's weight, the landing gear and engine thrust. It is important to understand how impact damage will affect the performance of the wing under these load cases.

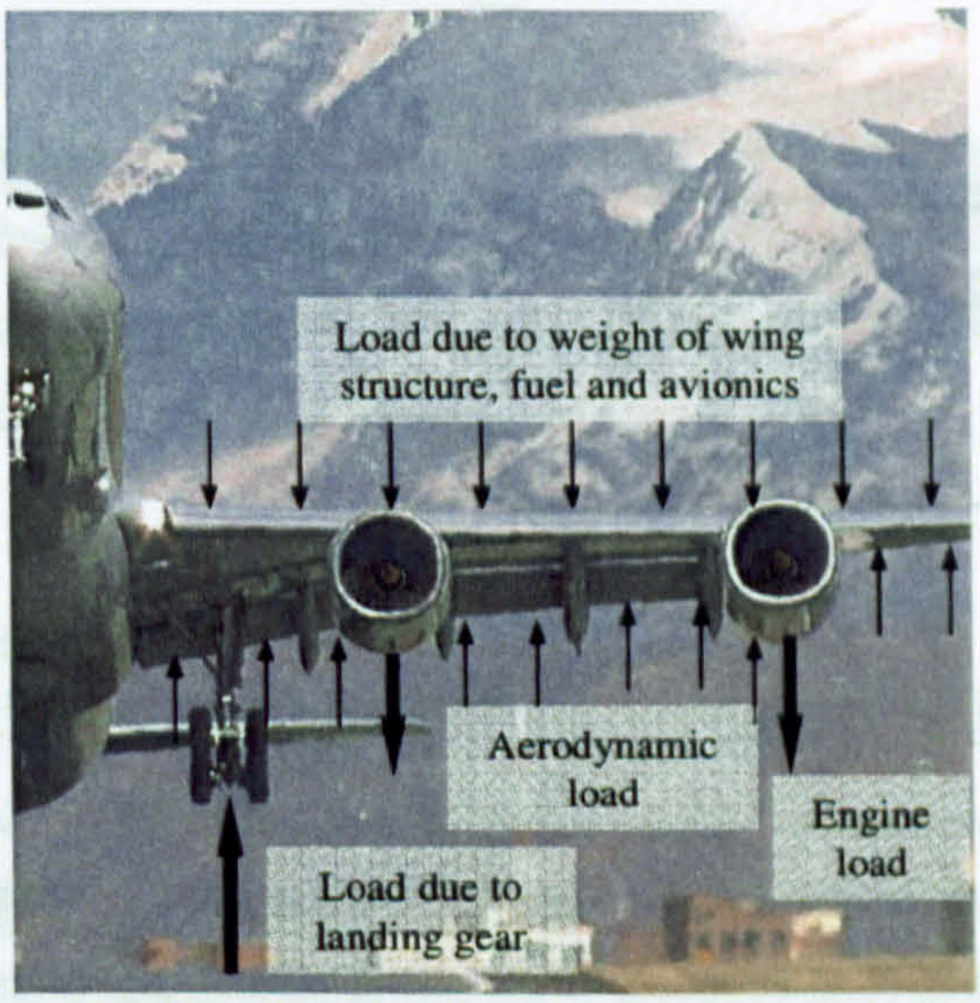

Figure 5.1 - Typical in-service loads a wing is subjected to

5.1.2 Aims

The first aim is to measure the residual strength of the impacted composite plates. The usual practice is to measure the compressive strength, as this is where the plate will experience the biggest strength drop due to the delaminations common in impacted laminates. The impacted plates were also tested in tension to measure the extent of fibre breakage. It is likely that the wing will sustain an impact to the lower skin, from runway debris for example, as it will to the upper skin, from a dropped tool for example, so it is important to study impacted plates in compression and tension. In addition both the upper and lower skins will experience compressive and tensile loads during service, depending on the load case for example high altitude cruise (up bend), strong down gust (down bend), and stationary (down bend), see Figure 5.2.

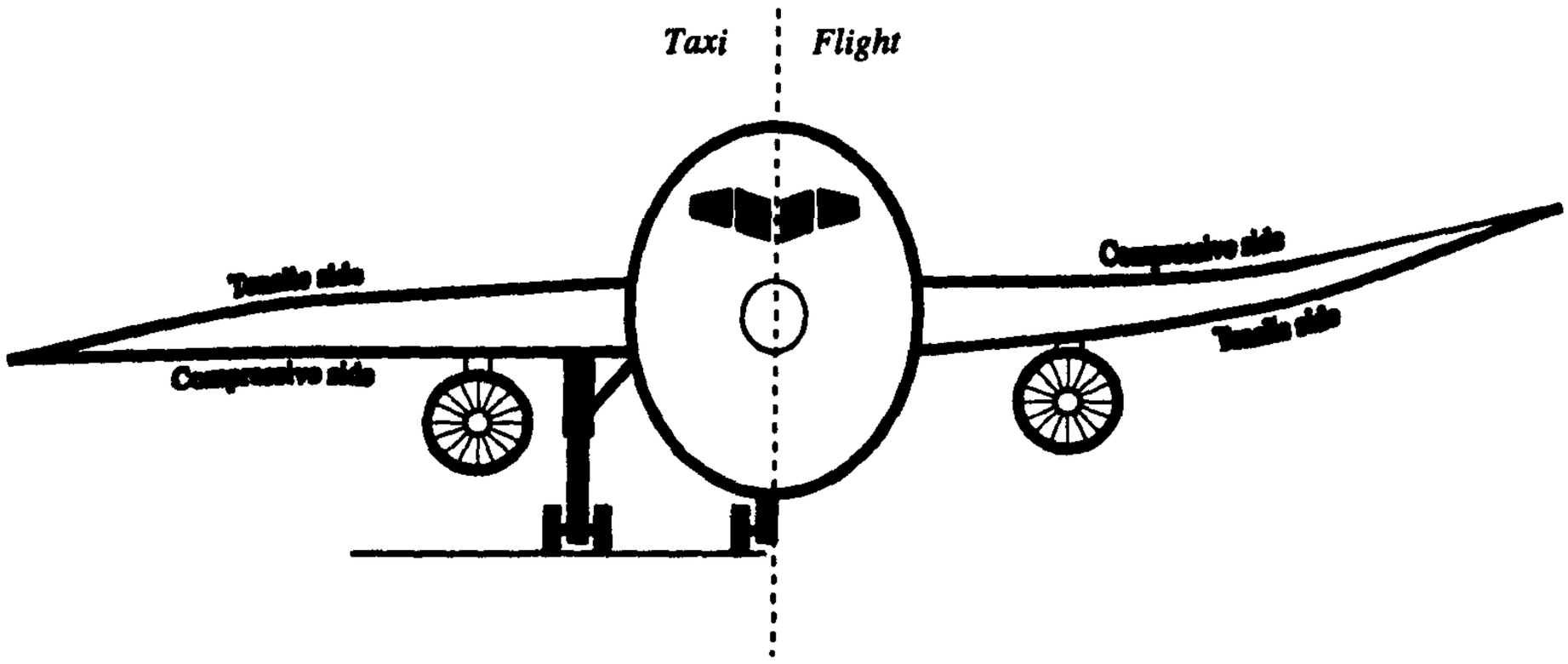

Figure 5.2 - Both top and bottom surfaces of a wing can be in compression or tension

The second aim is to further characterise the damage in the impacted plates. This is possible with a number of techniques. Firstly, the most simple, visual inspection of the surface and edges of the laminate can reveal information such as back face burst type splitting damage, impactor indent crush zone and in-plane edge cracking. Another, more useful, non-destructive technique, is the ultrasonic C-scan where a transducer is used to determine internal damage otherwise impossible to see with the naked eye. This system is best used to determine the extent of delaminations within the laminate, although it will not necessarily detect where delaminations overlap. Finally a destructive technique is employed, the resin burn-off and deply method. This is where, after careful pyrolysis, the laminate is deconstructed by removal of individual plies, after which damage (in particular fibre breakage) to the individual plies is obvious. It is difficult to detect delamination using this technique without using a penetrant that remains after the pyrolysis. These penetrants are usually gold based, and hence prohibitively expensive.

5.1.3 Chapter Structure

In this chapter, firstly, efforts to measure the residual strength of the laminates are presented with the results. Then the damage pattern analysis is presented, and the results from the various non-destructive and destructive techniques. Finally the results are discussed with a view to providing corroborating evidence to why the laminates failed at the load they did.

5.2 RESIDUAL STRENGTH

5.2.1 Introduction

The impacted plates had coupons cut from them with the damage in their centre. These coupons were loaded into a test machine and tested to destruction in either tension or compression in a standardised, repeatable manner. Initially, to obtain base line values, undamaged sections of laminate were tested.

5.2.2 Specimen Preparation

Coupons were cut from the impacted plate using a water-cooled circular diamond saw. The damage was always central to the coupon, and the coupons were cut to be 50 mm wide, as shown in Figure 5.3. This width was chosen as the widest possible that could still be failed in tension to encompass as much of the damaged region as possible. The capacity of the test machine was 500 kN, and the strength of undamaged laminate was 1 GPa (26 x 8 mm section, see Table 3.14). Thus, for 50 mm wide, 8 mm and 12 mm thick undamaged laminates the failure load would be 400 kN and 600 kN respectively. It was also known that, as the specimens were not end tabbed, the maximum load would be limited by shearing of the top layer of the coupon by the serrated grips, below 350 kN. This maximum possible applied load is proportional to the specimen width, so it was important that enough impact induced fibre damage was present to ensure the coupons would fail. By using narrower specimens, the maximum possible applied load would drop, but the failure load of the specimen would decrease by more as there would be a greater percentage of broken fibres. The specimens were not end tabbed because it was thought that the adhesive used to bond the tabs would fail before the specimen.

It would have been ideal to design specimens that encompassed all the impact damage, but as mentioned the capacity of the test machine limited what was possible. However this does not reduce the validity of the results as the significant damage is included, and all specimens were treated in the same manner.

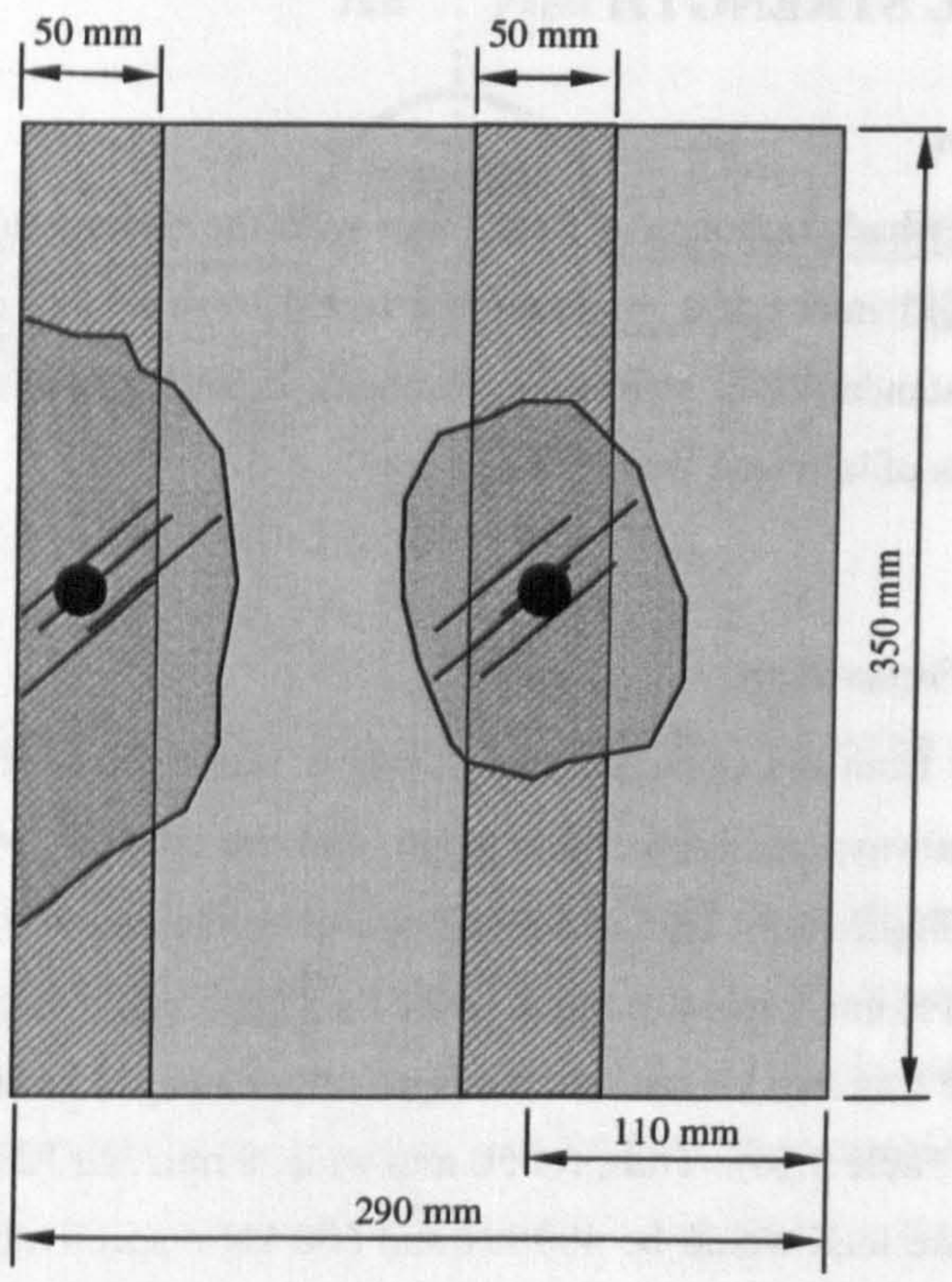

Figure 5.3 - Specimen cutting diagram

The specimens were measured, their width and thickness recorded in at least four different positions using a digital calliper and micrometer. Finally they were marked to show where they were to be gripped in the test machine: 110 mm gripping length at each end for all tensile tests and 100 mm for all compression tests. This left gauge lengths of 130 mm for tensile tests and 150 mm for compression tests. The reason for the difference was that it was desirable to have the gauge length as long as possible so that the longest delamination would not be between the grips. It was found, however, that more grip length was required for the tensile tests in order to fail the specimens, so the maximum possible of 110 mm was used.

5.2.3 Test Method

The Mayes 500 kN hydraulic test machine was used, the same machine as used for the simulated impacts and earlier laminate strength tests, see Section 3.4.4 and Figure 3.14. This machine was chosen because of its large load capacity and hydraulic grips. The grips

were important, as other gripping options were deemed unsuitable. Traditionally wedge grips are used in tensile tests, and they increase the gripping load on the specimen as the applied load increases by way of a wedging action (see Figure 5.4). With such a system it was thought that there was a strong likelihood that failure would occur compressively in the gripped portion of material as the applied load was expected to be very high, and hence the gripping load accordingly high. With hydraulic grips a gripping pressure is chosen and is independent of the applied load (although it still has to be high enough to prevent slippage).

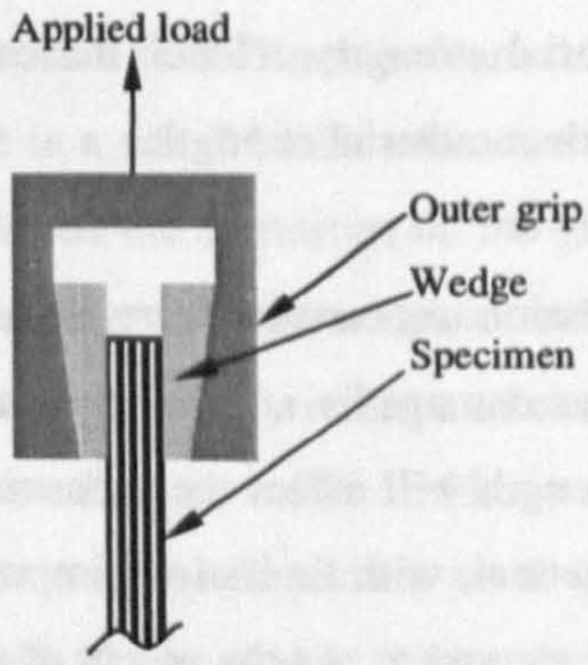

Figure 5.4 - Schematic of a wedge grip

The same test method as described in Section 3.4.4 was used, whereby the specimens were carefully loaded into the machine ensuring correct alignment along the loading axis by measuring the specimen's location, and then the machine, under displacement control, used to fail the specimen whilst recording crosshead displacement and force.

Care was taken in every test to ensure that the coupons failed in their gauge length and a sensible displacement rate was chosen to ensure that they were safely within the quasi-static region. No end tabs were used as it was thought that either the adhesive or the tab would likely fail before the coupon and the intention was that the damage in the coupon would be enough to ensure its failure before failure in the grips. A displacement rate of 0.01 mm/s was used in tensile tests and 0.005 mm/s in compression tests with failure occurring within 2 minutes.

It is common in some research to use an anti-buckling guide during compression tests to ensure that specimen buckling does not occur. Such a device is not employed in the compression tests in this research for two reasons. Firstly, and most significantly, the delaminations, in the edge impacted specimens especially, are very large: easily spanning the full width of the 50 mm wide coupons, and it was thought that to use an anti-buckling guide would be to, in effect, constrain any effect of the delaminations. It is the delaminations that have the greatest effect in reducing the in-plane compressive strength. Also when a plate is impacted on a real structure, it is the structural strength, not the material strength that will determine whether it fails, although the structural strength is dependent on the material strength. Hence the compression tests used here are more a structural stability test than material strength.

The tensile and compression tests are arbitrary as the results are dependent on the coupons' width and length. The damage is not wholly encapsulated by the coupon width, and changing the coupon length will affect the measured compressive strength. The reasons for this are entirely practical, with limitations imposed by the test machine, and its ability to deliver end load to the coupon. As the extent of the damage was commonly at least 100 mm across the width, a coupon width of 120 or 140 mm at least would have been ideal. However it would not have been possible to fail the specimen and new grip inserts would have been required. What the current test set-up and coupon design does allow is a repeatable and practical method to evaluate the damage in a way that enables comparison between different specimens. The extent of the delamination width is captured by C-scan. The compression tests will evaluate the effect of the number of delaminations and sub-laminates, and their length. The tensile tests will evaluate the effect of the amount of fibre breakage in the centre of the specimen. Hence no important damage mode is neglected.

5.2.4 Results and Discussion

5.2.4.1 Photographs and Descriptions of Specimen Failure

The tensile coupons failed by a sudden, brittle fracture. The compressively tested coupons failed either with a sudden brittle failure or a more gradual load reduction preceded by a linear load-displacement curve. The load-displacement curves are unreliable for estimating the coupon elastic modulus, as there is a small amount of slippage in the grips

as the serrations cut into the top layer of the composite, and the stiffness of the test machine is included also. The strain values on the abscissa of the following graphs are calculated using the cross-head displacement and hence should not be considered to be real strain values.

Here some specimens have been selected as producing typical results, and their failure has been recorded photographically for discussion.

Firstly, Figure 5.5 shows the stress-strain curve from a tensile test for an 8 mm thick coupon with central impact damage from a 200 J impact from 4.3 m, and a photograph taken the moment after failure. There is a small kink in the curve at approximately 240 MPa. This is thought to be the point when the serrations on the grips cut through the top layer of the composite; this is common to most tensile coupons and happens at around 110 kN. Following this the slope of the curve gradually reduces as the grips shear off the top layer of the composite, until the coupon fails in a full width catastrophic fracture. The shearing of the top layer of the laminate is not important as it does not affect the final failure of the specimen. The photograph shows that at failure the specimen failed across the width in the impact damaged area in its centre.

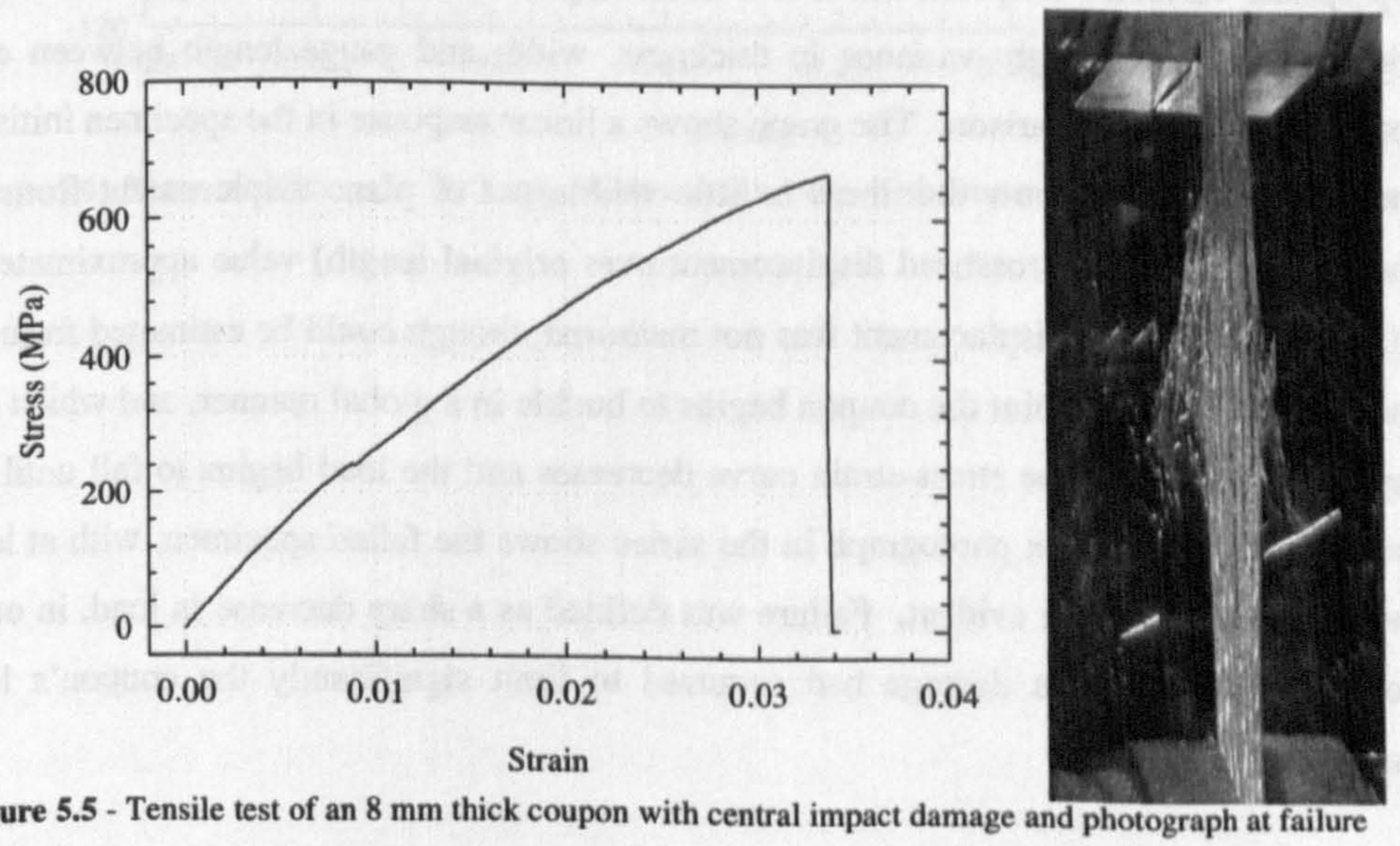

Figure 5.5 - Tensile test of an 8 mm thick coupon with central impact damage and photograph at failure

The full capacity of the Mayes test machine of 500 kN was never reached as the maximum possible load in tension was approximately 320 kN due to the reason already discussed in

Section 5.2.2, where the serrated grip inserts cut into the top layer of the composite, and proceeded to shear it off. In cases where this had started to happen, in order to save wasting the coupon, the gripping pressure was carefully increased as it always decreased during a tension test due to contractions in the thickness of the coupon. When the shearing of the top layer starts it is characterised by a decrease in the rate of increase of the applied load until the load displacement trace goes flat and then drops. Increasing the gripping pressure has the effect of relieving some of the applied load (squashing the ends of the coupon effectively puts a compressive load on it) and was done smoothly and slowly to prevent any failure between the grips. The gripping area was always as large as possible so it was not possible to grip a longer part of the coupon. Where increasing the gripping pressure did not succeed, some unfailed coupons were trimmed to a narrower width of 30 mm in an attempt to fail them in tension, but this had only limited success.

Figure 5.6 and Figure 5.7 illustrate the compressive failure of a 4 mm thick coupon that had edge impact damage from a 100 J impact from 4.3 m. Figure 5.6 shows the stress-strain curve (in the negative quadrant as it is a compression test) marked with nine points that refer to the corresponding photograph of the coupon in Figure 5.7. When dealing with a buckling type stability failure, stress and (axial) strain are not necessarily the most appropriate variables to quote, but it was necessary to normalise the compressive results with respect to the slight variance in thickness, width and gauge length between each coupon to enable comparison. The graph shows a linear response in the specimen initially, and the photographs show that there is little visible out of plane displacement from the coupon until a strain (crosshead displacement over original length) value approximately -0.0025. Out of plane displacement was not measured, though could be estimated from the photographs. At this point the coupon begins to buckle in a global manner, and whilst this happens the slope on the stress-strain curve decreases and the load begins to fall until the specimen fails. The last photograph in the series shows the failed specimen, with at least one major delamination evident. Failure was defined as a sharp decrease in load, in other words when significant damage had occurred to limit significantly the coupon's load carrying capability.

The compression tests attempt to simulate testing a structure, for example a plate between stringers. It could, however, be argued that a plate with damage reacts differently to a coupon with damage across its full width. As already described this does not invalidate

these tests as all specimens were treated in the same manner. The purpose of the tests was to investigate the effect of the different damage types arising from the different types of impact, and this is achieved as only the peripheral damage is omitted and clear patterns are observed in the results.

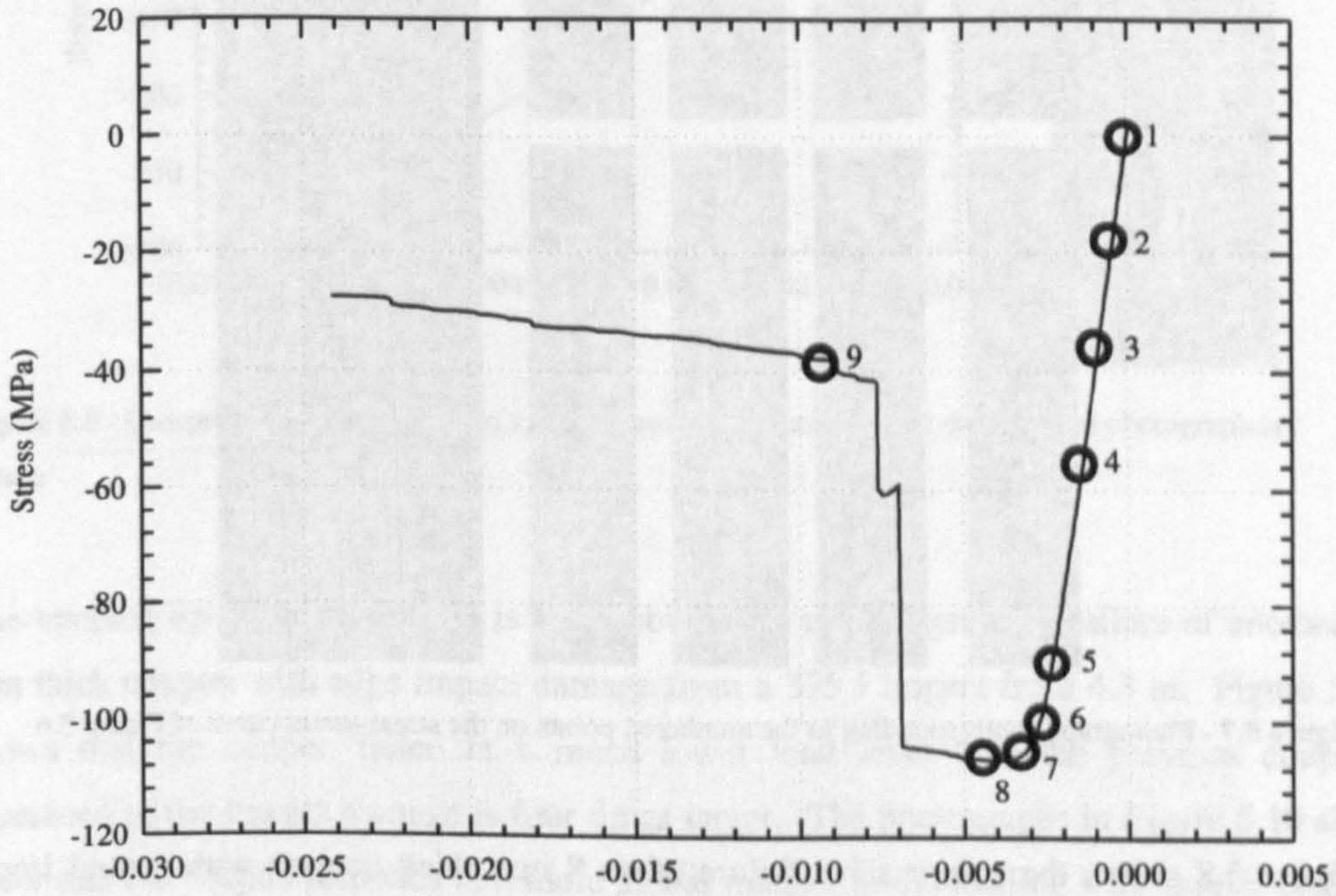

Figure 5.6 - Stress-strain curve for the compressive test of a 4 mm thick coupon with edge impact damage

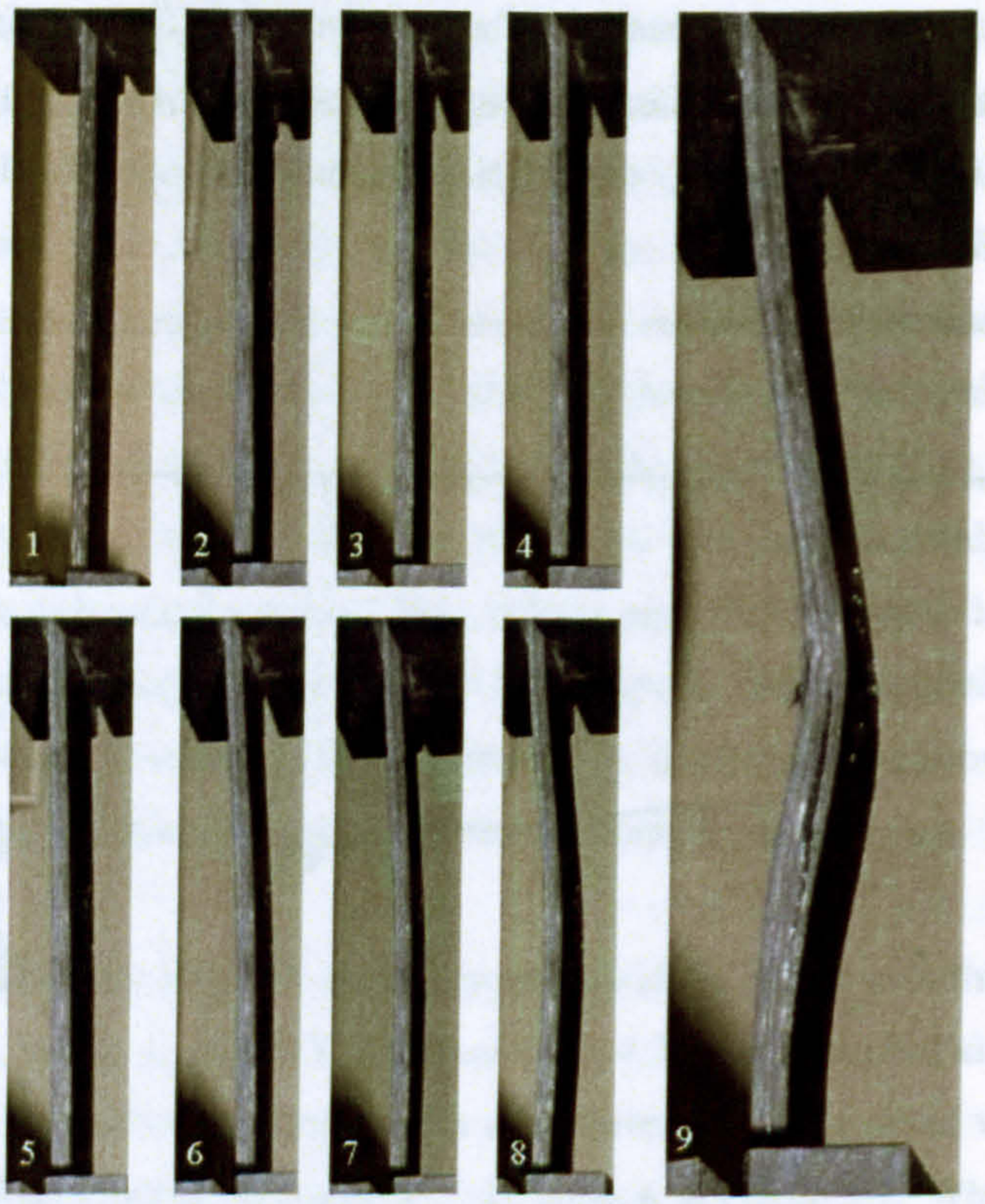

Figure 5.7 - Photographs corresponding to the numbered points on the stress-strain curve of Figure 5.6

Figure 5.8 shows the compressive failure of an 8 mm thick coupon with central impact damage from a 100 J impact from 4.3 m. The photograph of the specimen at failure shows that the specimen did not buckle globally, but with a more local failure with many delaminations opening up, showing at least five sub-laminates. The slight kink in the stress-strain curve at approximately –230 MPa corresponds again to the moment when the grips cut into the top layer of the composite, again at approximately 110 kN only this time in a compression test. Note that it may look like the grips have displaced sideways relative to each other in the photograph, but this is an illusion due to the angle of the picture and the fact that the grip inserts are much wider than the coupon.

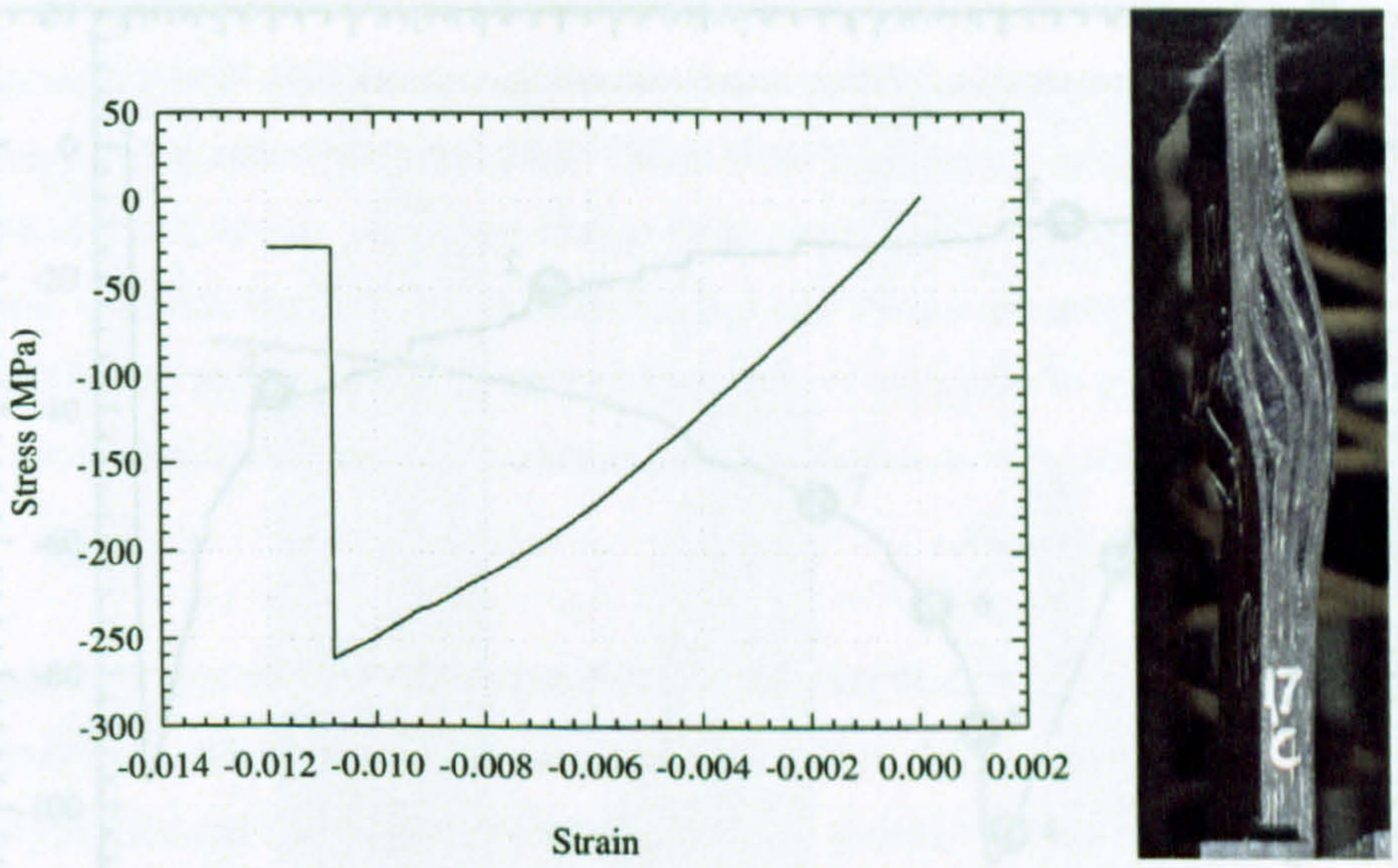

Figure 5.8 - Compression test of an 8 mm thick coupon with central impact damage and photograph at failure

The opening up of delaminations is more obvious in the compressive failure of another 8 mm thick coupon with edge impact damage from a 375 J impact from 4.3 m. Figure 5.9 shows that the coupon failed at a much lower load level than the previous coupon examined as the impact damage is four times larger. The photographs in Figure 5.10 also show that the coupon responds in a more global manner to the loading with several cracks apparent at failure spanning close to the whole length of the specimen. The ultrasonic C-scans will later show that the largest delamination caused by the impact was of that order of length also.

As the test continued post failure those delaminations were opened up further until it was possible to see that they indeed also spanned the full width of the specimen.

Figure 5.11 and Figure 5.12 show the compressive failure of a 12 mm thick coupon with edge impact damage from a 200 J impact from 4.3 m. The coupon's response is linear with no visible out of plane displacement until failure, which the photographs show to be a local buckling failure. The final photograph shows at least five cracks in the coupon.

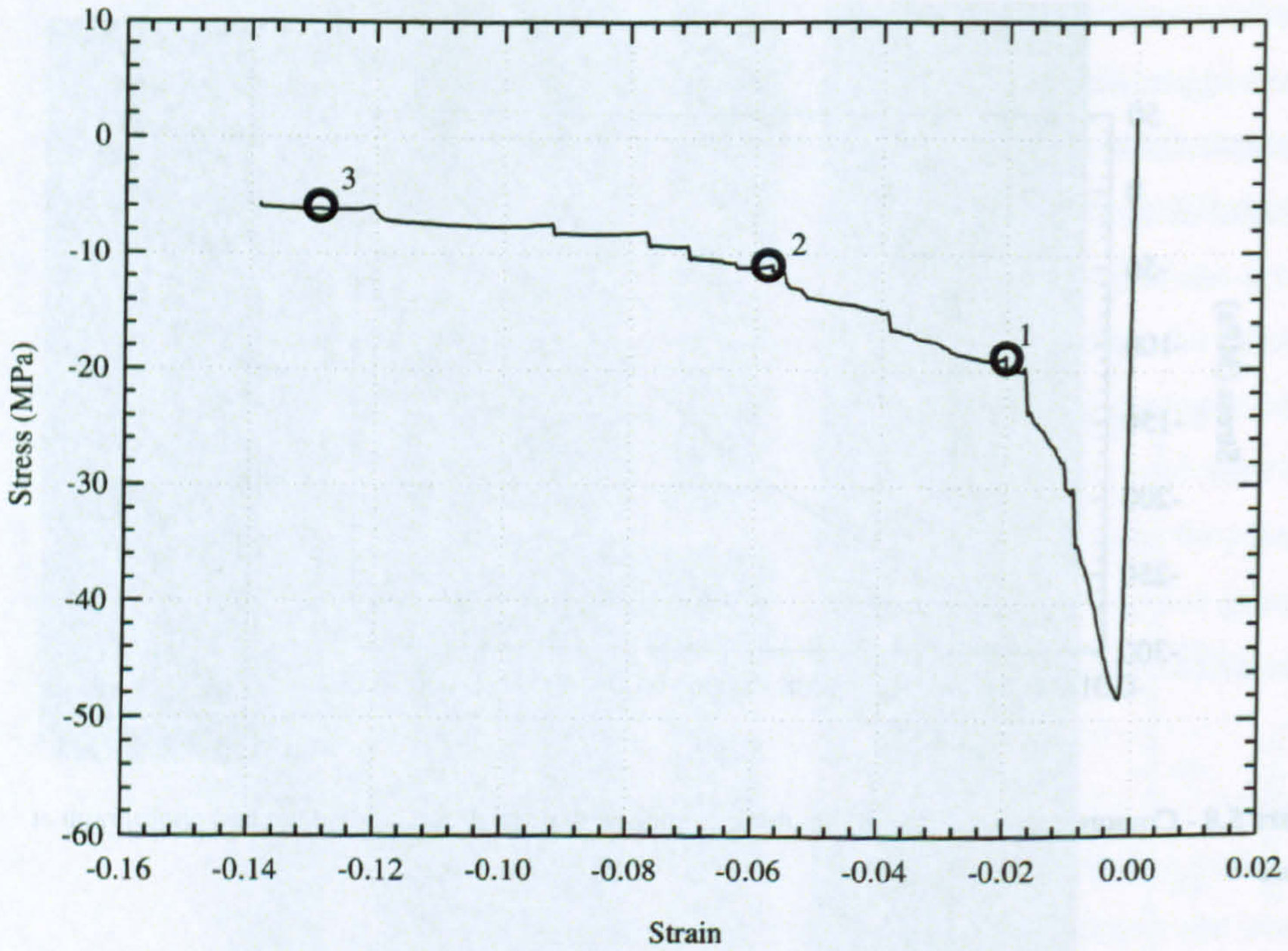

Figure 5.9 - Stress-strain curve for the compressive test of an 8 mm thick coupon with edge impact damage

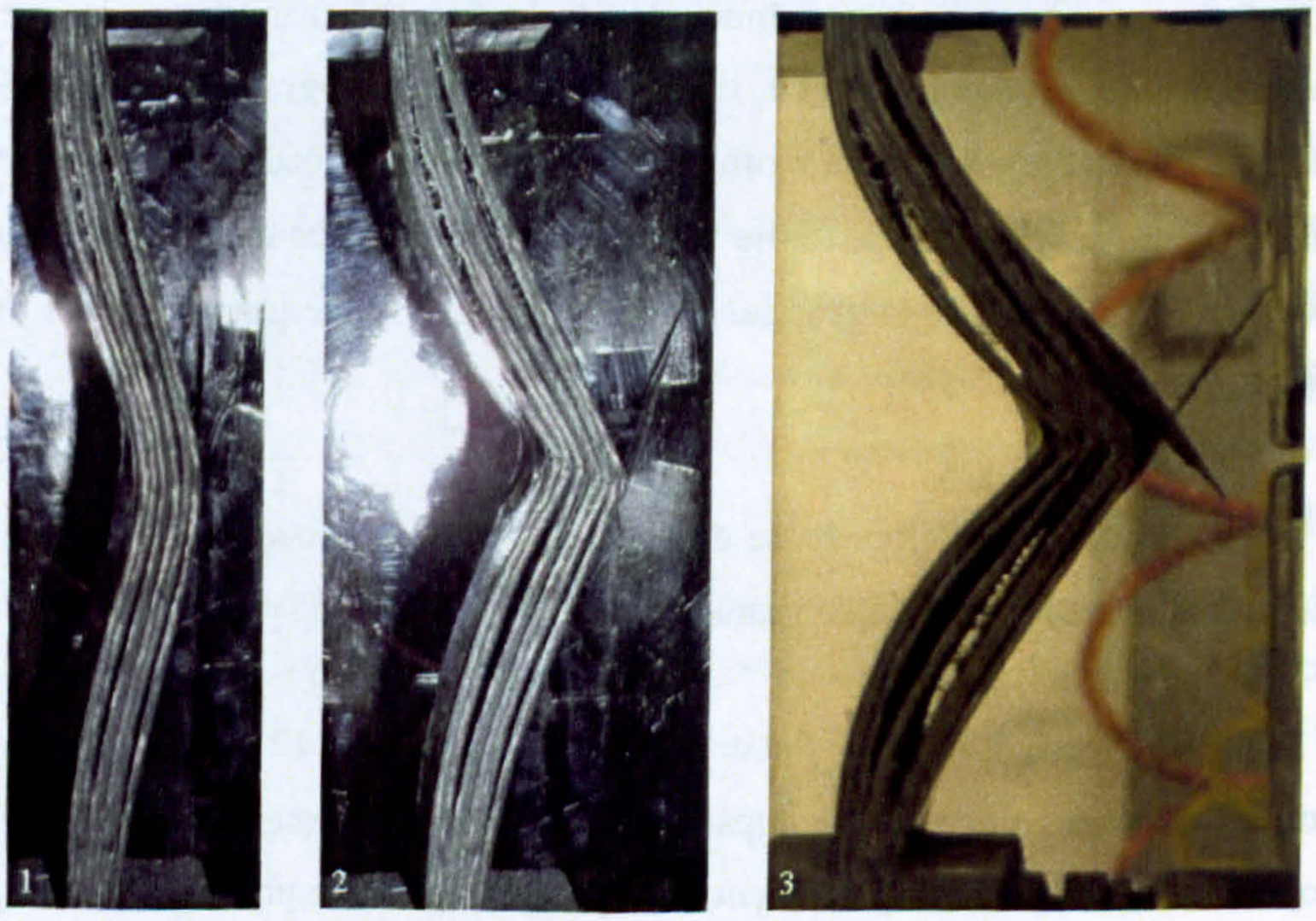

Figure 5.10 - Accompanying photographs to Figure 5.9 showing 8 mm thick coupon failing in compression

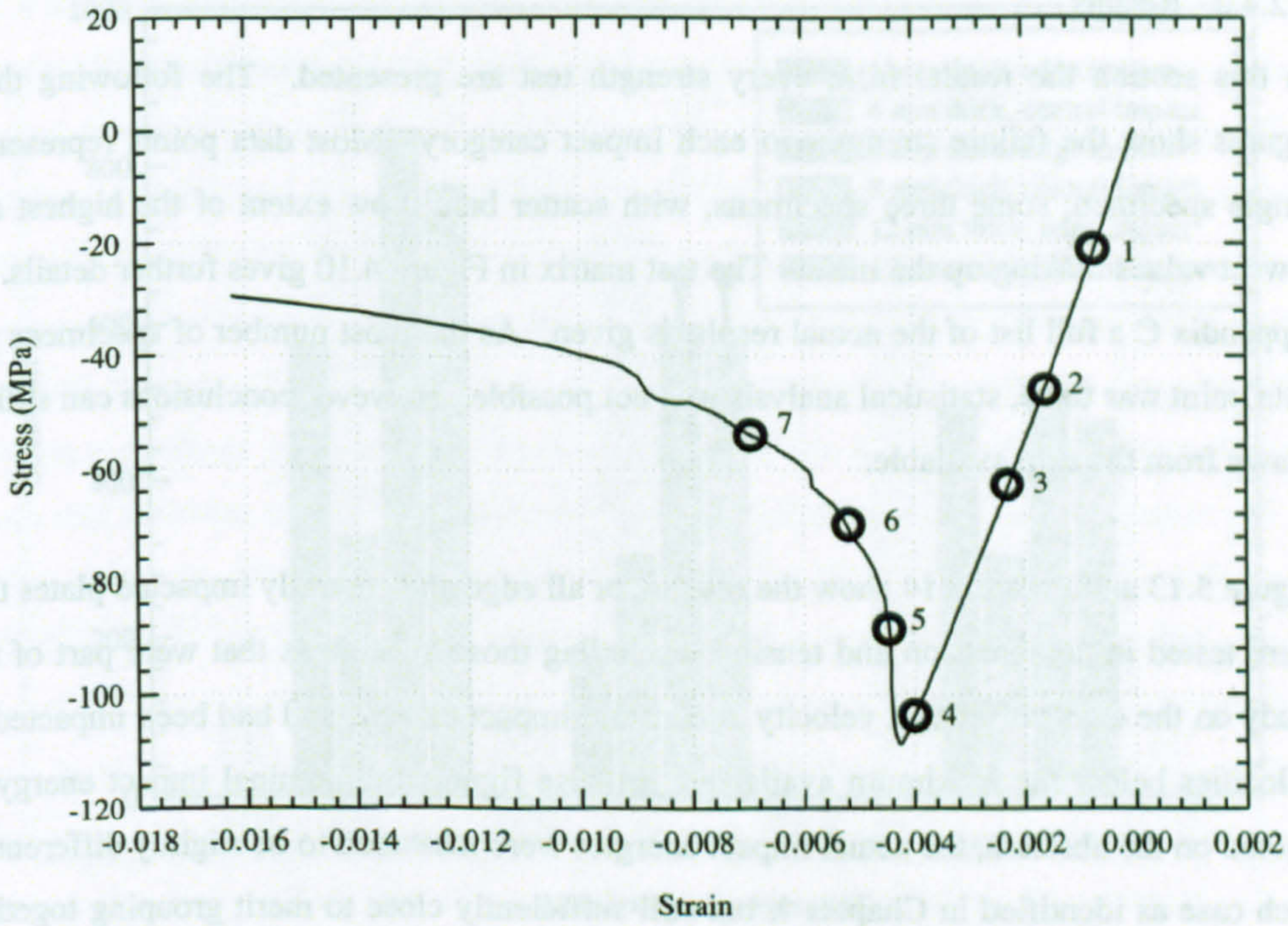

Figure 5.11 - Stress-strain curve for the compressive test of a 12 mm thick coupon with edge impact damage

Figure 5.12 - Accompanying photographs to Figure 5.11 showing failure of a 12 mm thick coupon

5.2.4.2 Results

In this section the results from every strength test are presented. The following three figures show the failure strengths in each impact category. Most data points represent a single specimen; some three specimens, with scatter bars show extent of the highest and lowest values making up the mean. The test matrix in Figure 4.10 gives further details. In Appendix C a full list of the actual results is given. As the most number of specimens per data point was three, statistical analysis was not possible. However conclusions can still be drawn from the data available.

Figure 5.13 and Figure 5.14 show the results for all edge and centrally impacted plates that were tested in compression and tension, excluding those specimens that were part of the study on the effect of impact velocity at constant impact energy, and had been impacted at velocities below the maximum available. In these figures the nominal impact energy is quoted on the abscissa, the actual impact energies were measured to be slightly different in each case as identified in Chapter 4, but still sufficiently close to merit grouping together of the results. In the same way in Figure 5.15 the nominal impact velocity is quoted. This figure shows the results from the study examining the effect of impact velocity.

As shown in the original test schedule, and obvious in the results from their absence, there were no 375 J impacts carried out on the 4 mm thick laminates and no 100 J impacts carried out on the 12 mm thick laminates. The reason for this was that firstly, it was thought that high energy impacts on the thin laminates would have penetrated the plate. The impactor was not designed for penetrative impacts and this would not have been a comparable result. Secondly it was thought that it would not be possible to fail 12 mm thick laminates that had been subjected to only a 100 J impact. In the end it was not possible to fail in tension the 12 mm thick laminates subjected to 200 J impacts as those impacts had not damaged the plates enough to reduce their strength to below the maximum practical test load of approximately 300 kN for a 50 mm wide coupon. The maximum practical test load arises from the shear strength of the top layer of the composite when being held by the hydraulic grips.

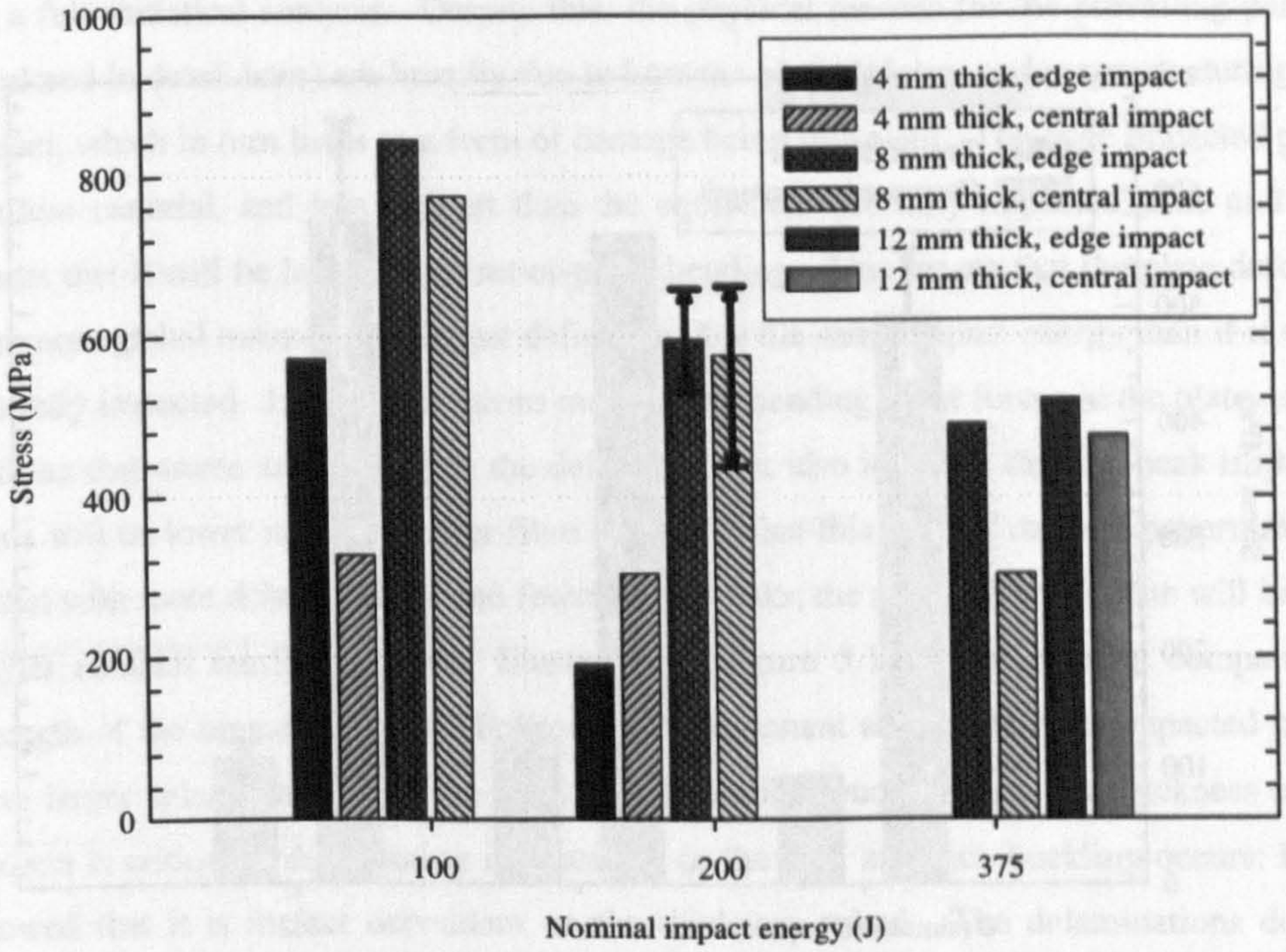

Figure 5.13 - Tensile strength results comparing edge and central impacted specimens

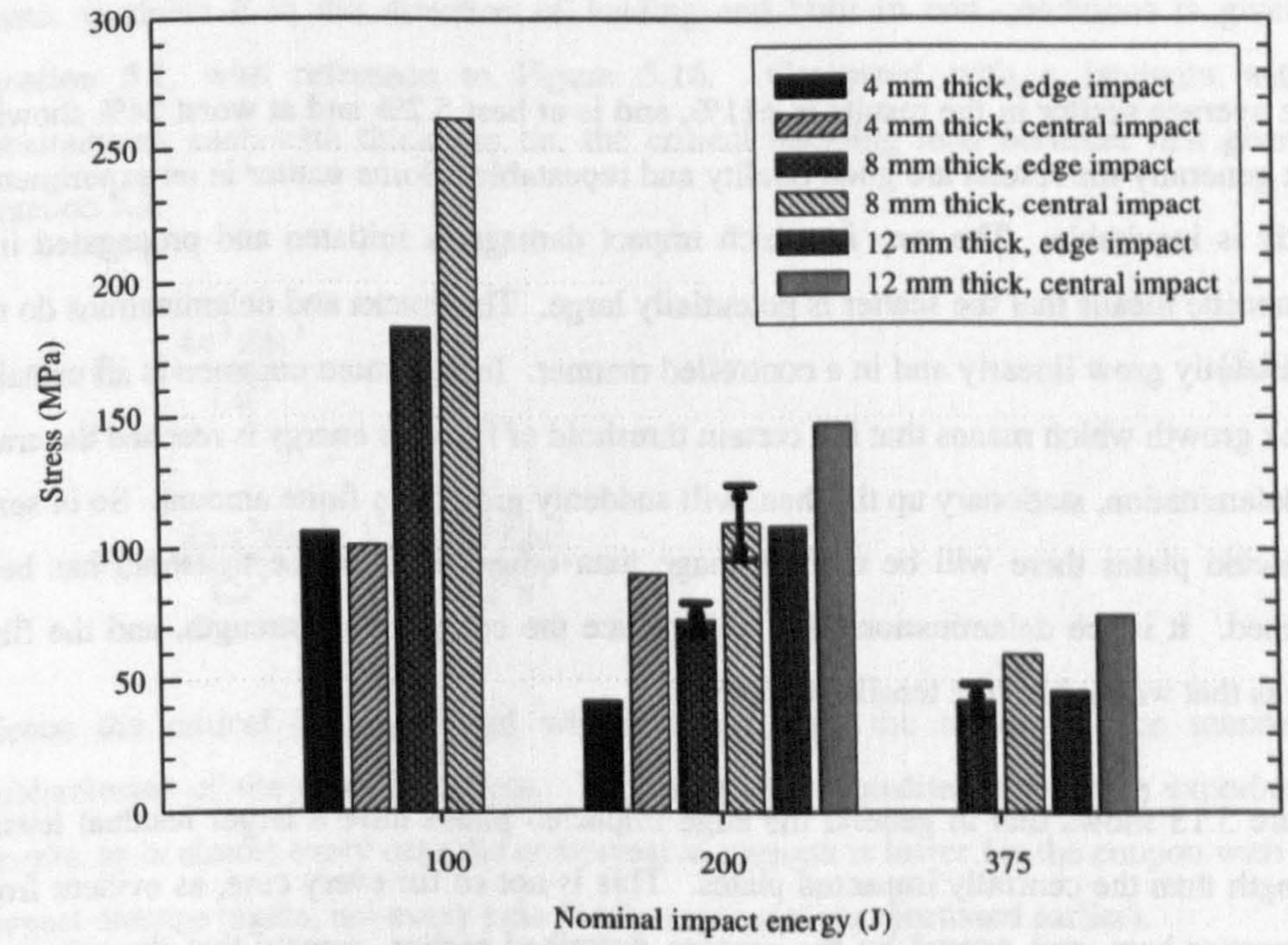

Figure 5.14 - Compression results comparing edge and centrally impacted coupons

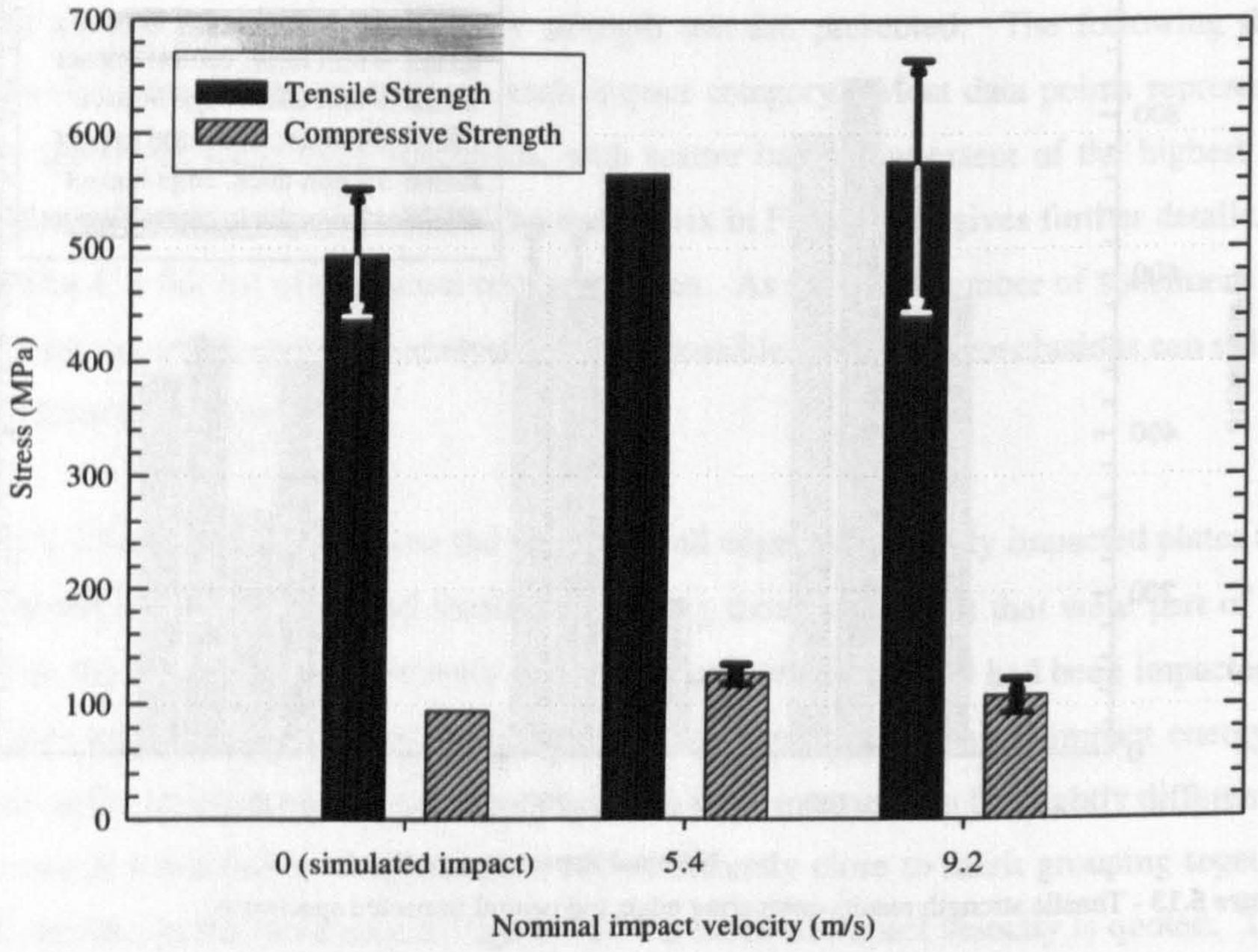

Figure 5.15 - Compressive and tensile results for plates impacted centrally at different velocities

The average scatter in the results is ±11%, and is at best 5.2% and at worst 24% showing that generally the results are good quality and repeatable. Some scatter in an experimental study is inevitable. The way in which impact damage is initiated and propagated in a composite means that the scatter is potentially large. The cracks and delaminations do not necessarily grow linearly and in a controlled manner. In fact more common is an unstable crack growth which means that if a certain threshold of force or energy is reached the crack or delamination, stationary up till then, will suddenly grow by a finite amount. So in some impacted plates there will be more damage than others because the threshold has been reached. It is the delaminations that will reduce the compressive strength, and the fibre cracks that will reduce the tensile strength.

Figure 5.13 shows that in general the edge impacted plates have a larger residual tensile strength than the centrally impacted plates. This is not so for every case, as evident from the scatter bars, and caused by the reasons described earlier, namely that the nature of impact tests means that scatter will be large and there were not enough specimens tested

for a full statistical analysis. Despite this, the physical reasons for the prevailing pattern (explored in detail later) are broadly due to how the plate deforms and responds during the impact, which in turn leads to a form of damage being prevalent. The edge impacted plate has less material, and less support than the equivalent centrally impacted plate and this means that it will be less stiff in out-of-plane bending. This means that the plate deforms in a more global manner with larger deflections for the same impact energy than if it were centrally impacted. Larger deflections mean larger bending shear forces in the plate, and it is these that create and propagate the delaminations; also it means that the peak impactor force will be lower meaning fewer fibre breaks. What this kind of damage pattern means is that with more delaminations and fewer fibre breaks, the edge impacted plate will have a higher residual tensile strength. Illustrated in Figure 5.14 is the residual compressive strength of the impacted plates. Following the argument above, the edge impacted plates have larger delaminations. As the test is of the stability/buckling type the thickness of the coupon is critical to determining its strength, or the load at which buckling occurs; Euler showed that it is in fact dependent on the thickness cubed. The delaminations do not reduce the thickness of the coupon, but they have the effect of dividing the coupon into multiple sublaminates. The critical buckling load , P_{cr}, for an undamaged laminate with elastic modulus E in the direction of loading and built in end conditions is given in equation 5.1, with reference to Figure 5.16. Compared with a laminate with n sublaminates, each with thickness t/n, the critical buckling load becomes that given in equation 5.2.

$$P_{cr} = \frac{4\pi^2 Ebt^3}{12l^2} \tag{5.1}$$

$$P_{cr} = \frac{4n\pi^2 Eb}{12l^2}\left(\frac{t}{n}\right)^3 = \frac{4\pi^2 Ebt^3}{12l^2 n^2} \tag{5.2}$$

Hence the critical buckling load will decrease with the square of the number of sublaminates of the same thickness. This is observed qualitatively in the experimental results, as in almost every case the compressive strength is lower for the coupon with edge impact damage (again, not every case for the same reasons discussed earlier).

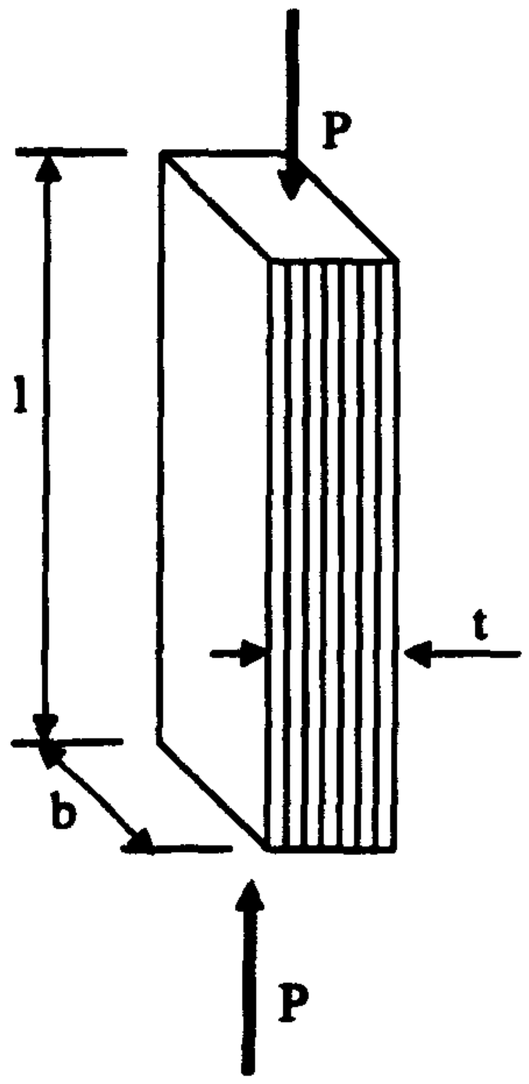

Figure 5.16 - Laminate coupon in compression - dimensions

Examination of the photographs in Figure 5.12 show that the 12 mm thick coupon failed in a fairly local manner (i.e. with a small buckled region only two or three times the thickness in length), indicating that the delaminations were small compared to those in the 8 mm and 4 mm thick coupons which failed in a more global manner (i.e. the buckled region extended the full length of the coupon). So the delaminations were quite small compared to those in the thinner laminates, but the plate still experienced a large decrease in the ultimate strength. If the plates were compressed further, the delaminations in the 12 mm thick plates would have spread, and the response of the coupon would have become gradually global. Chapter 3 presented the efforts to measure the undamaged strength of the laminates, and this was 356 MPa for an 8 mm thick plate in compression. The 12 mm thick coupons all failed well below this value in compression showing how significantly even a small delamination can affect the strength of a thick laminate.

Some specimens did not follow the pattern outlined above, particularly the 4 mm thick plates, (100 J impact in compression and 200 J in tension). These plates are significantly weaker and less stiff than the 8 mm plates and consequently the type of impact response is close to penetration, and hence will fall outside the scope of this study. These results therefore will appear to have more scatter.

Figure 5.15 shows fairly inconclusive results for the study looking at the effect of impact velocity in impacts of constant energy. It is postulated that a slow impact gives the plate more time to deform in a global manner and hence initiate more delaminations. This is similar to what has been shown to happen in the edge impacted plates in comparison with centrally impacted plates. However the range of impact velocities tested is possibly not wide enough to see a difference. The work of Olsson (2000) and Sjöblom, Hartness and Cordell (1988) show that there are three different velocity regimes to impact and to reach the high velocity region a significantly higher velocity is needed.

5.3 DAMAGE GEOMETRY

5.3.1 Introduction

In this section the physical reasons for the patterns found in the failure strengths of the coupons described above are explored with a number of techniques that examine and evaluate the damage internal to the laminates from the impacts. Understanding the kind of damage that is present in each type of laminate will help elaborate the reason for its particular failure strength. A number of destructive and non-destructive techniques are available that enable the examination of the damage present in the laminates; the delaminations, the cracking and surface damage including splitting and cracking.

5.3.2 Surface Damage

After impact there was a distinct difference between the damage evident on the front and back faces. On the front face there was an impact dent imparted by the impactor and some limited surface fibre (buckling) cracks. On the back face ply splitting and matrix cracking were visible. Figure 5.17 shows the typical surface damage from a 200 J impact (from 4.3 m) on to a 4 mm thick plate. The back face splitting is extensive and on the front face the dent is also evident, along with a surface fibre crack at the edge impact location (the fibre direction on the top layer is 45°). The plates are 350 mm by 290 mm, and the unsupported impact area is circular with a diameter of 200 mm.

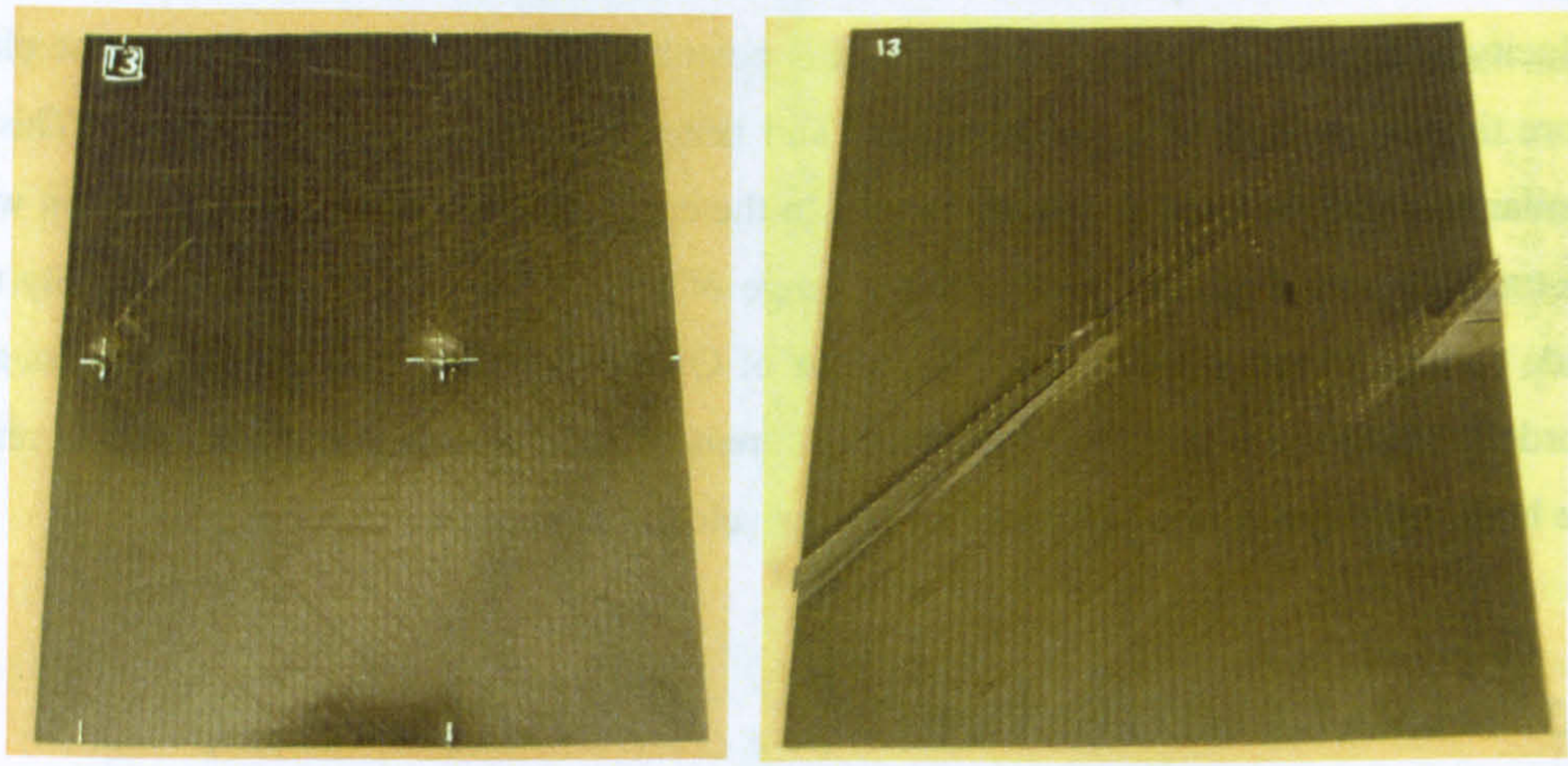

Figure 5.17 - 4 mm thick plate impacted with 200 J front and back face surface damage

Figure 5.18 shows the typical surface damage from a 200 J impact (from 4.3 m) on to an 8 mm thick plate. The back face splitting is less extensive compared to that shown in Figure 5.17, but still full width of the resulting residual strength coupon. The front face damage is also smaller, with the dents almost invisible in the photograph.

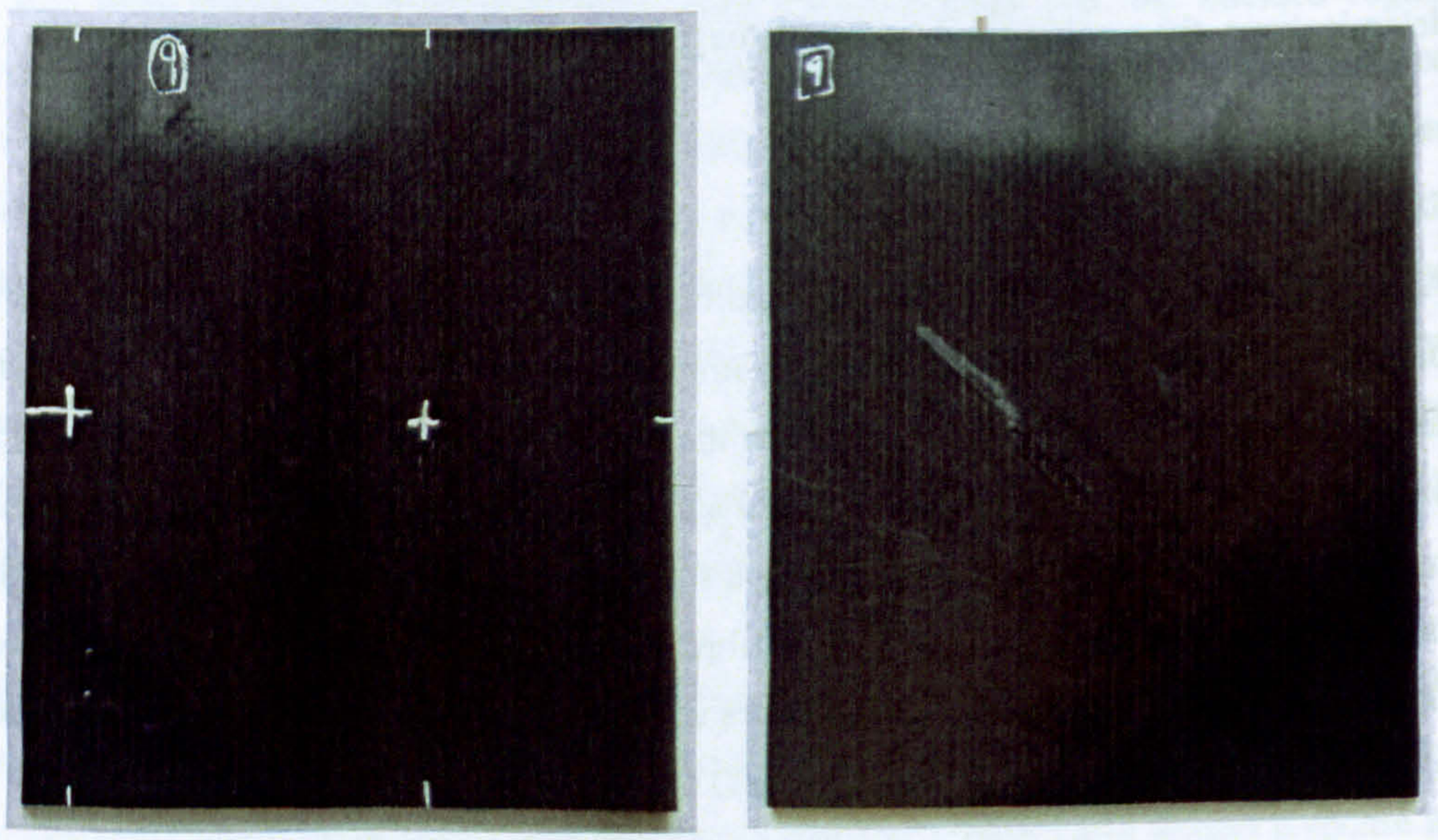

Figure 5.18 - 8 mm thick plate impacted with 200 J front and back face surface damage

Figure 5.19 shows the damage to an 8 mm plate impacted with 375 J (from 4.3 m) to the centre only, and the surface damage is much more extensive. The impact dent is more significant and there is some surface fibre cracking. The back face splitting is also more extensive.

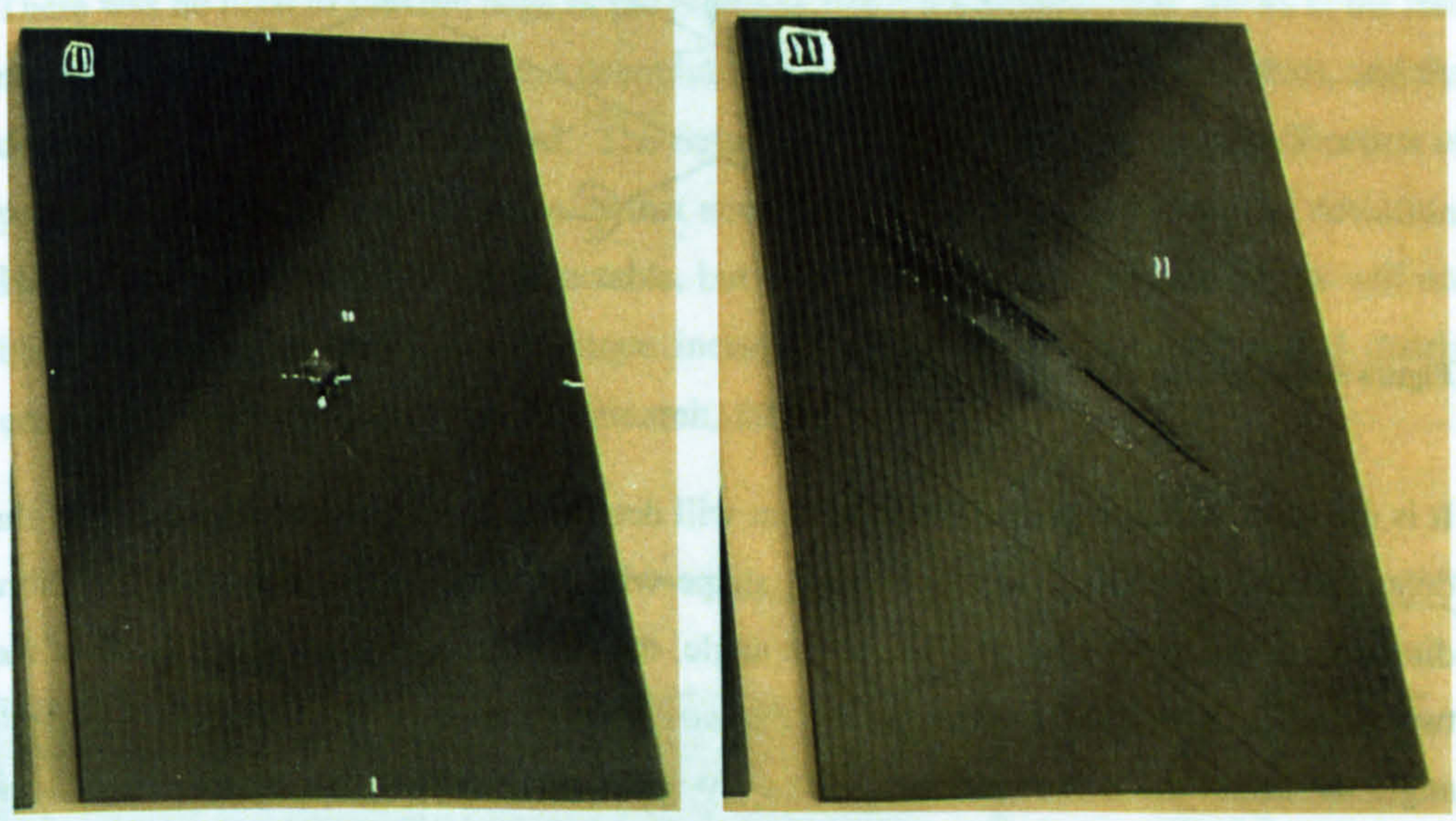

Figure 5.19 - 8 mm thick plate impacted with 375 J front and back face surface damage

The surface damage can give an indication to the damage that is within the composite, but further examination is required. Delaminations and internal fibre cracks are what most significantly affect the residual strength, and these are not directly evident from the surface in carbon fibre composites, hence other methods must be employed.

5.3.3 Delaminations

As a laminate is manufactured from several finite and distinct layers, each exhibiting different properties, a common damage mechanism is delamination where the laminated plies separate due to their mismatch in bending stiffness. Each ply is far less stiff in bending about its fibre direction compared to bending about its transverse in-plane direction. Thus, due to an impact two adjacent plies with fibres at 90° to each other will tend to bend in the manner illustrated in Figure 5.20 (Zukas et al., 1982).

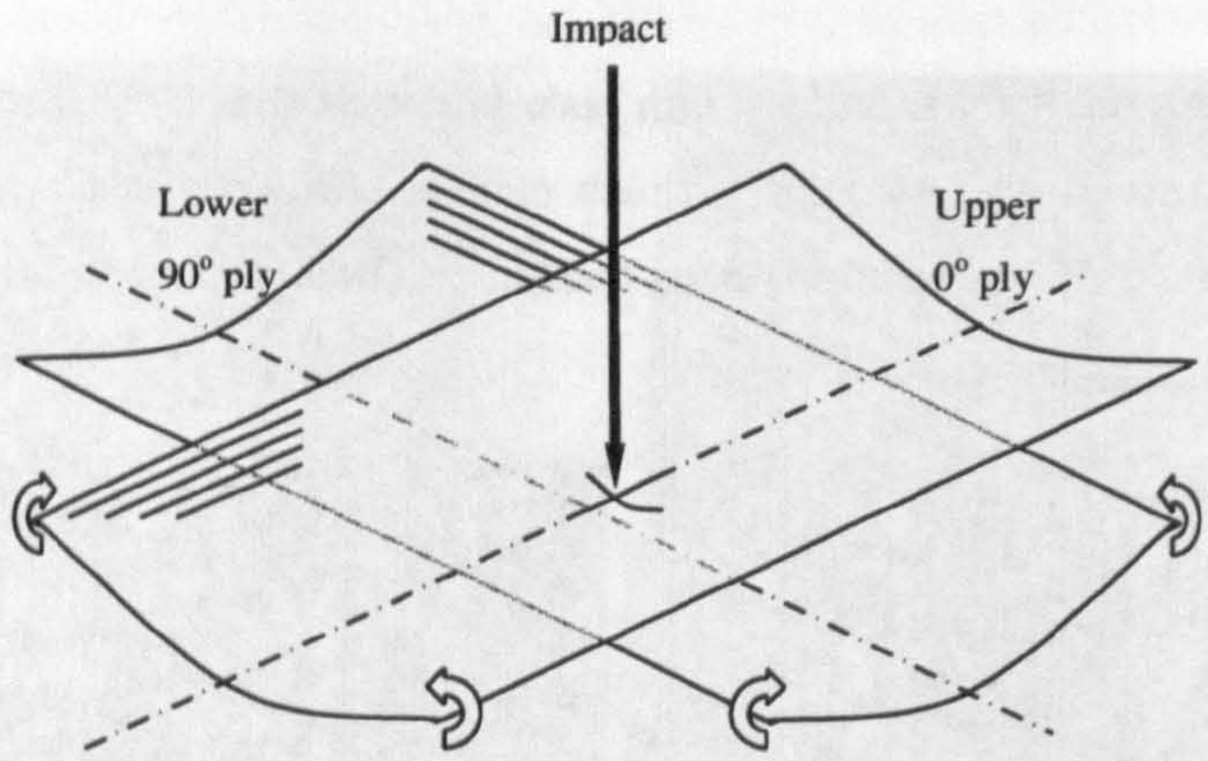

Figure 5.20 - Bending of a two ply laminate

It is the fibre direction of the lower ply that will determine the shape and orientation of the delamination, typically a figure of eight shape with its major axis lying along the fibre direction of the lower ply. It is the clock angle, the difference between orientations of the two adjacent plies, that determines the extent of the delamination, the bigger the clock angle the larger the delamination. With a lay-up like that used in this research the clock angles are minimised to 45° to give the laminate some resistance to delamination.

Delaminations are important because they change the ability of the laminate to support a compressive load, as seen in the previous section where delaminations significantly reduce the strength of the coupons. In glass fibre laminates the delaminations are readily detectable because those composites are translucent, and the presence of a delamination reduces the translucency. Holding the laminate up to a strong light reveals their extent. This is not possible with a carbon fibre laminate as they are opaque to visible light. They are not opaque to ultrasound however and this is the most successful means with which to detect internal defects such as a delamination.

The set-up used is illustrated in Figure 5.21. The transducer emits a pulse of ultrasound, and at every interface in the media through which it is travelling a portion of that signal will be reflected back to the transducer, the rest being transmitted through. These interfaces occur at the front and back faces of the laminate and at any internal defect, and their reflections arrive at different times at the transducer. What defines an interface is a

change in acoustic impedance. As the end of the transducer that emits the ultrasonic pulse is covered by a hard plastic, the change in impedance between that and the air is very high so very little will be imparted to the structure. Therefore is it extremely common to use a coupling agent, and water is commonly used. For this reason the specimen is fully immersed in a bath of water, having ensured that there were no bubbles on its surface. There was no need to seal the edge of the plates as water did not enter the cracks at the free edge (if this had happened then the delaminations would have been unobservable), and the delaminations were easily detected. The defect has to be perpendicular to the direction of propagation of the ultrasonic pulse so that enough energy is reflected to enable detection. Hence delaminations are easily detectable, but other defects such as matrix cracks will not be with this technique (use of oblique incidence ultrasonic testing does reveal matrix cracking, but not delaminations (Kaczmarek, 1995)).

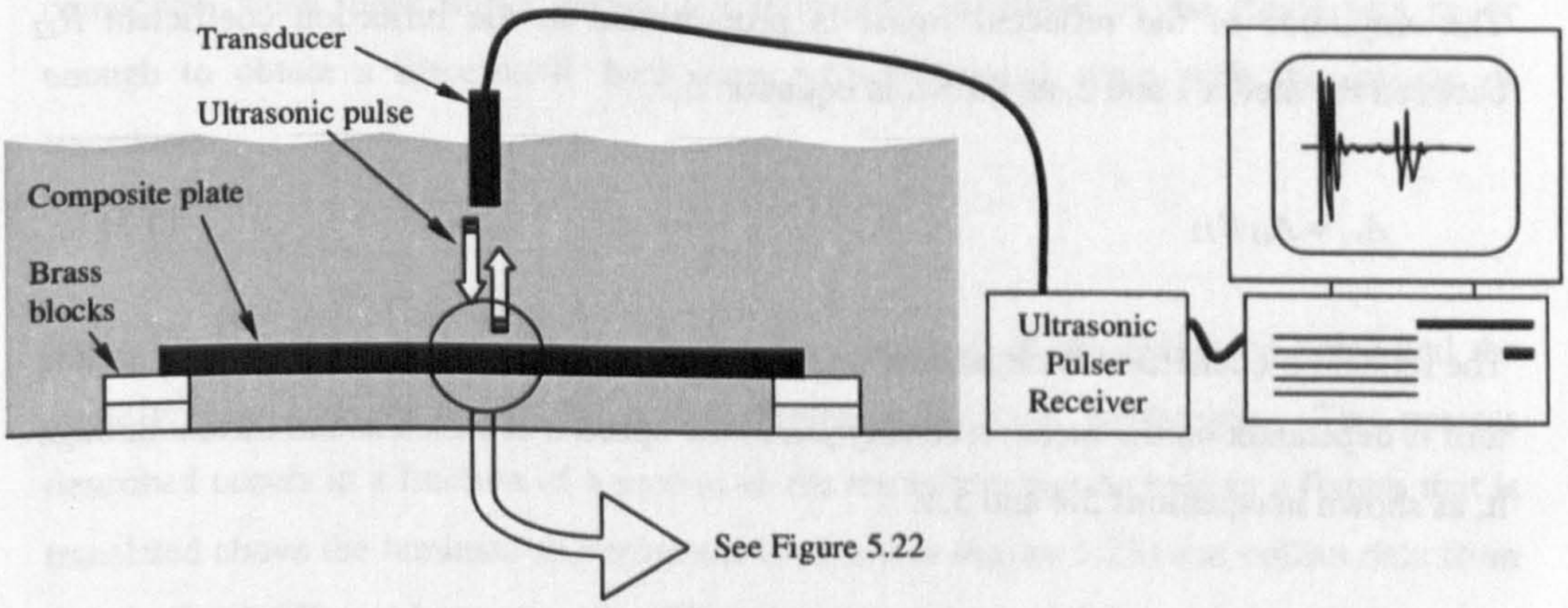

Figure 5.21 - Ultrasonic C-scan equipment set-up

Figure 5.22 illustrates what happens to the signal as it passes into the plate and why there is a difference between the reflected signal when there is a defect, and when there is no defect. Firstly we define two media, *1* (water) and *2* (composite), and whether the signal is incident (*i*) or reflected (*r*). Thus, the amplitude of the signal *A* incident to the plate in the water is defined A_{i1}, and the amplitude of the reflected signal from the front face of the plate A_{r1}.

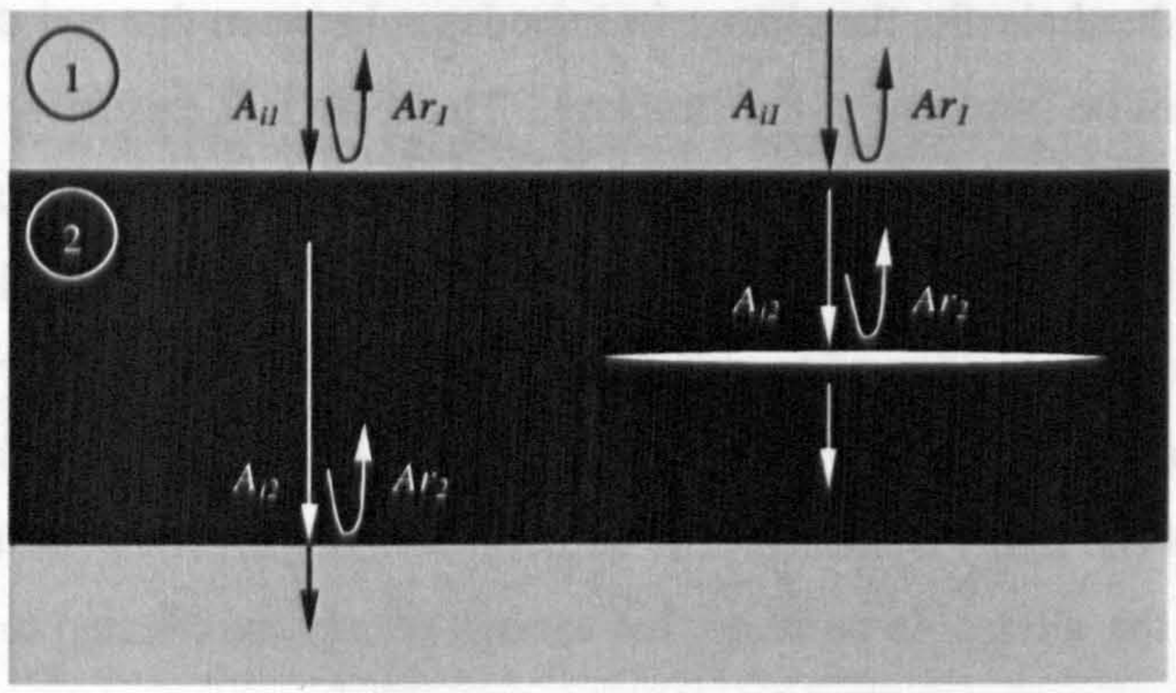

(a) No defect (b) Defect

Figure 5.22 - Schematic showing passage of the ultrasonic pulse through the plate and reflections at interfaces

The amplitude of the reflected signal is proportional to the reflection coefficient R_{12} between the media 1 and 2, as shown in equation 5.3.

$$A_{r1} = A_{i1} R_{12} \tag{5.3}$$

The reflection coefficient is dependant on the acoustic impedance Z of the media, and Z in turn is dependant on the media's density ρ and the speed c at which sound travels through it, as shown in equations 5.4 and 5.5.

$$R_{ij} = (Z_i - Z_j) / (Z_i + Z_j) \tag{5.4}$$

$$Z_i = \rho_i c_i \tag{5.5}$$

Thus, the amplitude of the reflected signal depends on the acoustic impedance of the two media that make up the interface (Krautkramer and Krautkramer, 1990). So, as the media within the delamination is likely to be air or a vacuum, its reflection coefficient will be significantly higher than at the back face composite-water interface. This is exacerbated by the fact that the carbon fibre composite is a highly attenuative material; the back face reflected signal has further to travel through the composite and will have a smaller

amplitude simply by having had to travel further. In addition the back face and defect reflected signals will be separated in time in the acquired results.

This attenuative property of the carbon fibre composite material made the choice of transducer important. There is a balance between using a high frequency transducer that has a high resolution (due to the consequently small wave length) and a low frequency transducer having greater penetrative power (the larger wavelength means that the wave is less scattered by the fibres). Further, a choice has to be made between a focussed or planar transducer, the focussed option giving a stronger reflected signal from defects at a known depth. As the delaminations were at unknown depths through the thickness of the plates, and ensuring a measurable back face reflected signal from an undamaged portion of the plate was a high importance, a planar transducer with a relatively low centre frequency of 2.25 MHz was used. In practice however, due to the attenuative nature of the carbon fibre composite, when there was a defect, the remaining amplitude of the signal was never enough to obtain a discernable back face reflected signal, even with this choice of transducer.

Specialised software and hardware controls the emission of the ultrasonic pulse and the amplifying and recording of the reflected signals for post processing. The process described occurs in a fraction of a second so the transducer can be held in a fixture that is translated above the laminate to perform a C-scan (see Figure 5.23) and collect data from thousands of different locations. Specific information from each location is saved, such as the amplitude of the back face reflected signal, and this is translated into a colour contour plot for ease of qualitative analysis. As well as signal amplitude, the time of flight is commonly recorded; this is simply the time elapsed from the output of the pulse from the transducer to the moment the reflected signal is received back. This time of flight is analogous to depth of the defect through the thickness of the plate, once the time for travelling through the coupling medium is accounted for. Within the data collection and processing software the data acquisition is started when a signal is detected with an amplitude above a given threshold, and within a given time band. This time band can be set based on the fact that it is known when the front face reflection will be received, and this time is constant over the whole plate within a certain tolerance to take into account variations in plate thickness and not being supported perfectly horizontally. Then data

collection regions can be defined as periods of time during which either a back face reflection is expected to be received, or some defect within the bulk of the material. In these data collection gates, either the amplitude of the biggest peak or the time of flight of that peak was recorded.

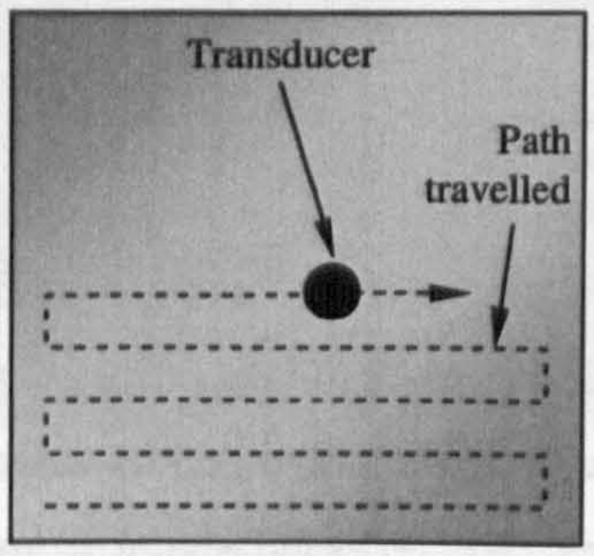

Figure 5.23 - The path that a transducer takes during a C-scan

To illustrate typical C-scan results, figures showing the back face amplitude (Figure 5.24), mid plane amplitude (Figure 5.25) and mid plane time of flight (Figure 5.26) have been produced. They are for a 12 mm thick laminate with damage from a 200 J impact in both the edge and central locations. In each the colour key indicates the meaning of the colours in the figure, either voltage for amplitude of signal or 10^{-6} s for time of flight: blue means a low amplitude signal and red a high amplitude signal in Figure 5.24 and Figure 5.25; in Figure 5.26 blue means a short time of flight, so the defect is close to the surface, and red a long time of flight so the defect is nearer the back face of the plate. In addition on each figure seven positions have been marked, and at each location the A-scan, or signal time trace at that location has been recorded, and will be discussed. In addition the approximate location of the plate support from the impact rig is shown in each figure for reference.

Figure 5.24 shows the full extent of the delaminations as two dark blue regions. The shape of the edge and central impact delaminations are very different, the central impact almost circular and the edge impact delaminated zone much longer and thinner in comparison where the crack has opened along the free edge. In the centre of each there is a black spot corresponding to the impact point, where there is no back face reflected signal due to the highly dissipative nature of the crushed composite. Surrounding that a uniform blue area for the bulk of the delamination, where there is a low amplitude reflection from the back face, and finally some regions within the delaminated zone that appear to give an almost intact level of amplitude to the reflected signal. The rest of the figure shows a rough

texture to the undamaged zone due to the fibre architecture, and high amplitude red spots at each corner where the plate was supported on brass blocks during the scan.

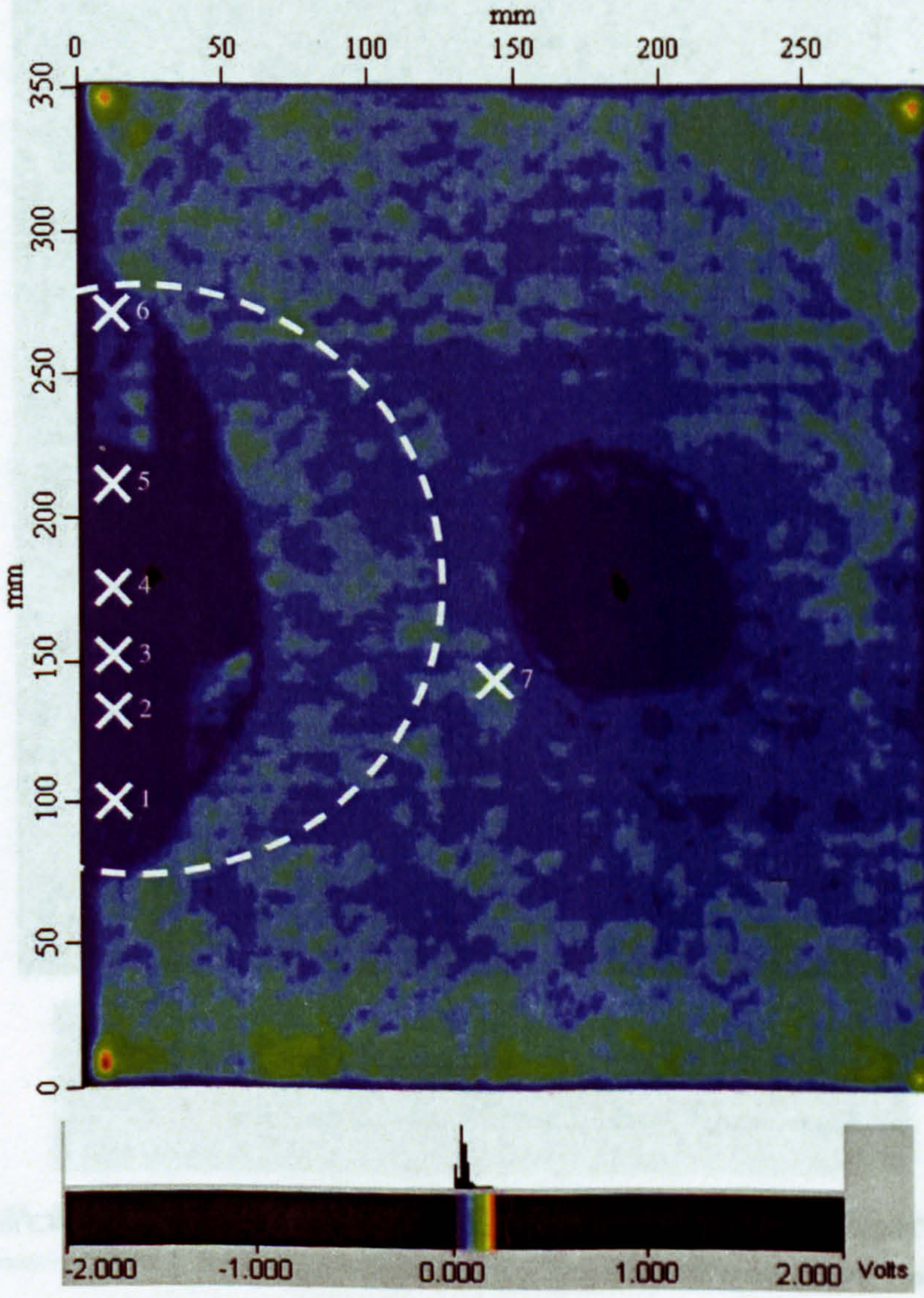

Figure 5.24 - Back face amplitude C-scan for a 12 mm thick plate impacted with 200 J from 4.3 m (X's indicate locations where A-scans have been presented in subsequent figures)

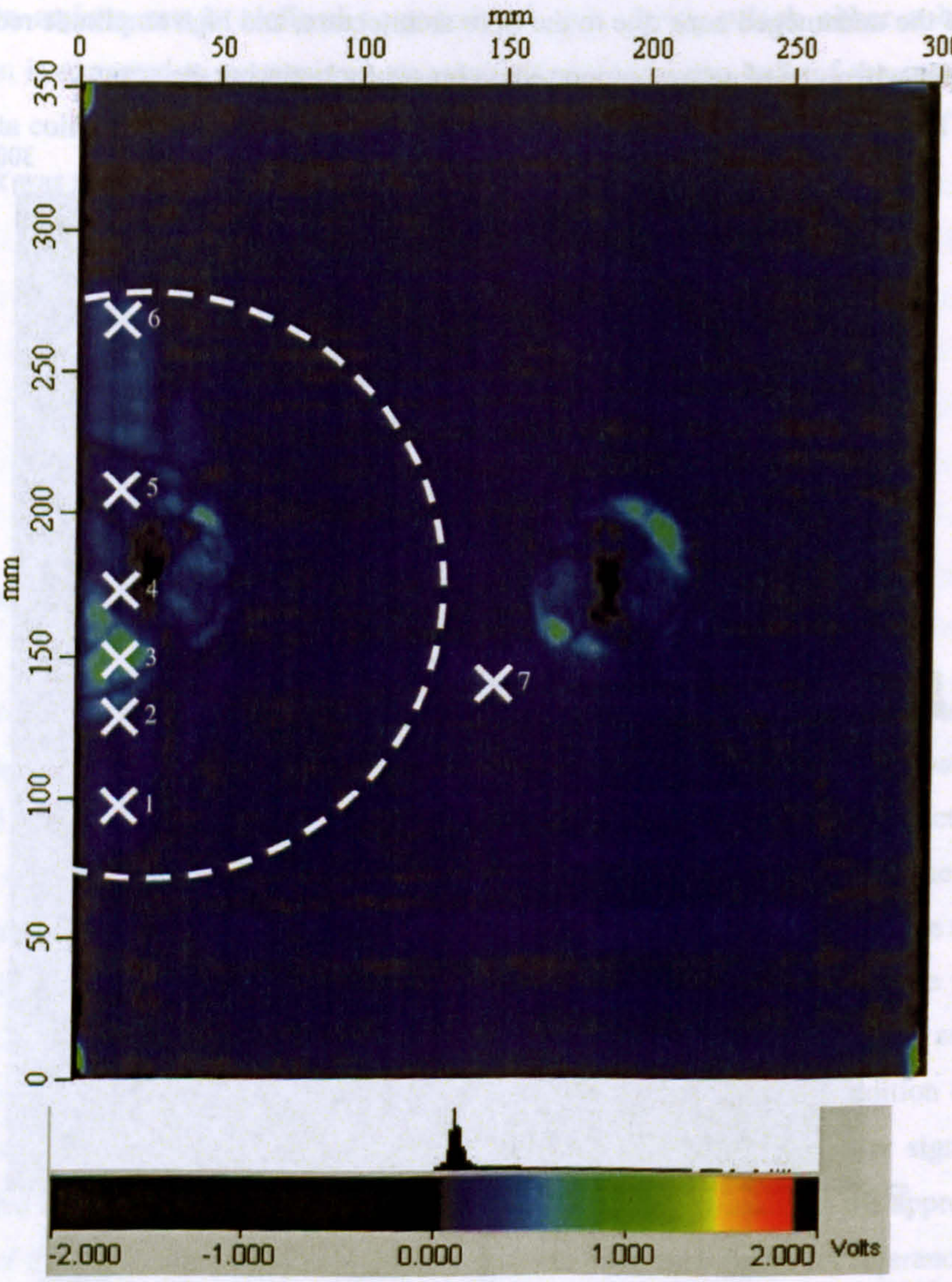

Figure 5.25 – Mid plane amplitude C-scan for a 12 mm thick plate impacted with 200 J from 4.3 m (X's indicate locations where A-scans have been presented in subsequent figures)

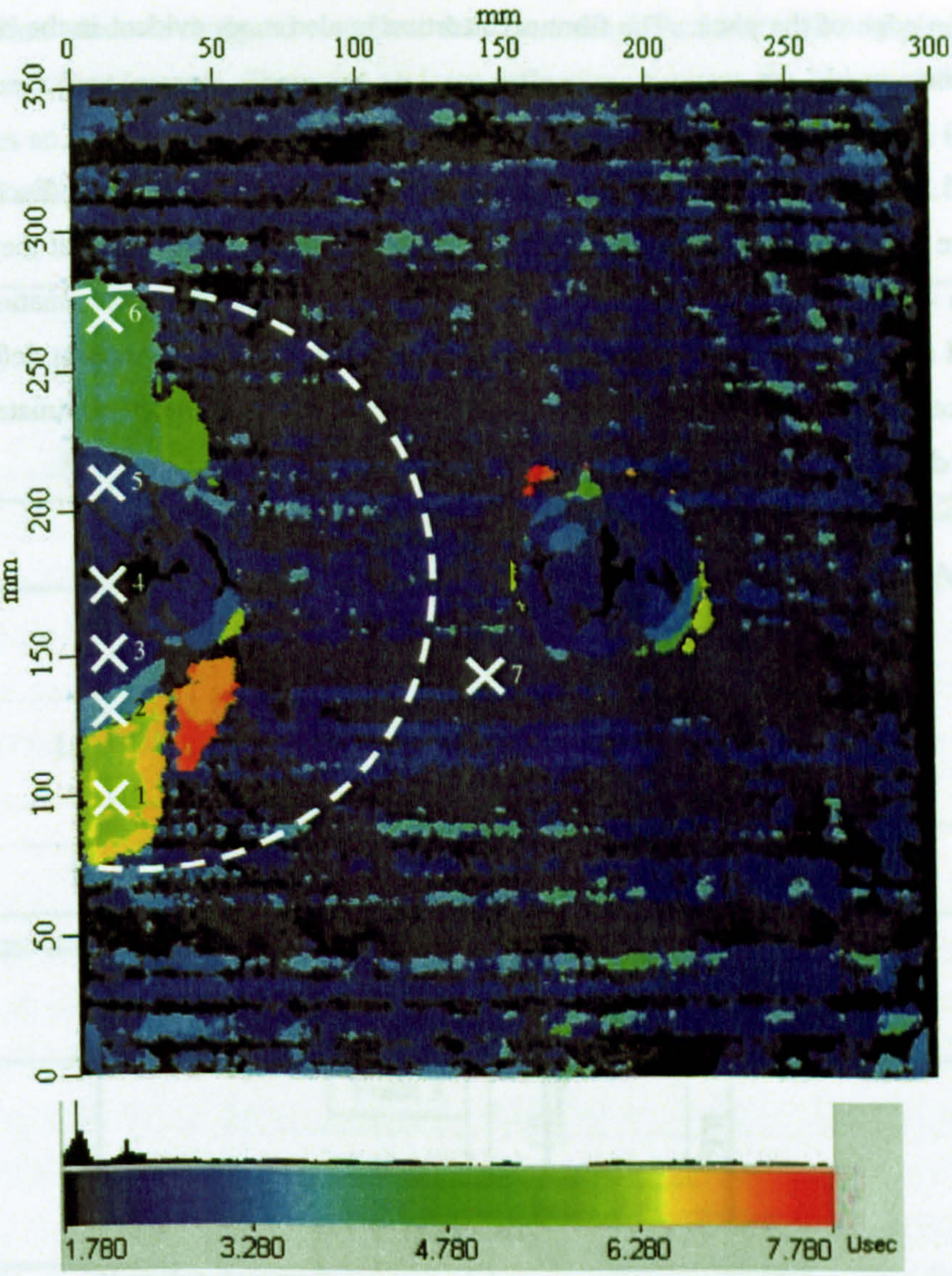

Figure 5.26 - Mid plane time of flight C-scan for a 12 mm thick plate impacted with 200 J from 4.3 m (X's indicate locations where A-scans have been presented in subsequent figures)

Figure 5.25 shows the mid plane amplitude C-scan. The mid plane region was chosen by selecting the data acquisition region so that all of the front face and back face reflected signals were omitted. The figure shows that the central and edge delaminated regions are made up of several smaller apparently separate delaminations. The central impact is surrounded by many, small delaminated areas without any real coherence or pattern. The same is true for the edge impact. However there are larger uniform areas of delamination above and below the central area of the edge impact where the delaminations have spread

along the edge of the plate. The fibre architecture is also more evident in the bulk of the rest of the scan.

Figure 5.26 shows why the smaller areas of delamination appear separate. Each of these areas are also evident, and they have a fairly uniform colour, indicating that they are at a uniform depth, and hence at a particular interface. Only the first delamination can be detected at any position as any remaining signal reflected from a subsequent defect or the back face is too small to detect. Hence what the figure shows is the approximate depth of the first delamination in the plate.

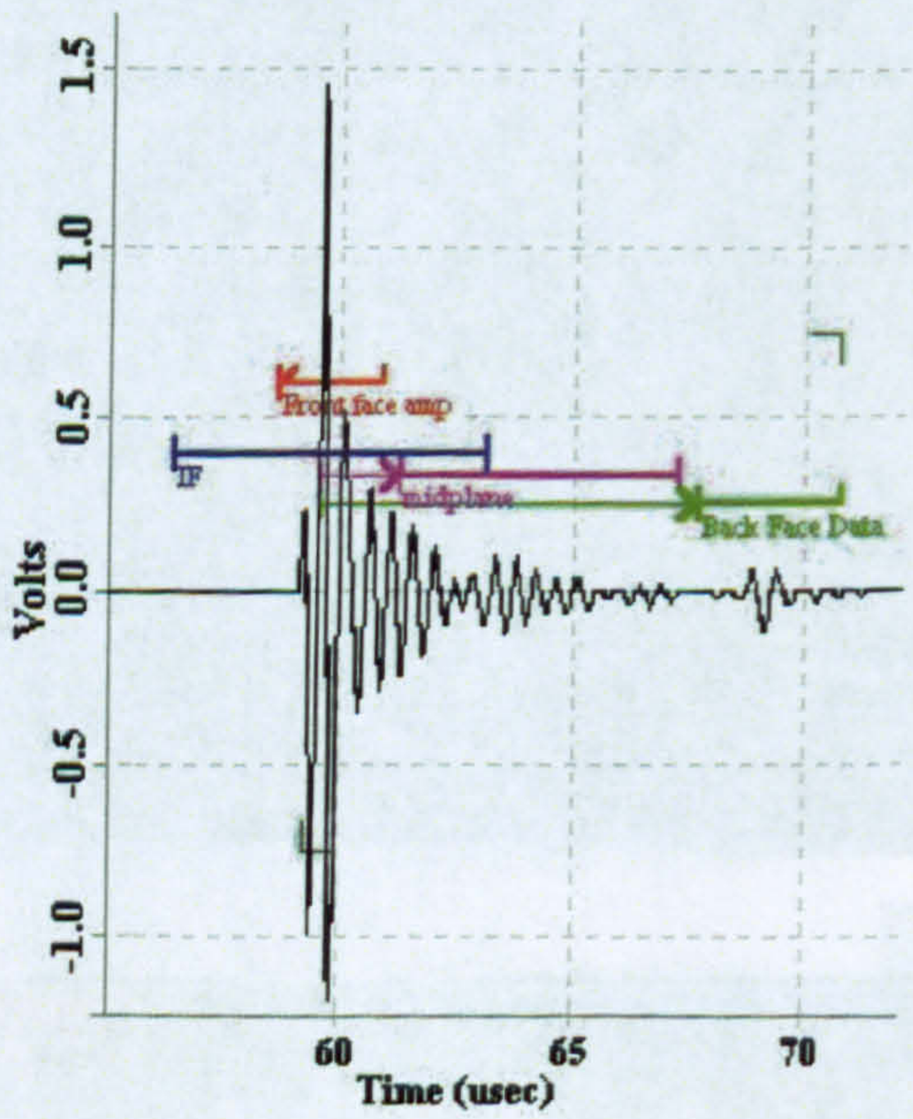

Figure 5.27 - A-scan at point 7 (12 mm thick laminate), see Figure 5.24 to Figure 5.26

Figure 5.27 shows an A-scan, or the time against amplitude plot, for a single specimen, although the same evidence was observed for all plates. For the pulse at point 7 (refer to Figure 5.24 to Figure 5.26), showing the signal at a normal undamaged portion of plate. At around 60 μs after the pulse was sent, the front face reflection is detected. Four regions have been marked on the graph showing where data collection takes place. The blue gate marked IF is the interface trigger that starts the data collection providing the front face reflection is detected within that time window above a given threshold. The three remaining gates are set to record the peak amplitude and time of flight of the signal within

defined time windows designed to collect data from the front face (red), mid plane (pink) and the back face (green). There are no large reflections between the front and back face reflections so it can be concluded that there is no defect in the mid plane. There is a clear back face reflected signal.

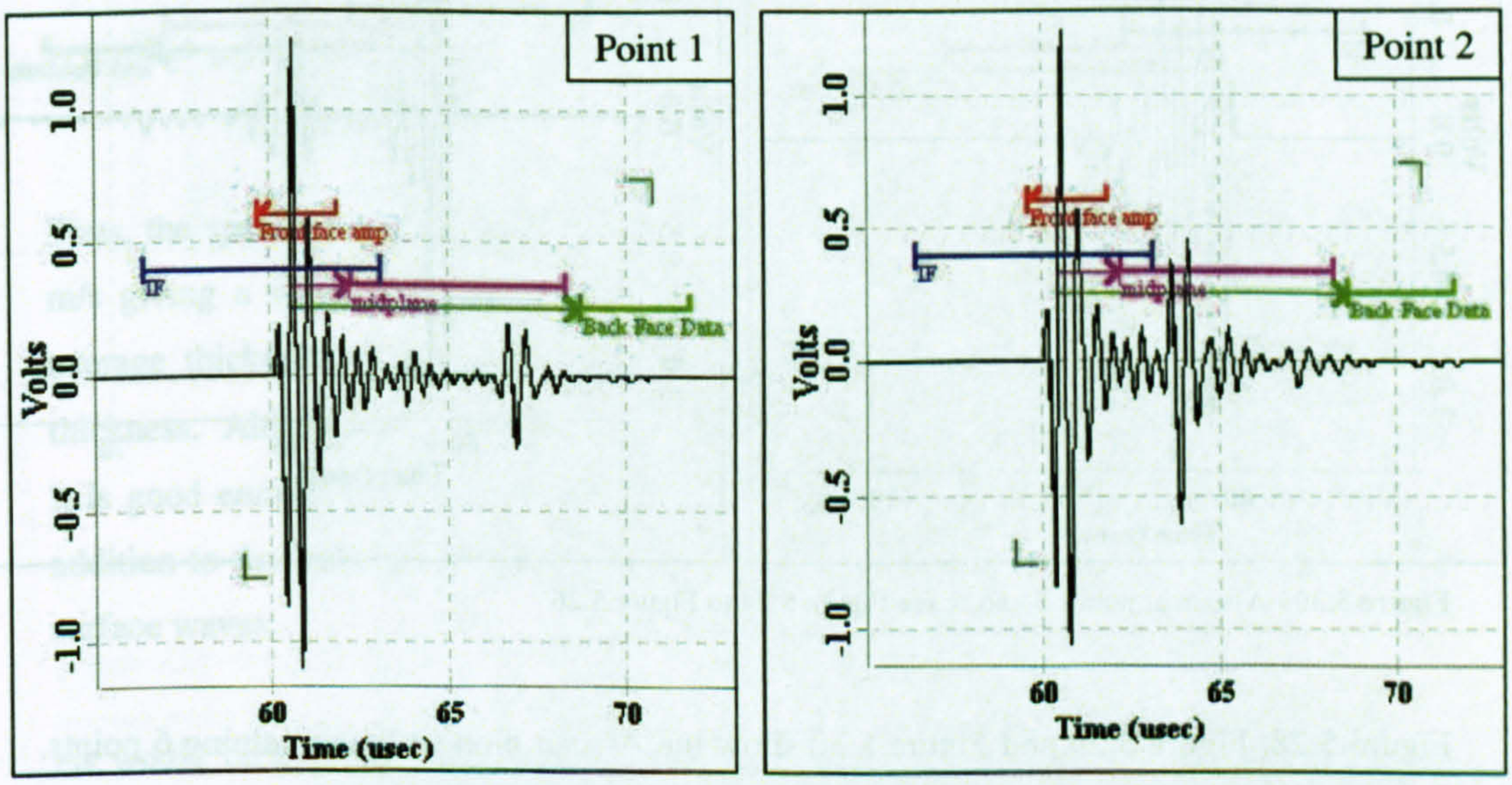

Figure 5.28 - A-scan at points 1 and 2, see Figure 5.24 to Figure 5.26

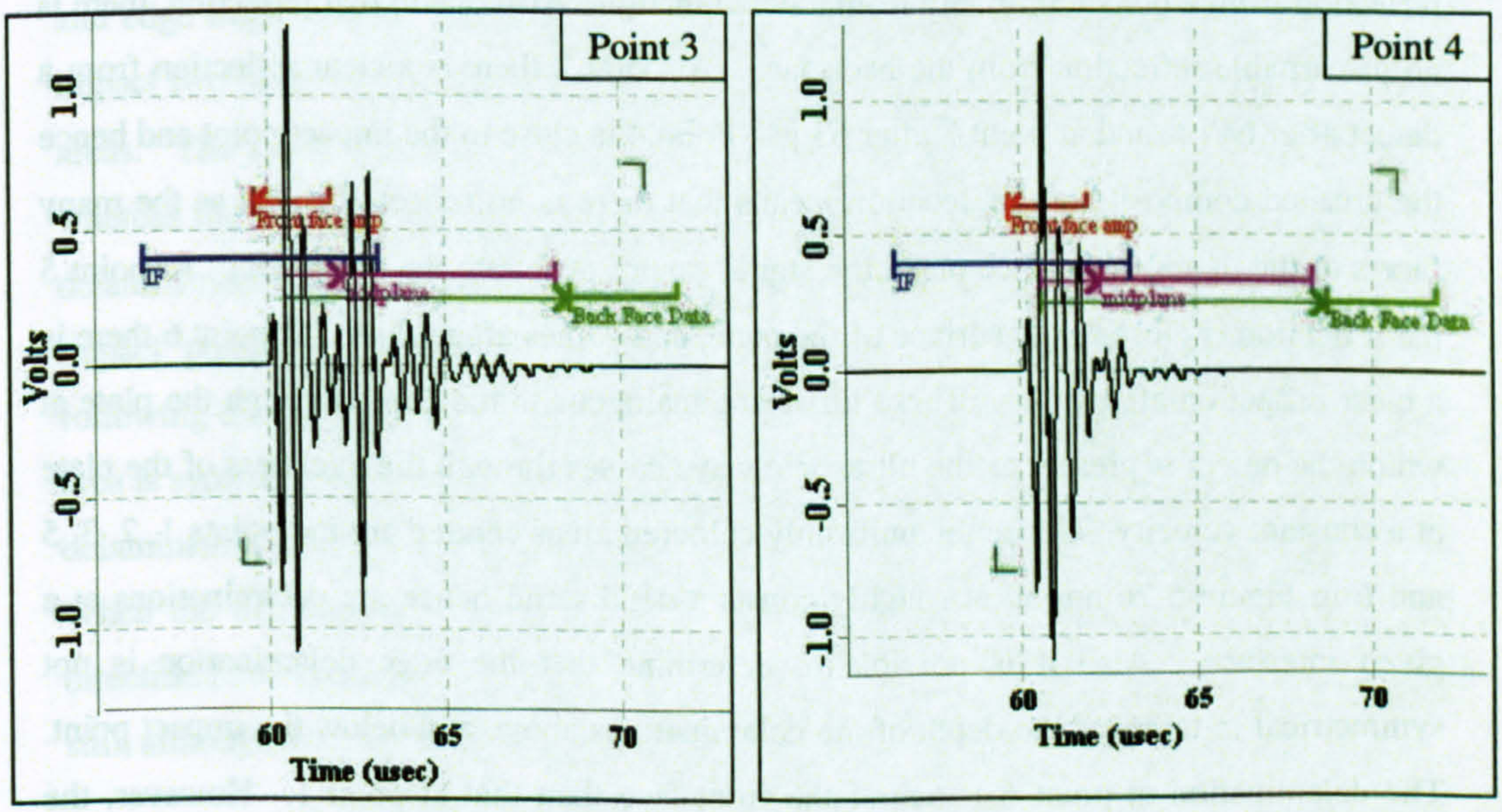

Figure 5.29 - A-scan at points 3 and 4, see Figure 5.24 to Figure 5.26

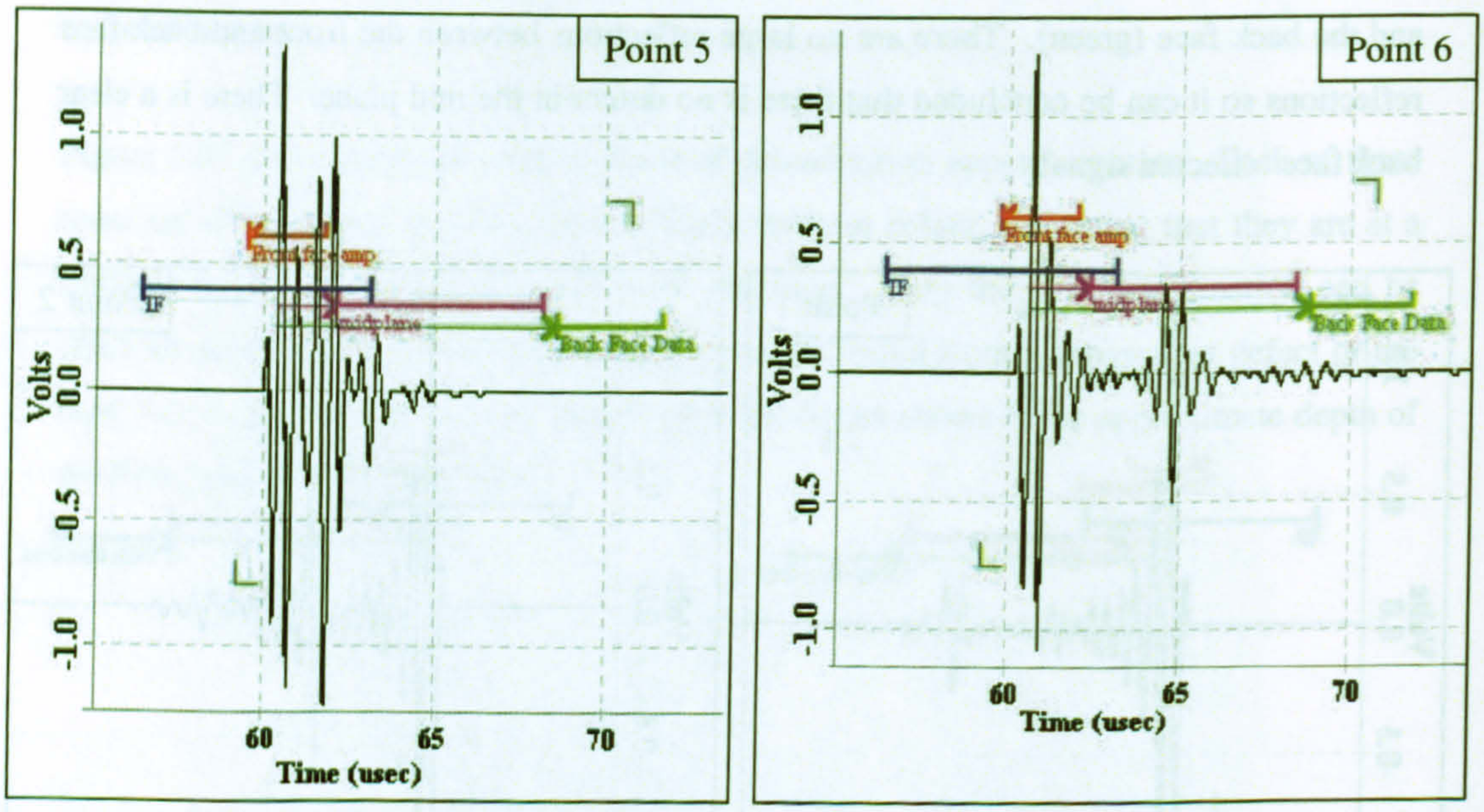

Figure 5.30 - A-scan at points 5 and 6, see Figure 5.24 to Figure 5.26

Figure 5.28, Figure 5.29 and Figure 5.30 show the A-scan plots at the remaining 6 points. By referring to these figures it is possible to see how the colour plots are created. At point 1 it is possible to see a dramatic increase in amplitude after approximately 67 μs: this is a reflection from a defect, probably from a delamination. Also due to that reflection, there is no discernable reflection from the back face. At point 2 there is a clear reflection from a defect after 64 μs, and at point 3 after 63 μs. Point 4 is close to the impact point and hence the crushed composite at this location means that there is no reflected signal as the many facets to the damaged surface mean the signal cannot penetrate the composite. At point 5 the reflection is close to the surface of the plate, and comes after 62 μs. At point 6 there is a clear reflection after 65 μs. These times are analogous to the depth through the plate at which the defect is present as the ultrasonic wave passes through the thickness of the plate at a constant velocity. Hence the uniformly coloured areas centred around points 1, 2, 3, 5 and 6 in Figure 5.26 are all at roughly constant depths and hence are delaminations at a given interface. Also it is possible to determine that the edge delamination is not symmetrical in terms of the depth of the delaminations above and below the impact point. The delamination at point 6 is nearer the front face than that at point 1. However, the spatial resolution through the thickness of the plate is not good enough to be able to pinpoint at which interface the delamination exists as the centre frequency of the

transducer is quite low, so the wavelength is correspondingly high. The speed of the ultrasonic pulse through the thickness of the plate can be calculated using equation 5.6 assuming it to be a semi-infinite body, valid if the wavelength is small compared to the thickness (Rose, 1999).

$$c^2 = \frac{E_2}{\rho}\frac{(1-\nu)}{(1+\nu)(1-2\nu)} \tag{5.6}$$

Thus, the speed of sound travelling transversely through the plate is approximately 3000 m/s giving a wavelength of approximately 1 mm, which is too large compared to the average thickness of a layer (0.2 mm) to give exact positional resolution through the thickness. Although this large wavelength means the assumption given above is not valid, it is good enough for a first approximation, what will be happening in reality is that in addition to the bulk wave there will be some additional wave forms created, for example surface waves.

As would be expected, the delamination area increases for impacts with higher energy. Figure 5.31 shows back face amplitude C-scans (in black and white for clarity) of impacts onto 8 mm thick laminates of three energies. For the two lower impact energies the central and edge impacts were performed on the same plate to conserve material. For the 375 J impact two plates were used to ensure there was no interaction between the larger damage areas. The scans show that edge delaminations grow considerably with impact energy, whereas the central delamination grows, but less dramatically. At 100 J the edge impact delamination is not symmetrical in shape, as the delamination has only spread above the impact point along the edge. This delamination is relatively deep within the plate following examination of the mid-plane time of flight plot. At 200 J the edge delamination area is symmetrical in shape, and appears bounded by the size of the specimen clamp. The delamination extends beyond the clamp along the free edge and enters the plate at 45°. When the delamination goes within the specimen support region the boundary changes direction to a vertical line in the 0° direction. At 375 J the edge delamination grew bigger still, although still apparently limited in extent by the specimen support.

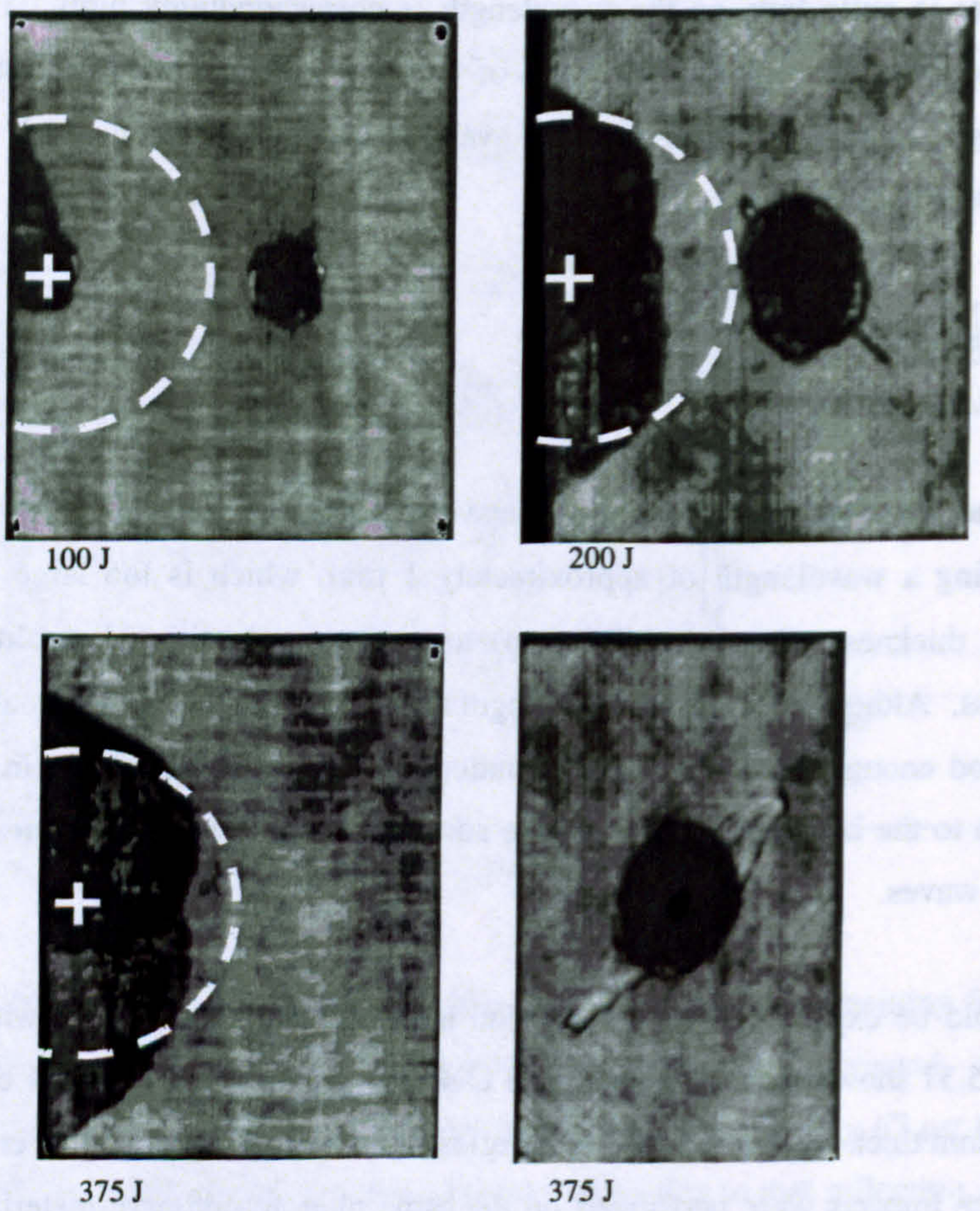

Figure 5.31 – Delamination area in 8 mm thick laminates subjected to increasing impact energy level

Figure 5.32 shows the full pattern of the delamination area against the impact energy, it shows the delaminated area from each impact where the full height of the impact machine was used. The area was measured from the C-scan results using ImageTool (Wilcox et al., 2002). Lines have been added to the graph that go through the average area at each impact energy for each plate thickness/impact position combination. Central impacts give a smaller delamination area in every case compared to the equivalent edge impact. In addition the increase in delamination area for each plate thickness and impact position is clear as the impact energy increases. The 4 mm plates do not exhibit such a dramatic increase, and this can be further explored by examining the C-scans directly, Figure 5.33.

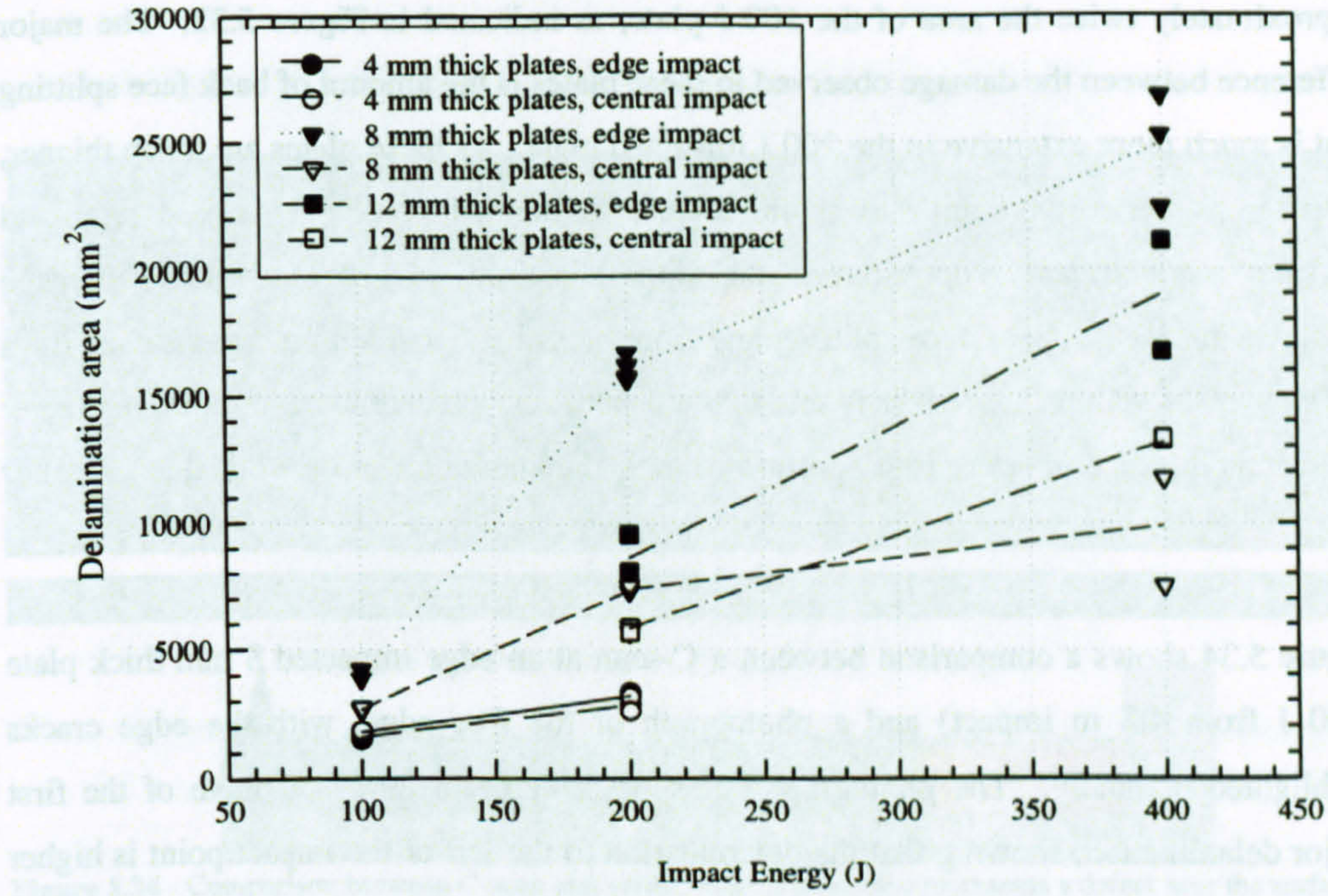

Figure 5.32 - Delamination areas for all specimens impacted from 4.3 m with lines passing through the average area at each energy

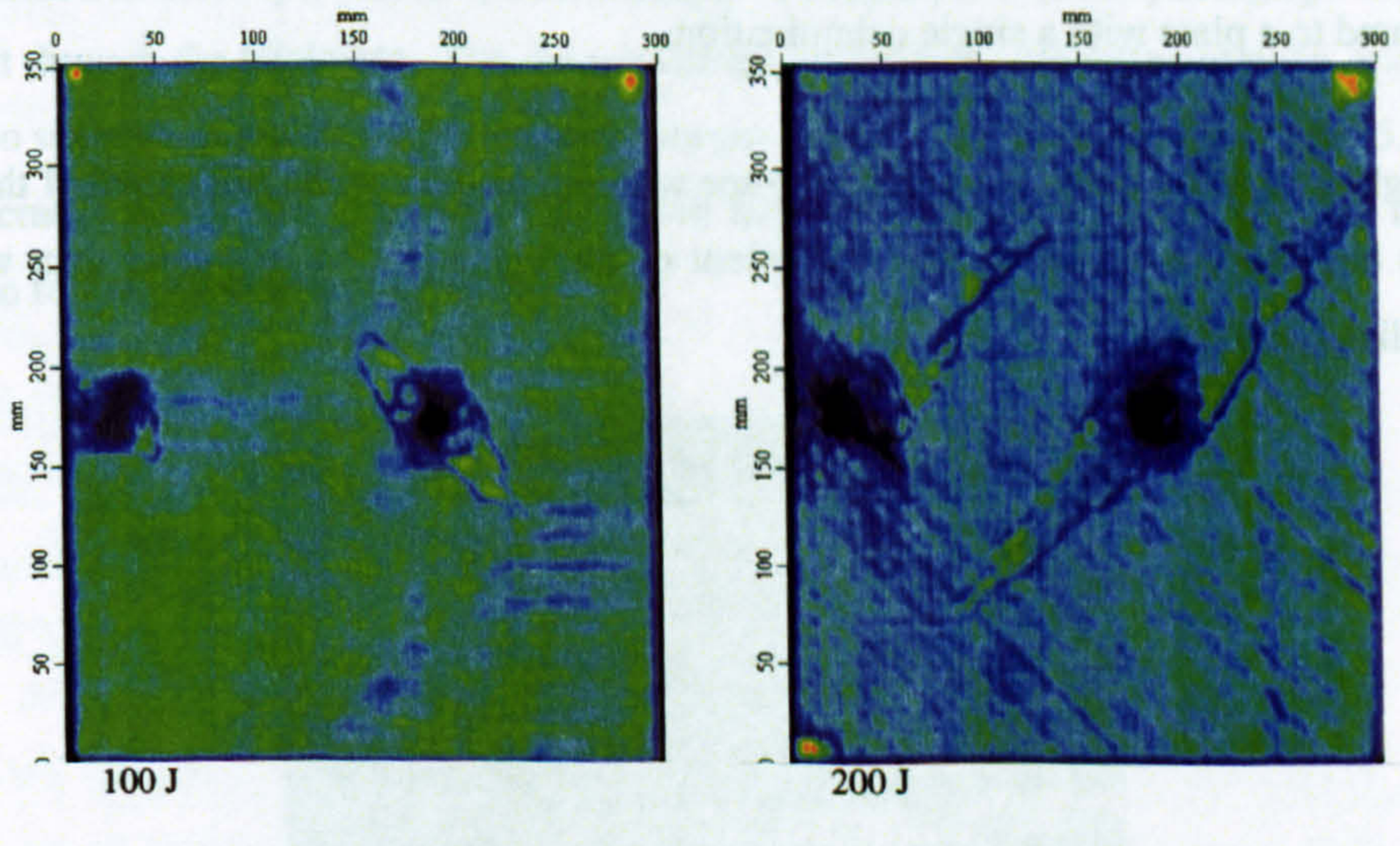

Figure 5.33 - Back face amplitude scans of two 4 mm plates impacted with different energies

Figure 5.33 shows the back face amplitude scans of two 4 mm thick plates, one impacted with 100 J and one with 200 J. The 200 J impacted plate shows delaminations with

approximately twice the area of the 100 J plate, as indicated in Figure 5.32. The major difference between the damage observed in these plates is the amount of back face splitting that is much more extensive in the 200 J impacted plate. As these plates are much thinner, at this impact energy the impactor is much closer to the threshold penetration energy, and as such a significant proportion of the impact energy goes towards other damage mechanisms such as back face splitting and fibre breakage. In addition, the distance from the edge that the impactor strikes is set at 20 mm for every plate thickness. In these thinner plates this distance is larger in proportion to their thickness and so the edge has a smaller effect.

Figure 5.34 shows a comparison between a C-scan at an edge impacted 8 mm thick plate (200 J from 4.3 m impact) and a photograph of the free edge, with the edge cracks highlighted manually. The photograph and C-scan agree in terms of depth of the first major delamination, showing that the delamination to the left of the impact point is higher than that to the right of the impact point. It also highlights the limitation of the C-scan in its inability to detect the delaminations below the first one detected, and as the photograph shows there are many delaminated interfaces. The existence of more than one large delamination means that the compressive strength of the plate will be much reduced compared to a plate with a single delamination.

As might be expected it is not possible to see with the naked eye the full extent of the edge cracks and the C-scan shows that the extent of the delamination is greater than what is immediately obvious.

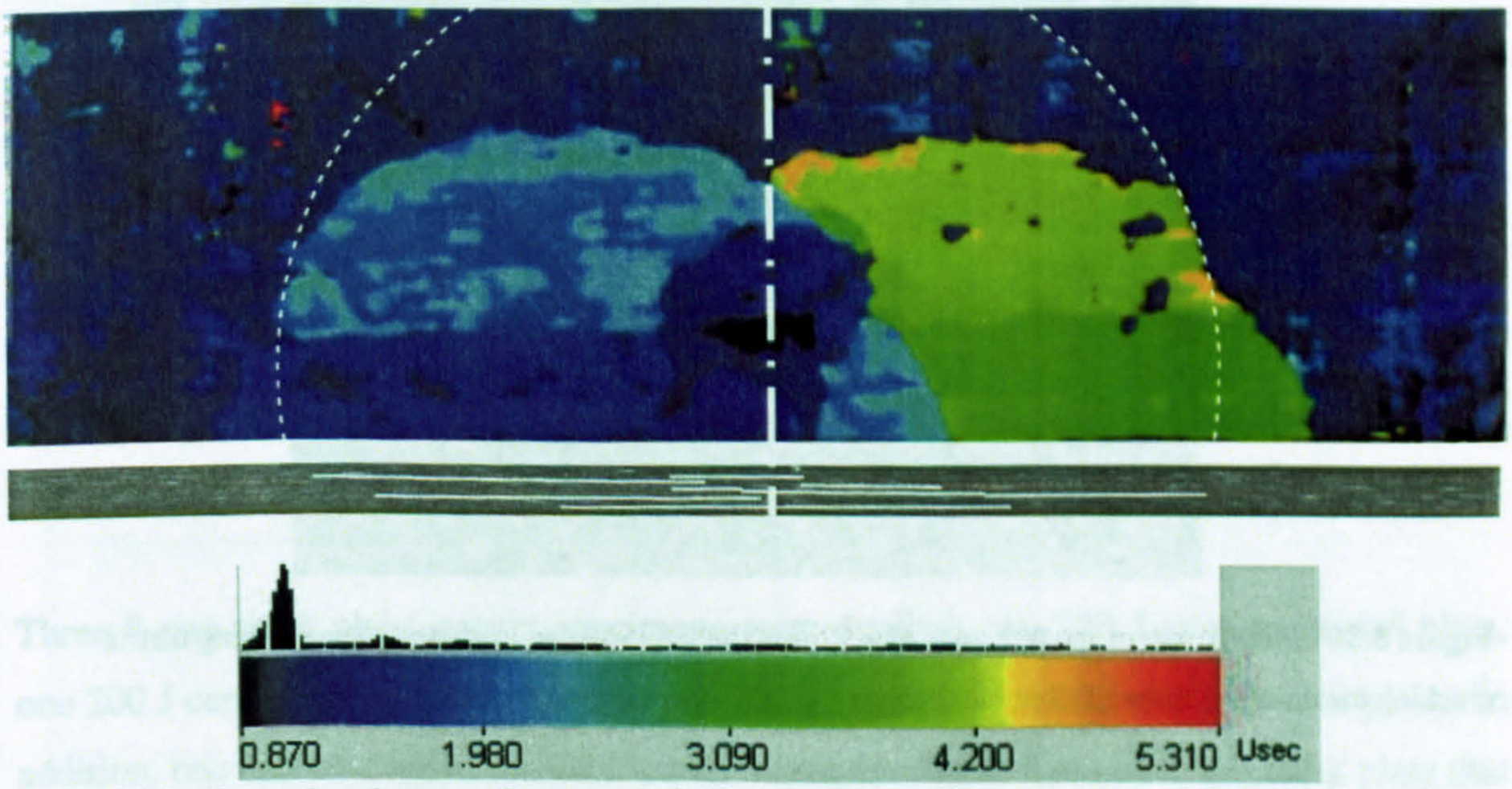

Figure 5.34 - Comparison between C-scan and visible edge cracks, blue represents a defect near the surface, red one nearer the back surface

Figure 5.35 shows a photograph of the free edge of a 12 mm thick edge impacted plate taken with a microscope. Clear are the multiple delaminations, in the photograph three are evident through the thickness. The delaminations are between the different plies, and there are also shear cracks as the delamination changes depth. As can be seen in Figure 5.36 the shear cracks follow the fibre bundles, which hence inhibit crack propagation by forcing them to follow more tortuous routes.

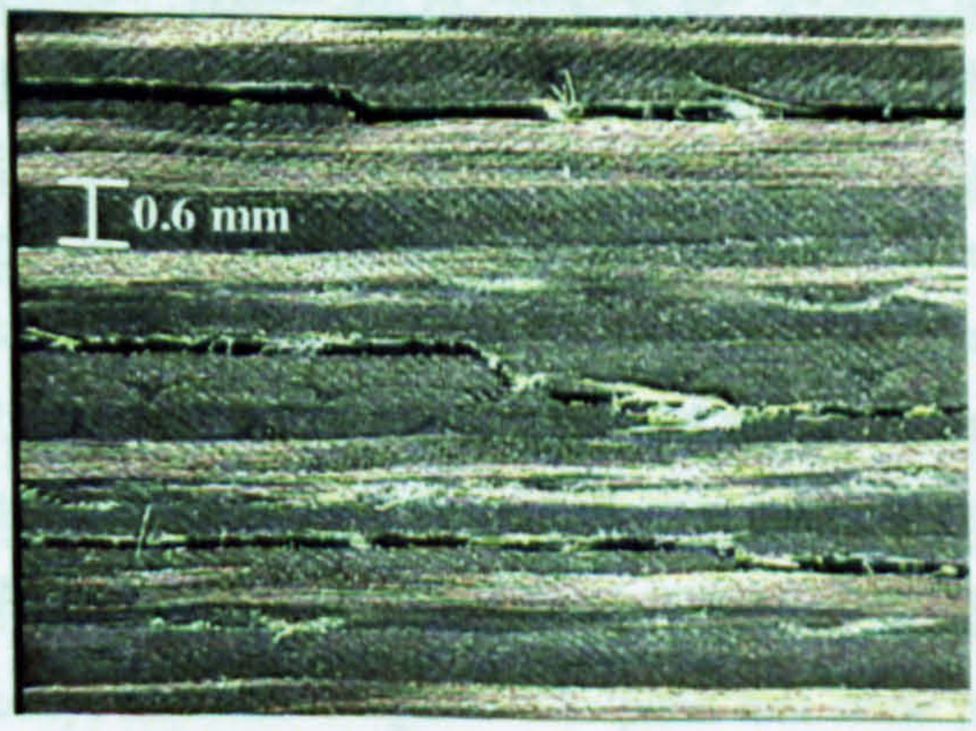

Figure 5.35 - Photograph of the free edge of a 12 mm thick 375 J edge impacted plate showing multiple delaminations

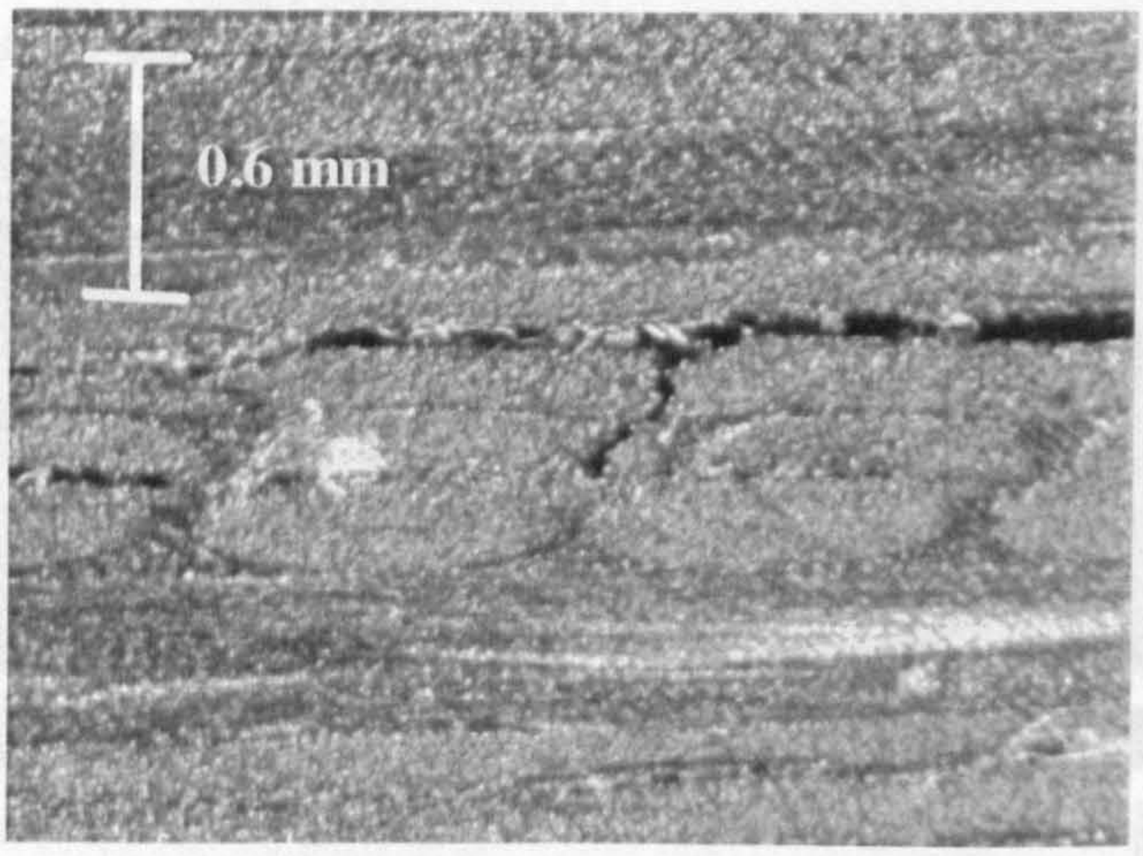

Figure 5.36 - Photograph of the free edge of a 12 mm thick 375 J edge impacted plate showing matrix cracking meandering between fibre bundles

5.3.4 Fibre Breakage

The best way to detect fibre breakage is the deply method as this enables direct observation of the individual plies. The method followed is similar to that used in previous research (Clarke, 1997). It involves heating the composite to pyrolise the resin in an atmosphere that will not allow the fibres to oxidise. The method was as follows:

1. Pre-heat furnace to 400°C.
2. The area of interest was cut from the impacted plate into a 100 mm x 100 mm square coupon with the impact point in the centre. The top right corner of each coupon was chamfered to allow easy orientation of the plies after the procedure.
3. In a small open container, the coupon was rested on a set of 8 metal rods 15 mm high to ensure the back face was open to the atmosphere. The container was filled with argon and placed into the furnace, which was then also filled with argon. Argon was chosen as it is heavier than air and prevents the fibres from oxidising. Once the pyrolysis of the resin had begun large quantities of smoke was emitted by the coupon, so an extraction system was employed and as this smoke is being emitted there is little chance of air entering the furnace so no further argon was added.

4. After 90 minutes the furnace was switched off and allowed to cool over night, after which the container was removed and the coupon carefully removed for deply. At this stage the coupon is delicate and is handled with care.
5. The deply procedure is carried out with sheets of clear adhesive film that are used to lift each layer from the coupon and seal it so it can be handled more robustly. A razor blade was occasionally used to aid the removal of the plies where there was some residue of adhesion.

The white polyester stitching was also totally burnt off so each individual ply was for one fibre direction. It was not possible to separate two adjacent plies with the same orientation.

Three 8 mm thick plain impact specimens were deplied: one 200 J edge impacted plate, one 200 J centrally impacted plate and one 200 J quasi-static simulated impacted plate. In addition, one half of a failed residual tensile strength coupon from an 8 mm thick plate that had been impacted centrally with 375 J was deplied in order to see the fracture surfaces of each ply. For each of the three plain impacted plates, a table showing the total fibre crack length in each ply has been produced. The crack length quoted is the effective crack length, i.e. perpendicular to the fibre direction irrespective of the actual crack direction and length. For all the deplied specimens a series of scale figures have been produced that accurately represent the fibre cracks in up to four plies in any one figure. A colour coding system was used to distinguish the fibre crack in one ply from another using the regime illustrated in Figure 5.37: red lines for cracks in 90° plies, green lines for those in +45° plies, blue lines for those in –45° cracks and black lines for those in 0° plies. A grid on each deply figure enables scaling, and the solid lines on the grid indicate the impact location. In the case of the edge impacted plate, the left hand edge of each figure corresponds with the free edge of the plate. In all cases ply 1 is on the top impacted surface, and ply 29 on the back surface of the plate.

Table 5.1 shows the perpendicular fibre crack length for each ply for an edge impacted 8 mm thick plate. Some crack lengths are asterisked (*) indicating that the crack on that ply extended beyond the coupon. Figure 5.38, Figure 5.39 and Figure 5.40 show the fibre cracks in ply graphically; from these figures it is plain that some plies did not show any fibre cracking. The grid spacing is 5 mm, with the impact point where the solid lines cross.

Similarly for Table 5.2 and Figure 5.41, Figure 5.42 and Figure 5.43 except for a centrally impacted 8 mm thick plate. From these figures it is plain that some plies did not show any fibre cracking. The grid spacing is again 5 mm with the impact point where the solid lines cross.

Similarly again for Table 5.3 and Figure 5.44, Figure 5.45 and Figure 5.46 except for a centrally simulated (quasi-static) impacted 8 mm thick plate. From these figures it is plain that some plies did not show any fibre cracking. The grid spacing is 10 mm.

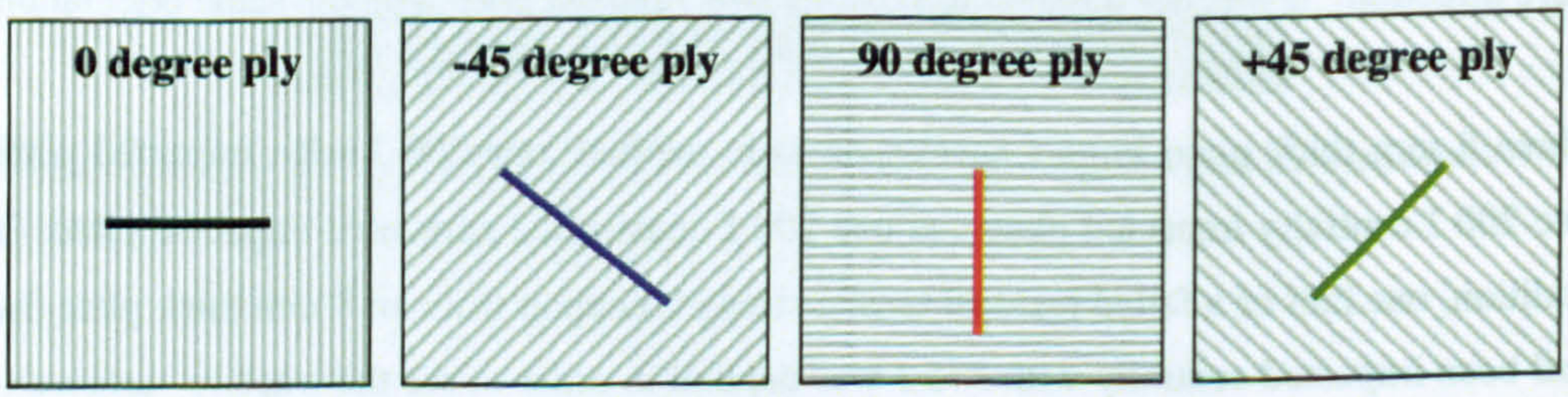

Figure 5.37 - Colour coding regime used in deply figures

Table 5.1 - Ply by ply fibre crack lengths for the 8 mm thick 200 J edge impacted plate. * indicates where the crack extends beyond the coupon and hence total crack length is unknown.

	Ply number	Fibre angle	Nominal Thickness (mm)	Crack length (mm)
(top)	1	-45	0.25	0
	2	90	0.1	5
	3	45	0.25	4
	4	0	0.6	9
	5	45	0.25	7
	6	90	0.1	0
	7	-45	0.25	0
	8	0	0.6	0
	9	-45	0.25	35*
	10	90	0.1	0
	11	45	0.25	0
	12	0	0.6	4
	13	45	0.25	0
	14	90	0.1	3
	15	-45	0.5	0
	16	90	0.1	40*
	17	45	0.25	0
	18	0	0.6	0
	19	45	0.25	17
	20	90	0.1	5
	21	-45	0.25	1
	22	0	0.6	0
	23	-45	0.25	25*
	24	90	0.1	0
	25	45	0.25	0
	26	0	0.6	0
	27	45	0.25	0
	28	90	0.1	0
(bottom)	29	-45	0.25	0

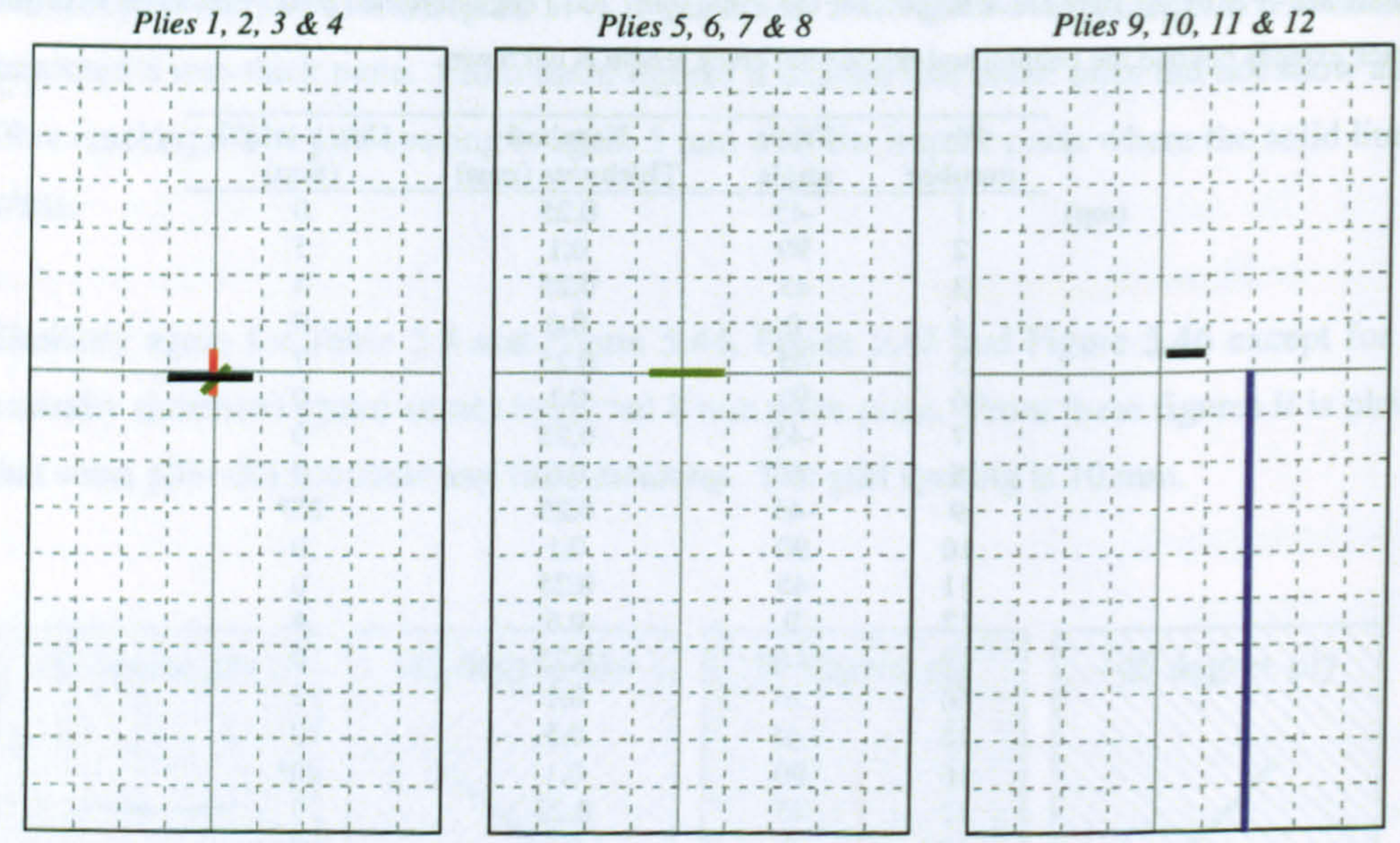

Figure 5.38 - Plies 1 - 12 showing fibre cracks following a 200 J edge impact on an 8 mm thick plate (5 mm grid spacing)

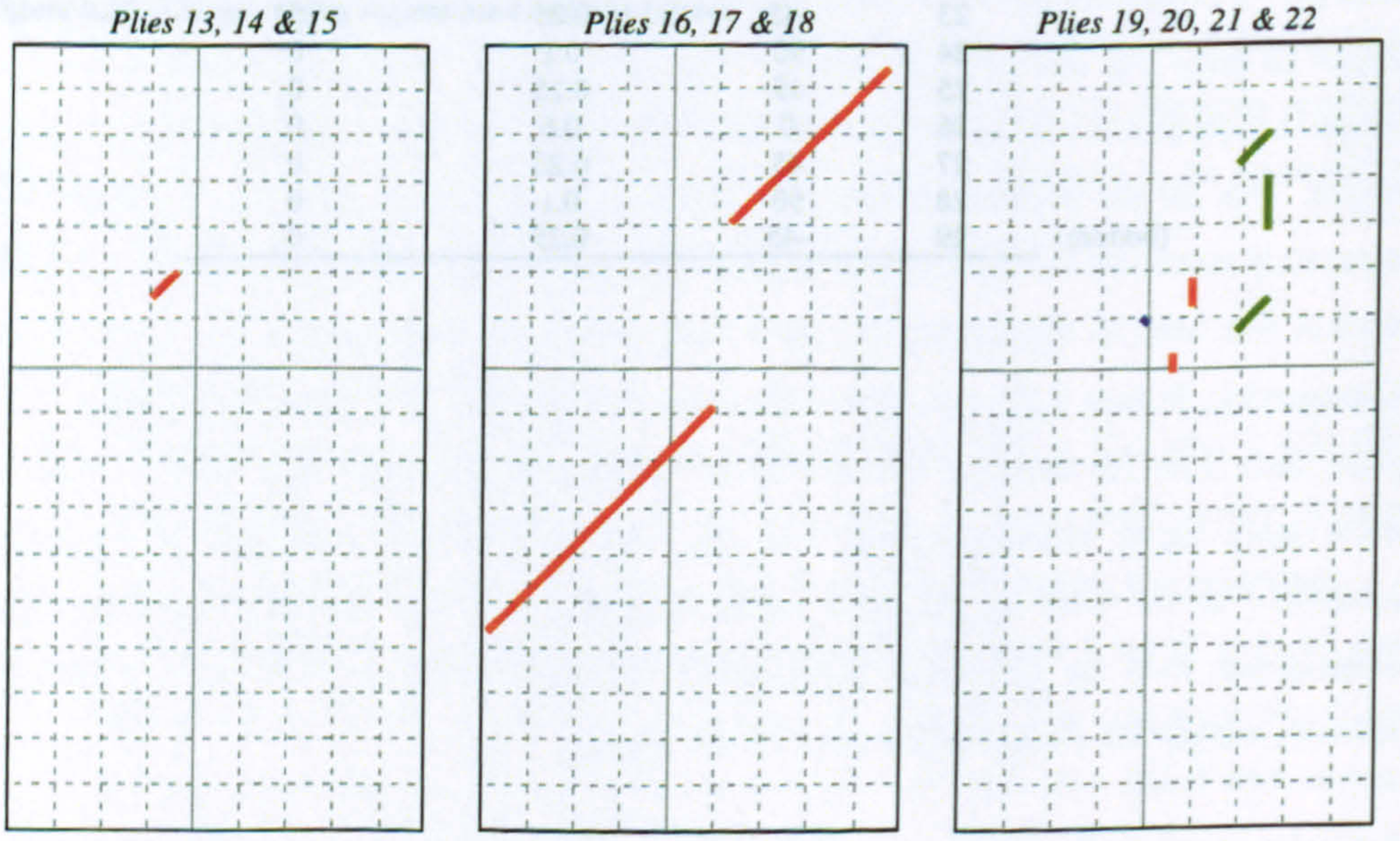

Figure 5.39 - Plies 13 - 22 showing fibre cracks following a 200 J edge impact on an 8 mm thick plate (5 mm grid spacing)

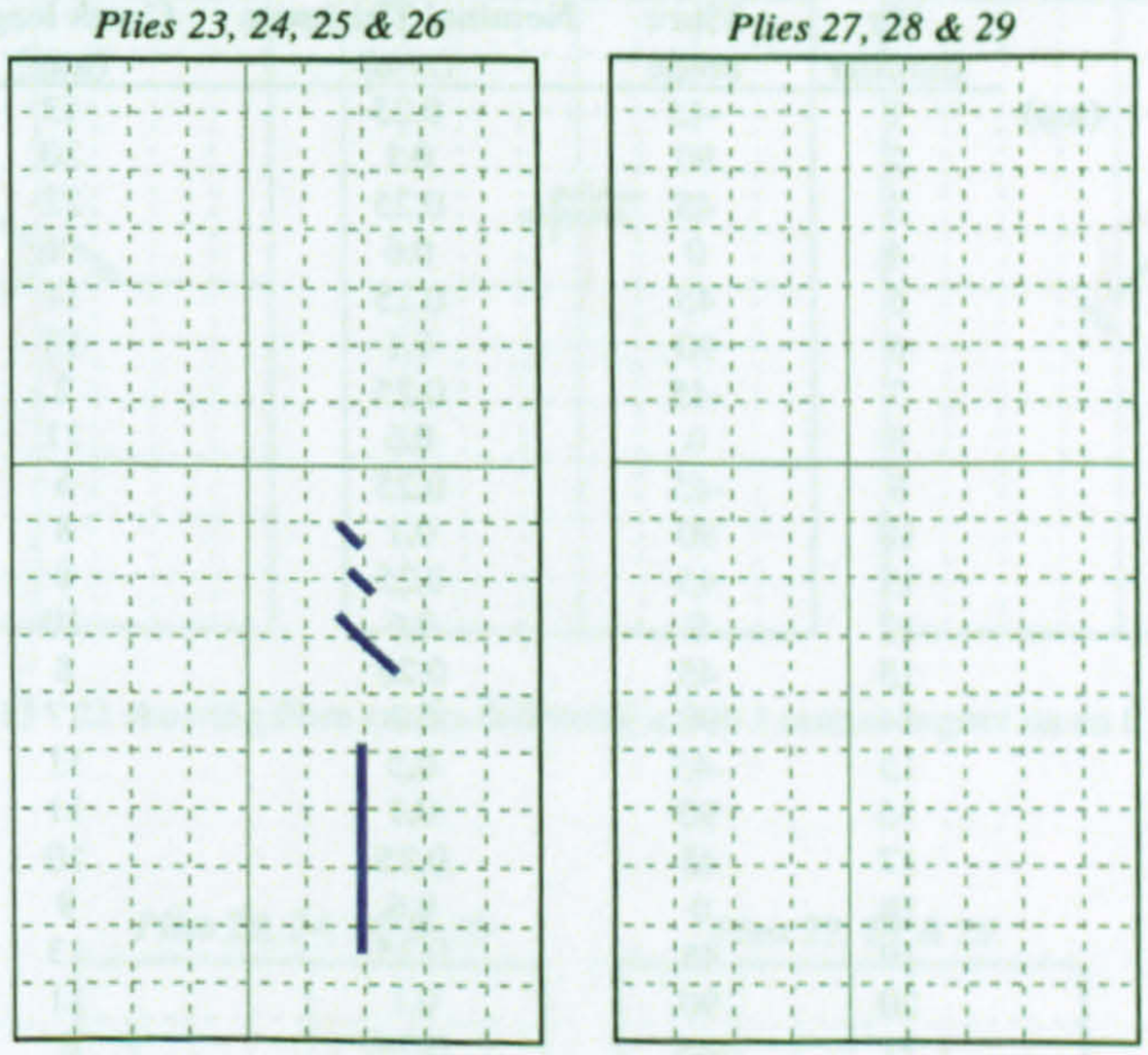

Figure 5.40 - Plies 23 - 29 showing fibre cracks following a 200 J edge impact on an 8 mm thick plate (5 mm grid spacing)

Table 5.2 - Ply by ply fibre crack lengths for the 8 mm thick 200 J centrally impacted plate

	Ply number	Fibre angle	Nominal Thickness (mm)	Crack length (mm)
(top)	1	-45	0.25	13
	2	90	0.1	30
	3	45	0.25	22
	4	0	0.6	11
	5	45	0.25	11
	6	90	0.1	13
	7	-45	0.25	2
	8	0	0.6	11
	9	-45	0.25	6
	10	90	0.1	8
	11	45	0.25	8
	12	0	0.6	10
	13	45	0.25	8
	14	90	0.1	17
	15	-45	0.5	11
	16	90	0.1	11
	17	45	0.25	10
	18	0	0.6	9
	19	45	0.25	13
	20	90	0.1	11
	21	-45	0.25	3
	22	0	0.6	0
	23	-45	0.25	8
	24	90	0.1	30
	25	45	0.25	0
	26	0	0.6	12
	27	45	0.25	20
	28	90	0.1	33
(bottom)	29	-45	0.25	4

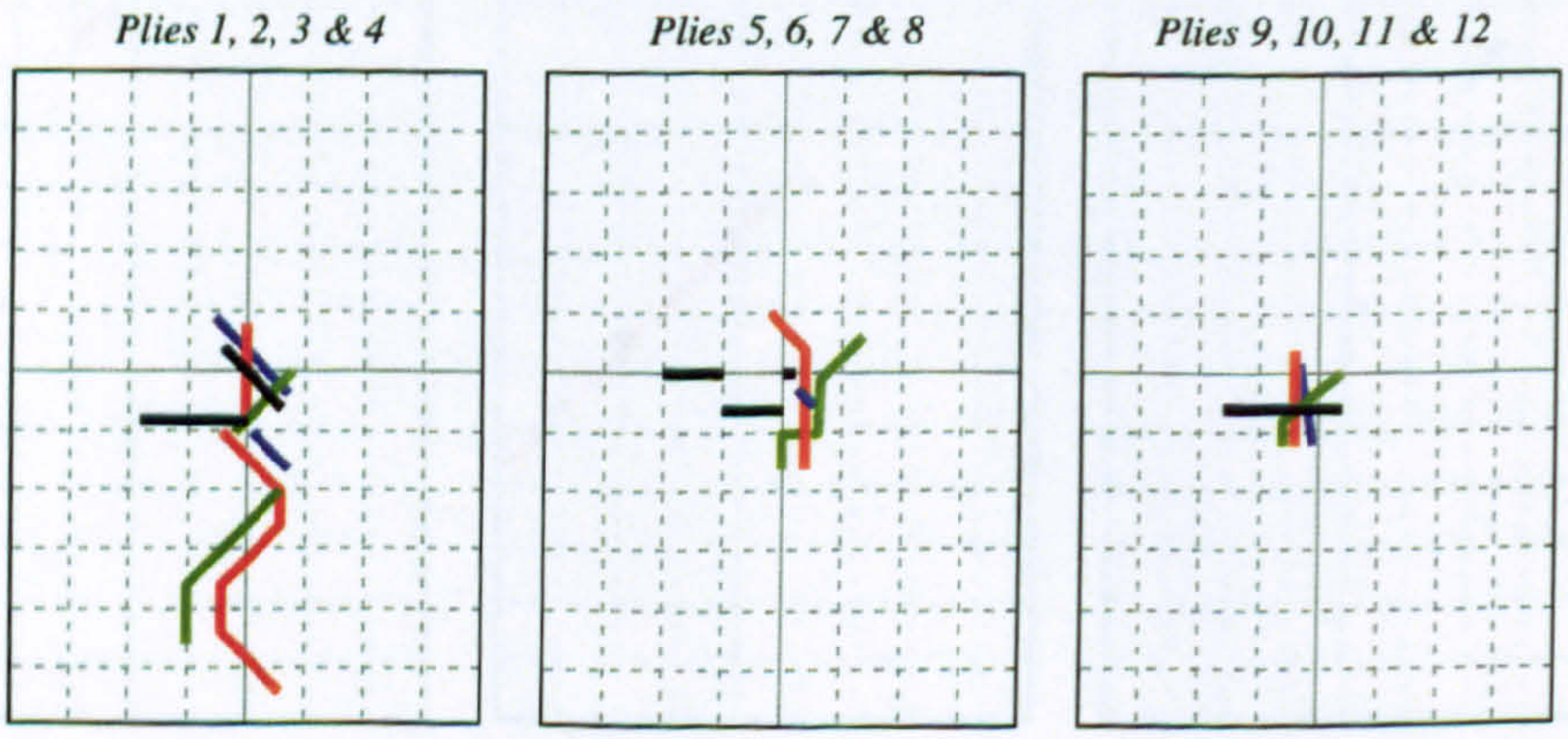

Figure 5.41 - Plies 1 - 12 showing fibre cracks following a 200 J central impact on an 8 mm thick plate (5 mm grid spacing)

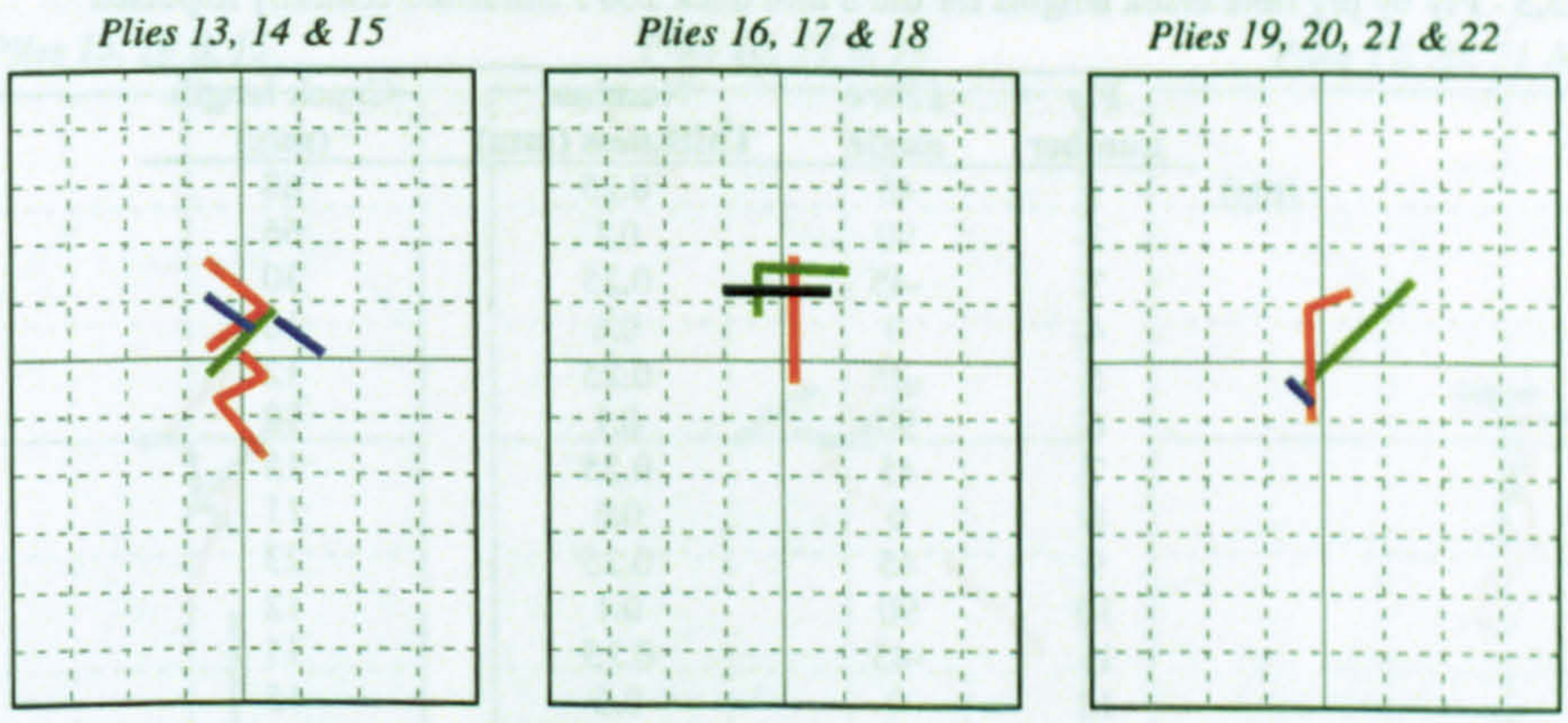

Figure 5.42 - Plies 13 - 22 showing fibre cracks following a 200 J central impact on an 8 mm thick plate (5 mm grid spacing)

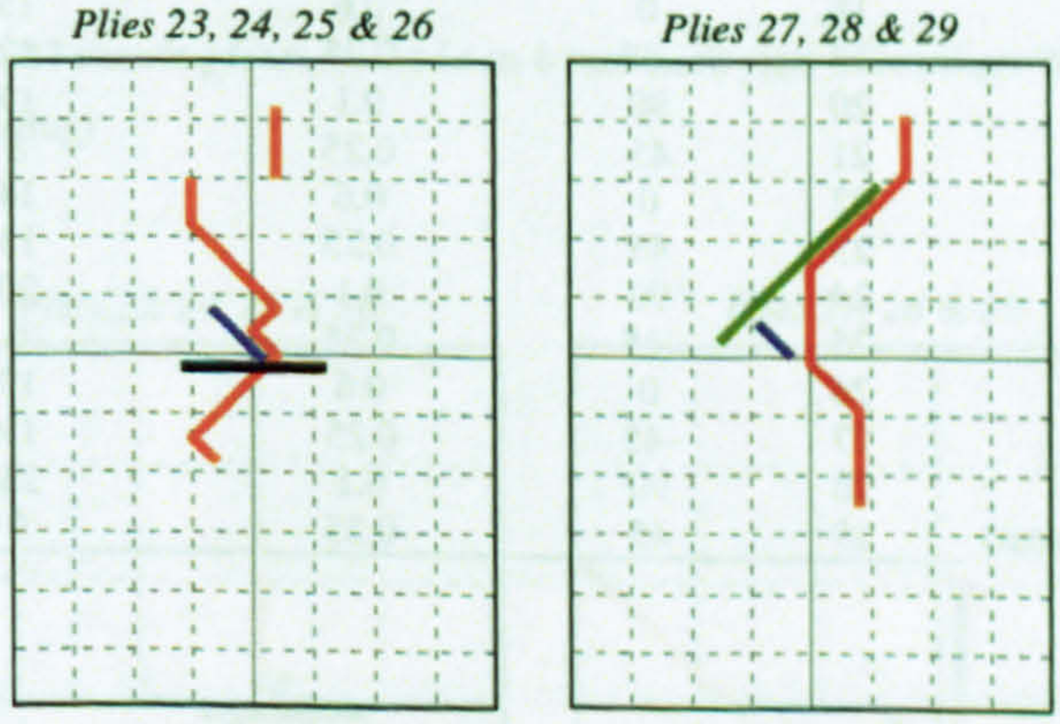

Figure 5.43 - Plies 23 - 29 showing fibre cracks following a 200 J central impact on an 8 mm thick plate (5 mm grid spacing)

Table 5.3 - Ply by ply fibre crack lengths for the 8 mm thick 200 J simulated centrally impacted

	Ply number	Fibre angle	Nominal Thickness (mm)	Crack length (mm)
(top)	1	45	0.25	68
	2	90	0.1	66
	3	-45	0.25	30
	4	0	0.6	10
	5	-45	0.25	12
	6	90	0.1	12
	7	45	0.25	15
	8	0	0.6	11
	9	45	0.25	23
	10	90	0.1	12
	11	-45	0.25	11
	12	0	0.6	15
	13	-45	0.25	21
	14	90	0.1	23
	15	45	0.5	11
	16	90	0.1	33
	17	-45	0.25	6
	18	0	0.6	15
	19	-45	0.25	12
	20	90	0.1	19
	21	45	0.25	8
	22	0	0.6	14
	23	45	0.25	13
	24	90	0.1	20
	25	-45	0.25	6
	26	0	0.6	15
	27	-45	0.25	19
	28	90	0.1	25
(bottom)	29	45	0.25	0

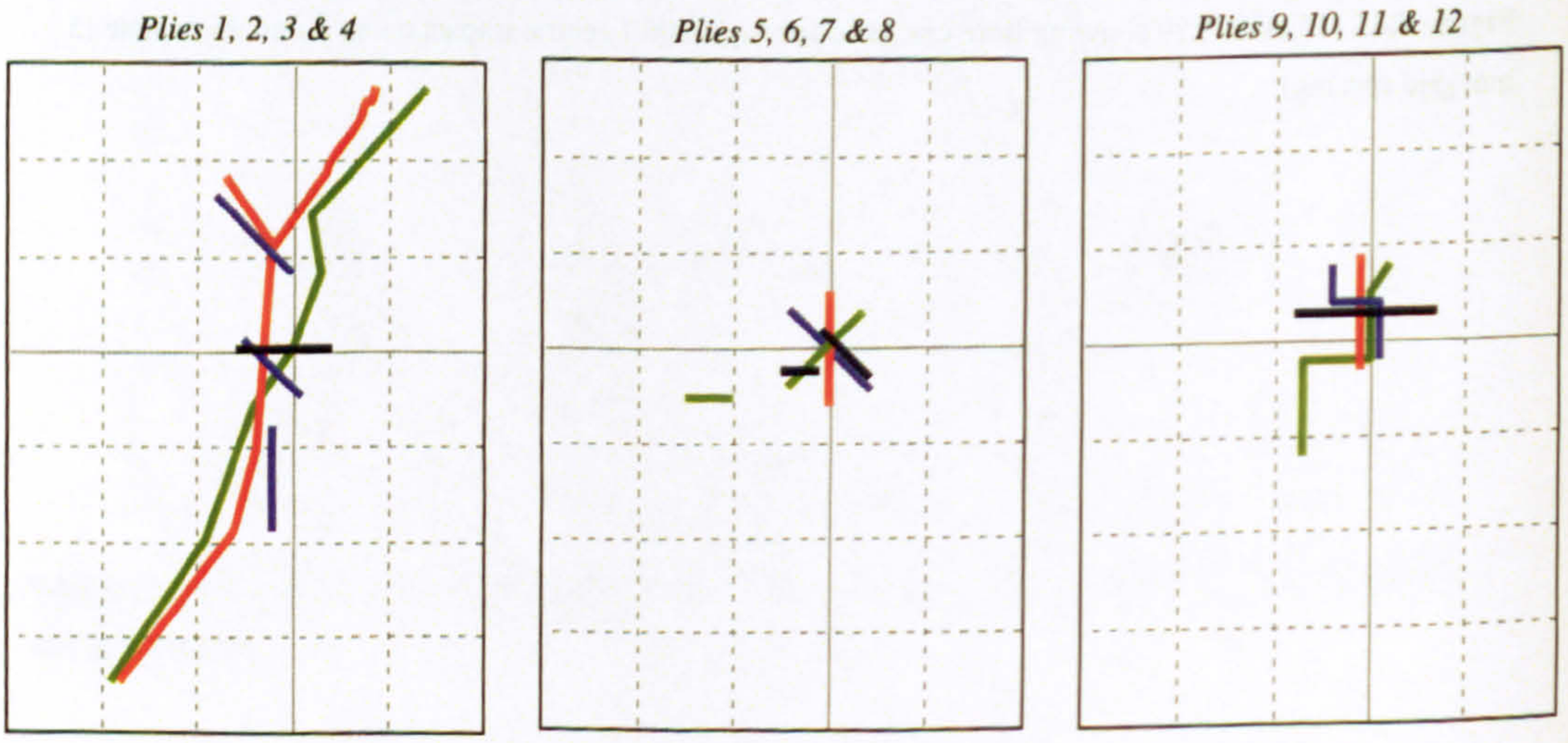

Figure 5.44 - Plies 1 – 12 showing fibre cracks in an 8 mm thick plate following a 200 J central simulated impact (10 mm grid spacing)

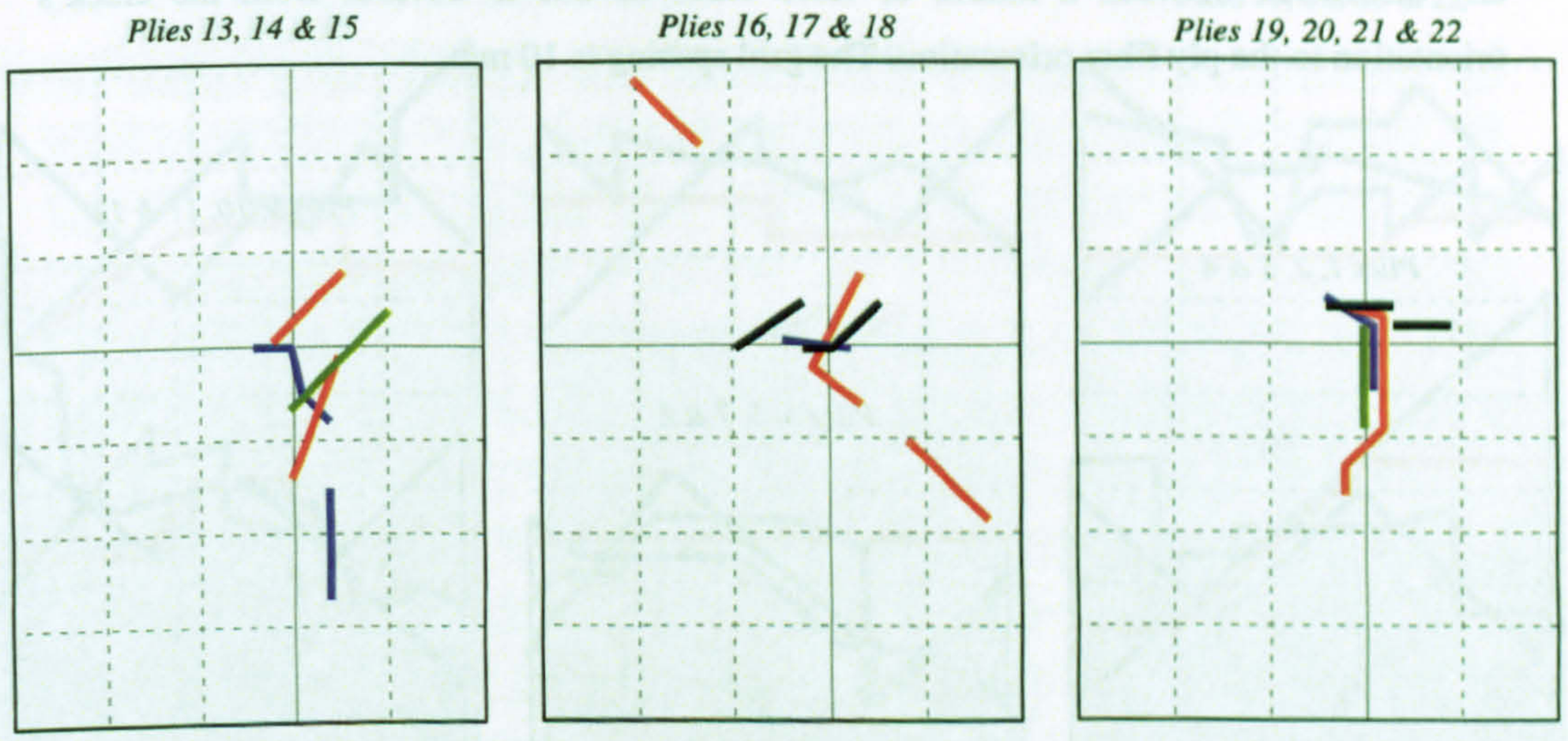

Figure 5.45 - Plies 13 – 22 showing fibre cracks in an 8 mm thick plate following a 200 J central simulated impact (10 mm grid spacing)

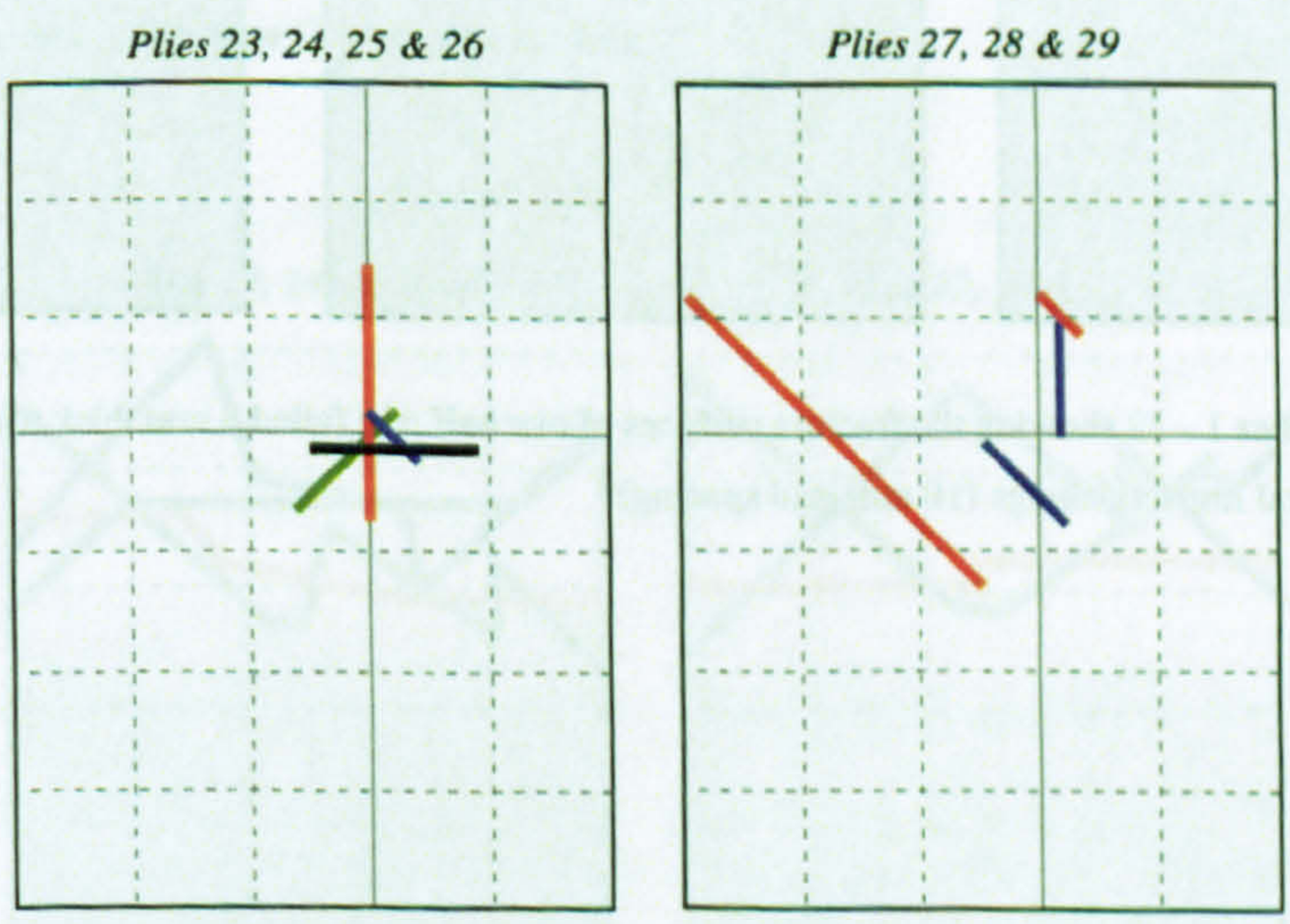

Figure 5.46 - Plies 23 - 29 showing fibre cracks in an 8 mm thick plate following a 200 J central simulated impact (10 mm grid spacing)

Figure 5.47, Figure 5.48 and Figure 5.49 show the fracture surfaces in one half of a failed tensile coupon with impact damage from a 375 J impact centrally onto an 8 mm thick plate. The lines show the total crack and fracture boundary of each ply without making

any distinction between a matrix or fibre crack as this is obvious from the crack's orientation to the ply fibre orientation. The grid spacing is 10 mm.

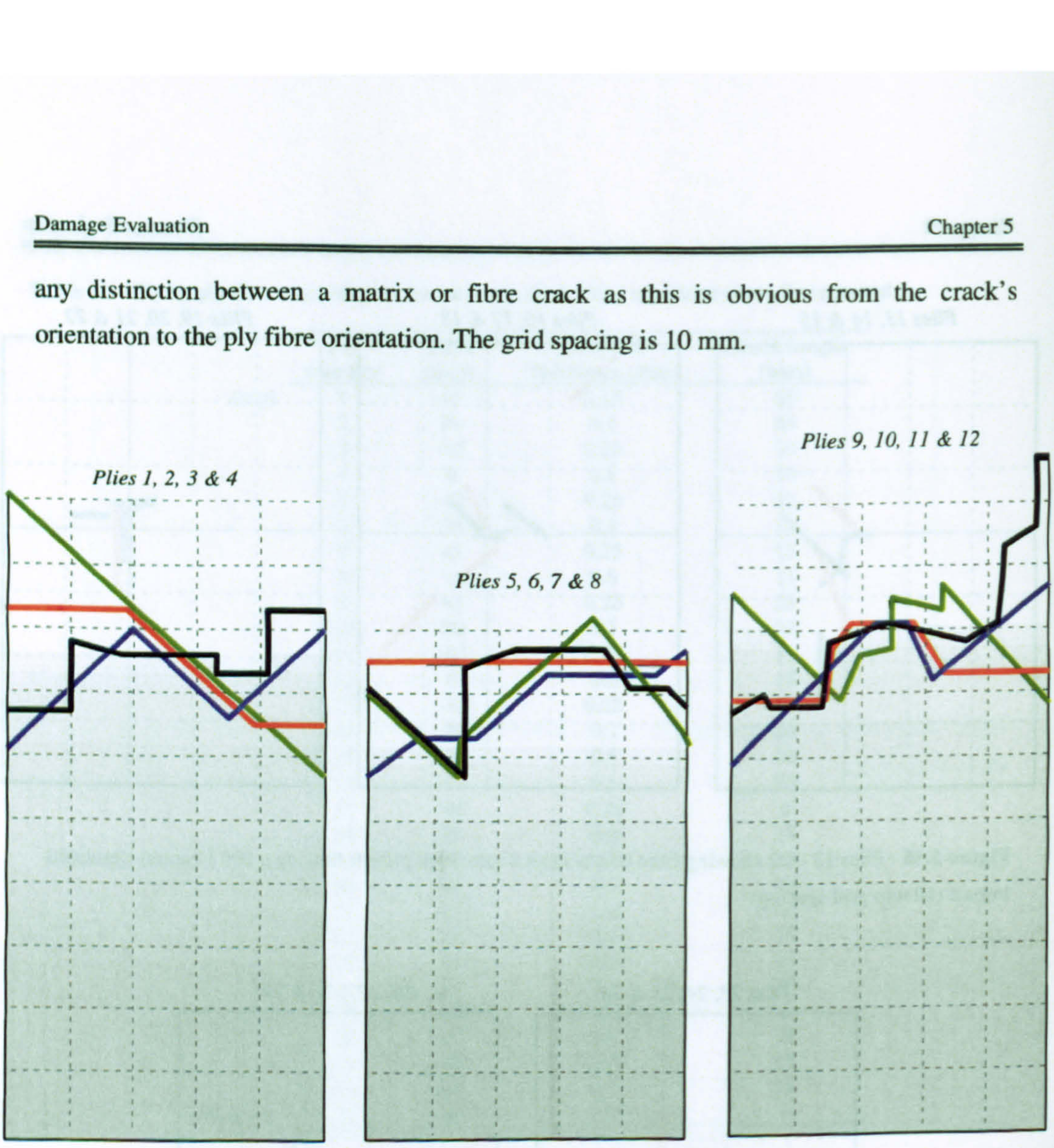

Figure 5.47 - Plies 1 - 12 showing the fracture surfaces of one half of a failed 8 mm thick tensile coupon with 375 J central impact damage (10 mm grid spacing)

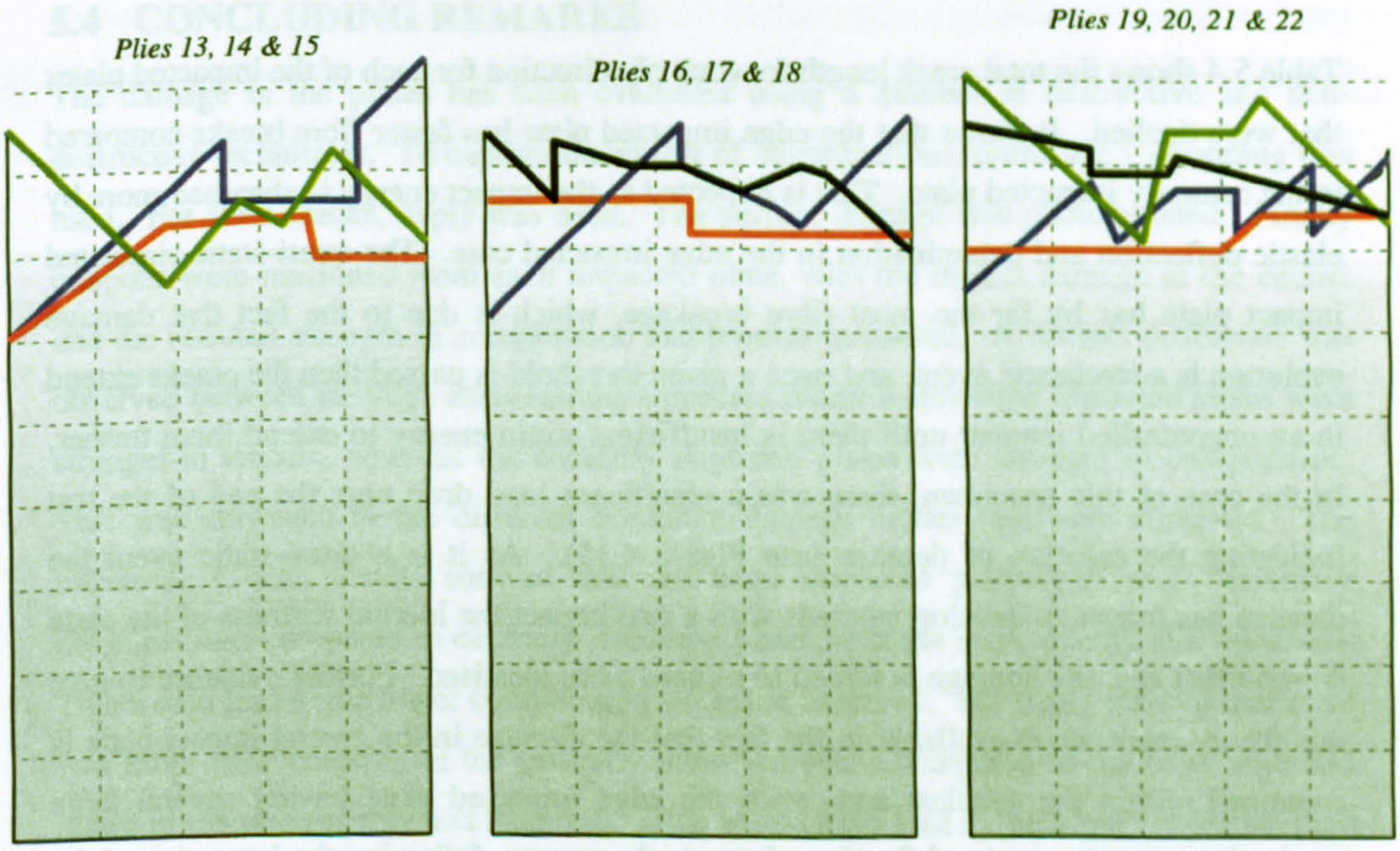

Figure 5.48 - Plies 13 - 22 showing the fracture surfaces of one half of a failed 8 mm thick tensile coupon with 375 J central impact damage (10 mm grid spacing)

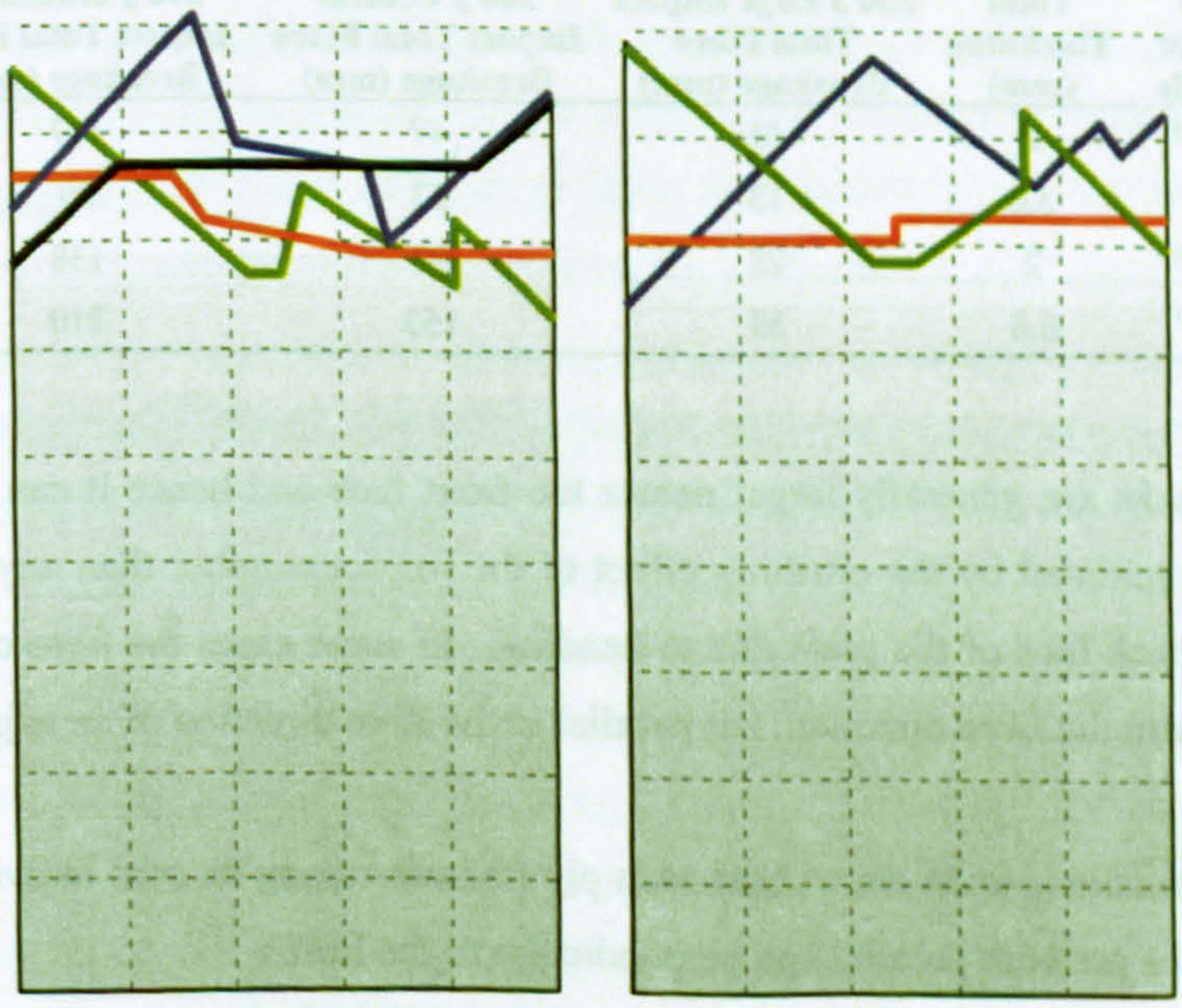

Figure 5.49 - Plies 23 - 29 showing the fracture surfaces of one half of a failed 8 mm thick tensile coupon with 375 J central impact damage (10 mm grid spacing)

Table 5.4 shows the total crack length for each ply direction for each of the impacted plates that were deplied. It shows that the edge impacted plate has fewer fibre breaks compared to the centrally impacted plate. This is expected as the impact energy is absorbed more by elastic deflection and delamination in the edge impacted case. The quasi-static simulated impact plate has by far the most fibre breakage, which is due to the fact that damage evolution is a stochastic event, and once a given threshold is passed then the cracks extend in an uncontrolled manner until there is insufficient strain energy to extend them further. In the case of this specimen, there was a significant load drop near the end of the test indicating the creation of damage (see Figure 4.15). As it is a quasi-static event the damage has longer to develop whereas with a real impact the inertial stiffness of the plate is important and any damage is forced to remain more localised. Further evidence to give this theory credence is available in the fact that the damage in the central impact plate is contained within the smallest area, with the edge impacted plate having several large cracks that extend outside of the size of the deply coupon, following the large size of the delamination.

Table 5.4 - Total fibre breakage for each ply direction on the three impacted plates deplied

Ply Fibre Angle	Total Thickness (mm)	200 J Edge Impact Total Fibre Breakage (mm)	200 J Central Impact Total Fibre Breakage (mm)	200 J Simulated Impact Total Fibre Breakage (mm)
-45°	2	61	47	117
0°	3.6	13	53	80
45°	2	28	92	138
90°	0.8	53	153	210

The fibre cracks are generally larger nearer the front face and hence it can be presumed that they are initiated by the crushing effect of the impactor rather than any large tensile force in the back face of the plate due to bending. In some cases the fibre cracks are not perpendicular to the fibre direction, but parallel to the fibre direction of an adjacent ply.

The deplied tensile coupon shows that each ply fractures along its own individual fracture path and cracks are both parallel and perpendicular to the fibres.

5.4 CONCLUDING REMARKS

The damage in the plates has been evaluated using a number of destructive and non-destructive techniques. To capture the extent of delaminations, ultrasonic C-scanning was used. For fibre cracks, deply was used. The surface damage was photographed. Finally coupons were machined from each impacted plate, with the impact damage in the centre, and the residual strength in compression and tension measured. A distinct difference was observed between the edge and centrally impacted plates where edge impacted plates were stronger in tension, whereas the centrally impacted plates were stronger in compression. This was attributed to the different dominant damage modes that were observed. The ultrasonic C-scan results showed that the edge impacted plates had more extensive delaminations compared to centrally impacted plates with the same energy and thickness. This would lead to the lower compression strengths observed. The deply showed that there was more fibre cracking in the centrally impacted plates compared to the edge impacted plates of the same energy and thickness. This would have lead to the lower tensile strength of the centrally impacted plates that was observed.

CHAPTER 6

FINITE ELEMENT ANALYSIS OF ELASTIC IMPACT

6.1 INTRODUCTION

6.1.1 Background

Materials can be analysed using simple constitutive laws, such as those devised by Hooke. These can, however, be limiting, and analysis of complex structures and loading requires more advanced techniques.

Tools and techniques have been developed that enable the prediction of the performance of a structure and its materials, such as more advanced analytical and numerical methods. The ideal is to be able to model a structure in order to assess the quality of the design before manufacture with the benefit of reduced cost of development.

To model a composite component from elastic behaviour through initial damage to final failure requires significant effort; hence today a lot of composites research is focussed on measuring characteristic properties and defining the mathematical relations that can be used to predict structural performance.

6.1.2 The Finite Element Method

As materials and their applications have become more complex so have the methods required to analyse them accurately. Analytical methods have become increasingly complex and specialised so that there is no single best way to solve a problem. To derive

an analytical solution requires rigorous mathematical modelling given a deep understanding of the material or empirical method of fitting a model to experimental results. Both have limitations either in the mathematics to model a complex non-linear event in a useable manner or the applicability of the experimental results that have been used to create the empirical relation.

By admitting that an analytical model cannot simulate a structural response, the approximation via numerical methods offers a welcome alternative. These methods do not necessarily require rigorous mathematical modelling but use general techniques given that we know the material and geometry of our problem. Finite element analysis was first conceptualised in the 1950's. However it was not until the 1970's, as computing power increased that our ability to use numerical methods such as finite element analysis also increased dramatically. When we have a characterised material, geometry and a loading scenario that we are unable to solve analytically, the finite element method offers an answer. The essence of this method is that the geometry is divided into discrete, or finite, elements. First a series of nodes are defined across the geometry that when joined up create a grid, or mesh, of enclosed finite elements. With the element material parameters and geometry known, the solution becomes a case of simultaneously solving the differential equations for continuity and equilibrium for every node. To achieve accurate results, the challenge becomes knowing how best to mesh the geometry, the element type to use, what simplifying assumptions can be made, all limited by how powerful the computing resource is that you have at your disposal.

Today a number of commercial finite element codes are available offering increased analysis potential together with ease of model creation and the flexibility to modify manually models to individual requirements.

6.1.3 Aims and Chapter Structure

In this chapter various analyses are presented. Analysis has been conducted as a part of this research for a variety of reasons, primarily to investigate the impact response of thick laminates. As will unfold, the main motivations for the analysis presented here are firstly to understand the impact response of large thick laminate plates in order to be able to confirm the validity of smaller scale coupon based experimental tests, and secondly to

understand the failure of the coupons. There are further studies to investigate the design of experimental rigs and, as the analyses are based on a series of simplifying assumptions, ways to make the analysis more representative of the actual material response are discussed.

As the analysis described in this Chapter was carried out before the experimental test schedule was finalised, the material properties of the laminates tested were not available. Also, different impact energies and impactor masses were analysed than those used during the tests, and the composite plate diameters were mostly larger than what was tested. This means that there is little that is directly comparable with the experiments; however the aim of the analysis was to gain qualitative understanding of the response of the plates, and investigate what might happen to plates with dimensions larger than what was actually tested.

The finite element modelling presented in this chapter largely used ABAQUS/Explicit, with axi-symmetric models. The general form of the models and analyses are presented in Section 6.2.

Section 6.3 examines the differences between impact and statically loading a plate and why explicit finite element analysis is needed.

Most often the experimental impact of composite laminates is on small coupons that are constrained in fixtures that are not representative of how they are used in practice. Wing skins on large aeroplanes can have in-plane dimensions of several metres, and be riveted, bolted, bonded or a combination at their edge. Unfortunately the cost of testing real structures in a detailed study is prohibitive, and researchers are forced to test coupon size specimens either simply supported or built in. To relate the response and damage found in experiment to that which might happen in a real structure is difficult. Hence in Section 6.4 the work conducted to find better ways of relating coupon tests to real structure response is presented. This is important to understand exactly the effect that varying the parameters of the system has on the response of the plate.

When impacting a specimen in an experiment, choice of a representative drop height and mass is important. Although it is often thought that purely the incident kinetic energy of

the impactor is enough for classification, circumstantial evidence has shown otherwise. Hence the experimental programme to investigate this further, and in Section 6.5 the complementary finite element study is presented.

To study the effect of impacting near a free edge, 3-dimensional models were used. Section 6.6 presents these results and discusses how these models show why the plates accumulated damage in the way observed experimentally.

Finally in Section 6.7 all further analyses are presented, particularly that which investigated the impactor design, and location of the accelerometer on the impactor.

6.2 PLATE IMPACT FINITE ELEMENT MODEL

6.2.1 Introduction

In this section, the common and generic properties of the models used in the subsequent two sections are presented. In addition the code used is introduced and the mesh convergence study discussed.

6.2.2 Common Model Properties

6.2.2.1 Finite Element Code

The dynamic impact of a plate is being modelled. Some researchers assume that a static approach is valid and model the impact using an implicit code, for example in Green, Morrison and Luo (2000). However this approach will not give a detailed history of the response of the plate to the impact. An explicit code will solve such a dynamic problem, and by the nature of the solution it derives detailed time-history results of the displacement and force in the system. In this research it was considered important to include any transient effects, due to the propagation of stress waves and hence an explicit solver was chosen.

The meshes used by each solver type tend to be different, the design of the mesh being driven by the opposing requirements of having accurate results that do not come at too great a computational cost. Assuming that the requirement of accurate results is common

then the meshes will differ in how the analyst ensures the simulation is efficiently solved. In an implicit code the computational cost depends mainly on the number of elements and degrees of freedom in the model, i.e. the more elements the longer it takes to solve. In an explicit code the computational cost depends on the smallest time taken for a stress wave to cross the smallest element (not across any particular element dimension), this depending on element dimensions and material properties. This time scale will determine the increment size in the analysis, and it is not uncommon for an explicit analysis to have up to 100,000 increments. Although both types of solver will require mesh refinement near a stress raiser, the mesh for an implicit analysis may have a greater refinement, whereas the equivalent mesh for an explicit analysis will have a more uniform mesh and many more increments. Optimised meshes are possible for both types, where further mesh refinement will not give significantly more accurate results.

For the reasons outlined above ABAQUS/Explicit was used to perform all the finite element analysis in this research. Versions 6.2, 6.3 and 6.4 were used. ABAQUS/CAE was used as the pre-processor to create the input decks defining the geometry, loading conditions and materials and also as the post-processor to process the results. The simulations were run on a Silicon Graphics Origin 200 server with a 133MHz processor and 128MB of RAM.

6.2.2.2 A Note on Explicit Finite Element Solvers

Explicit solvers include all transient effects in an analysis, and all solutions have a real time base. Unlike with an implicit analysis where the time period of the solution is arbitrary, that with an explicit analysis is the total time for which the analyst wishes to have a solution; in the case of this research the duration of an impact event. So, the time period has real physical meaning.

To perform the analysis, the code, in a time marching fashion, calculates the solution incrementally. The size of each increment is important and depends on the stable time increment, which in turn depends on the mesh and material. This increment, for the analysis to represent accurately the physical world, cannot be longer in duration than the shortest time taken for any stress wave to cross any element. The critical element will be the smallest in the model where an isotropic material is used. Where an anisotropic

material is used the critical element may not be the smallest, as the speed of a stress wave depends on the material stiffness.

So the time needed to run a simulation depends firstly on the size of the stable time increment, and then on the time period of the analysis. Further the number of elements and number of times data is written to the output database will also affect the computational cost.

6.2.2.3 Material Model

As described earlier, the lay-up of the laminates in this research involves many thin layers to create a thick plate. As the layers are small in comparison to the total thickness, and it is the global response that is required, the laminate can be modelled as homogenous in-plane with a reduced stiffness through the thickness by merging the ply properties. This is not seen as a limitation to the analysis; although the laminate lay-up is not quasi-isotropic, it is not far off, and the purpose of the analysis is not to provide quantitative results but a qualitative understanding of the impact response of a composite plate. This assumption can be verified by simply checking with classical lamination theory (Daniel and Ishai, 1994).

As the finite element analysis was carried out before any experimental work, the properties of the materials used were unknown. Therefore a set of material properties was chosen and used for the analysis in this Chapter, a set of generic carbon fibre composite properties (T300/934 carbon/epoxy) in a quasi-isotropic lay-up ((+45/-45/0/90)s). Note that this is different to the lay-up defined for the laminates in Figure 3.5. A quasi-isotropic lay-up was chosen to simplify the analysis and allow the use of an axi-symmetric model. The properties were taken from the data library supplied with the Classical Laminate Theory software, Laminator, (Lindell, 2001), and are presented in Table 6.1. Table 6.2 shows the apparent laminate properties resulting from this and consequently used in the analyses. Due to the quasi-isotropic lay-up and following the co-ordinate system defined (Figure 6.1) the two in-plane elastic moduli are equal ($E_1 = E_3$) and the two out of plane elastic shear moduli are equal ($G_{12} = G_{23}$). The co-ordinate system used in the analysis is different to that normally defined for laminates, due to the way the geometry is defined for an axi-

symmetric model in the finite element software; the out of plane (or through thickness) axis is 2 and the two in-plane axes are 1 (fibre direction) and 3, see Figure 6.1.

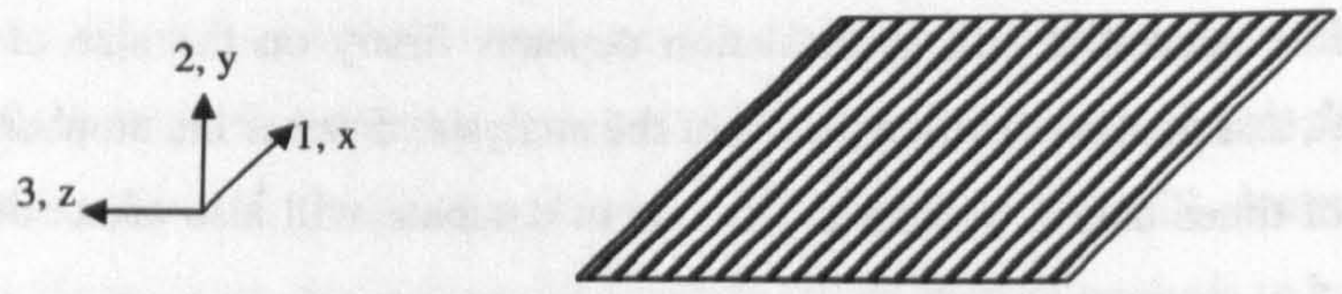

Figure 6.1 - Co-ordinate system as used for the Finite Element Analysis

Table 6.1 - Generic UD lamina CFRP properties

E_1 (GPa)	E_2 (GPa)	G_{12} (GPa)	v_{12}
148.0	9.655	4.552	0.3

Table 6.2 – Quasi-isotropic laminate properties using generic CFRP properties (using ABAQUS co-ordinate system)

E_1 (= E_3) (GPa)	E_2 (GPa)	G_{12} (= G_{23}) (GPa)	G_{13} (GPa)	v_{13}	Density (kg/m^3)
56.24	9.655	4.552	21.37	0.316	1620

The material properties were applied using the engineering constants method in ABAQUS/CAE: only linear elastic analyses were conducted.

To check the assumption that the laminate could be approximated by an in-plane homogenous plate The Laminator version 3.02 (Lindell, 2001) was used to perform Classical Lamination Theory analysis comparing laminates 4.2mm, 8.4mm and 12.6mm thick with an equivalent homogenous plate in tension and under pure moment. For this, new laminates were defined (and used only for this exercise), using the lay-up for the laminates presented in Figure 3.5 and the generic CFRP properties in Table 6.1. The apparent laminate properties are presented in Table 6.3.

Table 6.3 - Apparent laminate properties

E_1 (GPa)	E_2 (GPa)	G_{12} (GPa)	v_{12}
77.53	35.94	20.57	0.472

The analysis that The Laminator uses calculates three matrices (*A*, *B* and *D*) for performing stress and strain calculations; these matrices are common to all Classical Laminate Theory

analyses. The values in the matrices determine how the laminate will behave under loading. The single layer homogenous plate using the properties in Table 6.3 is effectively a balanced symmetric lamina and hence has a null *B* matrix (hence no coupling between in-plane loads to out-of-plane curvature or moments to in-plane strains) and an A matrix that implies no in-plane shear coupling. The actual 30 layer (counting the double 0° layers as single layers) 8.4 mm thick laminate (see Figure 3.5) produces similar results.

So, six laminates were analysed: a laminate and an equivalent single layer plate for three thicknesses. Each separately had applied a pure moment per unit width of 10^3 Nm/m and a tensile load per unit width of 10^3 N/m. The resulting total strain vector was examined, i.e. the strain and curvature of the laminate mid-plane, ignoring any shear coupling, coupling between in-plane loading and curvature, and moments to in-plane strain as being insignificant. As would be expected there is little difference between the laminates and their equivalent single layer plates when an in-plane tensile load is applied (0.06%); the lay-up will have no effect when it is balanced and symmetrical. However there is some difference with an applied bending load, as the results in Figure 6.2 show, in the resulting in-plane curvature K_x and K_y.

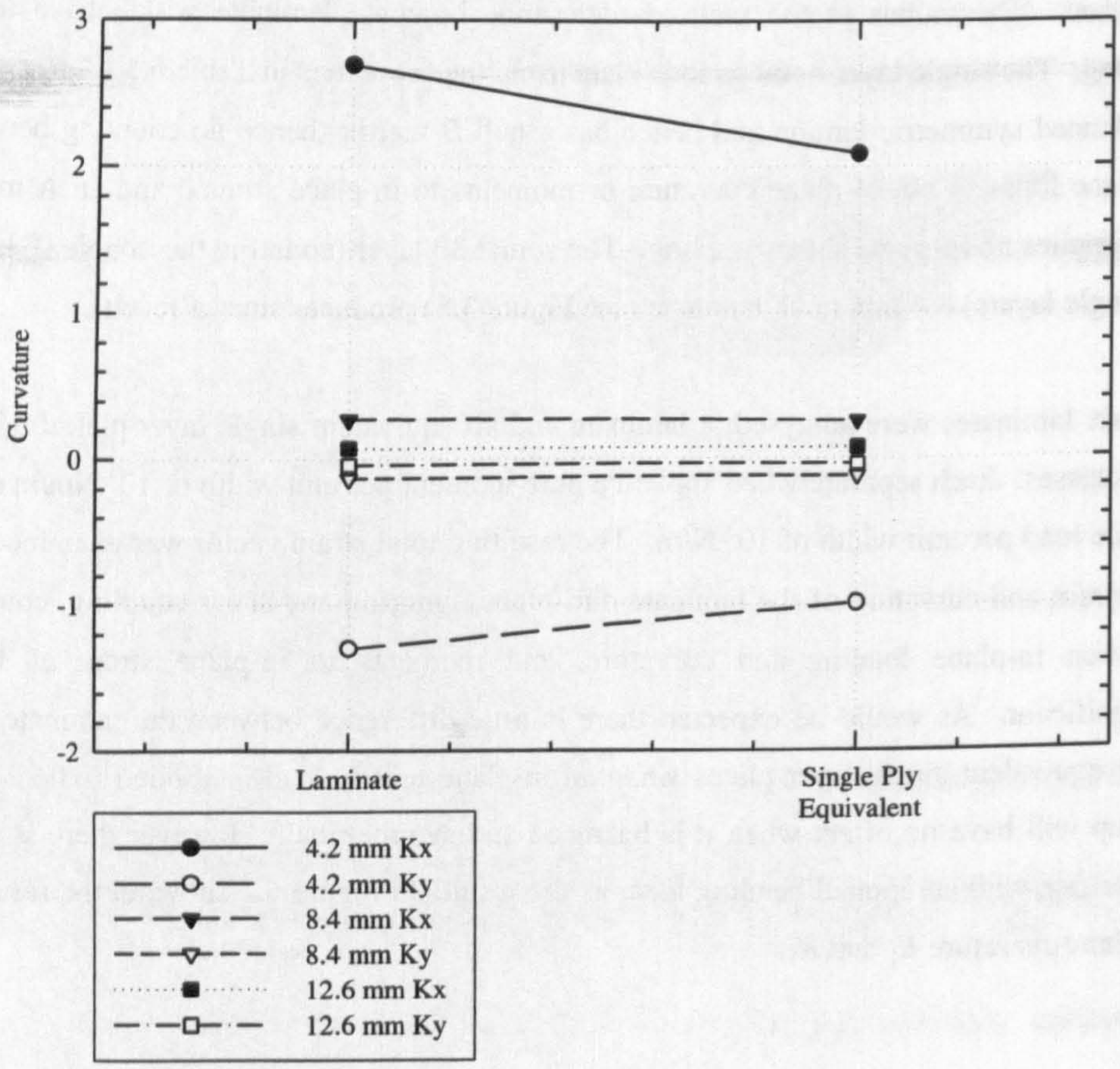

Figure 6.2 - Resulting curvature from an applied bending load

The thinnest, 4.2mm thick, laminate shows the greatest variation as would be expected. The layers have greater significance as their thickness is more comparable to the thickness of the laminate as a whole. With an explicitly defined laminate, when the stiffest layers are far from the mid-plane this will enhance the bending stiffness of the laminate without changing the in-plane elastic modulus. As the laminate becomes thicker, with the layer thicknesses remaining the same, their effect becomes smaller, hence the laminate experiences a curvature approximately 20% larger for the 4.2mm thick laminate, reducing to approximately 2.5% larger for the thickest laminate. Consequently the homogenised material model in Table 6.2 can validly be used in the finite element study of the thick laminates in this work. As previously stated, this finite element work was carried out before the experimental work and so material properties had to be assumed (the properties presented in Chapter 3 were not available).

6.2.2.4 Model Geometry

With the decision to model the material as isotropic in-plane justified by showing that the lay-up had little effect on the bending of the plate due to the large number of plies, the model can be simplified to enhance computational efficiency. An axi-symmetric model can be used to model the impact, as shown in Figure 6.3, using axi-symmetric (two-dimensional) elements. Use of an axi-symmetric model means that the geometry, loading and material properties have to be similarly symmetric. The material model and loading do not violate this principal. The geometry is modelled as a circular plate; this is acceptable as the composite plates are supported over a circular hole in a steel plate in the impact experiments.

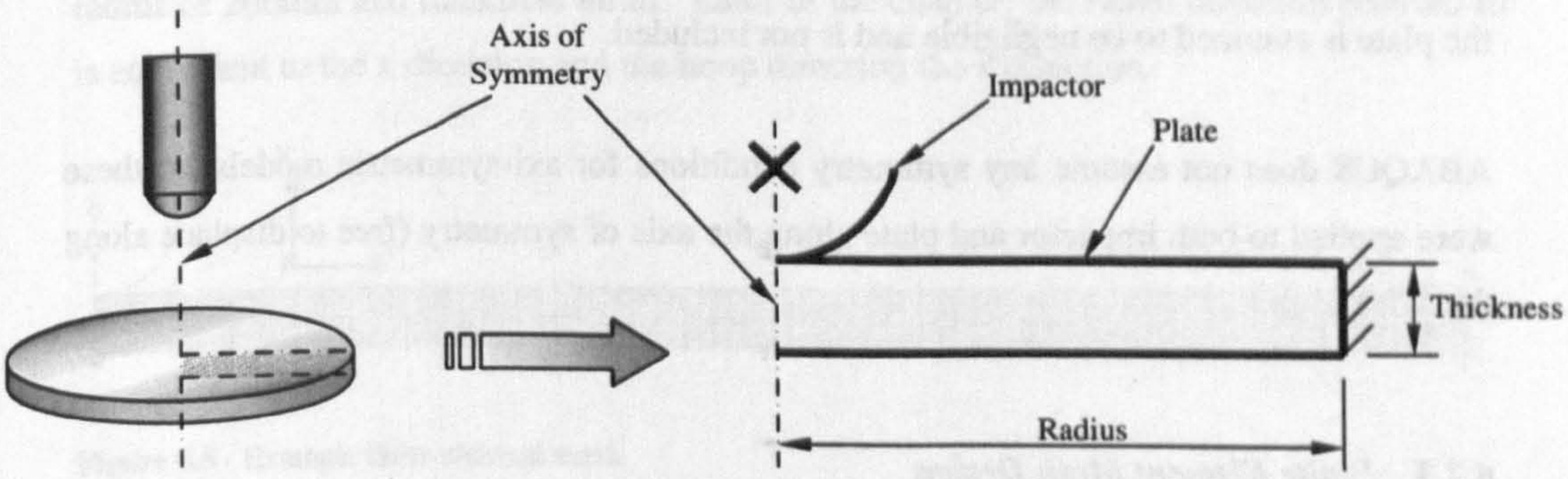

Figure 6.3 - Basic model geometry

Figure 6.3 shows that the impactor is modelled as a quarter circle and is assumed to be rigid in comparison to the plate. The circular plate is modelled as a single radial slice.

6.2.2.5 Model Boundary Conditions

The impactor is modelled as a rigid spherical body with diameter 25mm, and hence all the boundary and initial conditions are applied to its reference point at its centre. This impactor diameter is different to the 19 mm diameter in the experiments as the analysis was carried out prior to the impact machine being built. It is shown in Section 6.7.2 that impactor tup diameter has little effect. The analysis in Section 6.7.2 shows that the tup diameter has little effect on the plate's impact response. To simulate the impact, the model

is arranged at the moment before contact between impactor and plate. The following boundary and initial conditions are applied to the impactor:

1. An initial impact velocity (v) and a point mass (m). This initial kinetic energy of the impactor ($KE = \frac{1}{2}mv^2$) is equivalent to the impact energy, and these values are calculated assuming the impactor is dropped from a given height and falls under the influence of gravity.
2. A concentrated force, equivalent to that which it would experience due to gravity.
3. Hard and frictionless contact between the plate and impactor.

The plate is assumed to be built in around its circumference, so an encastré condition was applied to the appropriate edge in the model, as in Figure 6.3. This was assumed to appropriately represent the boundary condition of the test fixture. The effect of gravity on the plate is assumed to be negligible and is not included.

ABAQUS does not assume any symmetry conditions for axi-symmetric models, so these were applied to both impactor and plate along the axis of symmetry (free to displace along the axis only).

6.2.3 Finite Element Mesh Design

In this study the effect of various geometric parameters are considered, and hence it is important to ensure that the meshes are comparable. To that end in every mesh there is a region of square elements under the impactor. The size of this region and hence the size of the elements are exactly the same in every model. Four positions are examined in particular detail in every model, as shown in Figure 6.4. The deflections at points *A* and *B* and the stress at the integration point of elements *i* and *ii* are recorded. In the remaining part of the model, the element height remains constant, but their length in the radial direction gradually increases towards the outer edge of the plate. To ensure a good quality mesh the average aspect ratio (length to height ratio) is always between two and three, and the worst aspect ratio is never more than six.

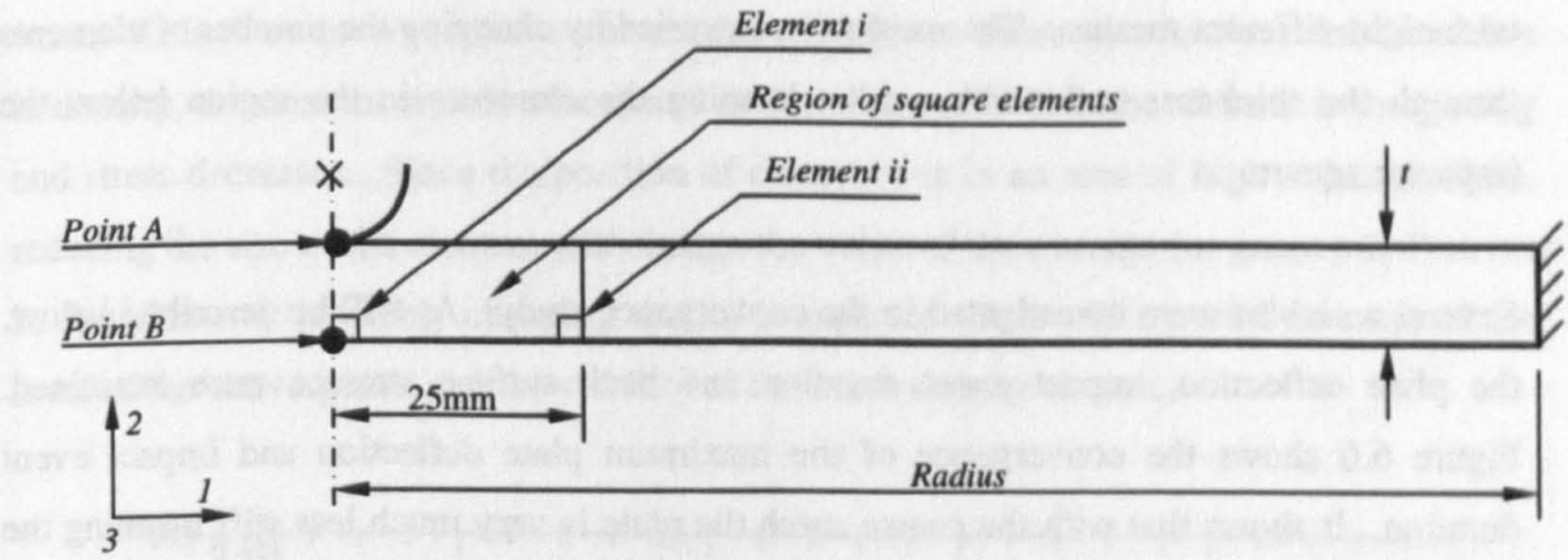

Figure 6.4 - Common mesh features

Figure 6.5 shows shows an example mesh as created by ABAQUS/CAE for a plate with a radius of 200mm and thickness 8mm. Later in the chapter, the radial direction referred to is equivalent to the x direction and the hoop direction the x direction.

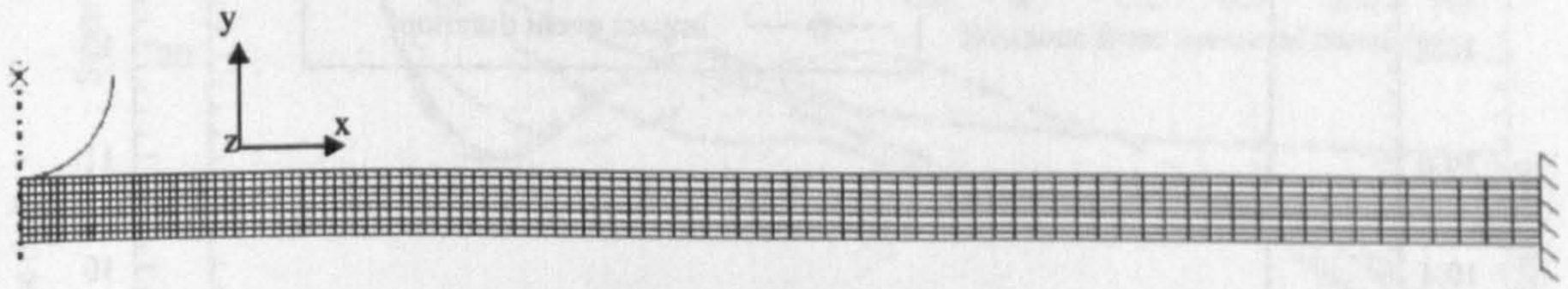

Figure 6.5 - Example finite element mesh

The element used in every mesh is a four noded, reduced integration, axi-symmetric element denoted CAX4R in ABAQUS. There are no quadratic elements available in ABAQUS/Explicit code.

6.2.4 Mesh Convergence Study

It is essential to carry out a mesh convergence study before attempting any finite element study to show that the optimised mesh has been used. With any simulation there is an optimum mesh where increasing the mesh density will not increase accuracy, only solution run time. The aim is to find the element size that gives the optimum mesh density.

A 500 mm radius, 8 mm thick plate with a 2 kg impactor impacting with 40 J was meshed with eight different meshes. The meshes were varied by changing the number of elements through the thickness and width, whilst keeping the elements in the region below the impactor square.

Several variables were investigated in the convergence study. As will be described below, the plate deflection, impact event duration and back surface stresses were examined. Figure 6.6 shows the convergence of the maximum plate deflection and impact event duration. It shows that with the coarse mesh the plate is very much less stiff meaning the event duration and maximum deflection are larger. The two finest meshes show converged values.

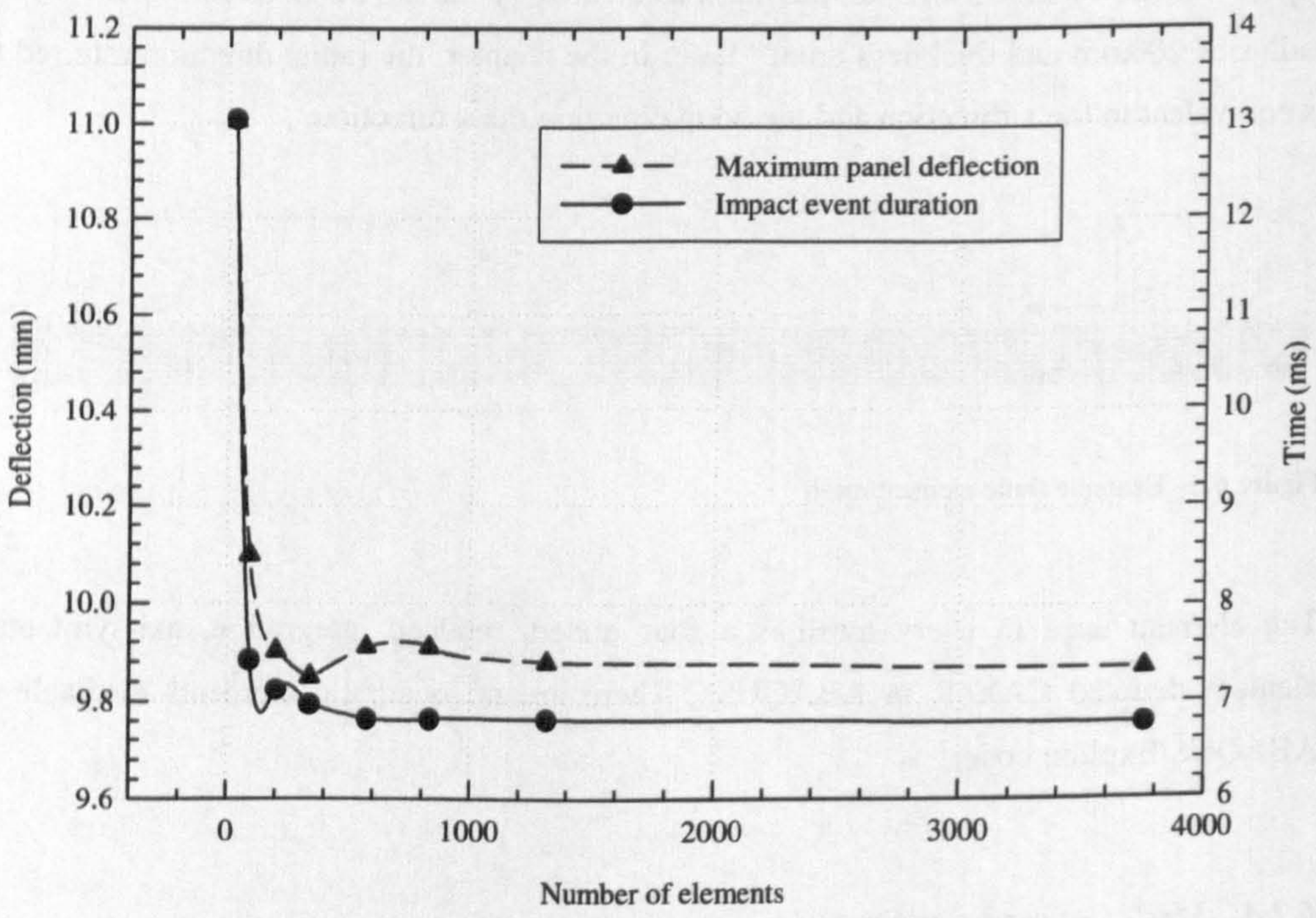

Figure 6.6 - Mesh convergence of maximum plate deflection and impact event duration

Figure 6.7 shows the back face (i.e. the non-impacted side) stress in the radial (σ_{11}) and hoop (σ_{33}) directions for each of the eight meshes after 2 ms of impact time. They show that as the mesh density increases the stress profiles get closer. This is further evidenced in Figure 6.8, which shows the maximum σ_{11} and σ_{33} values, in element *i*, (see Figure 6.4)

after 2 ms of impact time. This shows that the stress values are converging towards a value. This does not represent a true mesh convergence however. As the mesh increases in density, the element size decreases and so the area over which the element is integrating and stress decreases. Since the position of element *i* is in an area of high stress gradient, reducing the size of the element will change the value of the average (or gauss point) stress in that element, inevitably changing the value reported. It is still a useful measure of the level of the convergence and the stability of the mesh density chosen.

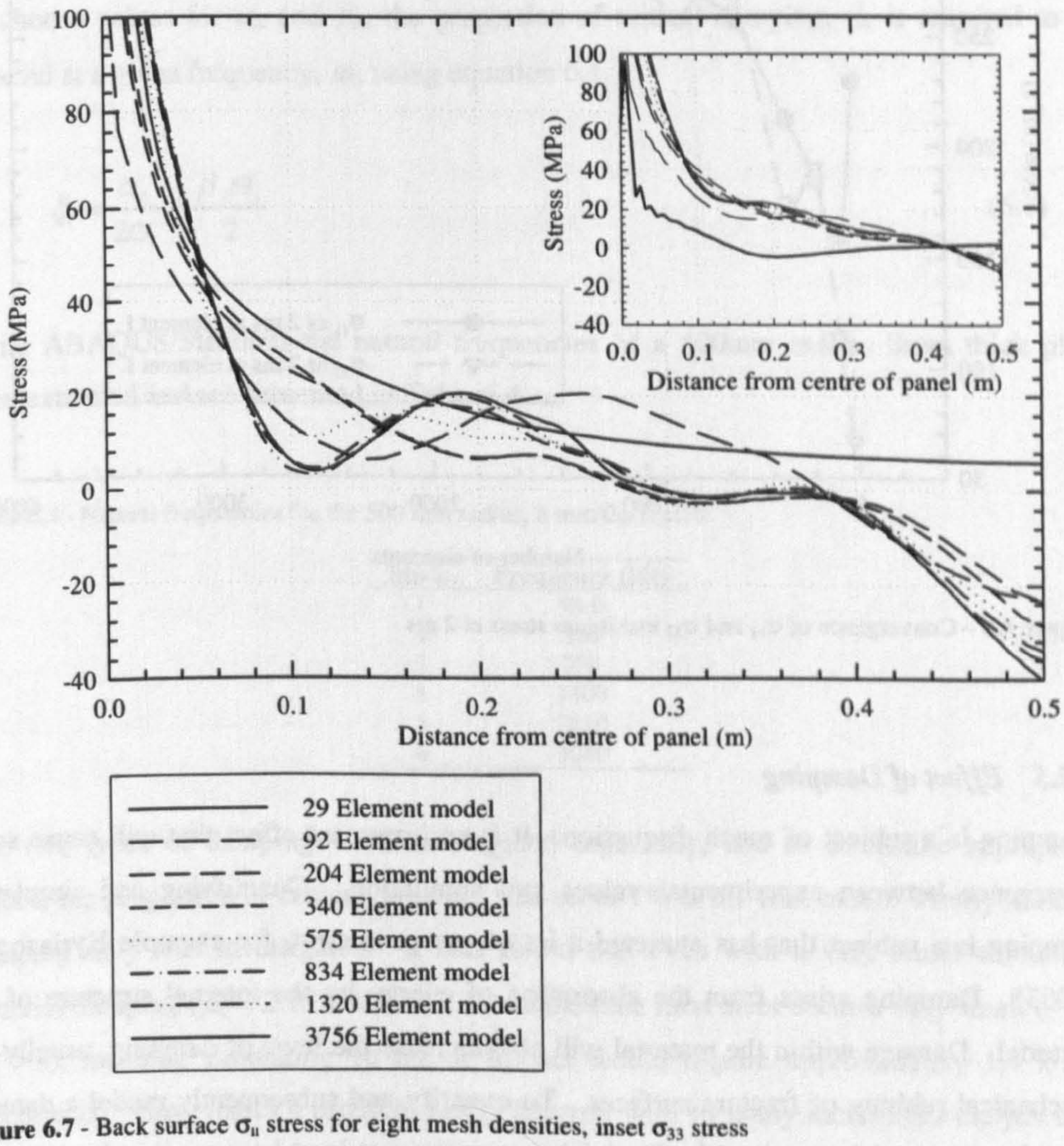

Figure 6.7 - Back surface σ_{11} stress for eight mesh densities, inset σ_{33} stress

Following this analysis it was decided that the mesh of 1320 elements represented the best trade-off between accuracy, stability and cost. This mesh corresponds to a density of one

element per 1 mm of thickness at the axis of symmetry, and this ratio was maintained in subsequent models.

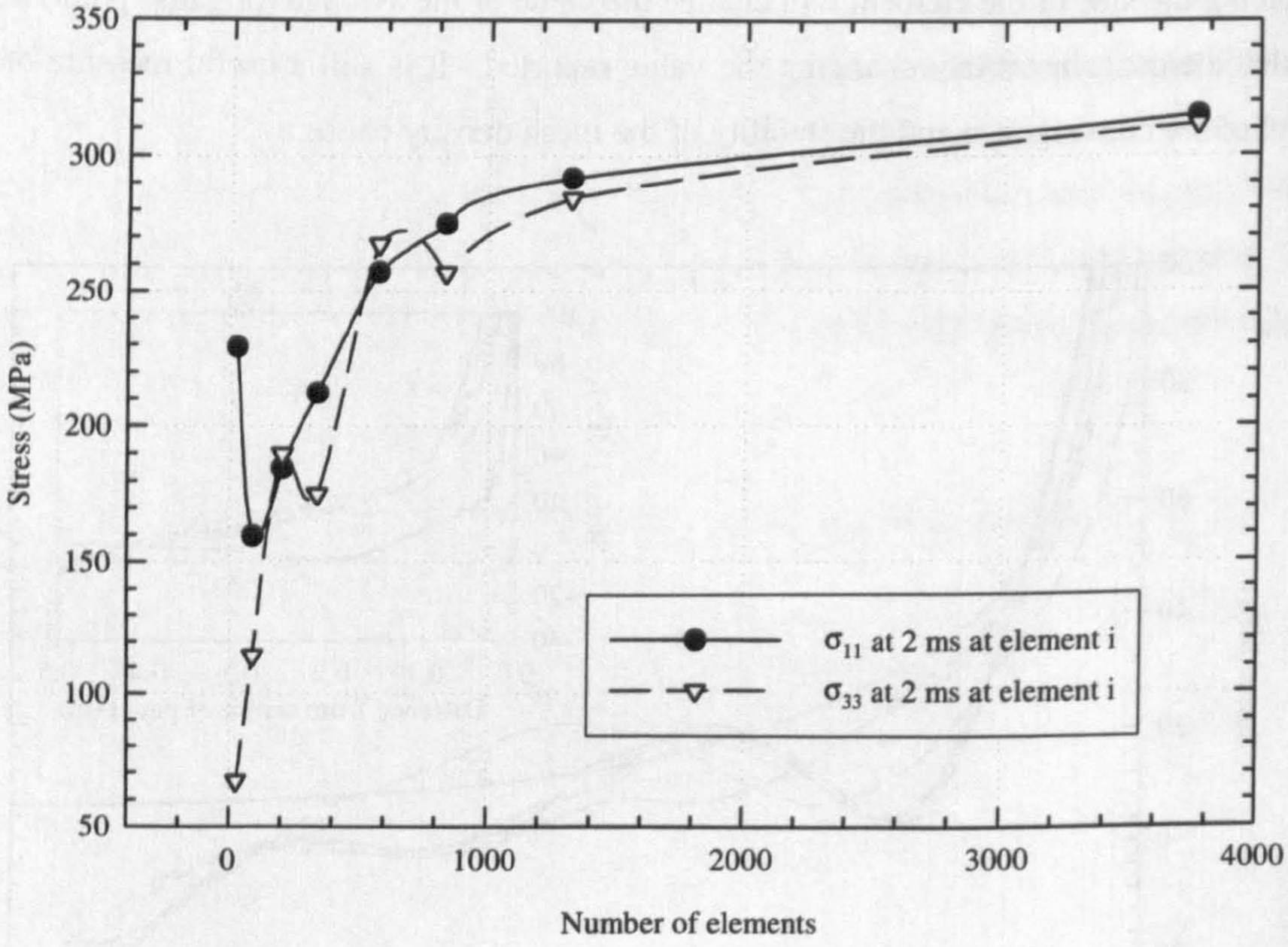

Figure 6.8 – Convergence of σ_{11} and σ_{33} maximum stress at 2 ms

6.2.5 Effect of Damping

Damping is a subject of much discussion. It is an important effect that will cause some divergence between experimental values and simulation. Quantifying and simulating damping is a subject that has attracted a lot of recent interest, for example Kyriazoglou (2003). Damping arises from the absorption of energy by the internal structure of the material. Damage within the material will also increase the level of damping, usually via mechanical rubbing of fracture surfaces. To quantify and subsequently model a damped material, the model presented by Rayleigh is popular not least because it is incorporated into the ABAQUS/Explicit code.

Rayleigh defined two variables: α_R and β_R, both of which can be directly defined as a material property in ABAQUS/CAE. The former is so-called mass damping and can be used to damp out low frequencies, the latter is stiffness or material damping and can be used to damp out high frequencies. In the following study the aim was to determine the effect of applying these damping parameters to an impact model, and thus establish the feasibility of using such a mathematical approximation to damping in the subsequent analyses.

To choose values for α_R and β_R, the proportion of critical damping, ξ_i, is required to be selected at a given frequency, ω_i, using equation 6.1.

$$\xi_i = \frac{\alpha_R}{2\omega_i} + \frac{\beta_R \omega_i}{2} \tag{6.1}$$

Using ABAQUS/Standard the natural frequencies of a 500mm radius, 8mm thick plate were extracted and are presented in Table 6.4.

Table 6.4 - Natural frequencies for the 500 mm radius, 8 mm thick plate

Mode	Frequency (Hz)
1	93.0
2	360
3	798
4	1400
5	2150
6	3040

The two types of damping were investigated separately, and to determine appropriate values, the proportion of critical damping was set to 1% at the first mode. Firstly material damping only was investigated. It was found that even with a very small amount of material damping ($\beta_R = 2.15 \times 10^{-4}$ s^{-1}), the stable time increment became very small (~ 7×10^{-11} s), meaning simulating 10 ms of impact would require approximately 1.4×10^8 increments. This creates a problem firstly because with so many increments the job time would become so large as to be impractical, and secondly round-off errors become significant when there are more than 3×10^5 increments. Hence it was not possible to study the effect of material damping. Mass damping, however, was possible. With the proportion of critical damping at 10%, α_R was calculated to be 18.6 s^{-1} at the first mode,

and 72.0 s^{-1} at the second mode. Simulations were run to compare these two levels of damping to a model with no damping, each impacted with a 2 kg impactor at 40 J.

It was found that, when looking at the displacement history, as shown in Figure 6.9, the effect of damping is minimal during the impact event, as all simulations show similar impactor and plate response, including impact event durations and maximum deflections. The simulations diverge post-impact; the greater the level of damping the faster the rate of reduction in plate vibration amplitude, though the frequency is unaffected as expected.

As forces and stresses in the system were also subject to investigation in later analyses, the effect of damping on impactor force was investigated. Figure 6.10 shows the impactor force histories during the impact event, and again there is little variation; the divergence between maximum forces between the undamped and most damped models is 8.7%, which is within acceptable limits.

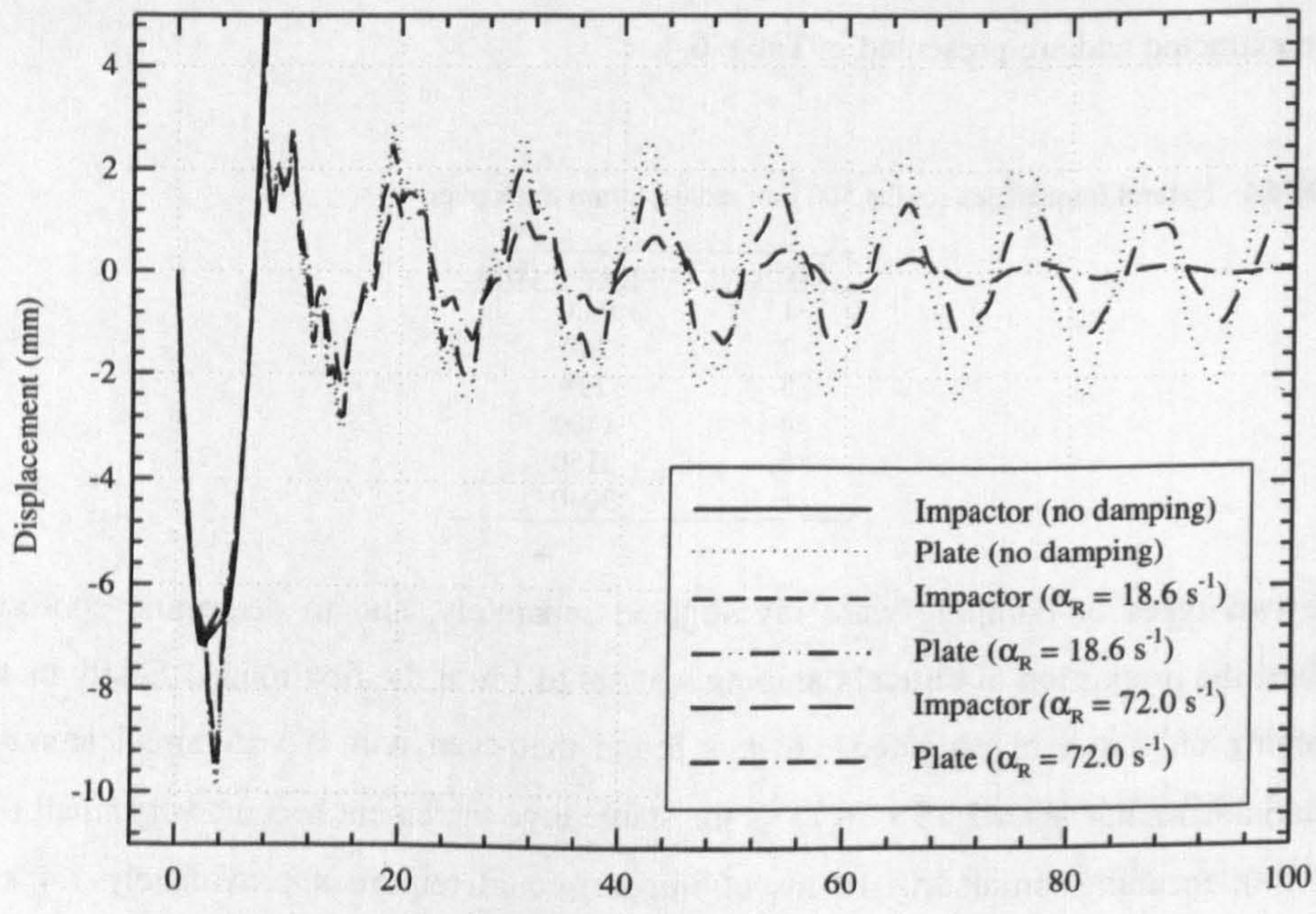

Figure 6.9 - Undamped versus damped plate and impactor displacement history

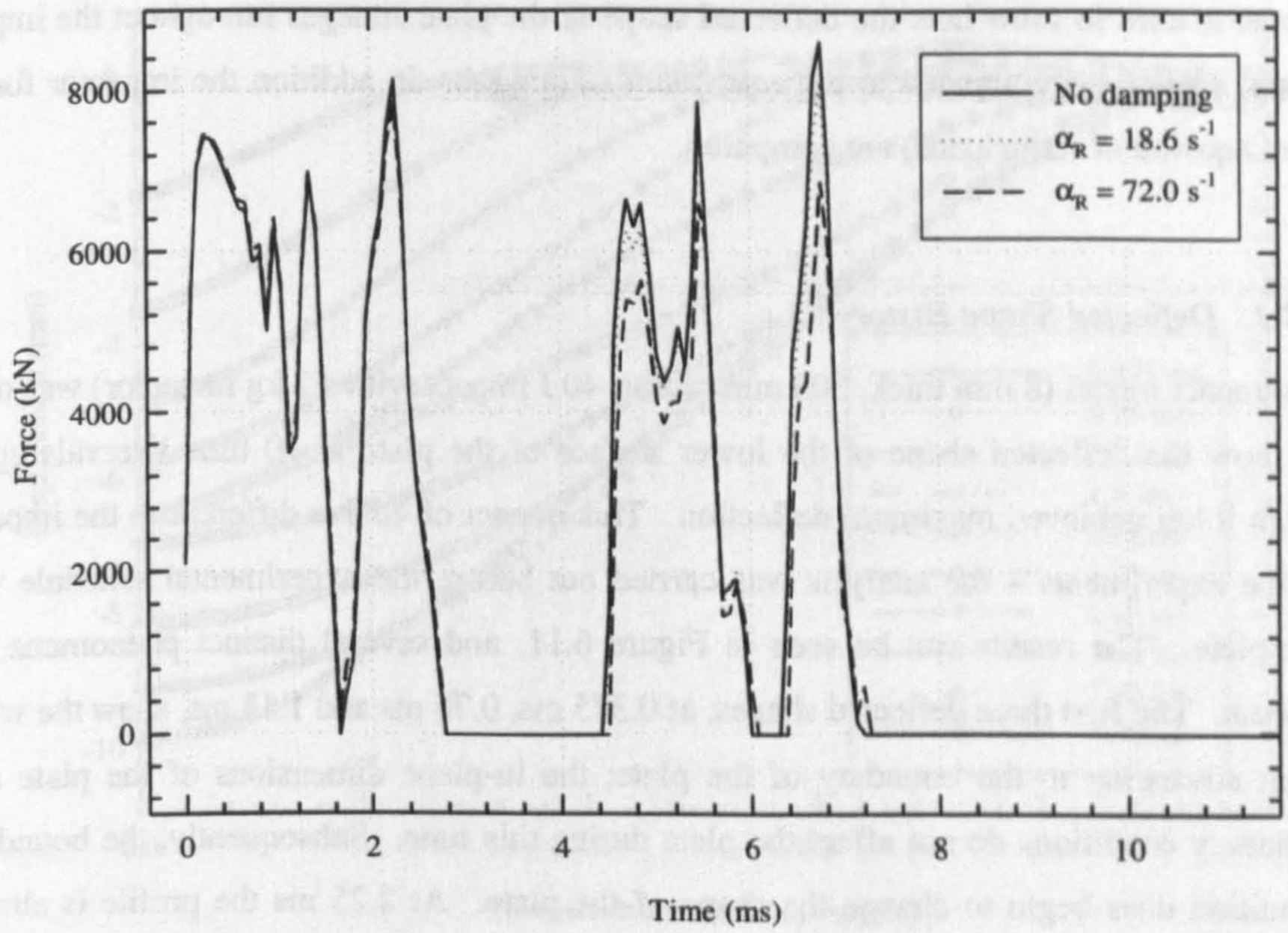

Figure 6.10 - Undamped versus damped impactor force history

Applying a realistic value for the damping is difficult, and though estimating values empirically is possible, it is not the subject of this research. In addition published values are available, as in Kyriazoglou (2003), and if damping is to be included it should have realistic values. However, as its inclusion does not greatly affect the plate's response, as shown, in terms of a qualitative study it was determined to not be important. Thus, the analysis does not include any damping effects.

6.3 CENTRALLY LOADED DEFLECTED SHAPE OF PLATES

6.3.1 Introduction

How a plate deflects during an impact, the nature of the stresses that are created during impact, and the shape of the plate need to be understood. In addition the need to study the impact with an explicit finite element code should be further verified by the comparison with equivalent static analysis. As discussed in the Literature Review, many authors take the assumption that impact can be analysed as a static event. The static deflection of a plate is well reported and analytical solutions are available. In this section a plate impact

model is used to show how the deflected shape of the plate changes throughout the impact event, and this is compared to the equivalent static case. In addition the impactor forces (and equivalent static loads) are compared.

6.3.2 Deflected Shape History

An impact model (8 mm thick, 500 mm radius, 40 J impact with a 2 kg impactor) was used to show the deflected shape of the lower surface of the plate at 10 time intervals up to when it has achieved maximum deflection. This impact of 40 J is different to the impacts in the experiments – the analysis was carried out before the experimental schedule was complete. The results can be seen in Figure 6.11, and several distinct phenomena are evident. The first three deflected shapes, at 0.375 ms, 0.75 ms and 1.13 ms, show the wave front advancing to the boundary of the plate; the in-plane dimensions of the plate and boundary conditions do not affect the plate during this time. Subsequently, the boundary condition does begin to change the shape of the plate. At 2.25 ms the profile is almost straight, the plate forming a cone shape, and this corresponds to the first peak in impactor force (see Figure 6.10). Then at 2.8 ms the plate leaves contact with the impactor (hence impactor force is purely that due to gravity 2 kg × 9.81 m/s^2 = 19.6 N) to achieve maximum deflection at 3.75 ms. To achieve the interruption in contact a large diameter plate is required, so it was not observed in the experimental impacts. To achieve an interrupted impact with the experimental set-up available, a very thin laminate with a low impact energy (and small impactor mass) would have been required.

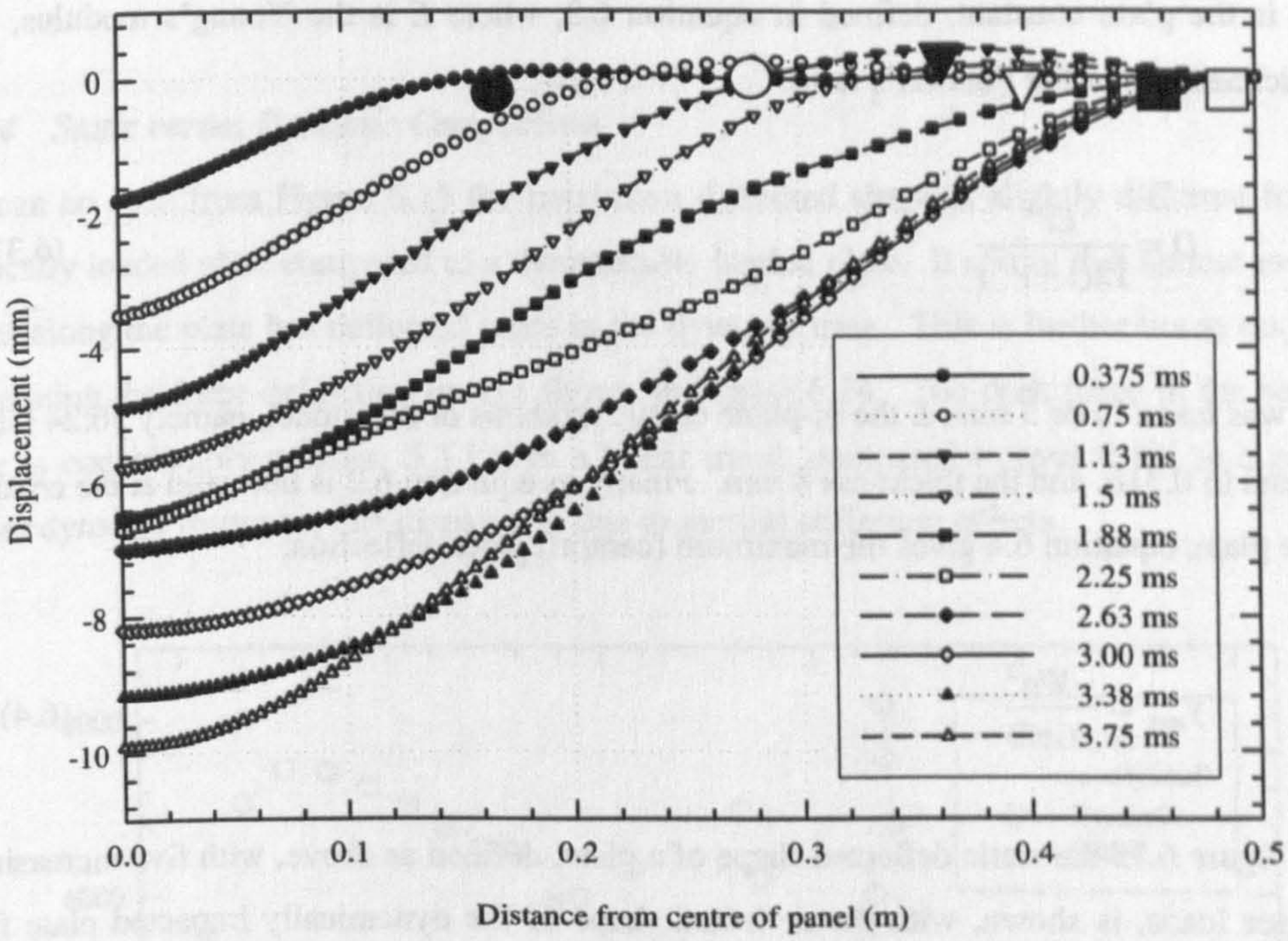

Figure 6.11 - Plate deflected shape history, with the large symbols indicating approximate hinge location

6.3.3 Static Deflected Shape

Young and Budynas (2002) presented Roark's solution for a centrally loaded circular plate. The deflection y at radius r of a plate of radius a with a central load W acting over a small area with radius r_o (see Figure 6.12), is given by equation 6.2, valid for $r > r_o$.

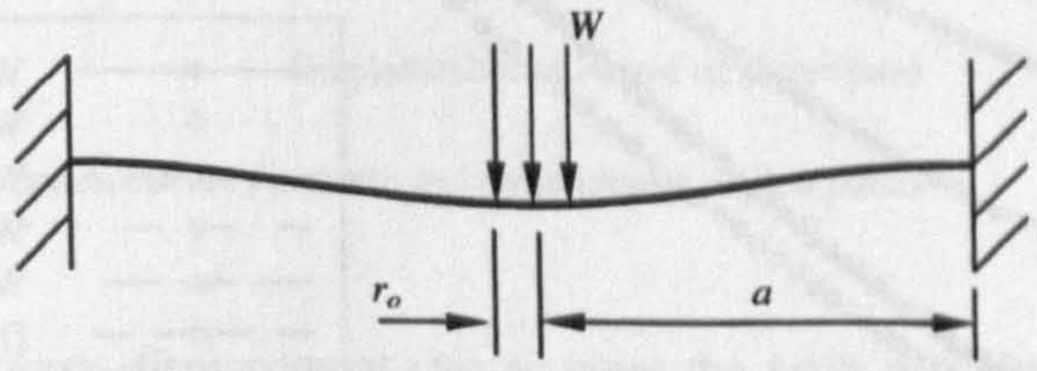

Figure 6.12 - Roark's centrally loaded circular plate

$$y = \frac{-W}{16\pi D}\left[a^2 - r^2\left(1 + 2\ln\frac{a}{r}\right)\right] \tag{6.2}$$

D is the plate constant, defined in equation 6.3, where E is the Young's modulus, t the thickness and ν the Poisson's ratio.

$$D = \frac{Et^3}{12(1-\nu^2)} \tag{6.3}$$

r_o was taken to be 5 mm, E the in-plane elastic modulus of the model, namely 56.24 GPa, ν equal to 0.316, and the thickness 8 mm. Finally as equation 6.2 is not valid at the centre of the plate, equation 6.4 gives the maximum (central) plate deflection.

$$y_{max} = \frac{-Wa^2}{16\pi D} \tag{6.4}$$

In Figure 6.13 the static deflected shape of a plate, defined as above, with five increasingly larger loads, is shown, with the deflected shape of the dynamically impacted plate from finite element analysis shown for comparison.

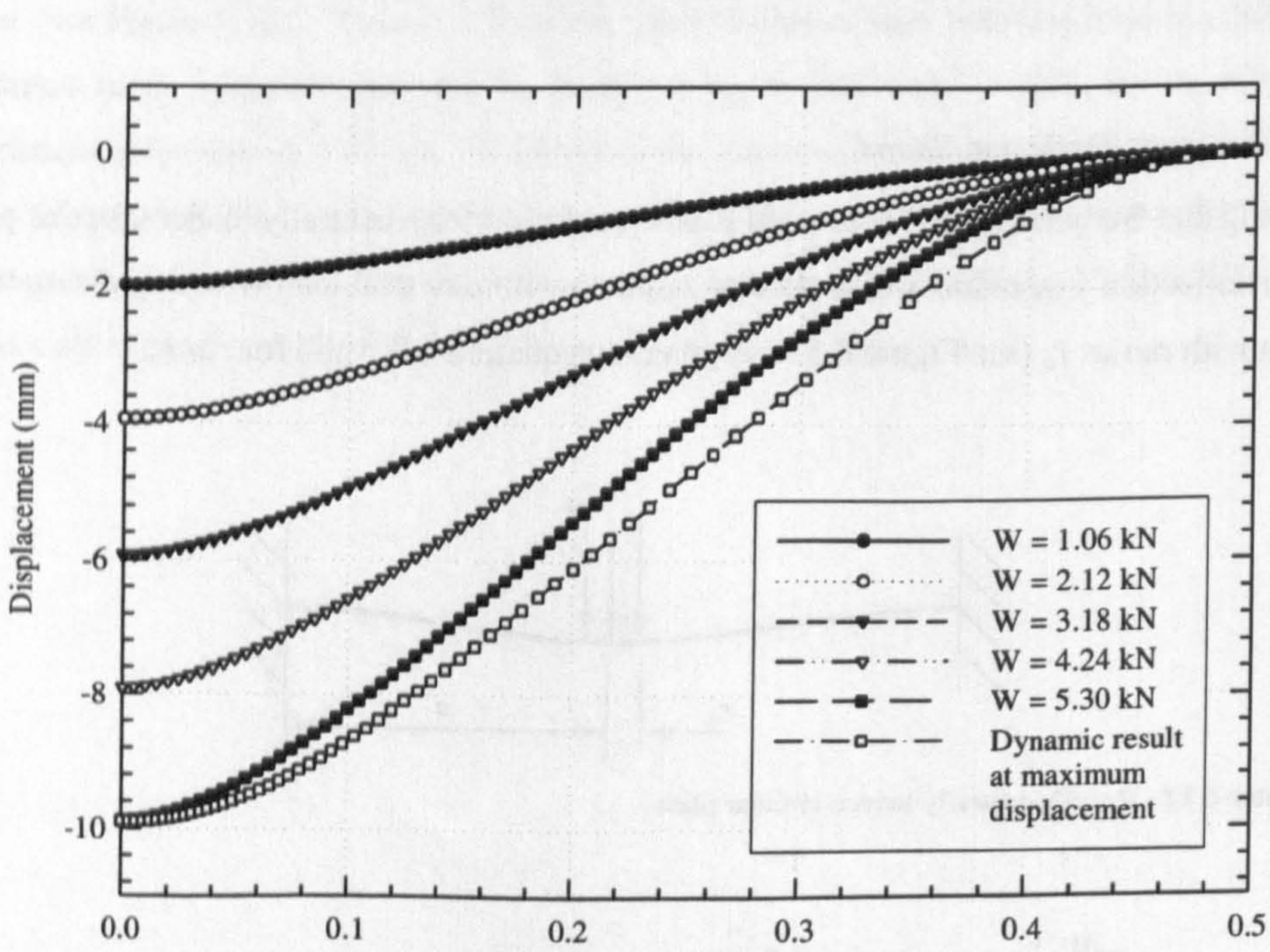

Figure 6.13 - Statically loaded plate deflections with maximum deflected dynamic profile

6.3.4 Static versus Dynamic Comparison

As can be seen from Figure 6.13 the maximum deflected shape is slightly different for a statically loaded plate compared to a dynamically loaded plate. It shows that almost every point along the plate has deflected more in the dynamic case. This is further borne out by examining the force-deflection curves shown in Figure 6.14. The peak force in the static case is considerably smaller, 5.3 kN in a linear trend, compared to over 8 kN in a non-linear dynamic response; this disparity is due to inertial stiffening effects.

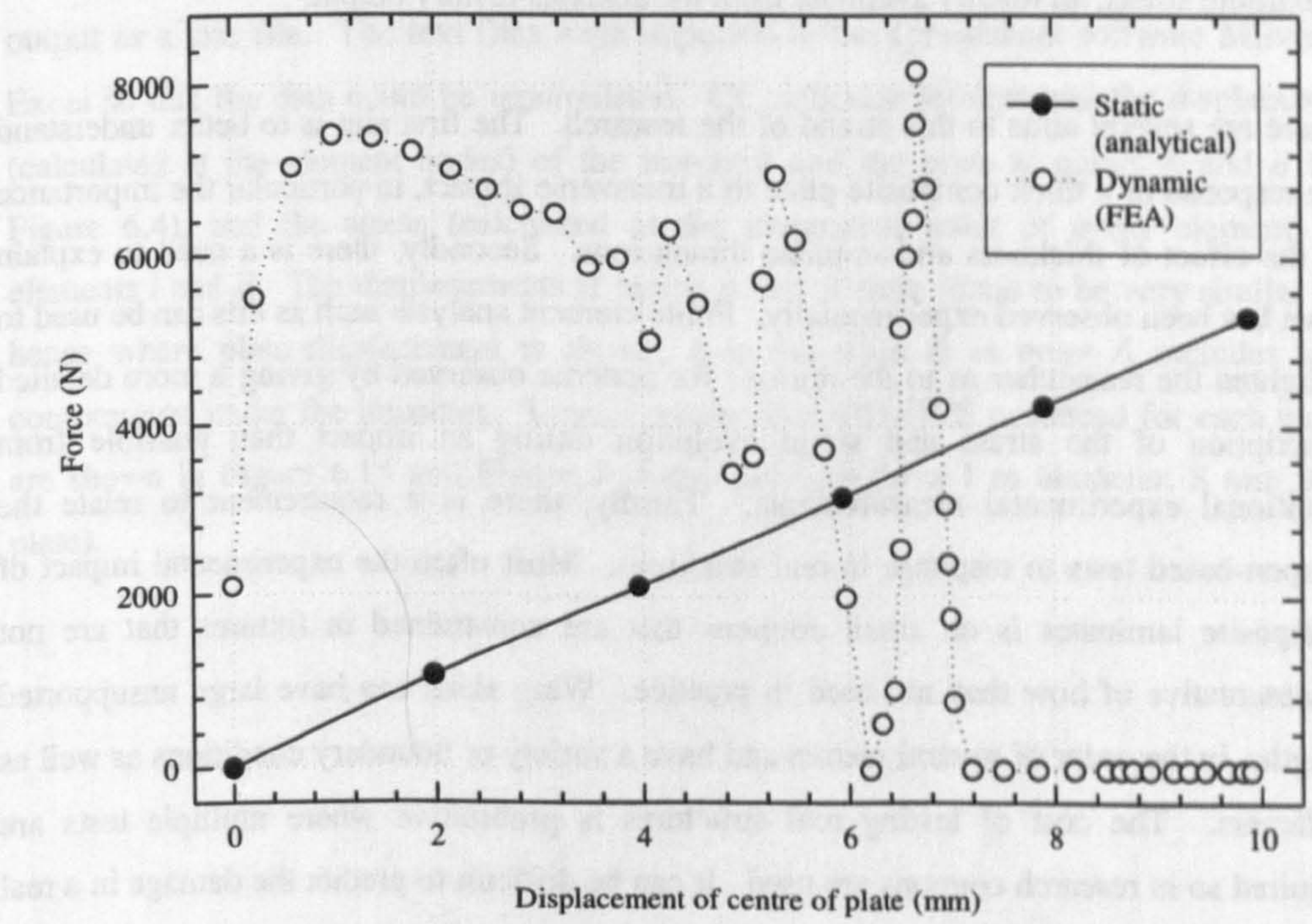

Figure 6.14 – Force-deflection curves for static and dynamically loaded plates

The area under the force-displacement curves gives the work done by the load applicator (the impactor or static indenter) and this is 26 kJ in the static case compared to 39 kJ in the dynamic situation. Without being able to say anything about the damage that might be sustained in each case, it is clear that inertial stiffening is a significant effect. The force and energy conveyed to the plate by the impactor is greater when loaded in a dynamic manner, hence it is valid to study impact with a series of explicit finite element models, and not static analyses.

6.4 EFFECT OF PLATE DIMENSIONS

6.4.1 Introduction

The purpose of this study is to understand the impact response of composite plates and identify the key variables determining that response. To achieve this, a parametric investigation has been undertaken, studying the effect of plate dimensions (plate radius and thickness) on the response. The response of the plate has been described with a number of measurable characteristics such as impact event duration, maximum deflection and maximum stress, all readily available from the analysis history output.

There are several aims to this strand of the research. The first aim is to better understand the response of a thick composite plate to a transverse impact, in particular the importance of the effect of thickness and in-plane dimensions. Secondly, there is a need to explain what has been observed experimentally. Finite element analysis such as this can be used to enlighten the researcher as to the reasons for patterns observed by giving a more detailed description of the stress and strain evolution during an impact than possible from traditional experimental measurements. Thirdly, there is a requirement to relate the coupon-based tests to response in real structures. Most often the experimental impact of composite laminates is on small coupons that are constrained in fixtures that are not representative of how they are used in practice. Wing skins can have large unsupported lengths, in the order of several metres and have a variety of boundary conditions as well as stiffeners. The cost of testing real structures is prohibitive where multiple tests are required so in research coupons are used. It can be difficult to predict the damage in a real structure having only tested small scale coupons.

6.4.2 Models Used and Method

In these analyses the generic geometry in Figure 6.4 is used. The impact event is the same in every case, whilst the plate radius and thickness are changed in the parametric study. Five plate radii and four plate thicknesses were studied giving an analysis matrix with 20 entries. The impactor is modelled as being 1.019 kg in weight, the impact velocity 8.86 ms^{-1} with an impact energy of 40 J, hence a theoretical drop height of 4 m. The converged

optimised mesh was used in every case, see section 6.2.4. As previously mentioned, the simulated impacts are different to the impacts in the experiments, as the analysis was carried out first. This means that the results are not directly comparable, but as the material properties used do not match the actual properties of the laminates, the aim of the analysis was to gain a qualitative understanding of the response of the laminates.

As requested in the input file, each model produced detailed time-history results for every requested variable (displacement, velocity, acceleration and stress components) in the specified areas of interest at nodal or element average positions as appropriate. These data were stored in the output database and during post-processing using ABAQUS/CAE were output as a text file. The text files were imported to the spreadsheet software Microsoft Excel so that the data could be manipulated. Of particular interest was the displacement (calculated at the element nodes) of the impactor and the plate at points *A* and *B* (see Figure 6.4), and the stress (calculated at the integration point of every element) for elements *i* and *ii*. The displacements at points *A* and *B* were found to be very similar and hence where plate displacement is shown, it is for point *B* as point *A* includes local compression under the impactor. Typical results that ABAQUS produced for each model are shown in Figure 6.15 and Figure 6.16 (in this case for a 1 m diameter, 8 mm thick plate).

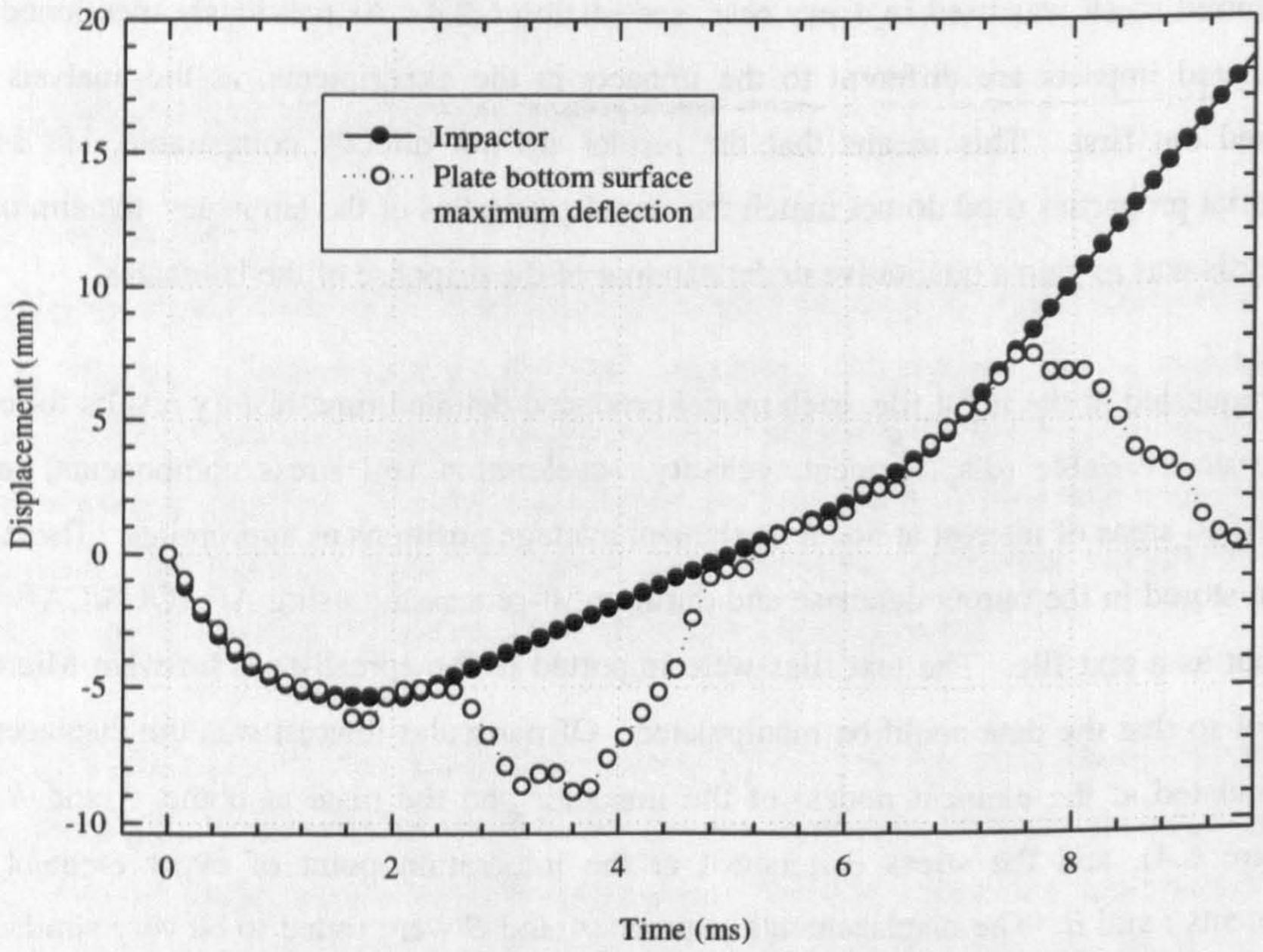

Figure 6.15 - Displacement time history results for the 8 mm thick, 1 m diameter plate

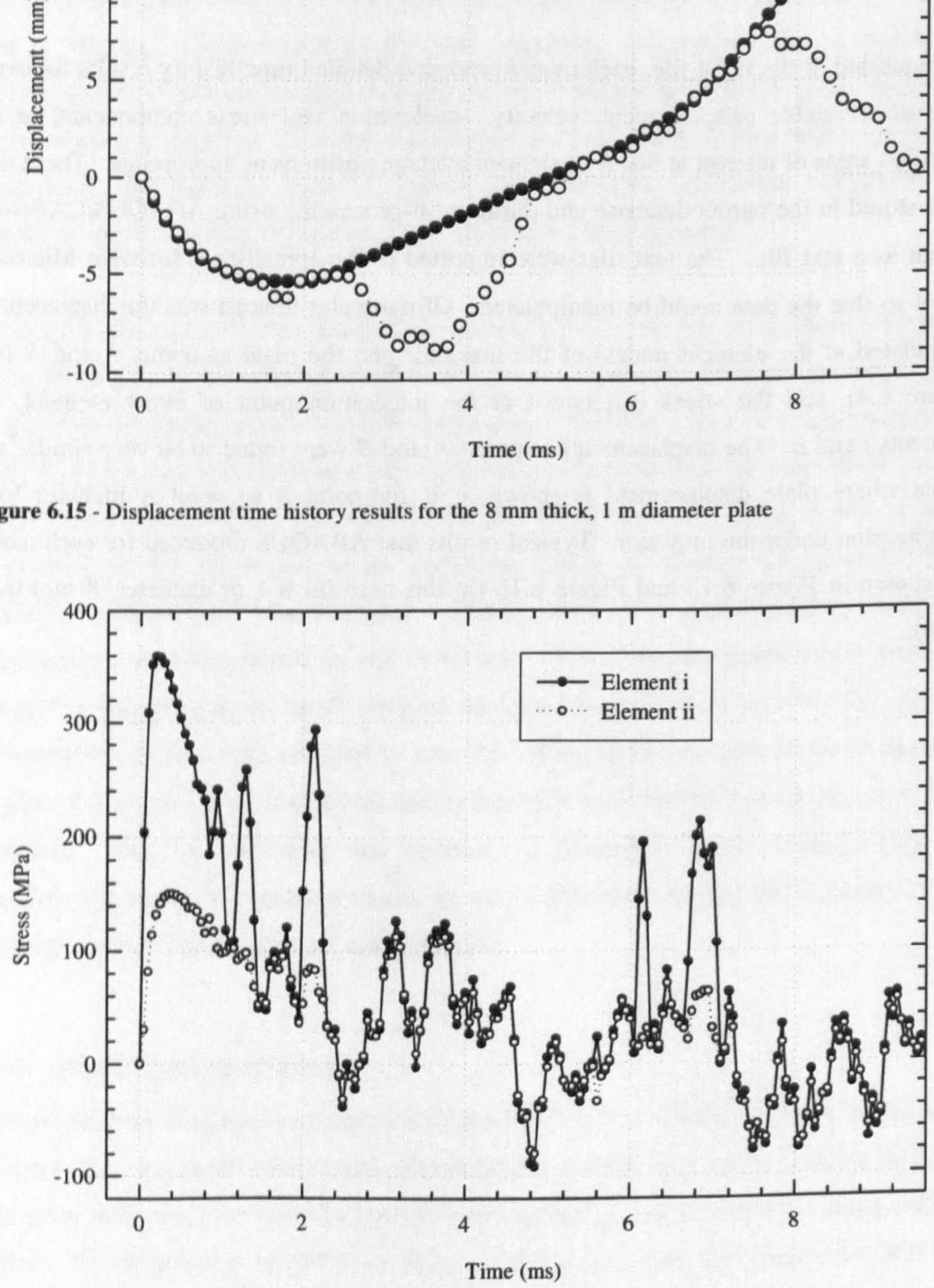

Figure 6.16 - Hoop stress time history results for the 8 mm thick, 1 m diameter plate

From graphs such as these various important pieces of data can be obtained. For example from Figure 6.15, the duration of the impact event and the maximum deflection of the impact event can be ascertained. From Figure 6.16 the maximum stress in the model can found by simple observation. Interestingly Figure 6.15 shows that the impact event is not one continuous period of contact, but in fact a series of interruptions in contact. For example, at about 1.5 ms after first contact the impactor and plate separate for a period of about 0.5 ms, and again at 2.5 ms for a duration 2.5 ms.

The radial and hoop stresses were found to be very similar to each other in their time history and magnitude, and so only the hoop stresses are reported. It was also observed that the radial and hoop stresses were significant in elements *i* and *ii*, whereas the through thickness and shear stresses were small in comparison and hence are not reported.

6.4.3 Results

Using the important data acquired from each model it is possible to build a picture of the effect that the geometrical parameters have on the impact response of a plate, in particular the maximum stress, maximum deflection and impact event duration. The following figures show the key trends found in the data. Figure 6.17 shows the variation of maximum hoop stress with plate thickness for each plate radius, Figure 6.18 shows the variation of impact event duration and Figure 6.19 shows the variation of maximum deflection.

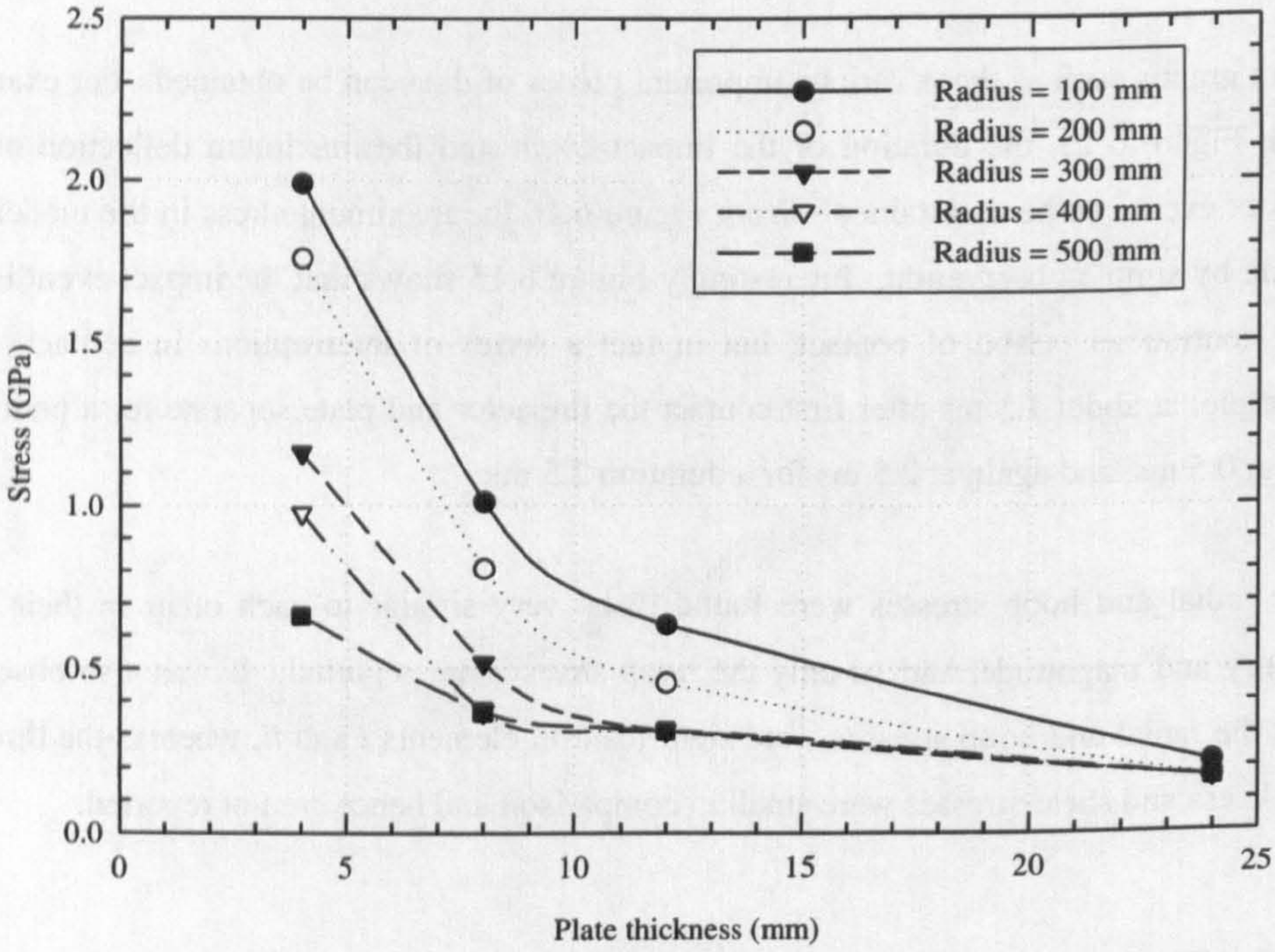

Figure 6.17 - Maximum hoop stress in every model (element *i*) with respect to plate radius and thickness

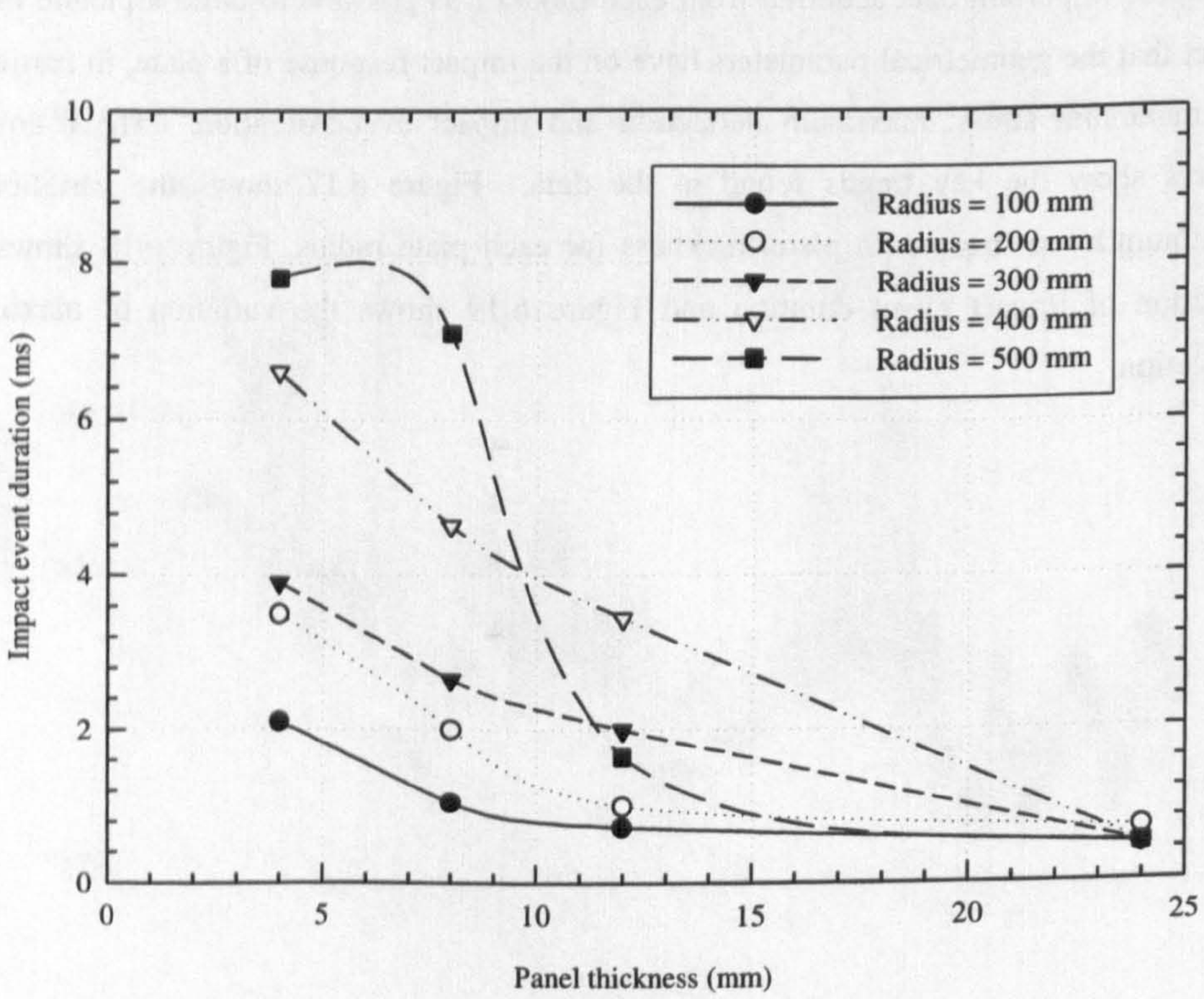

Figure 6.18 - Impact event duration in every model with respect to plate radius and thickness

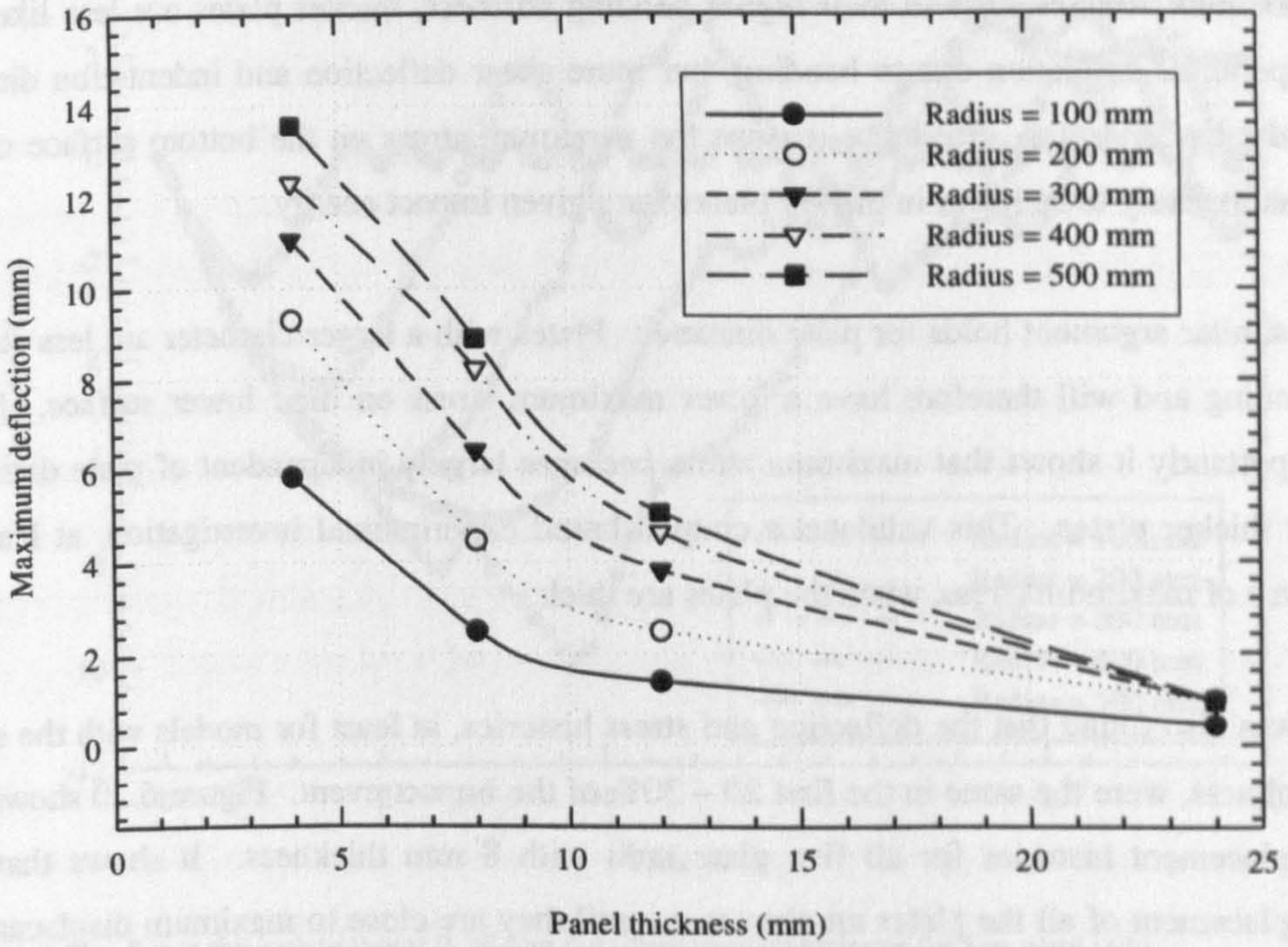

Figure 6.19 - Maximum deflection at the plate centre (point *B*) with respect to plate radius and thickness

6.4.4 Discussion

The impactor transfers some of its kinetic energy to the plate and during the first few milliseconds of the impact event (see Figure 6.9) the plate is in flexural vibration, with the motion of the front of the flexural wave visible as it progresses from the impact point to the model boundary (see Figure 6.11). Due to the superposition of different vibrational modes the centre of the plate accelerates downwards losing contact with the impactor which has already lost much of its initial impact velocity. The maximum deflection is obtained when the plate starts oscillating at first fundamental mode of vibration, and at this time the maximum amount of energy has been transferred to the plate from the impactor. Following the maximum of its displacement, on the plate's upward journey it meets the impactor again transferring energy back, reversing the impactor's initial downward velocity, and also ensuring that the amplitude of subsequent oscillations are smaller than the maximum.

Figure 6.17 shows that the smaller plates in both diameter and thickness have higher maximum stresses. Due to their higher bending stiffness, thicker plates are less likely to experience deflection due to bending, but more shear deflection and indentation directly under the impactor. For these reasons the maximum stress on the bottom surface of the plate is likely to be lower in thicker plates for a given impact energy.

A similar argument holds for plate diameter. Plates with a larger diameter are less stiff in bending and will therefore have a lower maximum stress on their lower surface. More importantly it shows that maximum stress becomes largely independent of plate diameter for thicker plates. This validates a coupon based experimental investigation, at least in terms of maximum stress, when the plates are thick.

It was also found that the deflection and stress histories, at least for models with the same thickness, were the same in the first 20 – 30% of the impact event. Figure 6.20 shows the displacement histories for all five plate radii with 8 mm thickness. It shows that the displacement of all the plates are the same, until they are close to maximum displacement when some divergence occurs. Only the 400 mm and 500 mm radius plates show any significant plate-impactor separation.

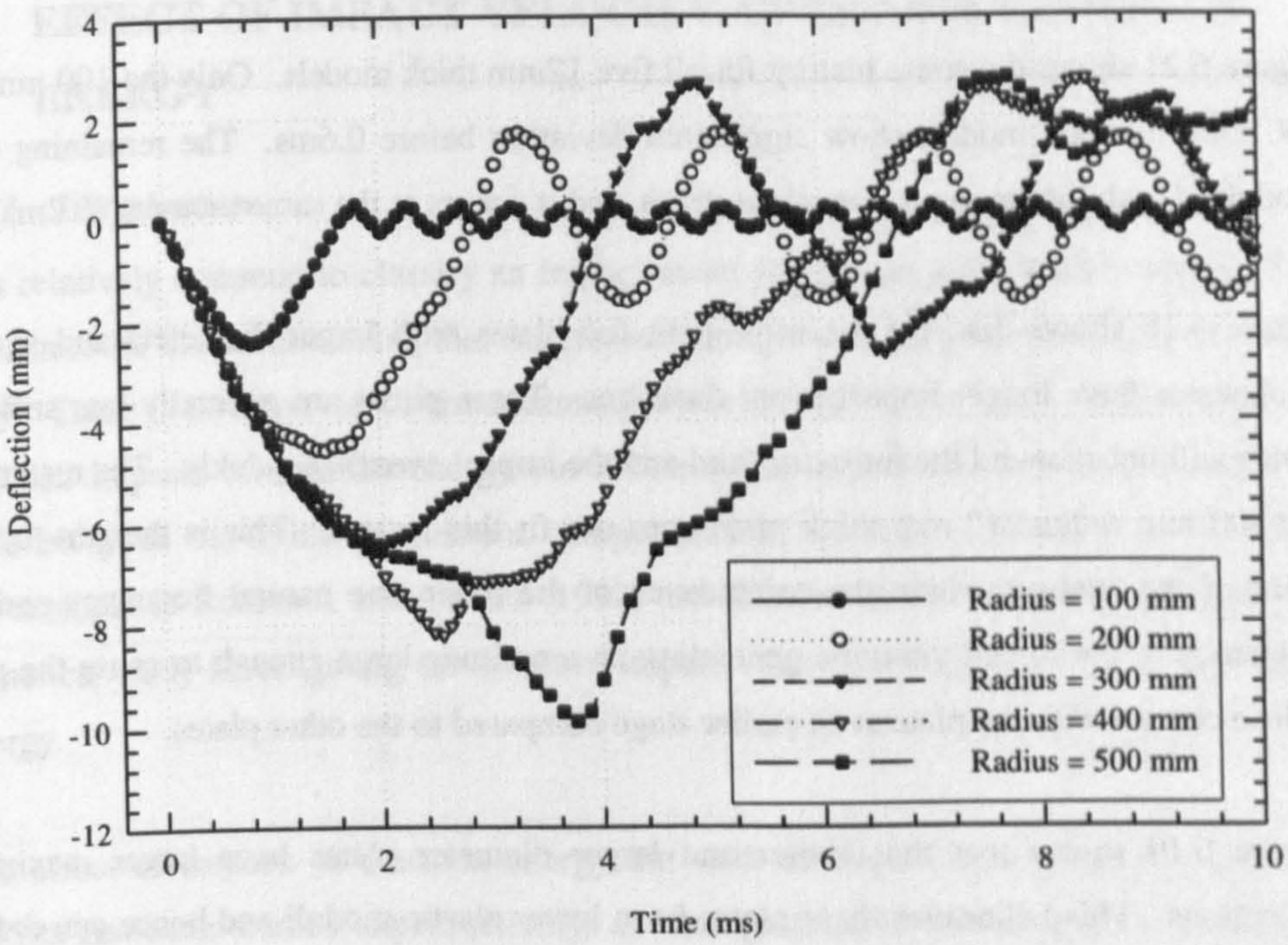

Figure 6.20 – 8 mm thick plate (point B, Figure 6.4) displacement histories for five plate radii

Figure 6.21 – 12 mm thick plate (element i, Figure 6.4) hoop stress histories

Figure 6.21 shows the stress history for all five 12mm thick models. Only the 100 mm and 200 mm diameter models show significant deviation before 0.6ms. The remaining three models all exhibit the same maximum stress, and it occurs at the same moment (0.2ms).

Figure 6.18 shows that, for the most part, the plates with larger diameters and smaller thicknesses have longer impact event durations. These plates are generally less stiff and hence will not rebound the impactor (and end the impact event) as quickly. The results for the 500 mm radius, 12 mm thick plate does not fit this pattern. This is thought to be a quirk of the analysis where the coincidence of the mode one natural frequency and the frequency of the forced vibration generating an amplitude large enough to cause the plate to lose contact with the plate at an earlier stage compared to the other plates.

Figure 6.19 shows that the thinner and larger diameter plates have larger maximum deflections. This is because these plates have lower elastic moduli and hence can deflect more from the impact. In addition, in a similar way to the maximum stress, there appears to be a convergence as the plates get thicker, where the maximum deflection becomes independent of the plate dimensions. Note this is the deflection at point *B* (see Figure 6.4) in the model, at the centre of the plate on the back face, and hence any effect due to indenting under the impactor will be minimised.

6.4.5 Conclusions

Thinner and larger diameter plates have larger maximum deflections and shorter impact event durations. Smaller plates in both diameter and thickness have higher maximum stresses. In particular it was shown that the maximum stress becomes largely independent of plate diameter for thicker plates, and hence it is valid to perform a coupon based experimental study as the application is for plates (wing skins) with large in-plane dimensions.

6.5 EFFECT OF IMPACT VELOCITY AT CONSTANT IMPACT ENERGY

6.5.1 Introduction

It is relatively common to classify an impact using just the incident kinetic energy of the impactor, the insinuation being that the impact damage is dependent on the impact energy only. There is however some circumstantial evidence that this is not a valid assumption, and that impacts of constant energy but different impact velocity will create damage of different types and of different extent. Some research has been carried out on this subject for example in Robinson and Davies (1992) and Olsson (2000). This section presents a numerical study investigating the effect of impact velocity for impacts of constant impact energy.

The effect of impacts at constant energy but with different impactor masses and drop heights has been studied experimentally, and the purpose of this study is to explain the effects seen in experiment. A series of finite element analyses were carried out. In addition, the theory of elastic impact of isotropic bars is examined for comparison.

6.5.2 Models Used and Method

The method used here is similar to that described in section 6.4.2, except that only two plate radii are considered (200 mm and 500 mm), both with the same thickness (8 mm). The generic geometry in Figure 6.4 is used, and the converged optimised mesh was used in every case. A 40 J impact energy impact was modelled in each case with an effective impactor mass varying between 0.4 kg to 20 kg giving a corresponding impact velocity range of 2 ms^{-1} to 14 ms^{-1}, see Table 6.5.

Table 6.5 – Impact velocities used, and corresponding impact parameters

Impact velocity (ms^{-1})	Impactor mass (kg)	Drop height (m)	Impact Energy (J)
1.98	20.39	0.2	40
3.13	8.15	0.5	40
3.84	5.44	0.75	40
4.42	4.1	1	40
6.25	2.05	2	40
7.67	1.36	3	40
8.86	1.02	4	40
9.9	0.82	5	40
10.85	0.68	6	40
11.72	0.58	7	40
12.53	0.51	8	40
13.33	0.45	9	40
14.01	0.41	10	40

Note that in subsequent figures the finite element results are plotted against the impact velocity squared as this gives equal increments, and is proportional to the kinetic energy.

6.5.3 Simulation results

Using the data gathered from each model it is possible to build a picture of the effect that impact velocity in impacts of constant impact energy have on the response of a plate, in particular the maximum stress, maximum deflection and impact event duration. Figure 6.22 shows the variation of maximum deflection of the plate with impact velocity for each plate radius and Figure 6.23 that for impact event duration. Figure 6.24 shows the variation of maximum impactor force (calculated by taking the product of the impactor acceleration (calculated by ABAQUS) and its mass) and Figure 6.25 that for maximum stress in the centre of the plate, on the back face. The stress results plotted in Figure 6.25 are the values of hoop stress; the values of radial stress are almost identical.

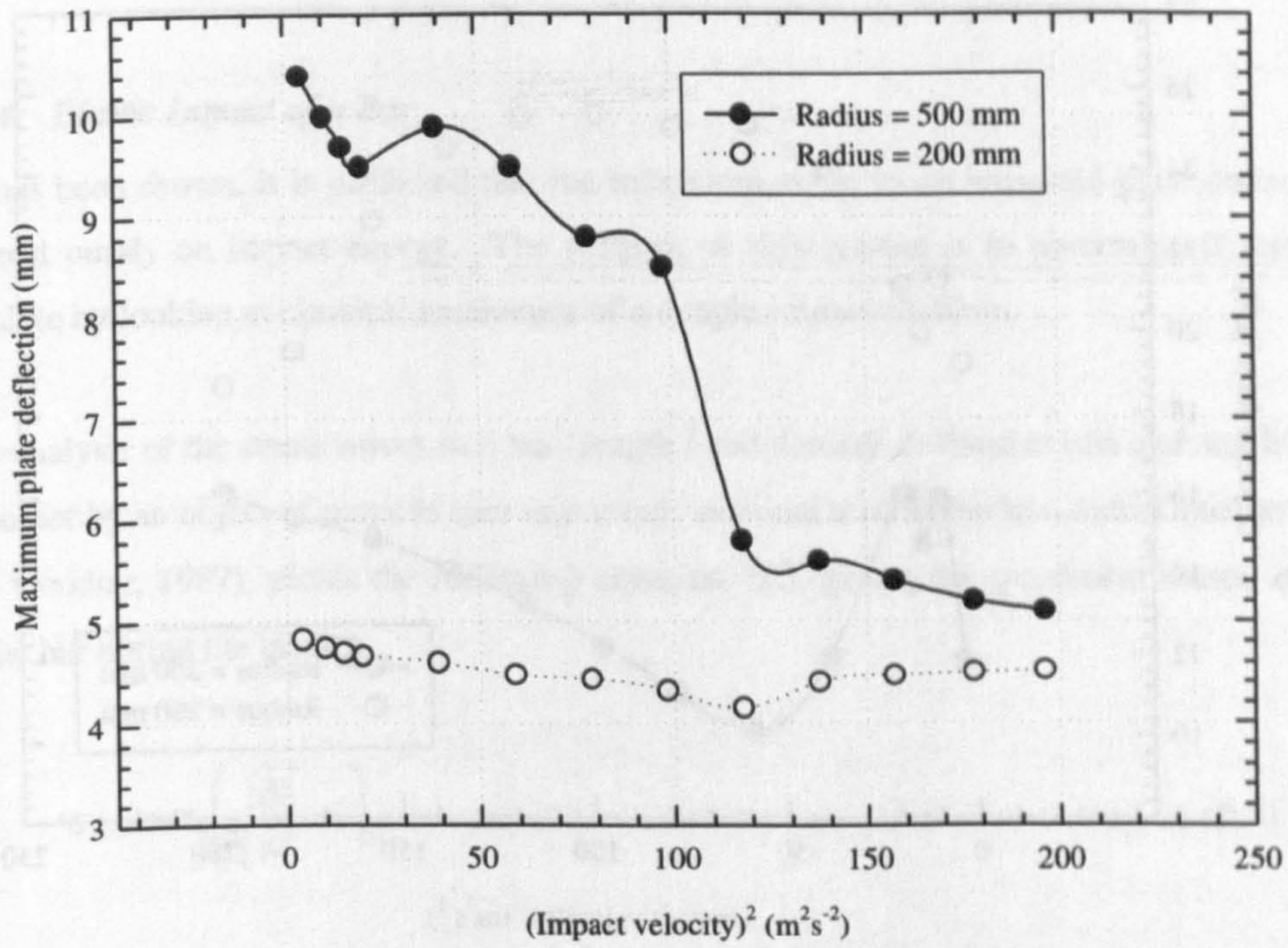

Figure 6.22 - Maximum plate deflection for both plate radii studied

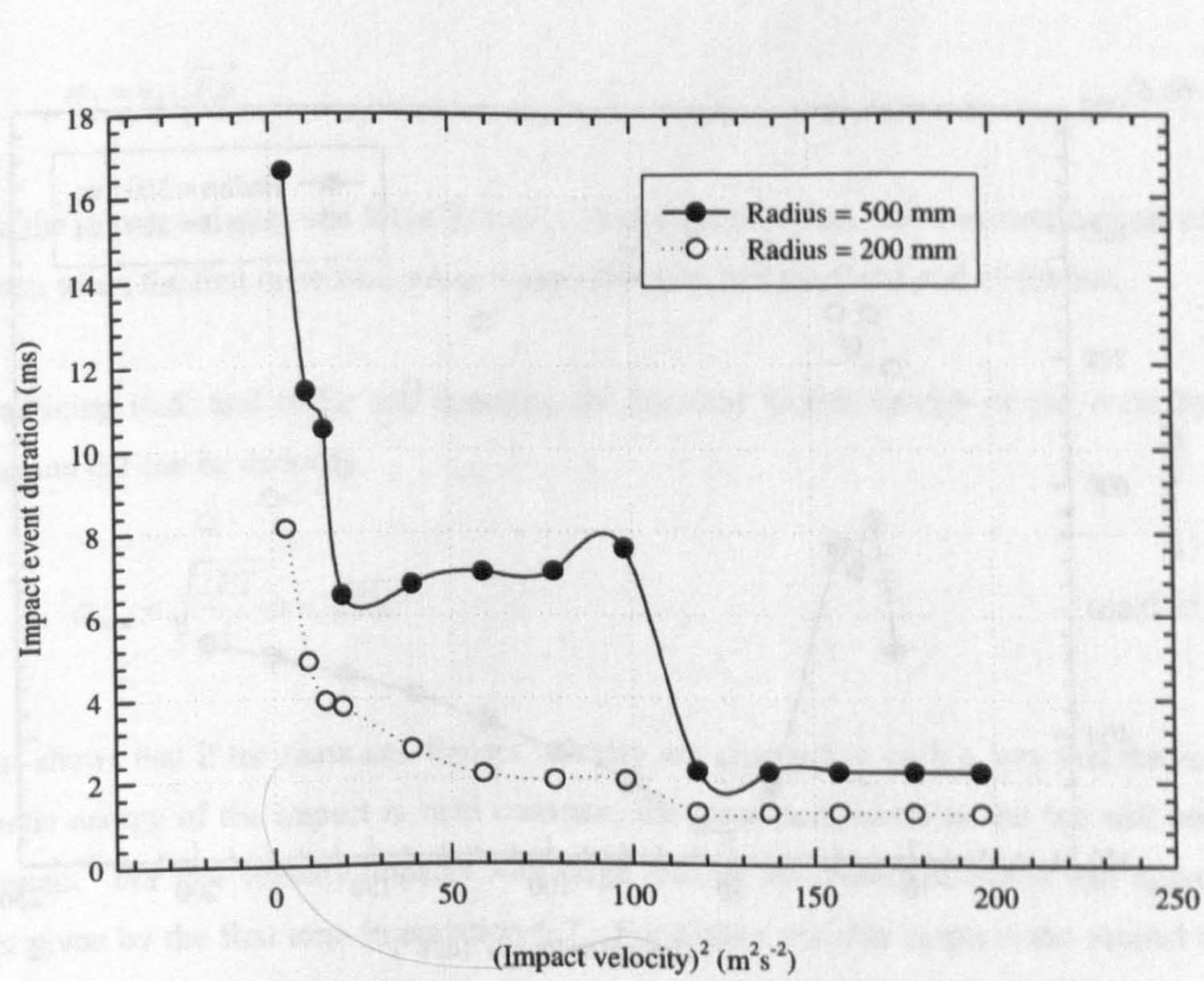

Figure 6.23 - Impact event duration for each plate radius

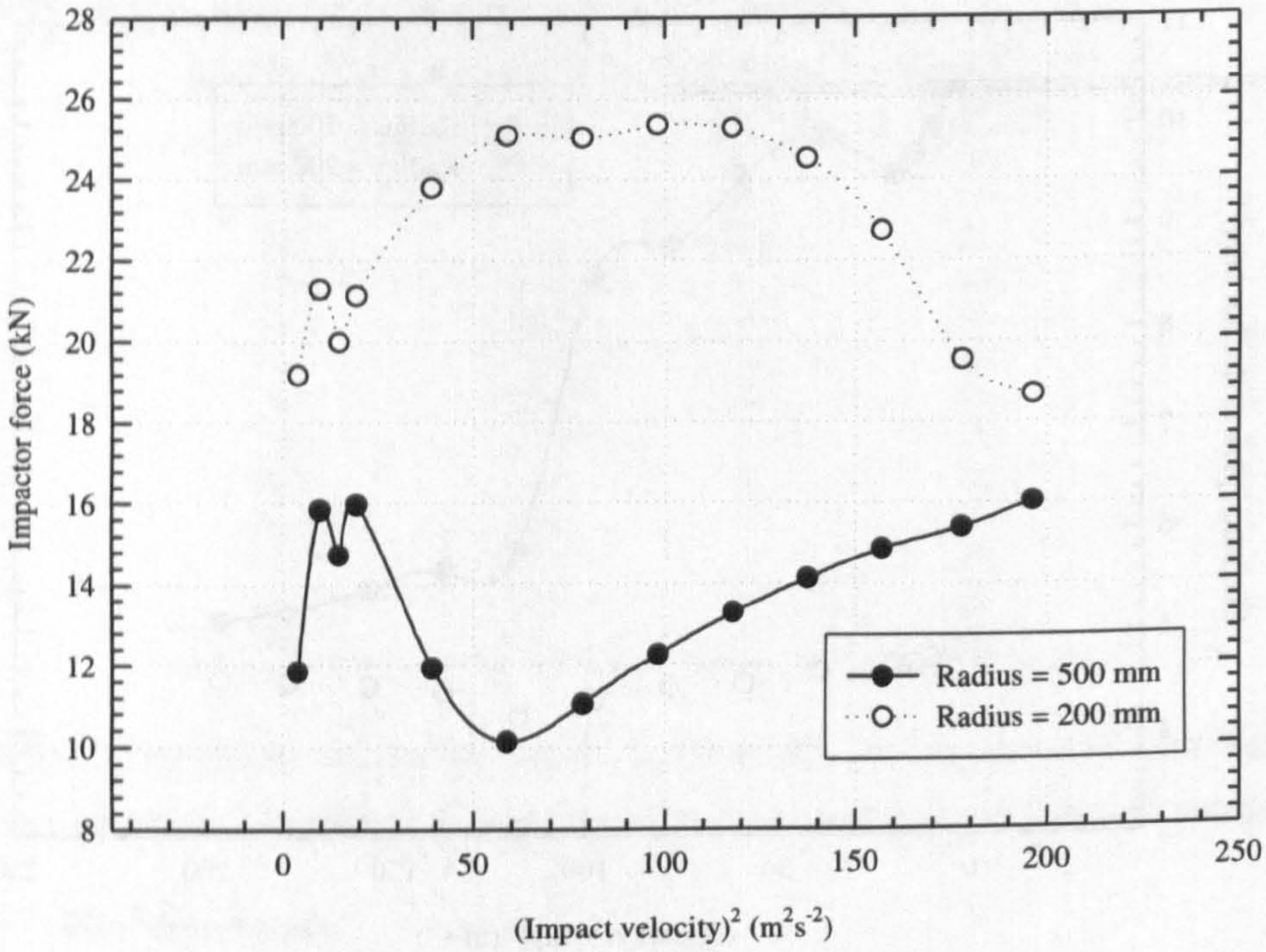

Figure 6.24 - Maximum impactor force for each plate radius

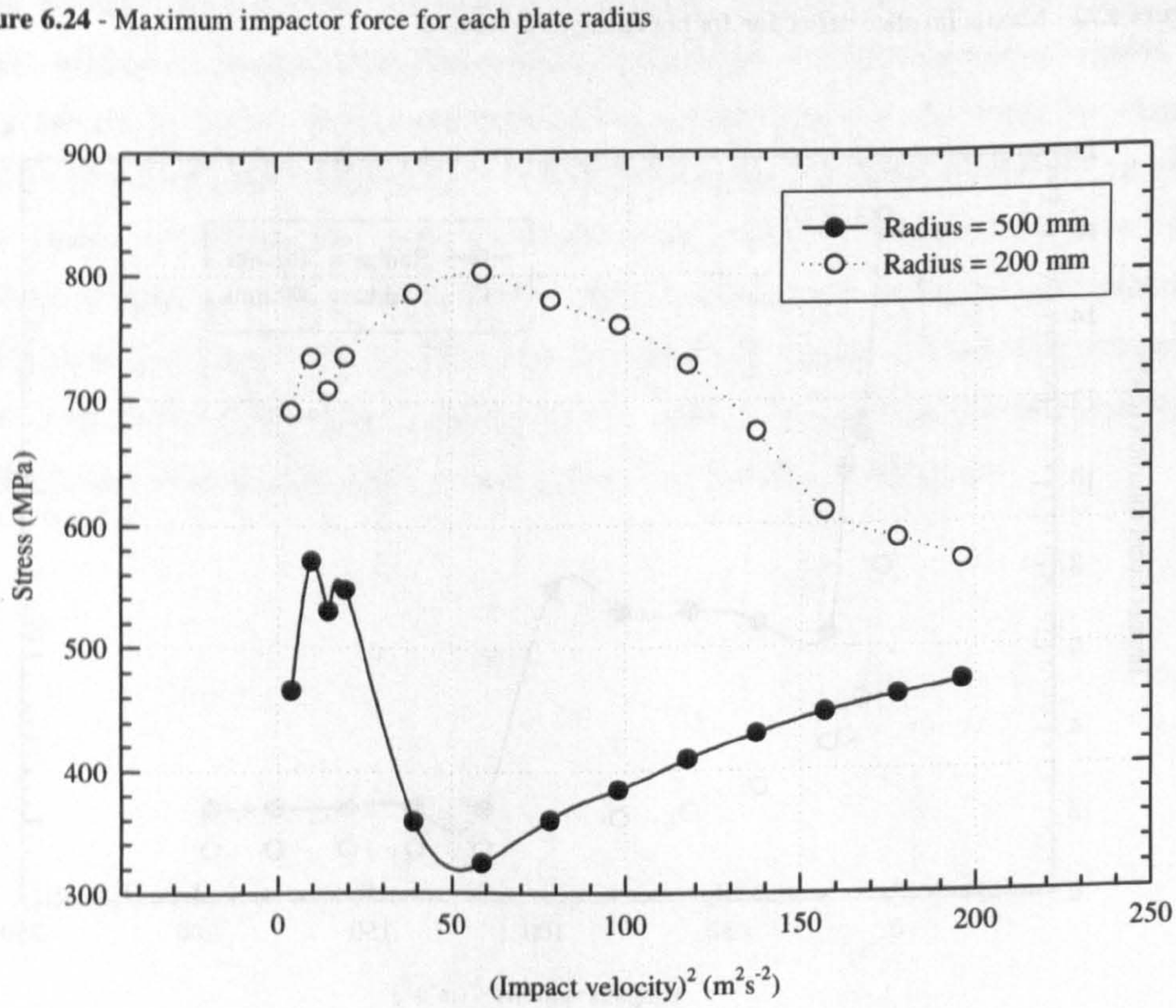

Figure 6.25 - Maximum hoop stress for each plate radius

6.5.4 Elastic Impact of a Bar

As has been shown, it is predicted that the maximum stress in an impacted plate does not depend purely on impact energy. The purpose of this section is to determine if this is sensible by looking at classical mechanics of a simple impact problem.

The analysis of the stress waves in a bar (length l and density ρ) fixed at one end and hit at the other by an object of mass M (per unit cross-sectional area of the bar) (see Timoshenko and Goodier, 1987), yields the following equation, 6.5, giving the maximum stress, σ_{max}, in the bar during the impact.

$$\sigma_{max} = \sigma_0 \left(\sqrt{\frac{M}{\rho l}} + 1 \right) \tag{6.5}$$

σ_0 is the initial stress in the bar and is given by equation 6.6.

$$\sigma_0 = v_0 \sqrt{E\rho} \tag{6.6}$$

v_0 is the impact velocity and E the Young's Modulus of the bar. The maximum stress often occurs when the first or second stress wave reflection hits the fixed end of the bar.

Combining (6.5) and (6.6), and denoting the incident kinetic energy of the mass by T, equation 6.7 can be derived.

$$\sigma_{max} = \sqrt{\frac{2ET}{l}} + v_0 \sqrt{E\rho} \tag{6.7}$$

This shows that if the mass and impact velocity are changed in such a way that the initial kinetic energy of the impact is held constant, the maximum stress in the bar will not be constant. For low velocity impacts with large masses the maximum stress will approach that given by the first term in equation 6.7. For higher velocity impacts the second term will cease to be negligible and the maximum stress will depend more on this term.

This analysis shows that in the case of end impact of a bar that is fixed at one end, the assumption that the maximum stress depends purely on the impact energy is false. It is reasonable to assume that the same is true for other impact scenarios, namely impact of a fibre reinforced, laminated wing skin panel.

6.5.5 Discussion

The maximum deflection for the 200 mm radius plate showed little variation, whereas the 500 mm radius plate showed a general reduction for faster impact velocities. Both plate geometries show a general reduction in impact event duration as impact velocity increases, with the smaller plate always having the shorter impact event duration and smaller maximum deflection. Both plate geometries seem to be tending towards the same value with faster impacts. The maximum impactor force and maximum hoop/radial stress at the centre of the back face show a similar variation with impact velocity, with both plates tending towards the same value with faster impacts.

The reason for the effects described can be attributed to inertial stiffening. As the impactor strikes the plate with a faster velocity, so the plate response is also faster; the plate is likely to enter into a higher fundamental mode of vibration than the first. Since the plate acceleration is higher so the local mass of the plate becomes more important compared to the elastic modulus. When the plate appears stiffer the deflection and impact event duration will be smaller. Inertial stiffening also accounts for the manner of the response of the plate and explains why the four parameters are tending towards common values for each plate geometry. A slow or simulated impact from a quasi-static test will deform the plate globally. Faster impacts will induce a more localised response meaning that the boundary conditions and in-plane dimensions are less important, illustrated in an exaggerated form in Figure 6.26. Hence at and above a certain impact velocity the values of maximum stress and impactor force will be the same for plates of a given thickness but of any radius, and this trend is observed in Figure 6.24 and Figure 6.25.

Figure 6.26 - Representative plate response to a slow impact (left) and a fast impact (right)

6.5.6 Conclusions

Two plate geometries have been numerically studied, each with 13 different impacts of constant impact energy using an explicit finite element analysis. There is a significant effect observed due to different impact velocities on the plate response. In particular the impact event duration and maximum deflection tend to decrease with faster impacts. More importantly the maximum stress in the plate was found to vary with impact velocity indicating that perhaps the type and extent of damage would vary in real impacts.

6.6 3D FE MODELLING OF EDGE IMPACT

6.6.1 Introduction

Significant impact testing has been undertaken in this work where the plate has been impacted near a free edge. This has been modelled in order to understand the pattern in the damage mechanisms that have manifested in the plates: delamination dominance in near edge impacts and fibre breakage dominance in central impacts. To conduct this analysis three-dimensional models have to be used. The same generic geometry is used, and the converged mesh of one element per 1 mm of plate thickness. The results from the analyses in this section are more thoroughly examined in Chapter 7. Both a central and edge 3D model were produced. Although the central impact model is accurately modelled using axi-symmetric elements it was also modelled in 3D to validate the method.

6.6.2 Models Used and Method

Two models were created, each for a 100 mm radius plate, with a 180 J impact from a 4.3 kg impactor, see Figure 6.27. In the edge impact model the impact occurs 25 mm from the free edge. As the same converged mesh was used, 8 linear, 8 noded elements were defined through the thickness, designated C3D8R in ABAQUS/Explicit.

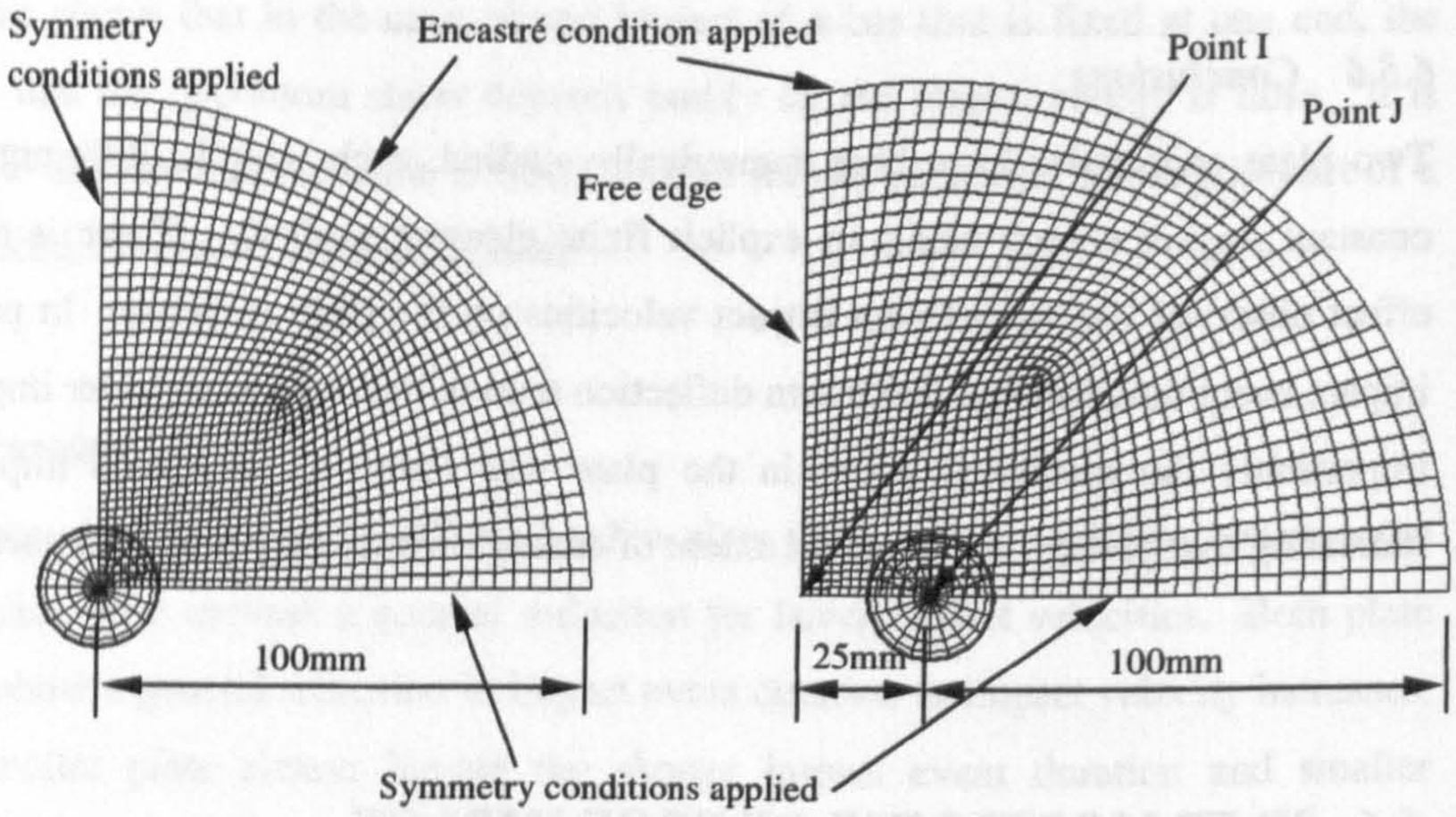

Figure 6.27 - Central impact (left) and edge impact (right) models

6.6.3 Results

By way of a simple comparison the displacement and direct stress histories were compared at the plate centre on the back face in the central impact model, and at points I and J on the back face of the edge impact model (see Figure 6.27). Figure 6.28 shows the displacement history. It is evident that the edge impact has a significantly longer impact event duration and a larger maximum deflection. This gives credence to the hypothesis that the edge-impacted plate absorbs impact energy through a large deflection. This will create larger bending shear stresses and give rise to delaminations. The centrally impacted plate deflects less and so delaminations will be smaller. Figure 6.29 shows the stress history for both models. Both show similar peak stresses. It is not possible to see the σ_{11} central impact stress plot in Figure 6.29 as it has plotted exactly behind the σ_{33} results. As with the axi-symmetric results the in-plane stresses are the same in each orthogonal direction.

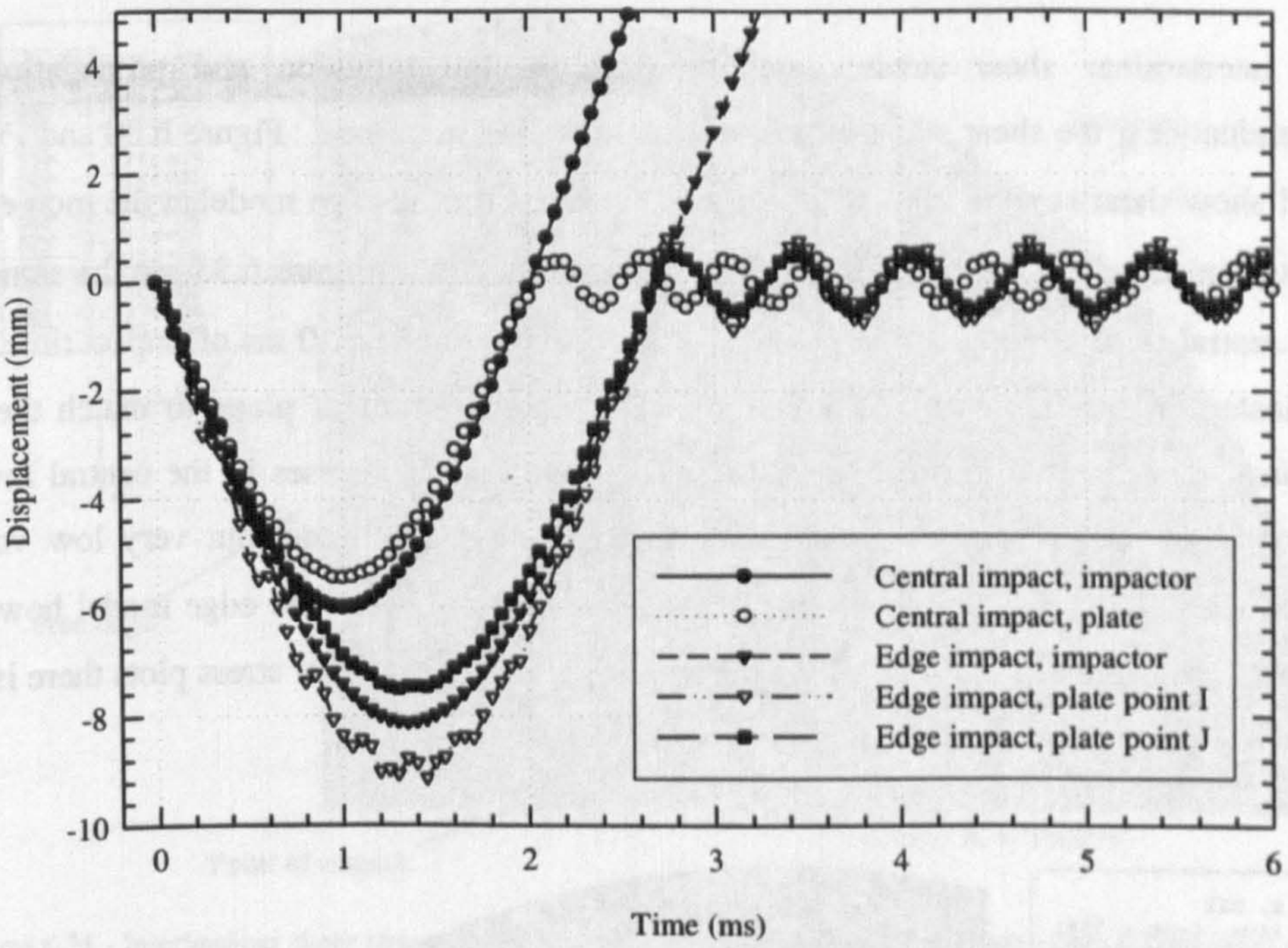

Figure 6.28 - Displacement histories for the edge and central impact models (see Figure 6.27 for I and J)

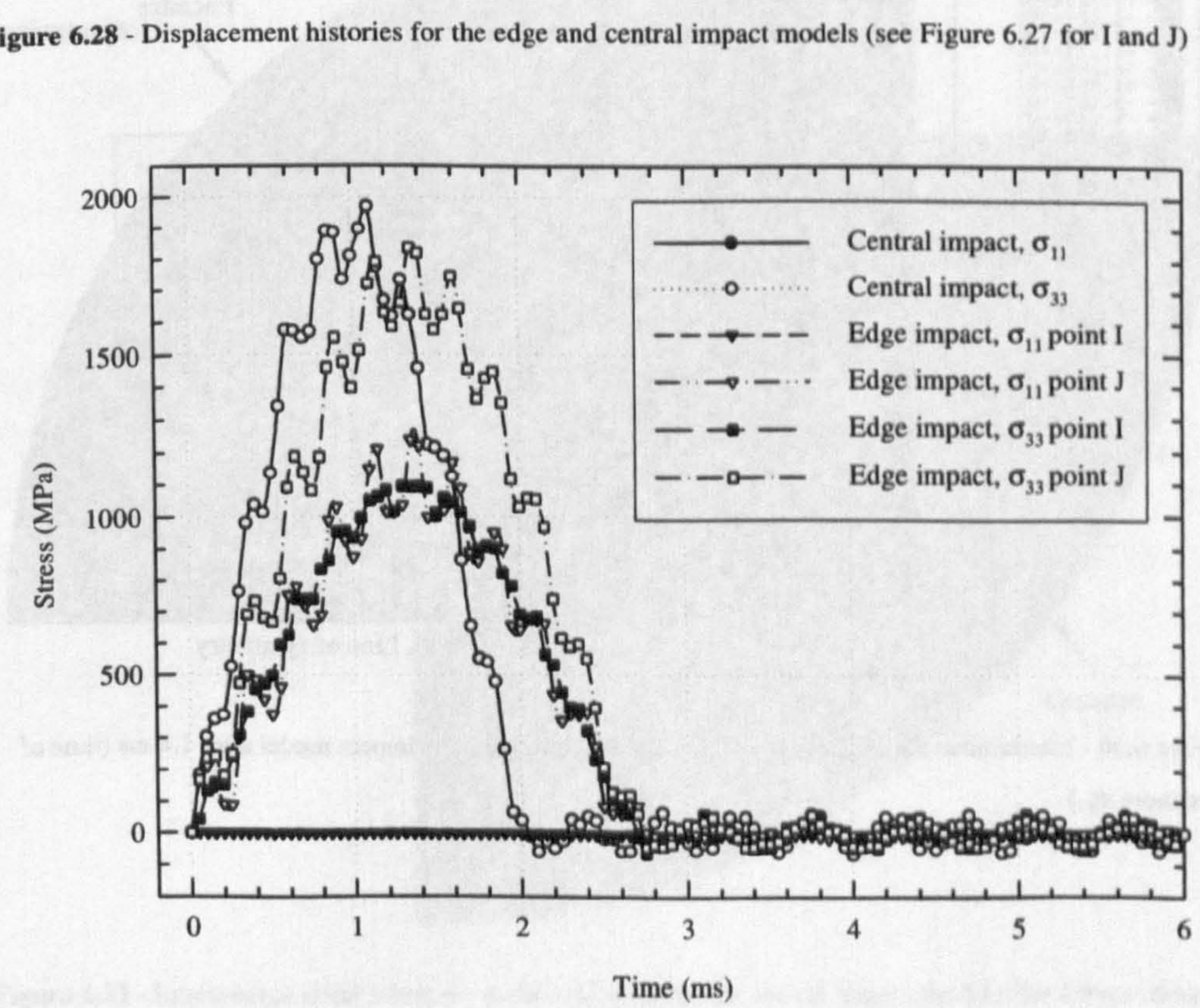

Figure 6.29 - Stress histories for the edge and central impact models (see Figure 6.27 for *I* and *J*)

As interlaminar shear stresses are important in the initiation and propagation of delaminations, the shear stress at mid-thickness is also examined. Figure 6.30 and Figure 6.31 show shear stresses σ_{12} and σ_{23} at mid-thickness for the edge model at the moment of maximum σ_{11} after 1.4 ms of impact time. Figure 6.32 and Figure 6.33 are the same for the central impact model at the moment of maximum σ_{11} after 1.0 ms of impact time. As indicated on the figures the 2 direction in the models is out of plane to match the co-ordinate system used in the 2d analysis work. Both shear stresses in the central impact model show peaks near the impact point with a high amplitude, but very low values elsewhere. The same is true for σ_{12} in the edge model. σ_{23} in the edge model however shows significant stress values along the free edge, unlike the other stress plots there is not only one peak.

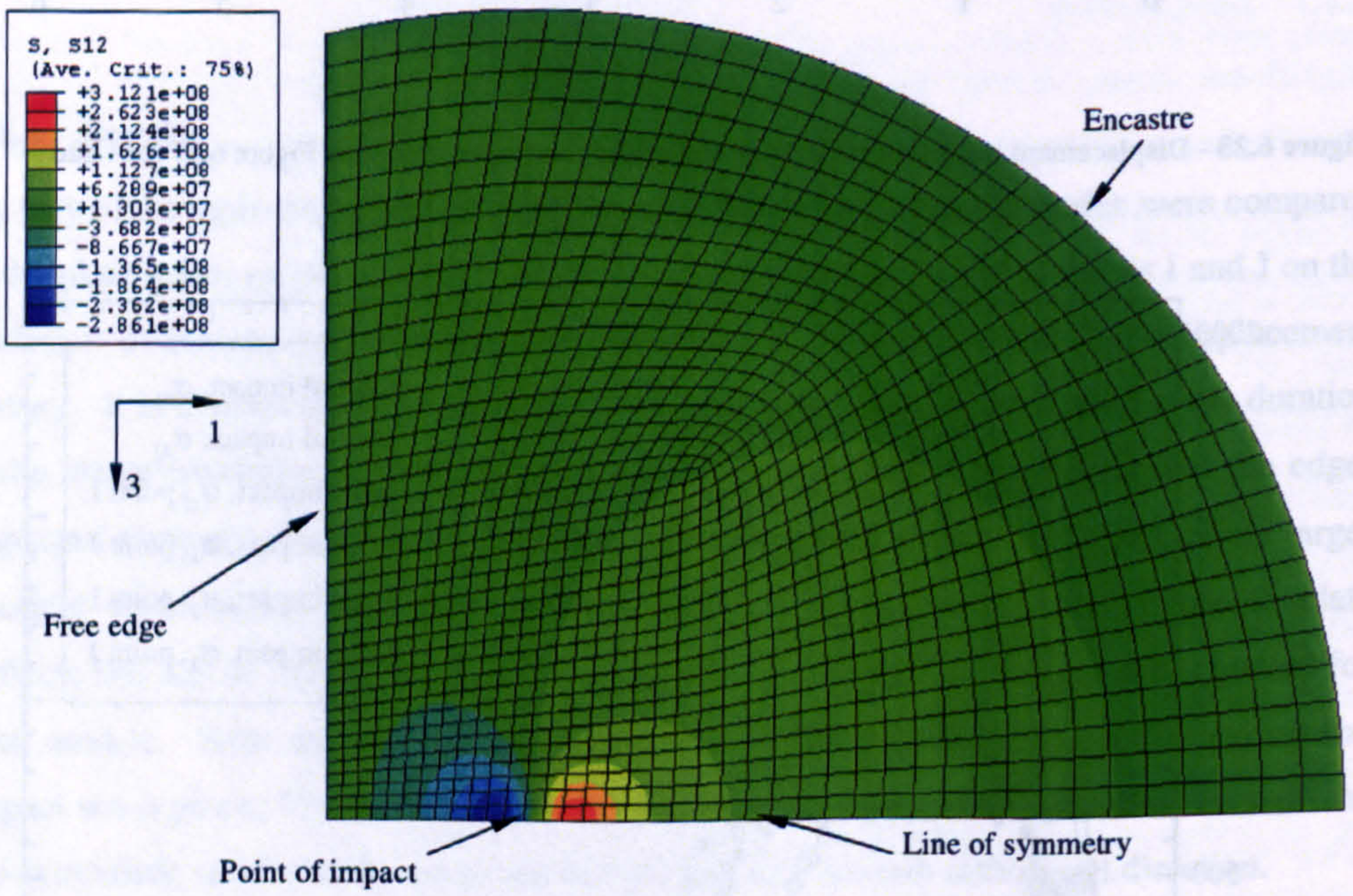

Figure 6.30 - Interlaminar shear stress σ_{12} at mid-thickness in the edge impact model after 1.4 ms (time of maximum σ_{11})

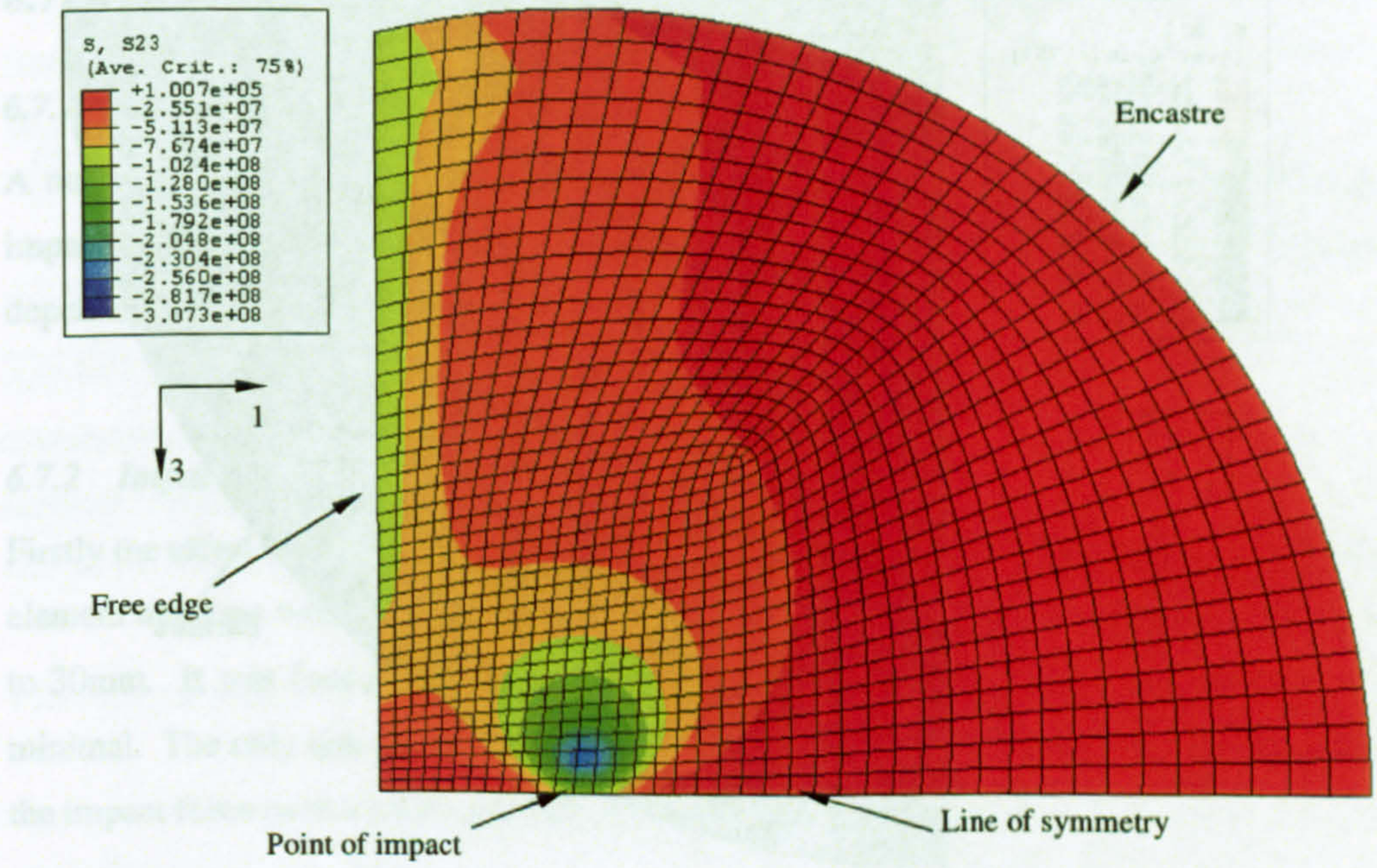

Figure 6.31 - Interlaminar shear stress σ_{23} at mid-thickness in the edge impact model after 1.4 ms (time of maximum σ_{11})

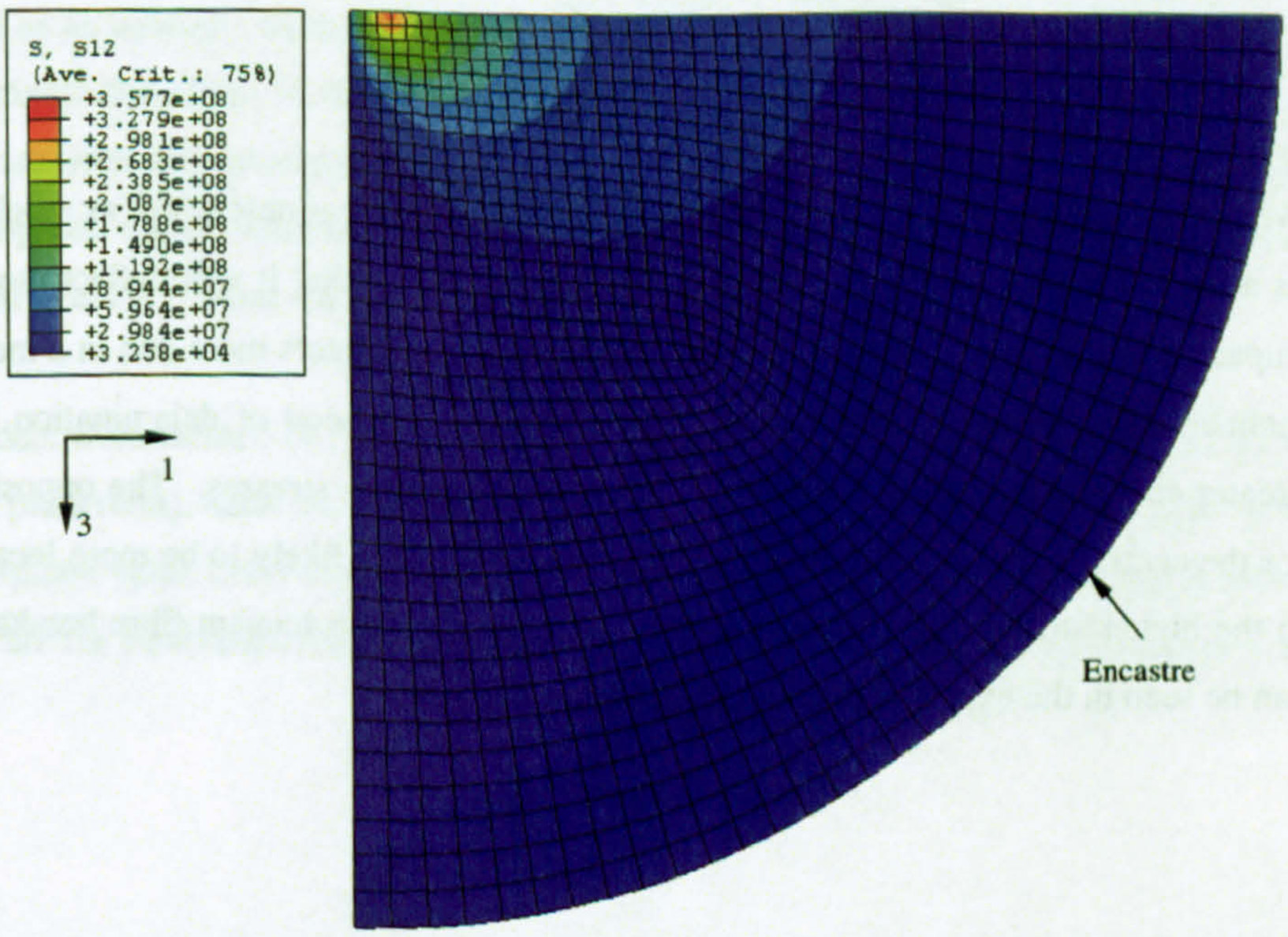

Figure 6.32 - Interlaminar shear stress σ_{12} at mid-thickness in the central impact model after 1.0 ms (time of maximum σ_{11})

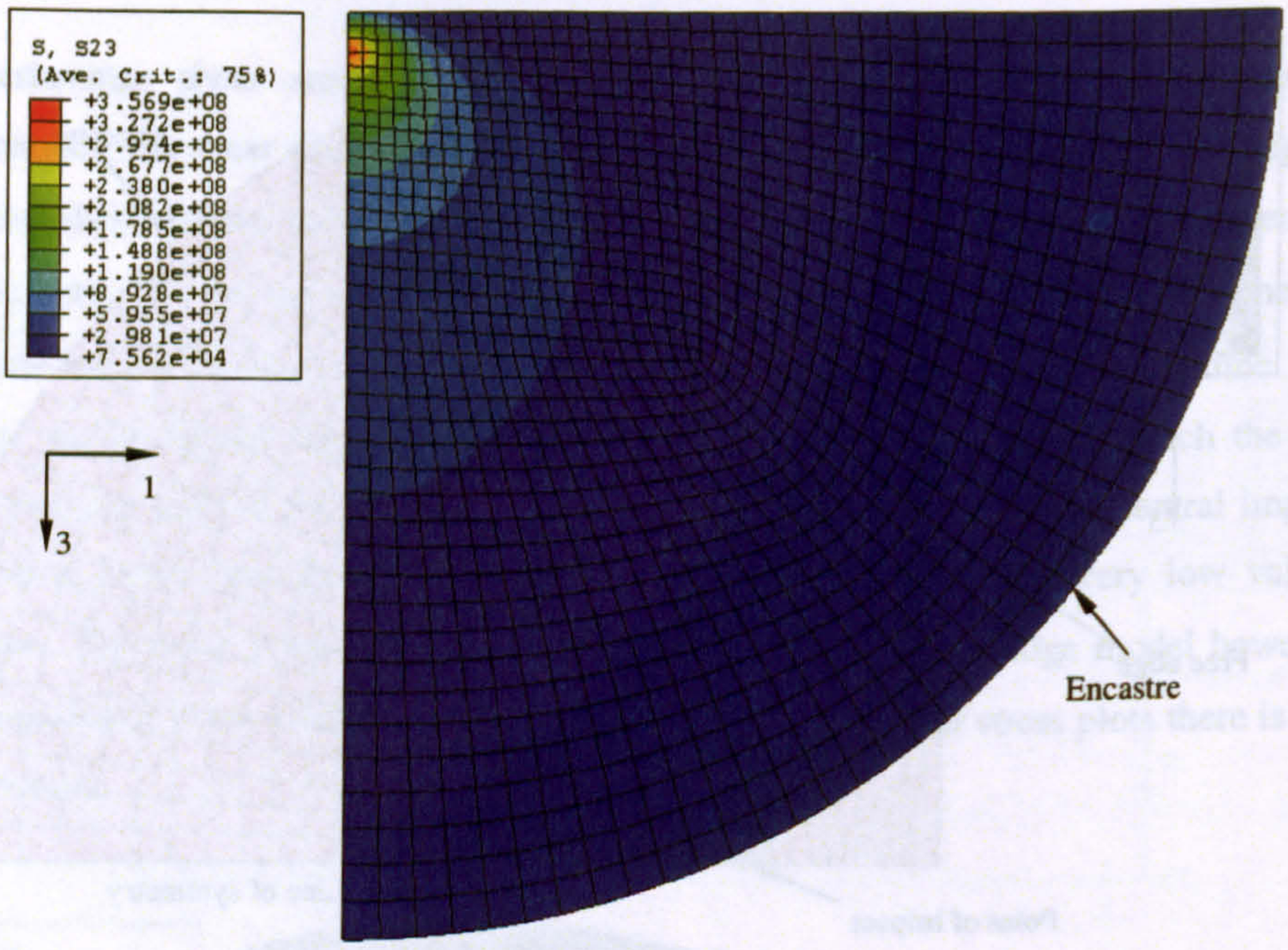

Figure 6.33 - Interlaminar shear stress σ_{23} at mid-thickness in the central impact model after 1.0 ms (time of maximum σ_{11})

6.6.4 Discussion

With an edge impact the plate is not as well supported and has nearly half as much material as a central impact specimen. The consequence of this is that it will deflect more than if impacted in the centre. Thus, for edge impact the plate deflects more and in a more global manner. This in turn means that there is a greater likelihood of delamination being the greater energy absorption mechanism due to shear bending stresses. The opposite is true for the centrally impacted specimens where the response is likely to be more localised due to the higher stiffness and the greater energy absorption mechanism fibre breakage. This can be seen in the experimental results in earlier chapters.

6.7 RIG VERIFICATION AND OTHER ANALYSES

6.7.1 Introduction

A number of other analysis studies were carried out in order to verify the design of the impact rig and give confidence that the main parameters upon which the plate response depended were being studied.

6.7.2 Impactor Tup Diameter

Firstly the effect of the diameter of the spherical impactor tup was investigated. Four finite element analyses were performed, each with an impactor of different diameter, from 5mm to 30mm. It was found that the effect on maximum stress and maximum deflection was minimal. The only noticeable difference came where the larger diameter impact tup spread the impact force over a wider area and so induced less indentation.

6.7.3 Through Thickness Elastic Modulus

The effect of through thickness elastic modulus was also investigated. The plates are modelled as an isotropic material in-plane with reduced through thickness elastic modulus. To investigate the effect of different through thickness elastic modulus a series of finite element analyses were performed where this elastic modulus was changed to be the same as the in-plane elastic modulus (so creating a fully isotropic material) and the effect on maximum stress and other impact response characteristics monitored.

Five models were created (40 J impact with 1.019 kg impactor, 8 mm thick plate with five different plate radii), each with the through thickness elastic modulus set to the same value as the in-plane value (56.4 GPa). The results are summarised in Table 6.6. The values in brackets are the equivalent results from analyses with the quasi-isotropic CFRP properties.

Table 6.6 - Selected results from the models using isotropic material properties (for comparison results from the standard analyses in brackets)

Plate radius (mm)	Maximum S11, element *i* (MPa)	Maximum S33, element *i* (MPa)	Duration of impact event (ms)	Maximum deflection (mm)
100	1108 (1010)	1108 (991)	1.0 (1.1)	2.3 (2.5)
200	882 (804)	868 (788)	1.9 (2)	4.4 (4.5)
300	569 (516)	569 (503)	2.6 (2.7)	6.4 (6.4)
400	448 (368)	448 (360)	4.7 (4.7)	8.2 (8.2)
500	387 (367)	387 (360)	7.3 (7.1)	8.8 (8.9

As can be seen from Table 6.6 there is little difference between the two types of model, no more than 10%, and hence in fact there is little effect due to the reduced elastic modulus through the thickness.

6.7.4 Plate Density

It has been shown that there are some unusual effects in the impact response of a plate, for example when it loses contact with the impactor during the impact event. These effects are in part due to the plate vibrating at the first natural frequency, and the superposition of in-plane stress waves reflecting off the plate boundary. The speed of these stress waves and the frequency of the first mode are dependent on the plate material density, for example consider the equation for the speed of sound, c, through an elastic plate in equation 6.8. To investigate this further, four finite element analyses were performed, where the density of the plate material was different in each case. The results are presented in Table 6.7.

$$c^2 = \frac{E}{\rho}\frac{(1-\nu)}{(1+\nu)(1-2\nu)} \tag{6.8}$$

Table 6.7 - Summary of results from the density analyses

Density Value (kg/m^3)	Maximum σ_{11} (MPa)	Maximum σ_{33} (MPa)	Duration of Impact (ms)	Max Deflection During Impact (mm)	% of Impact Event in Contact (ms)
1000	336	329	5.45	9.79	53
1620	367	359	7.1	8.91	34
2000	393	385	8	8.56	24
3000	447	438	3.1	5.49	58

There is variation between the results, with maximum stress increasing with density and maximum deflection decreasing as the inertial stiffness increases. The pattern of results for the impact event duration and proportion of this time the impactor spent in contact with

the plate is less clear. Clearly, however, the plate density has a significant effect, but as the material density is well known this should not be a problem. The plate density used in the parametric impact analysis was 1620 kg/m^3.

6.7.5 Impactor Design Analysis

The following analysis is to determine the suitability of using an aluminium impactor over one made from steel. In each case the same cross-section was used (25 mm radius cylinder) and the length varied to maintain the same mass (200mm for aluminium and 65mm for steel). Table 6.8 shows the results from an analytical analysis.

Table 6.8 - Stiffnesses of plates and impactors

Item	Stiffness (kN/mm)
Aluminium impactor	22.6
Steel impactor	67.7
CFRP plate, 24mm thick, 100mm radius (from FEA)	100
CFRP plate, 24mm thick, 100mm radius (from static theory)	465
CFRP plate, 12mm thick, 100mm radius (from static theory)	58.1
CFRP plate, 4mm thick, 100mm radius (from static theory)	2.15

Where the plate stiffness is quoted as coming from theory, it is calculated using equation 6.4. Where the plate stiffness is quoted as coming from finite element analysis (FEA), it was calculated from the gradient of impactor force against plate deflection from the relevant dynamic analysis.

Two finite element simulations were performed, to investigate what the difference between the two impactor designs (see Figure 6.34). The impactor tup in both cases was modelled with steel properties. The global element size for the impactor was set to 1mm, the same size as the elements under the impactor in the plate.

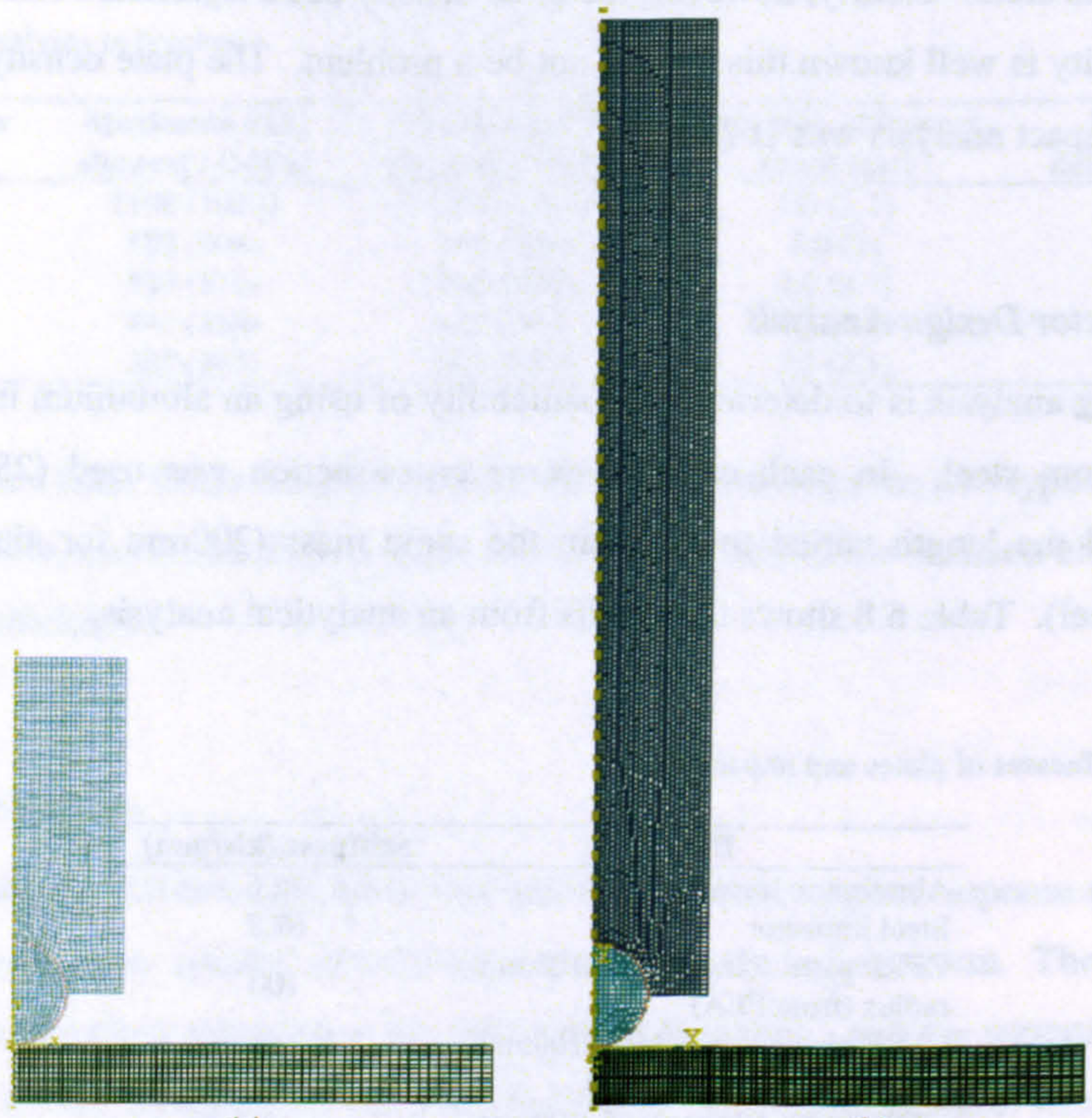

Figure 6.34 – (a) Steel impactor model; (b) Aluminium impactor model

The displacement history results for the plate, and the top and bottom of the impactor were in very good agreement between the two models.

The critical feature of the impactor, apart from its ability to transfer kinetic energy to the plate, is to allow acceleration readings using an accelerometer on the impactor. Ideally the accelerometer signal is as close as possible to representing the acceleration of the tip of the impactor. As will be shown, the position of the accelerometer is critical in this. The acceleration history results from the analyses show that whilst the acceleration of the bottom of the impactor follows that of the plate impact point very closely, the acceleration at the top of the impactor (the proposed position of the accelerometer in the first design iteration) is very different. For the first few milliseconds of the impact, arguably the most important, there is no noticeable trace, and when there is a trace it is much smaller than that of the plate and out of phase. Figure 6.35 compares the acceleration trace at the top of the impactor between the two models. It shows that the acceleration at the top of the

aluminium impactor varies greatly with that of the steel impactor. The top of the steel impactor does not pick up any acceleration for the first 0.1ms of the impact whereas the aluminium impactor has no acceleration for the first 0.3ms. This is because the stress wave speed in steel is faster due to its higher stiffness and it also has a shorter distance to travel. Hence if the accelerometer was mounted at the top of the impactor the preferred design would be to make it as short as possible, made from steel. However, with the current design of the impactor with the accelerometer mounted just behind the impactor tup the material dimension of the rest of the impactor is immaterial; this design being optimal for capturing the acceleration of the impactor, and the matching acceleration of the plate.

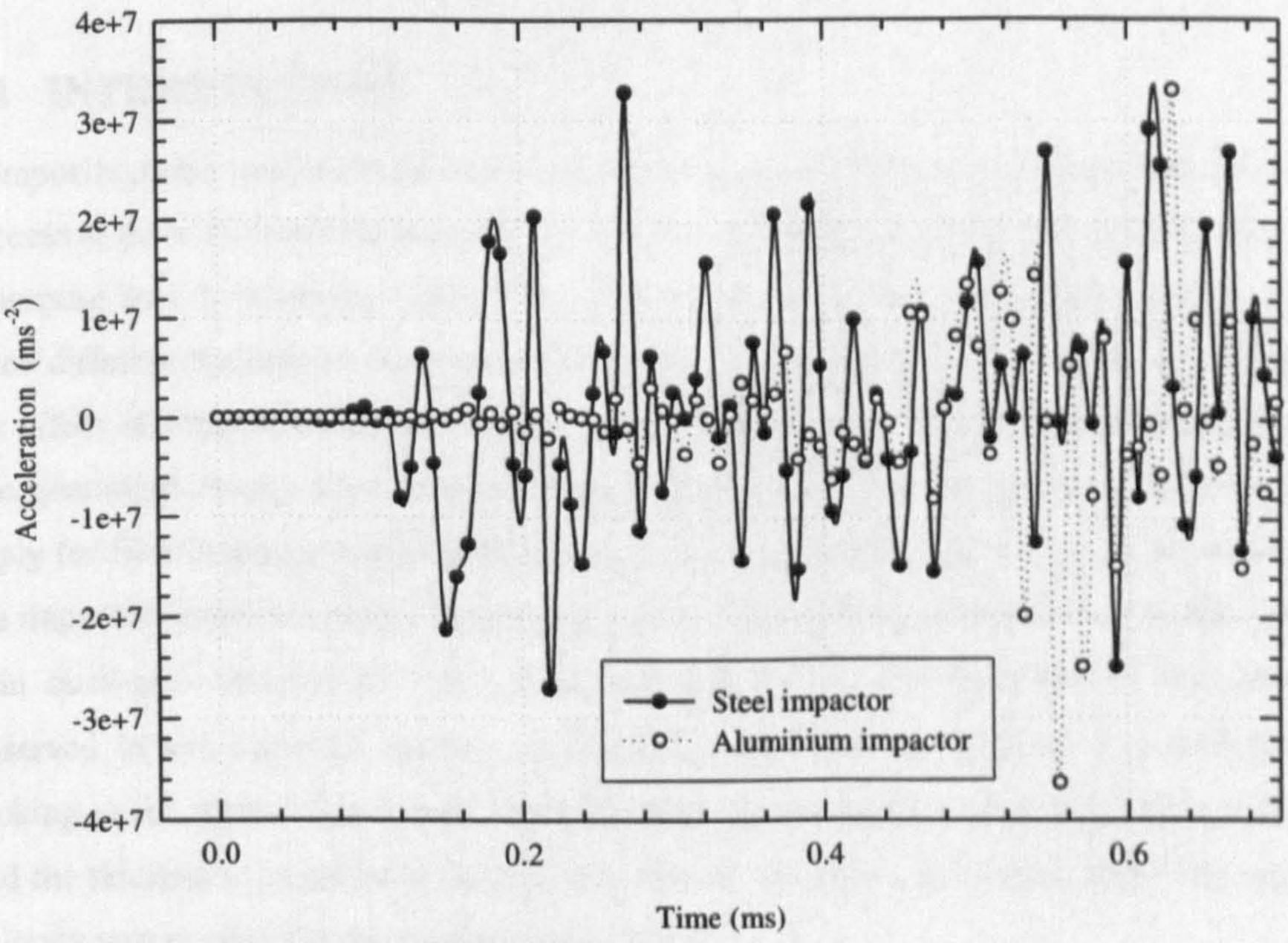

Figure 6.35 - Comparison of acceleration history from the top of each impactor

6.7.6 Conclusions

The design of the impact rig has been validated through use of finite element analysis. It was shown that the impactor tup radius is of little importance in the global response of the plate and the position of the accelerometer is important. It has also been shown that the density of the plate material has an effect on the response due to it affecting the velocity of

the stress waves, but that the through thickness elastic modulus of the material has little effect.

CHAPTER 7

DISCUSSION

7.1 INTRODUCTION

Composite plates were manufactured using non-crimped fabrics and the resin film infusion process to three different thicknesses. A detailed experimental study was performed, using a purpose built instrumented impact rig, that studied the effect of impacting laminates of three different thicknesses both near a free edge and centrally, and including a study into the effect of impact velocity in impacts of constant energy. Once impacted the damage was quantified using a number of techniques: ultrasonic C-scan for delamination detection, deply for fibre breakage and residual strength test on coupons machined from the centre of the impacted laminated plates. In parallel to this, finite element analysis was performed to gain qualitative agreement with experiment and further understanding of the damage observed in the impacted plates. A detailed parametric investigation was undertaken looking at the effect of geometric variables such as the in-plane plate dimension (radius) and the thickness. In addition the effect of impact velocity was studied where the impact velocity was varied in impacts of constant energy.

The results from these investigations have been discussed individually in the preceding chapters 3 to 6. In this chapter the results are discussed as a whole.

7.2 IMPACT CATEGORISATION

As has already been discussed in the literature review in Chapter 2, it has been observed that the response of the composite target plate and any resulting damage will change depending on at least four variables: plate thickness and in-plane dimensions, plate mass, impactor mass and impact velocity. Boundary conditions are also important, but were kept constant in this research. It has also been shown in detail that the resulting damage is dependent not solely on impact energy but the combination of the above listed factors. In this research similar observations have been made; the damage observed in experiment largely falls into two groups, one where delamination dominates and one where fibre breakage dominates. Within each experimental study, the defining variable can be used to categorise the type of result seen into one of the two damage pattern groups as follows:

- Impact location: Impact near a free edge gives rise to delamination as the dominant damage mode whereas impact centrally to a plate results in fibre breakage as the dominant damage mode.
- Thickness: The plates with nominal 8 mm thickness showed greater delamination area compared to the nominal 12 mm thickness plates for the same impact energy. Consequently fibre breakage was more pronounced in the 12 mm thick plates impacted compared to the 8 mm thick ones. The plates with nominal 4 mm thickness exhibited a different damage pattern again, showing a very small amount of delamination and significant back face splitting and fibre breakage as the impactor was of sufficient velocity and energy to induce a more local response close to penetrating the plate.
- Impact velocity: Slow velocity impacts showed extensive fibre breakage, though the cracks were longer and mainly concentrated in the upper layers where fibre micro-buckling would have occurred due to the large deflection. In the faster impacts the fibre cracking was more consistent in length through the thickness (see the deply results in section 5.3.4).

The categorisation of edge and central impact and the different damage modes that dominate has not been reported in the literature. This is important as it has implications for the integrity of impacted components that have free edges, especially if they are not stiffened or reinforced. Without the free edge the panel will react in the normal manner, with some fibre damage and some delamination. With the free edge, depending on the

proximity of the impact to the edge, the component will deflect much more and delaminate extensively with much less fibre breakage. Therefore having a free edge will mean impact may be less critical when the component has to sustain tensile loads as the absorbed impact energy will have been mostly used to create delaminations and not fibre breaks. A component that has to take significant compressive loads, with a free edge will similarly exhibit large delaminations near the hole, and will show a much reduced functional capacity, i.e. ability to sustain compressive loads. What this means is that careful consideration needs to be given to the location of free edges in a wing structure. If possible they should be located on the lower skin. Maintenance schedules should ensure careful inspection for impact damage around free edges in components that take large compressive loads, i.e. the upper skin. In the lower skin and other tensile load carrying components, the areas around holes and free edges are less critical, and more care should be paid to stiffer areas, for example near stiffeners like stringers and ribs where fibre damage will certainly result.

The reason for this is the manner of the plate's response, which is due to its apparent stiffness. When the plate is less stiff the deflection will be larger and bending (particularly shear) stresses greater, which consequently lead to matrix cracks and delaminations. A stiffer plate will deflect less overall but *will have a more localised* response with the damage absorbed by more fibre breakage. The local bending stress will be higher, giving rise to large in-plane tensile stresses below the centre plane of the plate. Also the action of the impact will induce fibre breakage through matrix crushing, both of which will spread to beyond the radius of the tup.

The plate's apparent stiffness depends on at least three different things. Firstly the support; the more supported a plate the less flexible it will be. So when comparing a centrally impacted plate with an edge impacted plate, the centrally impacted one has much more support, where the edge impacted plate has a large free unsupported edge. Secondly plate thickness is important. The bending stiffness is directly related to the thickness cubed of the plate, so a thinner plate will appear less stiff and a thicker plate more stiff. Finally impact velocity: a fast impact velocity will induce a more localised response as inertial forces will be higher and the plate will appear stiffer. Conversely with a slow impact the inertial forces are lower and a more global response will be induced. With a local

response, the effect of boundary conditions is much smaller or can be neglected, whereas with a global response the boundary conditions almost govern the mode of deflection.

The C-scan plots have shown that the maximum extent of delamination has been large in the case of edge impacts compared to equivalent central impacts, see section 5.3.3 and Figure 5.31 in particular. Fibre breakage has also been observed. Table 5.4 shows that the centrally impacted plate has significantly more fibre cracking compared to the edge impacted plate, and the figures in section 5.3.4 for the centrally impacted plate show that the majority of fibre breakage occurs at the top surface, where the impactor struck, and towards the back face where the in-plane tension stress was large due to bending. This was also seen in the finite element investigation where the back face in-plane tensile stress was greatest for a central impact compared to an equivalent edge impact. This is shown in Figure 6.29, where the peak σ_{33} edge impact stress is close to the peaks for the central impact σ_{11} and σ_{33} stresses, whereas the peak σ_{11} edge impact stress is approximately 60% of those values. It is these in-plane stresses that lead to fibre breakage. This description is only valid for certain impacts, governed by the impact energy and thickness of the target. The thinnest plates impacted with nominal thickness of 4 mm showed very different damage patterns, where the delamination was not larger near the edge of the plate, and did not grow with larger impact energy, see Figure 5.32 and Figure 5.33. In these cases the impact energy is being absorbed by more local damage with more surface damage evident, even at the lowest impact energy. Figure 5.17 shows evidence of this with significant denting and back face splitting. For 4 mm thick plates, at this impact velocity, the response is local and the major damage mechanism is not delamination. The boundary conditions are less important. Thus, when the residual strength is measured it does not follow the same pattern as that for the thicker plates, see Figure 5.13 and Figure 5.14. The energy is absorbed by more fibre breakage and the edge impacts, as they are more flexible, show more damage in tension and compression.

7.3 ESTIMATION OF LOSS OF STRENGTH

In section 5.3 the impact damage geometry was presented; this information can be used to estimate the residual strength of the laminates using simple assumptions.

It is assumed that all fibre cracks are contained within a 50 x 50 mm square area, and are all described by the data in Table 5.1, Table 5.2 and Table 5.3. Thus, the data in Table 5.4 (total crack length for each ply direction) was used to reduce the effective thickness of each ply to give the same strength reduction as a fibre crack. To do this each original ply thickness was factored by the ratio of the total crack length (for a ply orientation) to the maximum it could be. For example there are six 0° layers in an 8 mm thick laminate so the maximum possible crack length is 300 mm; the 0° ply total crack length for the 200 J edge impacted plate (see Table 5.4) is 13mm giving a factor of (300-13)/300=0.96. As the total thickness of all the 0° layers is 3.6 mm, the effective total 0° ply thickness is 3.4 mm. This procedure was followed for all ply orientations.

These new ply thicknesses were then used in a laminate analysis using Laminator (2001) to calculate effective damaged lamina ply strengths, which were compared with those already calculated for undamaged laminates in Table 3.13. The software used the maximum stress criterion to calculate factors by which the external applied load would have to be increased in order to fail that ply (with the properties as given in Table 3.12). This ply failure load was then divided by the original undamaged specimen thickness (the load is applied per unit width) to give a ply failure stress. The results are presented in Table 7.1. They show that the edge impacted plate has a 5% tensile strength reduction, whereas the centrally impacted plate an 18% reduction.

Table 7.1 – Predicted damaged laminate ply strengths

	Original and Damaged Ply Strengths						
		200 J Edge Impact		200 J Central Impact		200 J Simulated Impact	
Ply Orientation	Undamaged (MPa)	(MPa)	(%)	(MPa)	(%)	(MPa)	(%)
45	610	581	95.2	501	82.2	449	73.6
90	470	448	95.2	393	83.6	349	74.2
-45	610	581	95.2	501	82.2	449	73.6
0	765	727	95.1	635	82.9	565	73.9

These results can be compared to those measured from experiment, summarised in Table 7.2. Here it can be seen that the edge impacted 8 mm thick plate's tensile strength was reduced by 37%, the centrally impacted plate by 40% and the simulated impacted plate by 49%.

As expected the centrally impacted plate showed a greater reduction in tensile strength compared to the edge impacted plate. The predicted strength drop based on the calculation results in Table 7.1 do not show as great a percentage reduction in strength but agree in the order in which is stronger in tension post-impact. The reason that the percentage decrease in tensile strength does not agree between the predicted and measured values is due to the spread in results, the crudity of the assumptions in predicting the drop in strength and the fact that the tensile strength is affected by other factors than just the amount of fibre damage.

Table 7.2 - Laminate average tensile strength after impact

	Strength (MPa)	% of Undamaged Strength
Undamaged	960	100
200 J Edge Impact	600	63
200 J Central Impact	580	60
200 J Quasi-Static Simulated Impact	490	51

7.4 COMPARISON OF FEA AND EXPERIMENT

In Chapter 6 the work on finite element analysis of elastic impact was presented. In Chapter 5 the damage geometry from the impact experiments was presented, and in particular the shape of the delamination for edge impacts was shown, as in Figure 5.31. The interlaminar shear stresses are important in initiating and propagating delaminations. The 3D models used in section 6.6 can be used to display these stresses at mid-thickness of the model, and are presented in Figure 6.30, Figure 6.31, Figure 6.32 and Figure 6.33. The model has eight elements through the thickness and hence the mid-plane can be easily examined. The plots are taken from the moment when the direct σ_{11} stress is at a maximum in the models, after 1.0 ms in the case of the central impact model and 1.4 ms in the edge impact model. The plots show unrealistically high levels of stress as the laminate would have been damaged before those stresses were attained. However they show that in the central impact model there were concentrated zones of high shear stress near the impact point, with very low values elsewhere. In the edge impact model the σ_{12} follows a similar pattern. σ_{23} in the edge model however shows significant shear stresses that spread along the free edge in a similar shape to the delaminations seen in the C-scans. Therefore it is the high σ_{23} in the edge impact model that creates the large delaminations seen in experiment.

It is the direct stresses that break fibres, and the biggest tensile stresses in both edge and central impacts are found on the back face of the plate due to bending. As can be seen in Figure 6.29 the peak in-plane σ_{33} stresses in both edge and central impact models are of similar magnitude (the peak σ_{11} for the edge impact model being approximately 60% that for the centrally impacted model), and hence it could be thought that both will have similar amounts of fibre breakage. This was not found in experiment however, and the reason is that the edge impacted plate will have delaminated extensively before the fibre breakage had occurred due to the reason outlined in the previous paragraph. The interlaminar interface is weaker than the fibre strength, so the energy from the impact is absorbed in creating delaminations and thus the extent of fibre breakage is less in an edge impacted plate than in a centrally impacted plate of the same thickness.

CHAPTER 8

CONCLUSIONS AND FURTHER WORK

8.1 CONCLUSIONS

The conclusions to each component to the research in this project are summarised, then the main conclusions of the project are made.

The materials used in the project were characterised, and the required properties measured. The manufacturing methods were developed and used successfully to create many thick laminates of three different thicknesses up to 12 mm thick.

The impact machine was used to impact the plates and obtain relevant data from those experiments to produce impact energy absorption, maximum impact force and impact event duration data for each impact. The trends showed that the proportion of the impact energy absorbed by the plate is constant with impact energy at 70%, for both central and edge impacts. A consistently larger maximum impact force was recorded for thicker plates for both edge and central impacts whereas the impact event duration consistently decreased. In the impact of constant energy but variable impact velocity, the maximum impactor force is insensitive to the velocity, but the impact event duration decreases with faster impact velocities.

The damage in the plates was successfully evaluated using a number of destructive and non-destructive techniques. To measure the delaminations, ultrasonic C-scanning was used. For fibre cracks, deply was used. The surface damage was photographed. Finally

coupons were machined from each impacted plate, with the impact damage in the centre, and the residual strength in compression and tension measured. A distinct difference was observed between the edge and centrally impacted plates where edge impacted plates were stronger in tension, whereas the centrally impacted plates were stronger in compression. This was supported by the C-scan results that showed extensive delamination for edge impacted plates, much larger than equivalent centrally impacted plates, which lead to lower critical buckling load. The deply results show that centrally impacted plates suffered more fibre breakage, and hence a lower residual tensile strength.

Impact was efficiently modelled using an axi-symmetric linear-elastic model in ABAQUS/Explicit assuming quasi-isotropic in-plane properties. Inertial stiffening was shown to have a significant effect by comparing (static) indentation and (dynamic) impact. By using a parametric analysis of the elastic impact of composite plates it was shown that thinner and larger diameter plates have larger maximum deflections and longer impact event durations. Smaller plates in both diameter and thickness have higher maximum stresses. In particular it was shown that the maximum stress becomes largely independent of plate diameter for thicker plates. It was also shown that the impact event duration and maximum deflection tend to decrease with impacts with fast impact velocities compared to impacts with slow velocities but the same energy. Finally using ABAQUS/Explicit the edge impacts were modelled in a similar fashion to the earlier axi-symmetric models, but with a solid 3D model. It was shown for edge impacts the plate deflects more and in a more global manner compared to central impacts where the opposite was found to be true. Centrally impacted specimens were shown to have more local response due to the higher stiffness.

The experimental results showed a clear difference between the two impact locations that was also shown in the finite element analysis. The 3D models showed that the edge impacted model was effectively less stiff, and deflected more for a given impact energy. This greater deflection leads to greater bending shear stresses that lead to the delaminations seen in the damage evaluation. The reason for this lower stiffness is the fact there is less material and support for an edge impacted plate, and that hence its inertial stiffness will be lower. All these observations lead to the conclusion that having free edges, or access holes, is more critical when that component is in compression, as an impact near that edge will lead to damage that will reduce its ability to take high compressive loads. In the case

of wing skins, access holes should be placed on the lower skin, and those on the upper skin should have extra inspections.

In the finite element analysis it was also shown that in impacts of constant energy, there were differences in the plate response when the impact velocity was different. With faster impact from smaller masses, the response became more localised with smaller deflections and higher more concentrated stresses. It was attempted to replicate this in the experiments, comparing results from fast, intermediate velocity and quasi-static simulated impacts. Firstly, it is problematic deciding how to match a static indentation test to a dynamic falling weight test. With the method chosen, comparison proved difficult, plus with the range of velocities that were available using the drop weight impact machine, little variation was expected or seen. However, the FEA did predict a difference and that the size and velocity of an impactor would change the response and potentially the damage type observed in a composite. This means that it is insufficient to categorise impact purely as an energy to allow comparison with other impacts. Two of the impact energy, velocity or impactor mass should be quoted.

Using ABAQUS/CAE with the ABAQUS/Explicit solver it was shown that the axi-symmetric modelling capability could successfully be used to create a large number of models efficiently for a parametric analysis. A qualitative understanding of impact was obtained, including some agreement with experiment, particularly the fact that impact event duration was predicted to be longer for edge impacts and the fact that the delaminations in the edge impact were created by large in-plane shear stresses near the free edge.

8.2 FURTHER WORK

It would be useful to perform more tests in order to gain greater statistical confidence in the results presented from this research.

As the actual thickness of the wing skins that are going to be used on the future Airbus civil aircraft will be 20 or 30 mm thick, laminates of those thicknesses should be tested. There are significant challenges in doing so, in the manufacture, impact and strength

measurement of such laminates, but the results would provide a useful function to give more understanding.

Only two impact locations were studied – central and near free edge. The difference in the damage and response was clear, but what was not clear is what happens in between, and what the threshold might be. A programme of study to understand this would provide useful information on the criticality of the location of the impact.

A set of high velocity impact tests, using a gas gun apparatus perhaps, onto thick laminates would be of interest to find evidence of the variation of response due to impacts of constant energy where the impact velocity is changed.

A study of in-plane (onto a free edge) rather than the transverse impact studied in this research would be of interest. This type of impact is possible onto the internal structure, a stringer for example, or during manufacture and assembly. The damage that would result could be quite different to what has been observed for transverse impact.

Finally, more detailed finite element models would be useful in order to predict more accurately the composite plate's response. Modelling at the ply level would enable accurate ply stresses to be calculated and failure criteria to be included.

REFERENCES

Abrate, S., (1991), "Impact on Laminated Composite Materials", Applied Mechanics Review, Vol. 44 No. 4, pp 155 – 190

Abrate, S., (1994), "Impact on Laminated Composites: Recent Advances", Applied Mechanics Review, Vol. 47 No. 11, pp 517 – 544

Aymerich, F. and S. Meili, (2000), "Ultrasonic Evaluation of Matrix Damage in Impacted Composite Laminates", Composites: Part B, 31, pp 1 – 6

Balhi, N. S. S., "Evaluation and Analysis of Matrix Cracking in Composite Laminates", Ph.D. Thesis, Department of Mechanical Engineering, University of Bristol, 2007

Bar-Cohen, Y. and R. L. Crane, (1982), "Acoustic-Backscattering Imaging of Subcritical Flaws in Composites", Materials Evaluation, 40, pp 970 – 975

Bateman, M. G., O. H. Miller, T. J. Palmer, C. E. P. Breen, E. J. Kingston, D. J. Smith and M. J. Pavier, (2005), "Measurement of Residual Stress in Thick Composite Laminates using the Deep-Hole Method", International Journal of Mechanical Sciences, 47, pp 1718-1739

Callister, W. D., "Materials Science and Engineering an Introduction", 4th Ed., John Wiley and Sons Inc., 1997

Cantwell, W. J. and J. Morton, (1989), "Geometrical Effects in the Low Velocity Impact Response of CFRP", Composite Structures, 12, pp 39 – 59

Caprino, G., A. Langella and V. Lopresto, (2002), "Elastic Behaviour of Circular Composite Plates Transversely Loaded in the Centre", Composites: Part A, 33, pp 1191 – 1197

Chandrashekhara, K. and T. Schroeder, (1995), "Nonlinear Impact Analysis of Laminated Cylindrical and Doubly Curved Shells", Journal of Composite Materials, Vol. 29 No. 16, pp 2160 – 2179

Chang, F. and K. Chang, (1987), "A Progressive Damage Model for Laminated Composites Containing Stress Concentrations", Journal of Composite Materials, Vol. 21, pp 834 – 855

Chang, F., J. L. Perez and K. Chang, (1990), "Analysis of Thick Laminated Composites", Journal of Composite Materials, Vol. 24 August, pp 801 – 822

Chao, C. C. and C. Y. Tu, (1999), "Three-Dimensional Contact Dynamics of Laminated Plates: Part 1. Normal Impact", Composites: Part B, 30, pp 9 – 22

Chen, A. S., D. P. Almond and B. Harris, (2001), "In Situ Monitoring in Real Time of Fatigue Induced Damage Growth in Composite Materials by Acoustography", Composites Science and Technology, 61, pp 2437 – 2443

Chen, C. H. and S. Cheng, (1967), "Mechanical Properties of Fibre Reinforced Composites", Journal of Composite Materials, Vol. 1, pp30 – 41

Chen, J., S. V. Hoa, C. Jen and H. Wang, (1999), "Fibre-Optic and Ultrasonic Measurements for in-situ Cure Monitoring of Graphite/Epoxy Composites", Journal of Composite Materials, Vol. 33 No. 20, pp 1860 – 1881

Chen, Y. M. and K. J. Lee, (1979), "A Numerical Study on Effects of Fibre-Orientation of a Unidirectional Elastic Solid Under Impact", Journal of Composite Materials, Vol. 13 April, pp117 – 125

Choi, H. Y. and F. Chang, (1992), "A Model for Predicting Damage in Graphite/Epoxy Laminated Composites Resulting from Low-Velocity Point Impact", Journal of Composite Materials, Vol. 26, No. 14, pp 2134 – 2169

Choi, H. Y., H. S. Wang and F. Chang, (1992), "Effect of Laminate Configuration and Impactor's Mass on the Initial Impact Damage of Graphite/Epoxy Composite Plates Due to Line-Loading Impact", Journal of Composite Materials, Vol. 26, No. 6, pp 804 – 827

Choi, H. Y., R. J. Downs and F. Chang, (1991), "A New Approach toward Understanding Damage Mechanisms and Mechanics of Laminated Composites Due to Low Velocity Impact: Part I - Experiments", Journal of Composite Materials, Vol. 25 August, pp 992 – 1011

Choi, H. Y., H. T. Wu and F. Chang, (1991), "A New Approach toward Understanding Damage Mechanisms and Mechanics of Laminated Composites Due to Low Velocity Impact: Part II - Analysis", Journal of Composite Materials, Vol. 25 August, pp 1012 - 1038

Christoforou, A. P. and A. S. Yigit, (1996), "Impact of Composite Structures - The Momentum Balance Method", Journal of Composite Materials, Vol. 30 No. 10, pp 1068 – 1087

Clarke, M. P., "The Effect of Low Velocity Impact Damage on the Compressive Properties of Carbon Fibre Reinforced Composites", Ph.D. Thesis, Department of Mechanical Engineering, University of Bristol, 1997

Curtis, P. T., "CRAG Test Methods for the Measurement of the Engineering Properties of Fibre Reinforced Plastics", RAE Technical Report 85099, 1985

Daniel, I. M. and O. Ishai, "Engineering Mechanics of Composite Materials", Oxford University Press, New York, 1994

Drapier, S., A. Pagot, A. Vautrin and P. Henrat, (2002), "Influence of the Stitching Density on the Transverse Permeability on Non-Crimped New Concept (NC2) Multiaxial Reinforcements: Measurements and Predictions", Composites Science and Technology, 62, pp 1979 – 1991

Farrow, I. R., K. Potter, A. Fisher and M. Kelly, (2000), "Impact of Adhesively Bonded Composite Joints with Edge Effects", Advanced Composite Letters, Vol. 9 No. 6, pp 397 – 408

Fish, J. C. and S. W. Lee, (1989), "Delamination of Tapered Composite Structures", Engineering Fracture Mechanics, Vol. 34, pp 43 – 54

Fleming, D. C., (2001), "Delamination Modeling of Composites for Improved Crash Analysis", Journal of Composite Materials, Vol. 35 No. 19, pp 1777 – 1792

Fuoss, E., V. Straznicky and C. Poon, (1994), "Prediction of Impact-Induced Delamination in Composite Plates", Advanced Composite Letters, Vol. 3 No. 6, pp 193 – 196

Geubelle, P. H. and J. S. Baylor, (1998), "Impact Induced Delamination of Composites: a 2D Simulation", Composites: Part B, 29B, pp 589 – 682

Gorman, M. R., (1991), "Ultrasonic Polar Backscatter Imaging of Transverse Matrix Cracks", Journal of Composite Materials, Vol . 25 November, pp 1499 – 1514

Green, E. R., C. J. Morrison and R. K. Luo, (2000), "Simulation and Experimental Investigation of Impact Damage in Composite Plates with Holes", Journal of Composite Materials, Vol. 34 No. 6, pp 502 – 521

Guo, Y., D. Post and B. Han, (1992), "Thick Composites in Compression: An Experimental Study of Micromechanical Behaviour and Smeared Engineering Properties", Journal of Composite Materials, Vol. 26, No. 13, pp 1930 – 1967

Hashin, Z., (1980), "Failure Criteria for Unidirectional Composites", Journal of Applied Mechanics, Vol. 47, pp 329 - 334

Helms, J. E., G. Li and S. Pang, (2001), "Impact Response of a Composite Laminate Bonded to a Metal Substrate", Journal of Composite Materials, Vol. 35 No. 3, pp 237 – 252

Hexcel Composites, "Hexply M36 180°C curing epoxy matrix, Product Data", June 2001

Hou, J. P., N. Petrinic, C. Ruiz and S. R. Hallett, (2000), "Prediction of Impact Damage in Composite Plates", Composites Science and Technology, 60, pp 273 – 281

Johnson, A. F., G. Kempe and J. Simon, (2000), "Design of Composite Wing Access Cover Under Impact Loads", Applied Composite Materials, 7, pp 219 – 229

Joshi, S. P. and C. T. Sun, (1985), "Impact Induced Fracture in a Laminated Composite", Journal of Composite Materials, Vol. 19 January, pp 51 – 66

Kaczmarek, H., (1993), "Ultrasonic Analysis of Damage in CFRP Resulting from Static Indentation and Low Velocity Impact", Advanced Composite Letters, Vol. 2 No. 3, pp 101 – 106

Kaczmarek, H., (1995), "Ultrasonic Detection of Damage in CFRPs", Journal of Composite Materials, Vol. 29 No. 1, pp 59 – 95

Kessler, A. and A. Bledzki, (2000), "Influence of the fibre/matrix interphase on the post impact properties of glass/epoxy laminates", Advanced Composites Materials, Vol. 9 No. 2, pp 109 – 118

Kim, C. and E. Jun, (1992), "Impact Resistance of Composite Laminated Sandwich Plates", Journal of Composite Materials, Vol 26, No. 15, pp 2247 – 2261

Krautkramer, J. and H. Krautkramer, "Ultrasonic Testing of Materials", Springer-Verlag, Berlin, 4th Edition, 1990

Kyriazoglou, C., "Development of Vibration Damping for Structural Integrity Assessment of Composite Laminates", Ph.D. Thesis, Department of Mechanical Engineering, University of Bristol, 2003

Lin, H. J. and Y. J. Lee, (1990), "Impact-Induced Fracture in Laminated Plates and Shells", Journal of Composite Materials, Vol. 24 November, pp 1179 – 1199

Lindell, M., "The Laminator", version 3.02, 2001

Lord, A. E., D. R. Hay, (1972), "Ultrasonic Wave Propagation in Metal-Matrix Composites", Journal of Composite Materials, Vol. 6 April, pp278 – 285

McQuillen, E. J., L. W. Gause and R. E. Llorens, (1976), "Low Velocity Transverse Normal Impact of Graphite Epoxy Composite Laminates", Journal of Composite Materials, Vol. 10 January, pp79 – 91

Moon, F. C., (1972), "Wave Surfaces Due to Impact on Anisotropic Plates", Journal of Composite Materials, Vol. 6, pp62 – 79

Naylor, M., (2002), Airbus UK, Private communication

Oguibe, C. N. and D. C. Webb, (1999), "Finite Element Modelling of the impact reponse of a laminated composite plate", Composites Science and Technology, 59, pp 1913 – 1922

Olsson, R., (2000), "Mass Criterion for Wave Controlled Impact Response of Composite Plates", Composites: Part A, 31, pp 879 – 887

Park, R. and J. Jang, (2000), "Impact Behaviour of Aramid Fibre/Glass Fibre Hybrid Composites: Evaluation of Impact Behaviour Using Delamination Area", Journal of Composite Materials, Vol. 34 No. 13, pp 1117 – 1135

Penn, L. S., J. R. Jump, M. J. Greenfield and G. E. Blandford, (1999), "Use of the Free Vibration Spectrum to Detect Delamination in Thick Composites", Journal of Composite Materials, Vol. 33 No. 1, pp 54 – 72

Pickett, A. K., (2002), "Review of Finite Element Simulation Methods Applied to Manufacturing and Failure Prediction in Composite Structures", Applied Composite Materials, 9, pp 43 – 58

Potel, C., T. Chotard, J. de Belleval and M. Benzaggagh, (1998), "Characterisation of Composite Materials by Ultrasonic Methods: Modelisation and Application to Impact Damage", Composites: Part B, 29B, pp 159 – 169

Potter, K. D., F. Schweickhardt and M. R. Wisnom, (2000), "Impact Response of Unidirectional Carbon Fibre Rod Elements with and without an Impact Protection Layer", Journal of Composite Materials, Vol. 34 No. 17, pp 1437 – 1455

Raju, B. B., D. Liu and X. Dang, "Thickness Effects on Impact Response of Composite Laminates", Proceedings of the 13th Annual Technical Conference on Composite Materials, Baltimore, Maryland, USA, September, 1998

Reddy, J. N., (1982), "Transient Response of Laminated, Bimodular-Material, Composite Rectangular Plates", Journal of Composite Materials, Vol. 16 March, pp139 – 152

Richardson, M. O. W. and M. J. Wisheart, (1996), "Review of Low-Velocity Impact Properties of Composite Materials", Composites: Part A, 27A, pp 1123 – 1131

Robinson, P. and G. A. O. Davies, (1992), "Impactor Mass and Specimen Geometry Effects in Low Velocity Impact of Laminated Composites", International Journal of Impact Engineering (UK), Vol. 12, No. 2, pp 189 – 207

Rose, J. L., "Ultrasonic Waves in Solid Media", Cambridge University Press, Cambridge, 1999

Satish Kumar, Y. V. and M. Mukhopadhyay, (2002), "Transient Response Analysis of Laminated Stiffened Plates", Composite Structures, 58, pp 97 – 107

Scarponi, C. and G. Briotti, (2000), "Ultrasonic Technique for the Evaluation of Delaminations of CRFP, GFRP, KFRP Materials", Composites: Part B, 31, pp 237 – 243

Schoeppner, G. A. and S. Abrate, (2000), "Delamination Threshold Loads for Low Velocity Impact on Composite Laminates", Composites Part A, 31, pp 903 – 915

Schuster, D. M. and R. P. Reed, (1969), "Fracture Behaviour of Shock Loaded Boron-Aluminium Composite Materials", Journal of Composite Materials, Vol. 3, pp562 – 579

Short, G. J., "The Effect of Curvature on the Impact Performance of Flat and Curved Glass Fibre Reinforced Laminates", Ph.D. Thesis, Department of Mechanical Engineering, University of Bristol, 2001

Sjöblom, P. O., J. T. Hartness and T. M. Cordell, (1988), "On Low-Velocity Impact Testing of Composite Materials", Journal of Composite Materials, Vol. 22 January, pp30 – 52

Sun, C. T. and J. K. Chen, (1985), "On the Impact of Initially Stressed Composite Laminates", Journal of Composite Materials, Vol. 19 November, pp 490 – 504

Sun, C. T. and S. H. Yang, (1980), "Contact Law and Impact Response of Laminated Composites", NASA-CR-159884

Sun, C. T. and W. C. Liao, (1990), "Analysis of Thick Section Composite Laminates Using Effective Moduli", Journal of Composite Materials, Vol. 24 September, pp 977 – 993

Takeda, N., R. L. Sierakowski and L. E. Malvern, (1981), "Wave Propagation Experiments on Ballistically Impacted Composite Laminates", Journal of Composite Materials, Vol. 15 March, pp 157 – 174

Tenax Fibers GmbH & Co. KG, D-42097 Wuppertal, Germany, "Product Designation and Delivery Programme and Characteristics for Filament Yarn" datasheets, year unknown

Timoshenko, S. P. and J. N. Goodier, "Theory of Elasticity", McGraw-Hill Co., 3rd Ed., 1987

Tu, C. Y. and C. C. Chao, (1999), "Three-Dimensional Contact Dynamics of Laminated Plates: Part 2. Oblique Impact With Friction", Composites: Part B, 30, pp 23 – 41

Vasiliev, V. V. and A. F. Razin, "Anisogrid Composite Lattice Structures for Spacecraft and Aircraft Applications", Proceedings of the 15th International Conference on Composite Materials, Durban, South Africa, July, 2005

Vasudevan, V, "Developments in Advanced Materials", MSc. Thesis, Department of Mechanical Engineering, University of Bristol, 2004

Waddoups, M. E., S. K. Jackson and C. W. Rogers, (1972), "The Integration of Composite Structures into Aircraft Design", Journal of Composite Materials, Vol. 6 April, pp174 – 190

Whitney, J. M., (1967), "Elastic Moduli of Unidirectional Composites with Anisotropic Filaments", Journal of Composite Materials, Vol. 1, pp188 – 193

Whitney, J. M., (1969), "The Effect of Transverse Shear Deformation on the Bending of Laminated Plates", Journal of Composite Materials, Vol. 3 July, pp534 – 547

Wilcox, D., B. Dove, D. McDavid and D. Greer, (2002), ImageTool, University of Texas Health Science Centre at San Antonio, Texas, USA, available from the Internet by anonymous FTP from ftp://maxrad6.uthscsa.edu

Wisnom, M. R., M. I. Jones and G. F. J. Hill, (2001), "Interlaminar Tensile strength of carbon fibre epoxy - specimen size, layup and manufacturing effects", Advanced Composites Letters, Vol. 10 No. 4, pp 171 – 177

Wu, H. T. and G. S. Springer, (1988a), "Impact Induced Stresses, Strains and Delaminations in Composite Plates", Journal of Composite Materials, Vol. 22 June, pp 533 – 560

Wu, H. T. and G. S. Springer, (1988b), "Measurements of Matrix Cracking and Delamination Caused by Impact on Composite Plates", Journal of Composite Materials, Vol. 22 June, pp 518 – 532

Yang, N., (2005), Airbus UK, Private communication

Young, W. C. and R. G. Budynas, "Roark's Formulas for Stress and Strain", 7th Ed., McGraw-Hill, London, 2002

Yuan, Q., T. Czigany and L. Ye, (2000), "Failure Behaviour of Cross-Ply Carbon Fibre/Epoxy Laminates Subjected to Transverse Impact and Static Perforation", Advanced Composites Letters, Vol. 9 No. 5, pp 355 – 360

Zhou, G. and G. A. O. Davies, (1994), "Impact Response of Thick Glass Fibre Reinforced Polyester Laminates", International Journal of Impact Engineering, 16(3), pp 357 – 374

Zhou, G., J. C. Lloyd and J. J. McGuirk, (2001), "Experimental Evaluation of Geometric Factors Affecting Damage Mechanisms in Carbon/Epoxy Plates", Composites: Part A, 32, pp 71 – 84

Ziao, J. and J. Tao, (1996), "Investigation of interlaminar defects and their influence on interlaminar strength", Advanced Composites Letters, Vol. 5 No. 4, pp 117 – 120

Zou, Z., S. R. Reid, S. Li and P. D. Soden, (2002), "Application of a delamination model to Laminated Composite Structures", Composite Structures, 56, pp 375 – 389

Zukas, J. A., "Impact Dynamics", John Wiley and Sons Inc., 1982

APPENDIX A

In this appendix the drawings for the adapters for the Mayes test machine are shown. Figure A.1 shows the Mayes test machine with the adapters labelled. Figures A.2 to A.5 show the drawings for the adapters. Figure A.6 shows the spigot used for locating the adapters onto the grips.

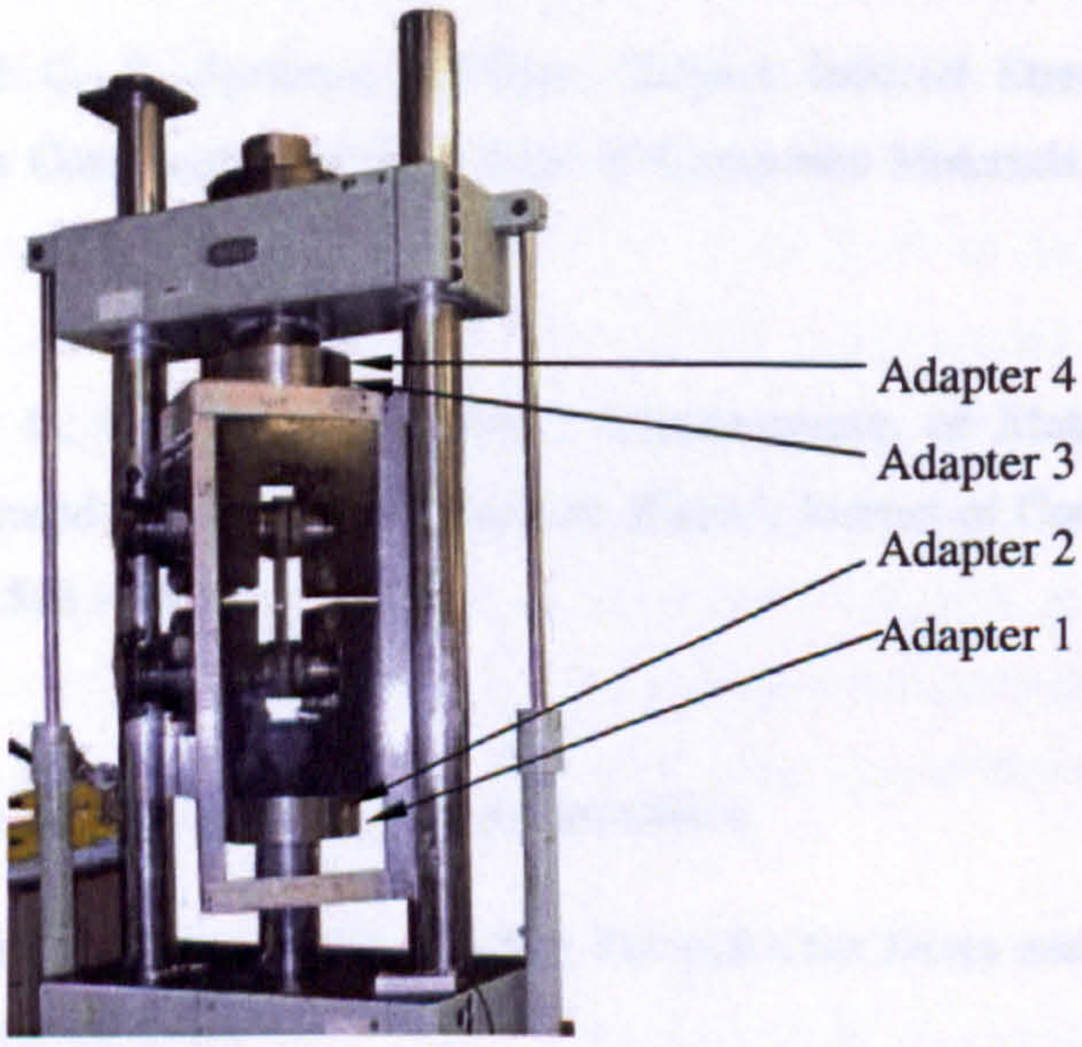

Figure A.1 – Location of the four hydraulic grip adapters on the Mayes test machine

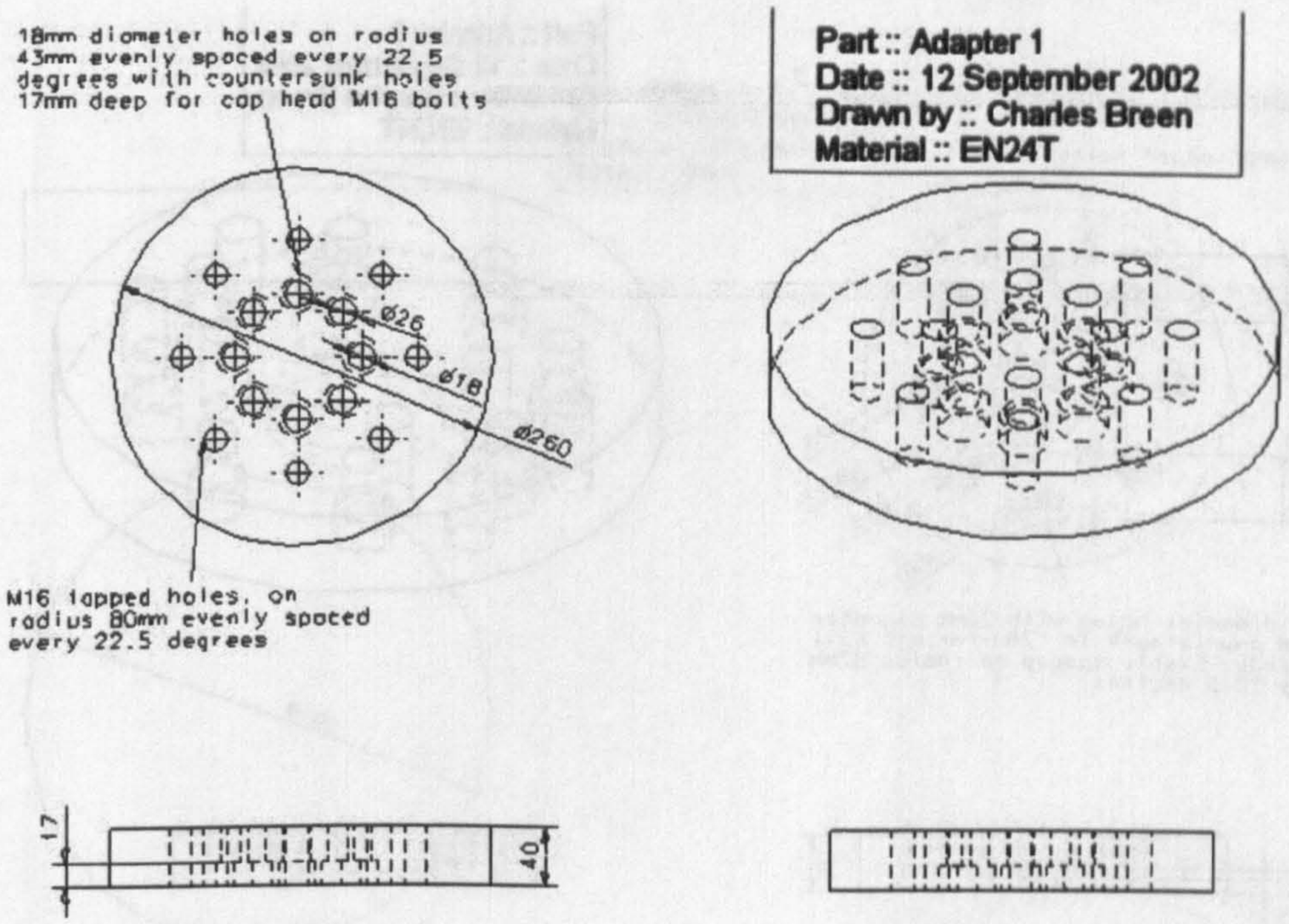

Figure A.2 – Drawing for adapter 1

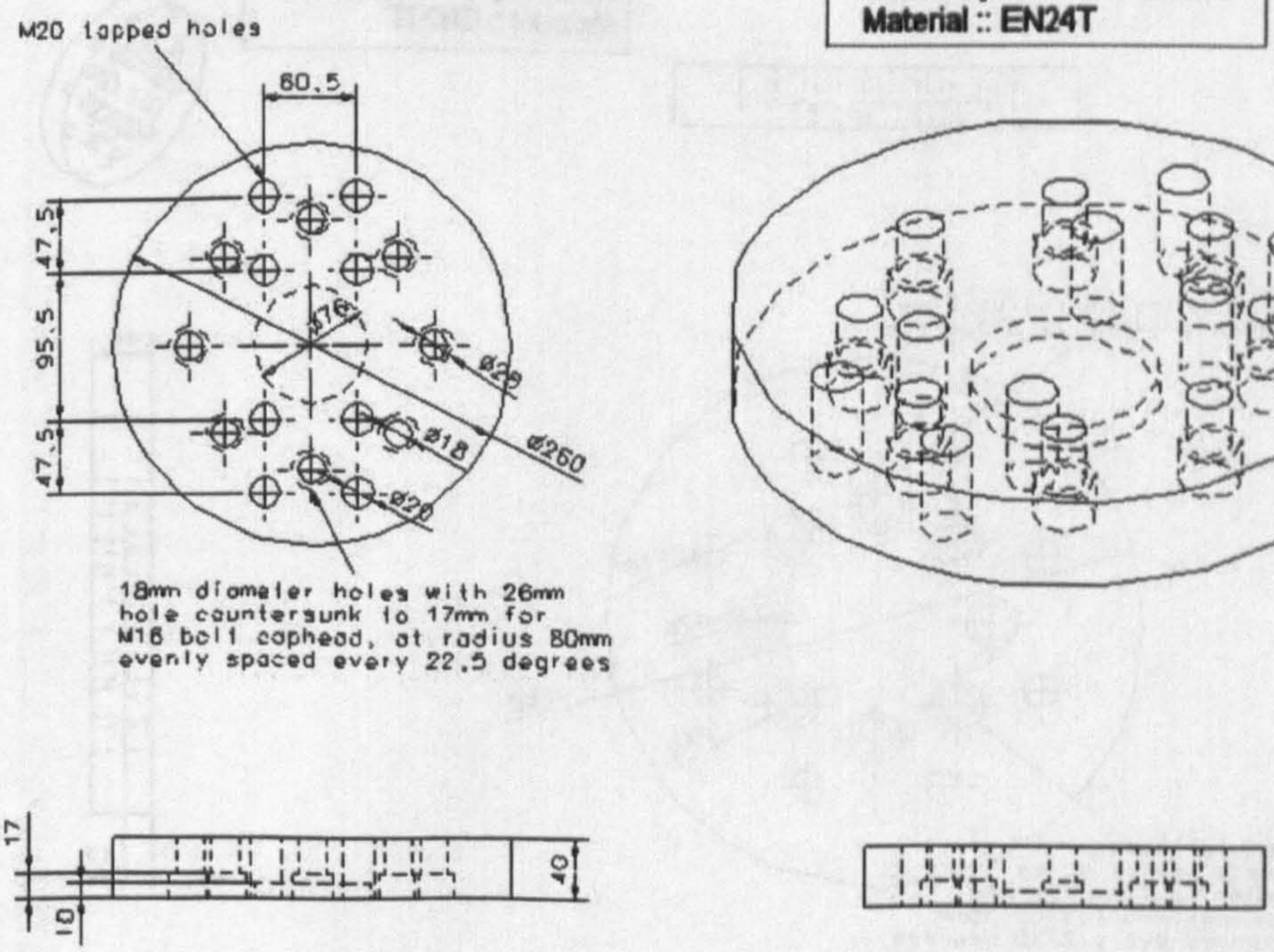

Figure A.3 – Drawing for adapter 2

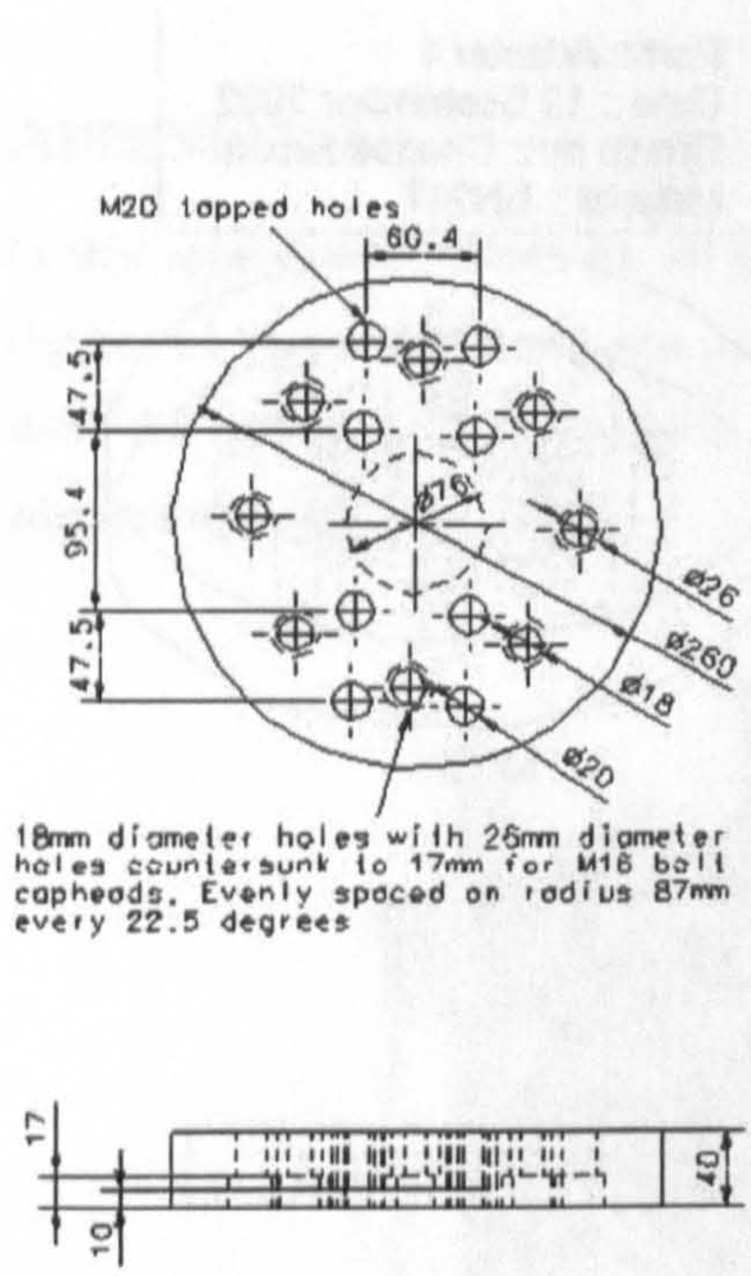

Figure A.4 – Drawing for adapter 3

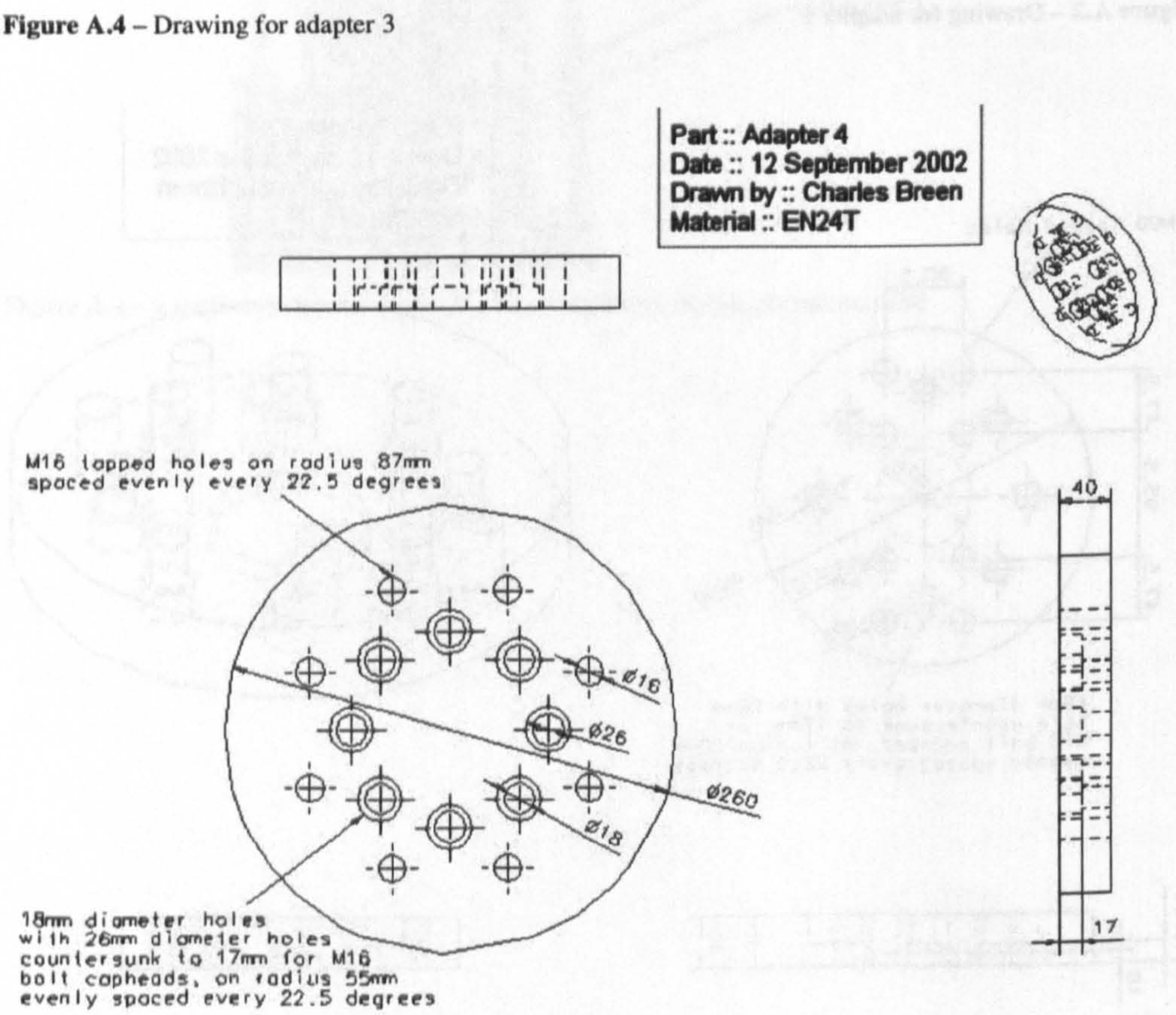

Figure A.5 – Drawing for adapter 4

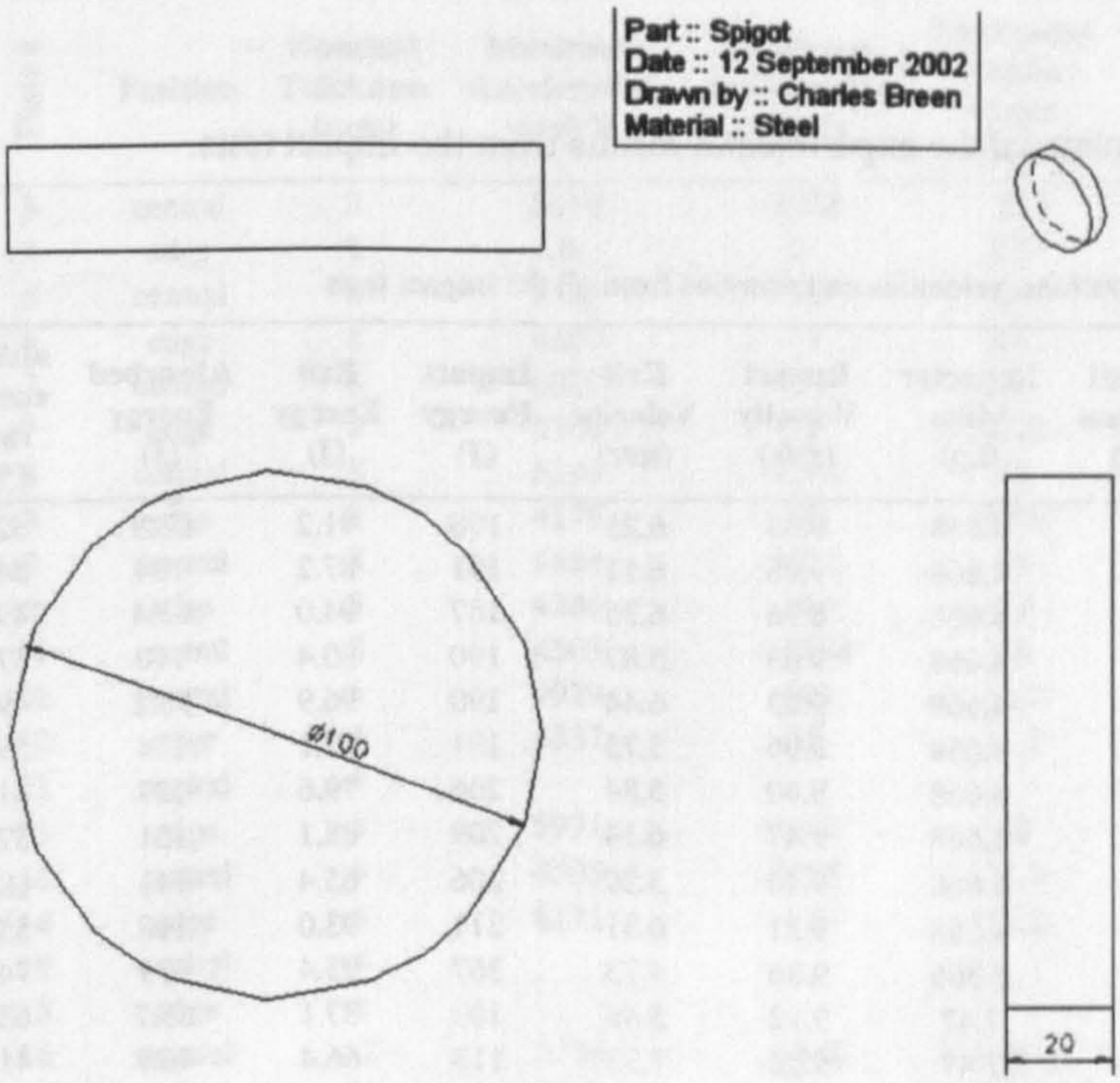

Figure A.6 – Drawing for the spigot

APPENDIX B

Tables B.1 and B.2 tabulate all the experimental results from the impact tests.

Table B.1 – Impact configurations, velocities and energies from all the impact tests

Plate #	Position	Nominal Thickness (mm)	Impactor Mass (kg)	Impact Velocity (m/s)	Exit Velocity (m/s)	Impact Energy (J)	Exit Energy (J)	Absorbed Energy (J)	ab/imp energy ratio (%)
3	central	8	4.668	9.03	6.25	190	91.2	98.9	52.0
3	edge	8	4.668	9.06	6.11	191	87.2	104	54.5
6	central	8	4.668	8.96	6.35	187	94.0	93.4	49.9
6	edge	8	4.668	9.03	5.87	190	80.4	110	57.7
7	central	8	4.668	9.03	6.44	190	96.9	93.2	49.0
7	edge	8	4.668	9.06	5.75	191	77.1	114	59.7
8	central	8	4.668	9.40	5.84	206	79.6	127	61.4
8	edge	8	4.668	9.47	6.14	209	88.1	121	57.9
9	central	8	4.668	9.40	5.29	206	65.4	141	68.3
9	edge	8	4.668	9.51	6.31	211	93.0	118	55.9
11	central	8	8.366	9.36	4.73	367	93.4	273	74.5
12	central	4	2.47	9.12	5.48	103	37.1	65.7	63.9
12	edge	4	2.47	9.58	7.33	113	66.4	46.9	41.4
13	central	4							
13	edge	4	4.668	9.31	5.87	202	80.4	122	60.3
14	central	4	4.668	9.51	5.10	211	60.7	150	71.2
14	edge	4	4.668	9.31	5.89	202	81.0	121	60.0
15	central	4	2.47	9.58	5.72	113	40.4	72.9	64.3
15	edge	4	2.47	9.47	7.65	111	72.2	38.6	34.8
16	central	12	8.366	9.54	5.79	381	140	241	63.2
16	edge	12	8.366	9.58	5.79	384	140	244	63.5
17	central	8	2.47	9.54	6.65	112	54.6	57.8	51.4
17	edge	8	2.47	9.58	6.33	113	49.5	63.8	56.3
18	central	8	8.366	9.47	4.54	375	86.3	289	77.0
18	edge	8	8.366	9.47	6.13	375	157	218	58.1
19	central	8	2.47	9.54	6.65	112	54.6	57.8	51.4
19	edge	8	2.47	9.54	6.60	112	53.7	58.7	52.2
25	edge	8	8.366	9.54	6.22	381	162	219	57.5
26	central	8	4.668	9.40	5.81	206	78.9	127	61.7
26	edge	8	4.668	9.47	6.36	209	94.4	115	54.9
27	central	12	4.668	9.43	5.76	208	77.4	130	62.7
27	edge	12	4.668	9.19	5.35	197	66.9	130	66.1
28	central	12	8.366	9.51	5.92	378	147	231	61.2
28	edge	12	8.366	9.54	5.59	381	131	250	65.6
30	edge	8	8.366	9.47	5.10	375	109	266	71.0
31	central	8	12.171	5.54	3.71	187	83.7	103	55.2
31	edge	8	12.171	5.58	3.56	190	77.2	112	59.3
32	central	12	4.668	9.29	5.66	202	74.7	127	63.0
32	edge	12	4.668	9.26	5.08	200	60.3	140	69.9
10a	central	8	12.171	5.51	3.92	185	93.7	90.8	49.2
10b	central	8	12.171	5.51	3.94	185	94.3	90.2	48.9

Table B.2 – Accelerations and forces from all the impact tests

Plate #	Position	Nominal Thickness (mm)	Maximum Acceleration (m/s2)	Minimum Acceleration (m/s2)	Maximum Impact Force (kN)	Minimum Impact Force (kN)	Impact Duration (ms)
3	central	8	5616	-1502	26	-7	3.50
3	edge	8	0	0	0.0	0.0	
6	central	8	5566	-703	26	-3	3.59
6	edge	8	4300	-71	20.1	-0.3	5.60
7	central	8	6020	-201	28	-0.9	3.76
7	edge	8	3768	-79	17.6	-0.4	6.12
8	central	8	5340	-3298	25	-15	4.46
8	edge	8	4179	-84	19.5	-0.4	5.89
9	central	8	4884	-1011	23	-5	3.77
9	edge	8	4286	-100	20	-0.5	5.86
11	central	8	4503	-11768	38	-98	5.30
12	central	4	4929	-133	12.2	-0.3	4.73
12	edge	4	4537	-55	11.2	-0.1	6.34
13	central	4					
13	edge	4	5931	-1637	28	-8	7.24
14	central	4	4503	-2685	21.0	-13	6.10
14	edge	4	6171	-178	28.8	-1	8.21
15	central	4					
15	edge	4					
16	central	12	6386	-6968	53	-58	3.83
16	edge	12	3717	-111	31.1	-1	6.70
17	central	8	9017	-400	22.3	-1.0	2.64
17	edge	8	6394	-152	15.8	-0.4	3.89
18	central	8	5220	-12585	44	-105	6.30
18	edge	8	5520	-333	46	-3	7.90
19	central	8	9041	-377	22.3	-0.9	2.68
19	edge	8	6365	-15	15.7	0.0	3.72
25	edge	8	3141	-65	26	-1	7.66
26	central	8	6084	-1073	28	-5	3.67
26	edge	8	4209	-42	19.6	-0.2	5.93
27	central	12	8473	-485	40	-2	2.75
27	edge	12					
28	central	12	5423	-641	45	-5	3.83
28	edge	12	3626	-134	30.3	-1.1	6.26
30	edge	8	3398	-4093	28	-34	7.69
31	central	8	2947	-1391	36	-17	5.76
31	edge	8	1632	-38	20	0	9.62
32	central	12	8024	-419	37	-2	2.72
32	edge	12	5142	-22	24.0	0	4.57
10a	central	8	2751	-1557	33	-19	5.77
10b	central	8	3897	-3300	47	-40	5.77

APPENDIX C

Table C.1 shows the residual tensile strength value for each specimen-impact configuration. The cells that have coloured borders are averaged values. The values that make up those averages are highlighted below in the same colour as the border.

Table C.1 – Tensile residual strength results for each specimen-impact configuration with average values colour-coded

Central Impact

	Impact Energy		
Thickness	100	180	350
4	329	305	
8	775	610	303
12		X	475

Edge Impact

	Impact Energy		
Thickness	100	180	350
4	573	191	
8	847	596	491
12		X	521

Effect of Impact Velocity

	Velocity		
Thickness	Q-Static	Slow	High
8	494	565	610

667	556	534
621	441	658
631	485	
521		

Table C.2 shows the same information, except for compression results.

Table C.1 – Compressive residual strength results for each specimen-impact configuration with average values colour-coded

Central Impact

	Impact Energy		
Thickness	100	180	350
4	102	90	
8	262	110	60
12		148	75

Edge Impact

	Impact Energy		
Thickness	100	180	350
4	107	42	
8	183	73	42
12		109	46

Effect of Impact Velocity

	Velocity		
Thickness	Q-Static	Slow	High
8	95	128	110

70	134	96	48
70	121	124	36
69			
77			
79			